Spatio-temporal reconstruction of satellite-based temperature maps and their application to the prediction of tick and mosquito disease vector distribution in Northern Italy

Von der Naturwissenschaftlichen Fakultät
der Gottfried Wilhelm Leibniz Universität Hannover
zur Erlangung des Grades

Doktor der Naturwissenschaften
Dr. rer. nat.

genehmigte Dissertation
von

Diplom-Geograph Markus Georg Neteler
geboren am 21.12.1969 in Thuine/Lingen

2010

Referent: Prof. Dr. Th. Mosimann

Korreferent: Prof. Dr. G. Kuhnt

Tag der Promotion: 26. April 2010

Acknowledgments

Summary

High temporal resolution data from remote sensing are of great relevance to the modelling of disease transmitting ectoparasites since they allow an assessment of vector and disease distribution and their potential spread. However, despite its potential, up to now, remote sensing has been used far below the expectations expressed in epidemiological literature.

In the present thesis, an innovative approach has been proposed for reconstructing incomplete time series of the new MODIS Land Surface Temperature (LST) sensor onboard the Terra and Aqua satellites. MODIS data are generated at daily resolution and freely available usually less than one week after image acquisition on a NASA server. Unfortunately, the satellite maps produced by this sensor are incomplete because cloud cover "contaminates" the data, and the maps also contain other pixel dropouts. Completion of these maps is essential for an efficient GIS based time series modelling, since these models can only be developed with complete data sets.

The MODIS LST map reconstruction was executed by performing an automated data download, reprojection to a commonly used map projection system, data format conversion for the GIS import, and a complex procedure to eliminate temperature outliers and to reconstruct the LST datum in areas with no data. For this last procedure, temperature gradient based models were used. Input data points were subsequently interpolated with volumetric splines to obtain complete LST maps.

Subsequently, these reconstructed daily LST maps were aggregated with various ecological indicators and were also thresholded to be able to search for signals relevant to tick and mosquito related ecological processes (e.g., onset of ticks activity in spring; mosquito moulting between life stages, etc.).

The obtained daily and aggregated LST maps were also compared to meteorological temperature measurements (instantaneous and aggregated measures) as well as to thermal maps from LANDSAT-TM in order to assess the quality of the data reconstruction. Both instantaneous and aggregated indicators derived from LST maps match related meteorological indicators with statistical significance. The correlation with thermal maps from LANDSAT-TM is less strong due to different sensor resolutions and a time shift between the overpasses of the LANDSAT-TM and Terra satellites.

As a result, a completely reconstructed remotely sensed thermal data set is available for parts of Northern Italy. Using temperature gradient based models which have been developed within the thesis together with high resolution elevation maps, it was also possible to increase the original resolution of the LST maps from 1,000 m to 200 m pixel size. Due to the subsequent aggregations of daily data, different derived temperature indicator data sets are now available at various temporal resolutions. In fact, more than 11,000 maps have been produced for the study area in Northern Italy. The produced maps were then applied in two case studies on disease vectors in order to understand seasonality and spatial distribution. The aggregated LST maps were used as input variables in these case studies.

In the first case study on the hard tick *Ixodes ricinus*, time series of larvae and nymphs counts were enriched with time series of LST derived ecological indicators. Probably because of the temporally limited tick data availability, no clear signal was evident, and it was not possible to obtain a model for predicting the distribution of different life stages. Since it was demonstrated

by comparison with meteorological data that the statistical significance of the LST data is high, an integration of further tick data will help to determine better temperature based models.

A second case study was performed on the invasive mosquito *Aedes albopictus*, a species known to be spreading in Northern Italy. Here, two different ecological indicators extracted from aggregated daily LST maps were applied successfully to obtain distribution maps of the vector. As a first indicator, January temperature threshold maps were generated in order to assess *Aedes albopictus* egg winter survival. A second indicator was based on growing degree days which were filtered with an autumnal minimum threshold in order to obtain a distribution map of adult mosquitoes. Both maps coincide significantly (89% of overlap), indicating good agreement and some variation in the survival of different life stages. Only two out of 594 positive municipalities result outside of the predicted distribution area of *Aedes albopictus* (false negative error of 0.3%). Reconstructed MODIS LST data can be accepted as a valid proxy for analysing the temperature profile in relation to mosquito survival.

Keywords

Zusammenfassung

Die Modellierung der Verbreitung von humanmedizinisch relevanten Parasiten in der Umwelt erfordert die Verwendung von hochauflösenden Datenquellen, insbesondere in Bezug auf die zeitliche Auflösung. Fernerkundungsdaten mit hoher zeitlicher Auflösung sind von großer Bedeutung für die epidemiologische Modellierung zur Erfassung und Neubewertung von aktuellen und potentiellen Verbreitungen von Krankheitsvektoren und Krankheiten. Diesem Anspruch konnte man jedoch bisher nicht gerecht werden – Fernerkundung wurde bislang nur unzureichend genutzt, wie in der Literatur kritisiert wird.

In dieser Arbeit wird ein innovativer Ansatz vorgeschlagen, der es ermöglicht, unvollständige Zeitreihen der neuen MODIS Land Surface Temperature (LST) Satellitensensoren der Aqua- und Terra-Satelliten vollständig zu rekonstruieren. Diese MODIS Daten werden viermal täglich erzeugt und nach wenigen Tagen auf einem NASA-Server öffentlich bereitgestellt. MODIS-Satellitenkarten sind häufig, bedingt durch Wolken oder andere atmosphärische Strömungen, unvollständig. Für eine effiziente GIS-basierte Zeitreihenmodellierung ist es wichtig, mit kompletten Datensätzen zu arbeiten.

Die Rekonstruktion der LST Satellitenbilder umfasst den automatisierten Daten-Download, die Reprojektion in eine gängige Projektion, die Konvertierung des originalen Datenformats in ein GIS-geeignetes Format sowie ein komplexes Verfahren zur Beseitigung der Temperaturausreißer und der Rekonstruktion fehlender Pixelwerte. Hierzu werden Temperaturgradienten-Modelle erstellt und eingesetzt. Die verwendeten Datenpunkte werden anschließend mit Volumen-Splines interpoliert, um schließlich komplette LST Karten zu erhalten.

Die rekonstruierten, täglich erzeugten LST Karten werden darüber hinaus aggregiert, um verschiedene ökologische Indikatoren zu ermitteln, und einer Schwellwertanalyse unterzogen, um nach für ökologische Prozesse von Zecken und Stechmücken relevanten Signalen zu suchen (z.B. Beginn der Zeckenaktivität im Frühjahr; Häutung der Stechmücken beim Wechsel von einem Lebensabschnitt zum nächsten usw.).

Die berechneten täglichen sowie die aggregierten LST Karten werden mit meteorologischen Temperaturmessungen (Instant- und aggregierte Messungen) sowie mit thermischen Karten von Landsat-TM verglichen, um die Qualität der rekonstruierten Daten zu bewerten. Die aus LST Karten extrahierten Indikatoren stimmen statistisch signifikant mit den entsprechenden Indikatoren aus meteorologischen Daten überein. Zu thermischen Karten von Landsat-TM besteht eine geringere Korrelation aufgrund der unterschiedlichen Sensorauflösung und einem Zeitversatz bei den Satellitenüberflügen von Landsat-TM und Terra.

Als ein Ergebnis steht nun eine komplett rekonstruierte Zeitreihe thermaler Fernerkundungsdaten für Teile Nord-Italiens zur Verfügung. Durch den Einsatz der Temperaturgradient-Modelle und von höherauflösenden Höhenkarten ist es möglich, die ursprüngliche Auflösung der LST Karten von 1.000 m auf 200 m pro Pixel zu erhöhen. Bei einer anschließenden Aggregation der täglichen Daten werden weitere Indikatorkarten mit verschiedenen zeitlichen Auflösungen abgeleitet. Insgesamt wurden mehr als 11.000 Karten für das Untersuchungsgebiet in Nord-Italien produziert.

In der ersten Fallstudie werden Zeitreihendaten von Larven und Nymphen von Schildzecken *Ixodes ricinus* durch Zeitreihen der aus LST erzeugten ökologischen Indikatoren ergänzt. Aufgrund der nur begrenzt zur Verfügung stehenden Zeckendaten konnte kein eindeutiges Sig-

nal identifiziert werden, mit dem sich ein räumliches Modell zur Verteilungvorhersage der verschiedenen Lebensphasen erstellen ließe. Da die LST-Daten im Vergleich mit meteorologischen Daten hohe statistische Signifikanz zeigen, dürfte die Integration von weiteren Zeckendaten helfen, bessere temperaturbasierte Modelle zu erstellen.

Eine zweite Fallstudie beschäftigt sich mit der sich in Norditalien verbreitenden tagaktiven Mückenart *Aedes albopictus*. Hier wurden zwei verschiedene ökologische Indikatoren aus täglichen LST-Karten aggregiert und erfolgreich eingesetzt, um eine potenzielle Verbreitungskarte des Vektors zu erhalten. Der erste Indikator ist die Minimumtemperatur im Januar, um die Überlebenswahrscheinlichkeit der Eier von *Aedes albopictus* im Winter zu bestimmen. Der zweite Indikator, benutzt für eine weitere Karte der Verteilung des Vektors, basiert auf der Berechnung von akkumulierten Gradzahltagen, die den Wert 1350 erreichen müssen bevor die herbstliche Mindesttemperatur von 10 °C unterschritten wird. Beide Karten zeigen große Übereinstimmung (89% Überschneidung), aber auch gewisse Unterschiede in den Überlebensraten der verschiedenen Lebensstadien. Nur zwei der insgesamt 594 Gemeinden, in denen *Aedes albopictus* auftritt, lagen außerhalb des prognostizierten Verbreitungsgebiet (falsch-negativer Fehler von 0,3%). Damit lassen sich rekonstruierte MODIS LST Daten bei Temperaturanalysen in Bezug auf Überleben von Mücken einsetzen.

Schlagwörter

Satellitenfernerkundung
Modellierung von Krankheitsvektoren
GIS Modellierung
Zeitreihenprozessierung
Landoberflächentemperatur
MODIS-Sensor
Raum-zeitliche Temperaturmodellierung
Ixodes ricinus Zecke
Aedes albopictus Stechmücke

Contents

List of Figures

List of Tables

List of abbreviations

CHIK: Chikungunya
DOY: Day Of Year
EVI: Enhanced Difference Vegetation Index
GDD: Growing Degree Days
GIS: Geographical Information System
HGA: Human Granulocytic Anaplasmosis
IPCC: Intergovernmental Panel on Climate Change
LB: Lyme Borreliosis
LST: Land Surface Temperature
MODIS: Moderate Resolution Imaging Spectroradiometer
NDVI: Normalized Difference Vegetation Index
RMSE: Root Mean Square Error
RS: Remote Sensing
TBE: Tick-Borne Encephalitis
WHO: World Health Organization
WNV: West Nile Virus

1 Introduction

Many continents, including Europe, are facing an increasing risk of introduction or spread of tropical vector-borne diseases transmitted by insects, ticks and rodents threatening human and animal health (Nurdan, 2005; Randolph, 2006; Senior, 2008). Zoonoses already present in Europe include Tick-borne Encephalitis, Lyme disease, Leishmaniasis, Bluetongue, Chikungunya, and diseases caused by West Nile virus, Toscana virus and Hantavirus (Grunewald et al., 2003; World Health Organization, 2004; Bengis et al., 2004; Kuhn et al., 2004; Nurdan, 2005; Niedrig et al., 2006; Randolph, 2006; Senior, 2008). Since arthropod vectors such as ticks and insects are ectotherms, their activity depends directly on environmental conditions (Grunewald et al., 2003; Frumkin, 2005; Intergovernmental Panel on Climate Change, 2008). Especially relevant is temperature which controls winter survival, vector population growth, feeding behavior, susceptibility of the vector to pathogens, synchrony among life stages, and the spread of the vectors to more northern latitudes (Nurdan, 2005). Until 2100, an increase of winter minimum temperatures is expected in northern Europe along with increased annual precipitation, while in southern and central Europe higher-than-average summer temperatures are expected with a decrease of annual precipitation (World Health Organization, 2008). Consequently, new ecological niches are being and are expected to be established and (re-)colonized by vectors along the northern limits of tick (e.g., *Ixodes ricinus*), tiger mosquito (*Ae. albopictus*), and sand fly (Diptera: Phlebotominae) distributions in Europe (World Health Organization, 2008) concurrent with the increase of the suitable habitat for these vectors.

Moreover, secondary infection routes have been recently identified: for example, the Chikungunya virus (see Section 1.1.2) has been imported into a northern Italian region by a tourist returning from an endemic country, and it was transmitted to more than 200 people by *Ae. albopictus* (Rezza et al., 2007). The presence of a competent vector would also allow local outbreaks in other regions.

A variety of methods have been developed to analyse natural and introduced disease patterns and spread, including the modelling of host-pathogen systems. The model outputs have been helpful in improving our understanding of specific aspects of spatial epidemiology of disease. Most models are strongly data-driven and rely on the input of related environmental variables which are ideally collected in a spatially distributed way and at high temporal resolution designed to capture disease dynamics. For this purpose, remote sensing environmental correlates have been an extremely relevant source of information; up to now, low and medium resolution remote sensing (LRRS and MRRS) have been especially and increasingly important as data source for disease modelling. This thesis focuses on data preparation and analysis of temperature maps from MRRS and demonstrate the integration of the resulting ecological indicators in the analysis of two case studies.

1.1   The spread of emerging infectious diseases: selected disease vectors and vector-borne diseases

In the following section, selected disease vectors and vector-borne diseases are briefly presented with focus on the relevance of environmental factors driving spread and disease transmission.

1.1.1   Tick-borne diseases: TBE, Lyme and HGA

Tick-borne diseases (TBD) are continuously spreading in Europe and in other regions of the world (Senior, 2008). After mosquitoes, ticks are considered to be second most important as vectors of human infectious diseases in the world (Parola and Raoult, 2001). In the temperate zones of the Northern hemisphere, ticks rather than insects are responsible for the majority of vector-borne pathogens (Randolph, 2001b). In Europe, the hard tick *Ixodes ricinus* (Linnaeus 1758) (family Ixodidae, order Ixodida, class Arachnida, phylum Arthropoda; vernacular names: sheep tick or castor bean tick) acts both as vector and reservoir for a series of wildlife zoonotic pathogens. *I. ricinus* transmits a range of pathogens including bacteria (e.g., Lyme disease spirochaetes such as *Borrelia burgdorferi* spp., or rickettsiae such as *Ehrlichiae* spp.), and viruses (e.g., tick-borne encephalitis virus) and protozoans (e.g., *Babesiae* spp.) (Randolph and Storey, 1999; Faulde and Hoffmann, 2001). Particularly the agents of Lyme diseases, tick-borne encephalitis and human granulocytic anaplasmosis are emerging in many parts of Europe. A rise of tick-borne diseases is caused by the shortening of the developmental cycle of ticks because of several ecological changes including higher average temperatures throughout the year and because of the increased availability of reservoir hosts (Stanek, 2002; Bengis et al., 2004; Kruse et al., 2004). In Italy, the tick *I. ricinus* has been recorded in most regions, especially in thermo-mesophilous woods and shrubby habitats where the relative humidity allows the tick to complete its 3 year developmental cycle (Rizzoli et al., 2004).

Ticks can cause paralyses, toxicoses, allergic reactions in humans and animals (Estrada-Peña and Jongejan, 1999). Due to their ability to transmit both bacteria and viruses, tick-borne diseases are considered as major public health concern. Humans and animals are exposed to Ixodid ticks (hard ticks) in infested vegetation as ticks are attaching through physical contact to the host.

The abundance of ticks is driven by various factors. In terms of emerging diseases, landscape changes are an important factor: for example, the increase of ecosystem patchiness leads to a different distribution and abundance of wildlife species and their ectoparasites (Ostfeld et al., 1995). The rise of *Ixodes* tick-borne diseases is further amplified by increased reforestation and in particular by the increase of deer populations in European and other countries (Barbour, 1998; Chaput et al., 2002; Gray et al., 2009; Rizzoli et al., 2009). Landscape composition (types of elements) and configuration (spatial location of those elements) influence disease risk or incidence – this suggests that a true integration of landscape ecology with epidemiology will be fruitful (Ostfeld et al., 2005). Landscape composition has impact on both abiotic conditions (e.g. abundance of edges or changes to environmental gradients) and species interactions that are important to disease spread and prevalence. A major research challenge is to understand the level of ecological complexity in order to accurately predict spatial dynamics; this includes the assessment of niches as abiotically defined as well as trophic interactions (Ostfeld et al., 2005). Other factors of tick-borne disease spread are the changes in human behaviour that have brought

more people into contact with infected ticks (Randolph, 2001b). Both political changes in Europe and changes in the leisure activities are suspected reasons for the observed increase of infectious diseases. Infections are commonly acquired in outdoor work or recreational activities which suggests that human behaviour is a strong predictor of tick-borne disease risk (Barbour, 1998; Chaput et al., 2002).

Climate warming will affect biological systems, both vegetal and animal but its impact is yet unclear (Intergovernmental Panel on Climate Change, 2007). Climate models predict an increase in temperature and significant increases in precipitation in Europe during the next century (Intergovernmental Panel on Climate Change, 2007). Results from biological and statistical models suggest that these changes could influence or increase directly or indirectly the risk, particularly of malaria, tick-borne encephalitis and Lyme disease (Randolph and Rogers, 2000; Randolph, 2002; Grunewald et al., 2003; Randolph, 2004a). With respect to ticks, the already observed temperature increase may lead to a prolonged tick questing activity, and a possible increased tick survival rate. Reservoir host survival and reproductive rates are also affected. Consequently, suitable habitats may shift northwards (Randolph, 2002). However, other authors suggest that an increase of vector-borne diseases would only occur in combination with vector competence, land cover and socio-economic factors changes (Kuhn et al., 2004; Sumilo et al., 2007).

Available European maps of the risk estimation of acquiring a tick-borne disease (published e.g. in Estrada-Peña (1999b) or Randolph (2002), see also Baxter GmbH[1]) show strong differences among each other. A first European *Ae. albopictus* risk maps was published by the European Centre for Disease Prevention and Control (2009). With more data becoming continuously available, updated versions of these maps are expected.

Ecology of ticks

I. ricinus ticks, a non-nidiculous species, live in leaf litter and low vegetation of temperate deciduous woodlands and mixed forests. In case of high rainfall, they also appear in coniferous forests and open space such as grasslands (Gern and Humair, 2002). Their habitats are affected by biotic (vegetation, host) and by abiotic factors (climate). Since ticks spend a large proportion of their life-cycle off the host, the habitat in which they live is of particular importance. Infected ticks are usually found in forest edges, forest plantations with brushwood and shrubbery, in the transition between deciduous and coniferous forests or between timber and coppice (Süss, 2003).

The *Ixodes* tick life cycle lasts for 2-6 years (typically 3 years) and consists of three parasitic stages evolving from an egg: larva (6 legs), nymph and adult (both eight legs; see Fig. 1.1). During these three active stages, ticks need a blood meal to pass from one stage to another which lasts two to ten days on the vertebrate host. Eggs are laid by an adult female tick in spring and hatch into six-legged larvae in summer which begin seeking their first blood meal. After this meal, the larval tick moults into an eight-legged nymph which undergoes a developmental diapause (dormancy) until the next late spring or early summer. The induction of the diapause is largely determined by changes in temperature and in day length due to a photo-periodic reaction (Sonenshine, 1993; Gray, 2001). The nymph seeks a blood meal, then moult into a similar but larger adult tick. The adult *Ixodes* seeks a medium- or large mammal host in mid-autumn of the

---

[1]Baxter Deutschland GmbH, `http://www.zecken.de/fsme/krankheiten_verbreitung_von_fsme.asp`
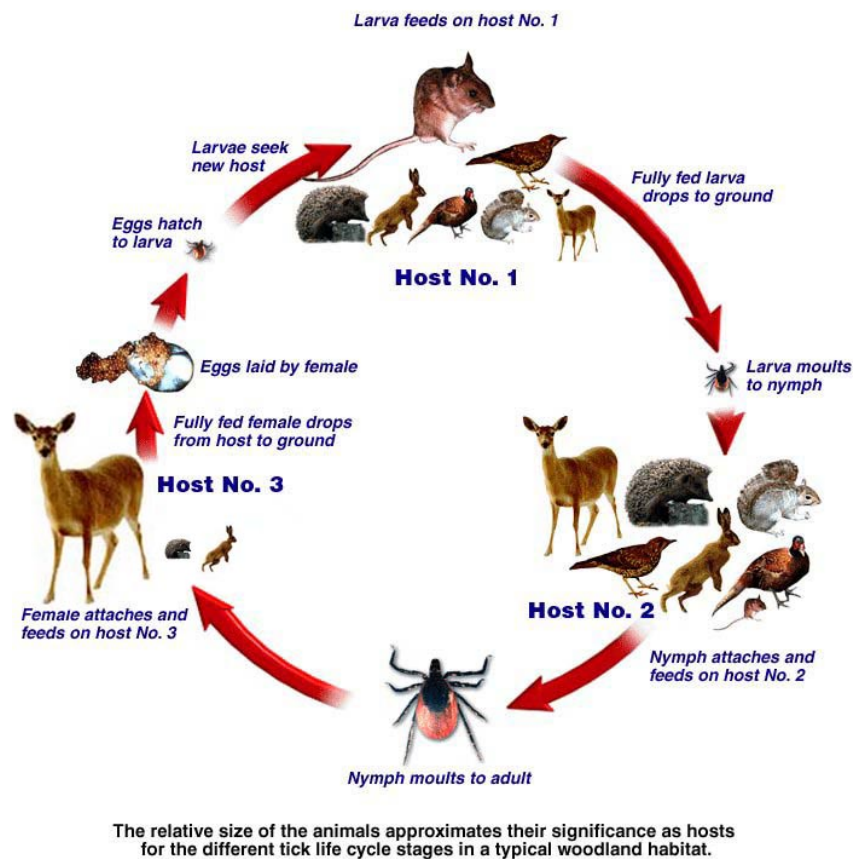
Figure 1.1: **Life cycle of ticks** (courtesy EUCALB – European Union Concerted Action on Lyme Borreliosis, `http://www.oeghmp.at/eucalb/`)

same year for the next blood meal (Süss, 2003; Ostfeld et al., 2006). Unsuitable environmental conditions can trigger a quiescence of unfed ticks (behavioural diapause, Gray, 2001).

In central Europe, *I. ricinus* ticks show a bimodal activity pattern with two activity peaks in spring and autumn (Rizzoli et al., 2004). While nymphs and adults usually show higher activity in spring in some areas, larvae do so in autumn (Gern and Humair, 2002). Peak seasons of tick-borne diseases are often preceded by population peaks in forest rodents in the preceding year which leads to synchronised disease transmission (Korenberg et al., 2002). A cold, dry winter tends to destroy ticks, particularly in the absence of snow cover (Süss, 2003). *Ixodes* tick species proliferate and survive between temperatures of -10 °C and +35 °C with low tolerance for extremes. They need relative air humidity to be 80 % or more with soil nearly saturated with water (Barbour, 1998). Also a low saturation deficit correlates with habitat conditions for *I. ricinus* (Randolph and Storey, 1999; Knap et al., 2009). During their intermittent periods of host seeking (questing), ticks are vulnerable to desiccation due to their exposure on plants which they climb (Gray et al., 2009).

Three components of the ecological system of (tick-borne) disease transmission depend on each other: the pathogens, the vectors (pathogen transmitting ticks) and the reservoir hosts (pathogen transmitting tick hosts, Kahl et al., 2002). The presence of these components along with suitable environmental conditions can lead to enzootic cycles of a disease. In ticks, three

transmission routes are observed: systemic from tick to host (via blood meal), non-systemic through tick to tick cofeeding (two ticks feeding on the same host closely together), and transovarial transmission where females transmit the pathogen to their eggs.

The maintenance of an enzootic cycle depends on several life stages occurring together as ticks are intermittent parasites as well as the condition that two life stages are feeding on the same host (Randolph, 2004b). In the summer, temperatures must be high enough to allow rapid tick development; in autumn rapid temperature decline stimulates a behavioural diapause of the emergent larvae (a kind of suspended animation) for the winter (Randolph and Rogers, 2000; Randolph et al., 2002; Gern and Humair, 2002). In the following spring, in case of rapid warming, nymph and larvae become active in synchrony which increases the probability of co-feeding on hosts This is a requirement for the TBEv transmission cycle. Those ticks, which exhaust their nutrient reserves and fail to find a host, die quickly (Korenberg, 2000). Also human granulocytic anaplasmosis and Lyme borreliosis are considered seasonal zoonoses, since most of the human cases occur in the summer half of the year due to the activity of the tick vectors.

The risk of infection is greatest from April to August, when ticks are most active. Larvae, nymphs and female adults can attach to humans. In this period, disease transmission depends on the type of disease. Due to the fact that *Ixodid* ticks only feed once per life stage, infection is usually acquired by one stage (e.g., nymph) that feeds on a reservoir host. It is then transstadially maintained to the next stage (e.g., larva). Seasonality is considered a key issue for predicting the focal distribution of TBE and other tick-borne diseases (Randolph et al., 1999).

Questing ticks wait passively for passing hosts. A wide spectrum of hosts from birds, reptiles and small to large sized mammals (rodents, ungulates, etc.) serve as hosts, but with a preference depending on the life stage of the tick. Known important competent reservoirs in Europe are mice, voles, rats, squirrels, deers and other mammals (Randolph et al., 2002). A relationship between mast production of trees, subsequent rodent peak and abundance of host-seeking nymphs has been established (Ostfeld et al., 1995; Ostfeld, 1997; Jones et al., 1998; Ostfeld et al., 2006).

The analysis of the causes of variation in infected ticks (in particular nymphs) is an ongoing research issue (Ostfeld et al., 2006). A tick is able to transmit multiple infections at one time, but the spatial disease patterns are known to be different in the same area (Randolph, 2001b).

The duration of host infectivity to ticks is shorter for the TBE virus (a few days) than for Lyme borreliosis (several months), which leads to different patterns of circulation (Randolph, 2001b). On the other hand, the exceptional longevity of ticks leads to prolonged periods of time for carrying tick-borne viruses. As a result, ticks are not only vectors but also excellent reservoir hosts for the viruses they carry (Labuda and Nuttall, 2004).

In Europe, infection prevalence in *I. ricinus* for Lyme spirochaetes is typically 2-20 % for questing nymphs; for TBE virus it is typically 0.1-5 % (Randolph et al., 1999). Prevalence of the human granulocytic anaplasmosis agent in questing *I. ricinus* is usually higher in adult ticks than in nymphs and ranges from 0-30 % (Strle, 2004). However, prevalences vary considerably in different European countries.

Tick-borne Encephalitis (TBE)

Tick-borne encephalitis is a tick-borne viral infection of the central nervous system affecting humans as well as most other mammals. In the last 10-20 years a significant increase of TBE

in Central Europe and the Baltic States has been reported (Haglund, 2001; Randolph, 2001b; Sumilo et al., 2007; Donoso et al., 2008).[2]

The responsible virus, TBEv (tick-borne encephalitis virus), is a member of the genus flavivirus. It is also known as spring-summer encephalitis. In Europe, it is transmitted through bites by *I. ricinus* ticks to vertebrate hosts. The virus can also be passed on in untreated milk and milk products from infected goats or sheep (Randolph and Rogers, 2000; Haglund, 2001; Rizzoli et al., 2004, 2007a). The distribution in Europe is highly focal (microfoci) because the virus occurs only in a subset of suitable tick habitats.

Ixodes ricinus is the main vector of the infection in Italy and other European countries, where fortunately clinical neurological manifestations, typical of the more serious phase of the disease, are very rarely observed. This behaviour is different from other endemic Euro-asiatic areas where numerous cases of encephalitis are described. E.g., in the Aut. Province of Trento (northern Italy), TBE infection in humans has been observed since 1992 (Rizzoli et al., 2004).

TBEv is efficiently amplified through co-feeding ticks which take a coincidental blood-meal on rodents, e.g. on *Apodemus flavicollis* (yellow-necked mouse). Large vertebrates do not take part in the virus amplification while they serve as main feeding host for all the developmental stages of the ticks (Randolph, 2001b).

In a study in the province of Trento and Belluno in northern Italy, the abundance of questing ticks and ticks feeding on roe deer was greater in TBE positive hunting districts than in hunting districts where TBE complex viruses were only probable or believed to be absent (Hudson et al., 2001). A synchrony in the seasonal dynamics of larvae and nymphs of *I. ricinus* was observed in TBE positive areas. The study suggests that roe deer may play an important role in the maintenance of tick density and in the persistence of TBE virus. In other studies on small mammals, it was found that since TBEv is very short-lived in its rodent hosts, it must be transmitted by nymphal and larval coincident feeding (co-feeding) on the same host which requires seasonal synchrony of activity (Labuda et al., 1997; Randolph, 2001b; Perkins et al., 2003; Randolph, 2004b). In Northern Italy, changes in the mountain forest use and wildlife management are affecting the TBE upsurge, resulting in an increase of selected vertebrate tick hosts which enhanced the potential of TBE virus circulation (Rizzoli et al., 2009). These hosts include the small mammals rodent which act as reservoir of TBE virus (especially *Apodemus flavicollis*) and the roe deer, one of the favourite *Ixodes ricinus* feeding on wild host.

Lyme Borreliosis (LB)

Lyme disease or Lyme borreliosis is a bacterial infection which causes symptoms like fever, fatigue, headache, and a characteristic skin rash called erythema migrans. If the disease is left untreated, the infection can spread to joints, the heart, and the nervous system. Lyme disease was named after Lyme, Connecticut (USA) where a cluster of human cases occurred in 1975 – the disease, however, was known for a longer time. Pathogen and vector were discovered at the same time (Gern and Humair, 2002). Lyme borreliosis (LB) is caused by a gram-negative spirochaete (thin spiral-shaped bacterium), *Borrelia burgdorferi* (*Borrelia burgdorferi* sensu latu (s.l.)) which circulates between ticks and vertebrate hosts. In Europe, three relevant *Borrelia*

---

[2]Human cases per European country are reported at
`http://www.tbe-info.org/upload/medialibrary/Reported_Cases.pdf`

burgdorferi species are present: *B. burgdorferi* sensu stricto, *B. garinii,* and *B. afzelii* (Gern and Humair, 2002; Piesman and Gern, 2004). Some *Ixodes* tick species are known to transmit *Borrelia* infections; the vector in Europe is *Ixodes ricinus* (Barbour, 1998). This tick is capable to transmit even more than one disease at a time (multiple infections, Gern and Humair, 2002).

The *Borrelia* species circulate between ticks (and other vectors), and mammalian or avian reservoirs. In Europe small mammals (including mice and bank voles), medium sized mammals (especially squirrels) and a number of birds and reptiles are competent host reservoirs (Dennis and Hayes, 2002; Piesman and Gern, 2004).

Ticks are transmitting spirochaetes through cutaneous inoculation of saliva after the beginning of the blood meal. The nymphal tick stage is considered responsible for the majority of the Lyme borreliosis cases (Dennis and Hayes, 2002), despite the fact that infection prevalence can be higher in adult ticks (Jouda et al., 2004). Reason for this is the adult's size; adult ticks are often removed from humans before the disease transmission takes place while nymphal ticks are harder to recognise. Larvae are rarely infected. Horizontal transmission is considered to be most important for the continuous transmission of *B. burgdorferi*, which requires a sufficient number of vertebrate hosts to be present (Cortinas et al., 2002). Lyme borreliosis requires that humans, infected vector ticks, and infected hosts all occur in close spatial proximity (Killilea et al., 2008), with forests as most important spatial determinant.

B. burgdorferi s.l. is able to survive in vertebrates for weeks or months which leads to a more wide-spread and more prevalent disease than e.g. the tick-borne encephalitis virus (TBEv). The natural cycles of Lyme disease are robust and maintained under a wide variety of conditions (Randolph, 2001a). Kahl et al. (2002) define a detailed terminology related to the ecology of *B. burgdorferi* s.l.

Human Granulocytic Anaplasmosis (HGA)

Human Granulocytic Anaplasmosis (HGA, formerly called Ehrlichiosis) is caused by several rickettsia-like bacterial species in the genus *Ehrlichia* which belong to the family *Ehrlichiaceae* of gram-negative bacteria of the order *Rickettsiales* (class Alpha-Proteobacteria, phylum Proteobacteria). *Ehrlichia spp.* species have been known in animals since 1935; human granulocytic anaplasmosis and ehrlichiosis have been more recently recognised as diseases that infect the white blood cells. The taxonomy of *Anaplasma* and *Ehrlichia* was revised only a few years ago with the help of molecular phylogenetics (Dumler et al., 2001).

Three emerging tick-borne diseases related to human infections have been recognised (Mcquiston et al., 1999):

- Human Granulocytic Anaplasmosis (HGA, formerly known human granulocytic ehrlichiosis – HGE), which was first described in 1994 in the United States and 1995 in Europe; it is caused by *Anaplasma phagocytophilum* (formerly known as *Ehrlichia phagocytophilia* and *Ehrlichia equi*);
- Human Monocytic Ehrlichiosis (HME), which was first described in 1987; it is caused by *Ehrlichia chaffeensis*;
- *Ehrlichia ewingii*, which was described in 1999 as an agent of human ehrlichiosis.

The following description focuses on the emerging Human Granulocytic Anaplasmosis (HGA).

Most patients show a non-specific febrile illness occurring within short time after tick exposure or tick bite (Robert Koch-Institut (RKI), 1998; Stuen, 2007). Symptoms resemble those of Rocky Mountain spotted fever (RMSF). While mortality in US series is estimated to 0-5 %, no deaths have yet been reported in Europe (Blanco and Oteo, 2002).

The European vector of *A. phagocytophilum* is the same as that of Lyme borreliosis and tick-borne encephalitis: the hard tick *I. ricinus* (Parola, 2004; Mantelli et al., 2006). HGA has a similar epidemiology to that of *B. burgdorferi* infection. Across Europe, *I. ricinus* is infected to a variable extent (0.4-66.7 %) with the causative agent *A. phagocytophilum* genogroup (Blanco and Oteo, 2002). The disease prevalence in questing ticks was found to be higher in adult ticks than in nymphs (Strle, 2004).

A. phagocytophilum is transstadially maintained by the vector ticks and, to date, there is no evidence of transovarial transmission (Bown et al., 2003). Some data suggest that tick co-feeding may transmit the bacteria which is well known for TBEv (Strle, 2004).

The mammalian host range of *A. phagocytophilum* is wide. Domesticated animals such as dogs, sheep, cows, and horses, as well as wildlife species such as deer and rodents can be infected (Bown et al., 2003). The role of small mammals is considered to be important: wood mice *Apodemus sylvaticus*, yellow-necked mice *Apodemus flavicollis* and bank voles *Clethrionomys glareolus* appear to be reservoirs for *A. phagocytophilum* (Strle, 2004; Parola et al., 2005). Studies on rodents, however, suggest that rodent infections are generally short-lived and that ticks rather than rodents may maintain the infection over the winter (Parola et al., 2005). Also roe and red deer were found to be seropositive in several European countries (Stuen, 2007).

However, there is a discordance between relatively presence of *A. phagocytophilum* in ticks, small mammals and deer and the rather low number of patients with proven HGA which suggests an inadequate awareness among European physicians, incomplete reporting of the disease, or other factors such as the lack of standardised diagnostic approaches (Strle, 2004). Some authors assume that human cases of unexplained febrile illness may be related to HGA (Nuti et al., 1998).

First studies on seasonality and vegetation types with respect to ticks and deer infections with *A. phagocytophilum* did not show seasonal patterns in Scotland (Walker et al., 2001). There, the infection prevalence was found to be higher in nymphs than adults (larvae not considered).

1.1.2   Mosquito-borne diseases: Chikungunya and West Nile Virus

Mosquitoes (e.g., *Anopheles* spp., *Aedes* spp., and *Culex* spp.) are important human disease vectors, from Malaria to filariosis as well as viral pathogens such as Dengue, Chikungunya, Yellow Fever and West Nile virus (Eritja et al., 2005; Fontenille et al., 2007).

Ecology of* Aedes albopictus *and* Culex pipiens *mosquitoes

The Asian tiger mosquito, *Ae. albopictus* (Skuse) (Diptera: Culicidae), is native of the forests of south-east Asia where it breeds in tree-holes (Hawley, 1988). In other parts of the world, temperate *Ae. albopictus* populations have adapted to use a variety of man-made containers including discarded tires and vases for breeding (Alto and Juliano, 2001b). While the mosquito itself flies only half a kilometre (Kitron et al., 1998), it has been introduced to the North-,

Central- and South-America, Indo-Pacific and Australian regions, as well as to Europe and some countries in Africa over the past 30 years by transportation of eggs in used tires or Lucky Bamboo plants (*Dracaena sp.*; Medlock et al. (2006); Scholte et al. (2008)). *Ae. albopictus* is an ecological generalist as it is adapted to both tropical and temperate climates (Hawley, 1988; Alto and Juliano, 2001b). Temperate populations of *Ae. albopictus* are able to produce diapausing eggs, allowing the species to survive the winter period outside the tropics. Since eggs are drought-resistant, they can survive long international trade passages for several months, leading to a global dispersal of the mosquito (Tatem et al., 2006; Benedict et al., 2007). For example, after 1990 Italy was colonised for 75 % of its territory in 15 years including the Autonomous Province of Trento, generating annual expenses of around 15 millions euros at the national level (Pilani et al., 2004).

Ae. albopictus is a vector of at least 23 arboviroses (*a*rtropod-*bo*rne viruses) and dirofilariasis (Mitchell, 1995; Medlock et al., 2006). Several of these viruses are human pathogens including Dengue, Yellow fever, West Nile Virus, Chikungunya and other meningoencephalitis (Mitchell, 1995; Fontenille et al., 2007). *Ae. albopictus* usually feeds at daytime; it is highly anthropophilic, which in combination, leads to a high contact rate between the vector and the hosts.

The distribution of *Ae. albopictus* in temperate areas is influenced by a number of factors including the adaptability of this species. Environmental factors such as patterns of precipitation, winter temperatures and their effect on population survival, and season length may also influence regional differences in the dynamics and spread of *Ae. albopictus* (Hawley, 1988). Temperature patterns in combination with certain precipitation patters are regulating the production of adults (Alto and Juliano, 2001a). Expected increase in average temperatures and frequency of summer droughts may lead to a higher spread of *Ae. albopictus* in future (Alto and Juliano, 2001a). Temperatures are considered a basic limiting factor, especially winter mean temperatures and annual mean temperatures. Temperate populations of *Ae. albopictus* are able to produce diapausing eggs, allowing the species to survive the winter period. Mean January temperature is an especially relevant ecological indicator (Medlock et al., 2006; Benedict et al., 2007; Straetemans, 2008).

The common house mosquito *Culex pipiens* (L., 1758) (Diptera: Culicidae) is a species complex with the most widespread distribution in the world (Vinogradova, 2000; Fonseca et al., 2004). *Cx. pipiens* lays its eggs in tin cans, buckets, discarded tires and other artificial containers that hold stagnant water. It usually feeds at night. *Cx. pipiens* is a vector for a number of diseases, especially arboviruses. It is able to transmit West Nile virus, filariasis, Japanese encephalitis, St. Louis encephalitis and avian malaria. The *Cx. pipiens pipiens* form is primarily rural and a bird feeder in Europe; the *Cx. pipiens molestus* form is urban and antrophofilic (Vinogradova, 2000), while the hybrid *Cx. pipiens-molestus* form is the vector of West Nile in the United States (Fonseca et al., 2004). The female of the true "pipiens" passes the winter in diapause in temperate areas (Vinogradova, 2000).

Chikungunya virus

Chikungunya (CHIK; an alphavirus) is an enveloped single-stranded positive-sense RNA virus which was first isolated in 1952 in Tanzania (Tsetsarkin et al., 2007). CHIK is a viral disease caused by arbovirus (arthropod-borne virus) transmitted to vertebrates including humans by mosquitoes, usually of the *Aedes* genus (Vazeille et al., 2008). Chikungunya is primarily trans-

mitted through bites by *Ae. aegypti* (yellow fever mosquito) but also by *Ae. albopictus* (tiger mosquito). The infection, with almost two million cases in the tropics, is usually not fatal. It has spread recently to Europe from the Indian Ocean coastlines and the Indian subcontinent.

At the genetic level, a mutation has been identified that caused a significant increase in CHIKV infectivity for *Ae. albopictus*. It was responsible for an unusual high outbreak of Chikungunya (2005–2006) on the La Réunion island (Tsetsarkin et al., 2007). The same mutation was found in Italy (Rezza et al., 2007).

The virus incubates in humans for a few days and creates an acute infection with typically high fever, arthralgia, myalgia, headache, and rash which last about 10 days. The arthralgia may last for several months.

The Chikungunya outbreak in Italy in 2007 in the Emilia-Romagna region was unexpected and the first known example of Chikungunya transmission outside the tropics (Rezza et al., 2007; Enserink, 2007). Since then, an increasing risk is expected for Europe as seen in the Italian outbreak due to the ongoing spread of *Ae. albopictus* in southern Europe (Vazeille et al., 2008).

West Nile virus

West Nile virus (WNV; a flavivirus), is a single-stranded positive-sense RNA virus (Kilpatrick et al., 2008). WNV is, globally, one of the most widespread flaviviruses (Rizzoli et al., 2007b). With human and equine outbreaks of fatal encephalitis, it has become a major health concern (Zeller and Schuffenecker, 2004). The virus is carried by migratory birds and transmitted to humans and animals by ornithophilic mosquitoes, especially by the *Culex* genus (Rizzoli et al., 2007b). Wild birds, including migratory birds, are instrumental in the introduction of the virus (Hubálek and Halouzka, 1999). The West Nile virus has been isolated from 43 mosquito species, predominantly of the *Culex* genus (Hubálek and Halouzka, 1999).

The role of wild birds is two-fold as they may carry emerging zoonotic pathogens, either as a reservoir host or by dispersing infected arthropod vectors which increases the risk of establishment of new endemic disease foci at great distances from where an infection was acquired (Reed et al., 2003). It has been rarely isolated from mammals. Humans and horses are considered dead-end hosts (Zeller and Schuffenecker, 2004).

The virus is pathogenic to humans and many animal species, with asymptomatic symptoms (typically febrile, influenza-like illness with increased mortality recorded in patients older than 50 years) with thousands of human cases each year in the USA.[3]

While the role of climate change in the future epidemiology of this disease is uncertain, it may play a role on bird migration patterns in terms of the distribution of West Nile fever (Hubálek et al., 2006). A major public health concern for an increased spread risk is the colonisation by the West Nile virus competent vector *Ae. albopictus*, considering that the West Nile virus and several other viruses are known to circulate sporadically in the Mediterranean region (Eritja et al., 2005).

1.2   Epidemiological remote sensing

For several years, satellite data have been successfully used in health and epidemiological applications. They are crucial for providing detailed environmental spatial databases for the analysis

---

[3]US Center of Disease Control and Prevention: West Nile Virus, `http://www.cdc.gov/ncidod/dvbid/westnile/`

and the understanding of disease patterns (Hay et al., 1996; Wood et al., 2000; Thomson and Connor, 2000; Rogers and Randolph, 2003). Changing environmental conditions can be retrieved from geocoded remotely sensed data and integrated into GIS (Geographic Information Systems) databases for further analysis. A list of potential links between remotely sensed indices and infectious diseases is found in Beck et al. (2000). Satellite data, as surrogates of meteorological station data, are gaining interest due to the fact that they are intrinsically spatialised: instead of point data a continuous field of observations is obtained (Goetz et al., 2000; Randolph et al., 2000; Neteler, 2005).

Some authors consider the use of remote sensing in human health applications far under its expected potential and especially driven by price and data availability instead of suitability to the problem (Herbreteau et al., 2005). In recent years, the availability of new satellite sensors is reducing the gap between high spatial resolution versus high temporal resolution. New opportunities are offered through the satellites Terra (launched in December 1999, data available from 3/2000 onwards) and Aqua (launched in May 2002, data available from 8/2002 onwards). Together they provide four LST coverages per day at various resolutions; additionally, data sets aggregated over 8 and 16 days to minimise cloud effects are offered (maximum value composition, Holben (1986)). These new satellite systems significantly improve the data availability for scientific purposes and predictive epidemiological studies (Tatem et al., 2004). The key instrument onboard both the Terra and Aqua satellites is the Moderate Resolution Imaging Spectroradiometer (MODIS). Each MODIS sensor delivers twice a day global coverages at 250 m, 500 m and 1000 m resolution in different spectral bands in a hierarchical spatial scheme (Justice et al. 1998; see also Section 3.1.2). The processed data are usually published less than one week after acquisition on a NASA FTP site[4]. Thanks to the data policy of the U.S. government to make these data sets available in the public domain, they are also frequently used in Europe and other parts of the world. This compensates for the fact that most European high priced data sources are effectively inaccessible (even within EU funded projects such as EDEN EU/FP6).

MODIS can be considered as a much enhanced successor of the AVHRR (Advanced Very High Resolution Radiometer) instrument onboard the NOAA series of satellites. MODIS improves upon the performance of AVHRR by providing both higher spatial resolution and greater spectral resolution; it has been used as a major source for the design for AVHRR's planned operational successor VIIRS on NPOESS satellite[5], currently expected for launch in 2013. The current NPOESS mandate, which is the underlying program, extends to the year 2026.

Numerous products derived from MODIS data including Land Surface Temperature (LST; Wan, 1999, 2003), vegetation indices (NDVI[6] and EVI[7], Huete et al., 2002) and snow cover are made available by NASA. The maps can be used to derive indices relevant for disease monitoring and risk modelling. Of particular interest are daily Land Surface Temperature maps, which can be aggregated to extract annual/monthly minima/maxima temperatures, late frost periods, hot summer temperatures, growing degree days, and autumnal temperature decrease. Aggregated EVI maps permit to detect seasonal vegetation differences, spring/autumn detection and the length of growing season. Furthermore, the Normalised Difference Water Index (NDWI) can be calculated (Gao, 1996) as well as other indices.

---

[4]NASA MODIS FTP site, `ftp://e4ftl01u.ecs.nasa.gov/`
[5]VIIRS, `http://npoess.noaa.gov/index.php?pg=instr`
[6]Normalised Difference Vegetation Index
[7]Enhanced Vegetation Index

Remote sensing data integrated into a GIS database, combined with methods of spatial analysis provide a powerful tool for understanding the epidemiology of diseases and for improving disease prevention and control. Rogers et al. (1996) developed Temporal Fourier Analysis (TFA) to assess habitat seasonality in AVHRR satellite maps and to obtain seasonality trends. The Temporal Fourier Analysis technique was later expanded to MODIS LST 8-day composites by Scharlemann et al. (2008). Estrada-Peña (1999a) linked time-series of AVHRR satellite images and other GIS layers to generate a habitat suitability map of cattle tick. Hendrickx et al. (2001) derived from AVHRR and Meteosat images tsetse distribution and abundance maps through discriminant analysis. Randolph (2001b, 2002) linked NDVI and LST to co-feeding transmission route of TBEv due to effects on the seasonal population dynamics of *I. ricinus*. Especially a higher than average rate of the autumnal temperature decrease ("autumnal cooling") is suggested as an index to a specific pattern of the population dynamics (Randolph et al., 2000; Carpi et al., 2008): the overwintering of unfed larvae which then emerge synchronously with nymphs in the following spring. Rapidly rising temperatures in spring ("spring warming") synchronise the emerge of two different life stages (nymphs and larvae). This synchronisation amplifies the establishment of a TBEv focus.

To enhance the temporal and spatial data richness in a GIS database, continuous field data such as land surface temperatures, snow coverage, and vegetation indices are commonly derived from satellite data. The integration of satellite data into epidemiological research enhances the spatio-temporal resolution of climatological data in particular in mountainous regions, where climatic stations and ground surveys are unavailable or sparse (Hess et al., 2002).

1.3   Thesis integration in the EDEN FP6/EU project and the RISK-TIGER project

This thesis contributes to the EDEN project (*E*merging *D*iseases in a changing *E*uropean *EN*vironment, Integrated Project of the 6th Framework Program, GOCE-CT-2003-010284 EDEN (2004-2009), `http://www.eden-fp6project.net/`) which is established at European level by a consortium of 48 institutes from 24 countries (equivalent to 200 research years) focusing on environmental analysis; epidemiology; social, medical and veterinary science; functional ecology; genomics; and information and communication science (Randolph, 2006). The goal of EDEN is to create a set of generic tools for monitoring, understanding and predicting diseases that do now, and will in future, threaten the health of Europe. EDEN aims at the identification, evaluation and cataloguing of those European ecosystems and environmental conditions that can influence the spatial and temporal distribution and dynamics of human pathogenic agents. Within EDEN, generic methods, predictive models, early warning and monitoring tools are developed to be used by decision makers for risk assessment, decision support for intervention and public health policies. EDEN covers ecosystems from the polar circle to the south the Mediterranean basin with some links to West Africa.

Furthermore, the thesis contributes to the RISKTIGER project (*Risk* assessment of the emergence of new arboviruses diseases transmitted by the *tiger* mosquito *Ae. albopictus* (Diptera: Culicidae), 2007-2010, `http://risktiger.fem-environment.eu/`). This is a post-doctoral research project at FEM-CRI (formerly Centre for Alpine Ecology) funded by the Autonomous Province of Trento. In this project, the current spatial distribution, spreading and seasonal dynamics of *Ae. albopictus*

in the Aut. Province of Trento are assessed. The influence of climatic and ecological variables is evaluated, and predictive models shall be developed to determine high risk areas for the potential establishment of this invasive species, and to optimise control strategies. High risk areas for the potential establishment of this invasive species will be identified and predictive models produced on the possible future spread of this species and the risk of emergence of several human and veterinary diseases in the Aut. Province of Trento.

2 State of the art and aims of the thesis

Epidemiological remote sensing is an emerging, rapidly evolving discipline. Despite the advances in remote sensing platforms and the increasing availability of data, several authors (e.g. Herbreteau et al. 2005) state that the role of remote sensing in health applications has not reached its expected potential, and that relationships of environmental variables extracted from remote sensing and geospatial data from other sources are not integrated adequately enough for health investigations.

This thesis aims at contributing to the improvement of high temporal resolution land surface temperature modelling in a GIS framework and its application to landscape epidemiological problems. For this, medium resolution remote sensing data (MRRS, at approximately 1000 m pixel resolution), which are characterised by high temporal resolution (multiple maps per day), are used as a data source. These data provide the relevant visible, infrared and thermal channels which render them suitable for the creation of eco-climatic data or vegetation cover and status. Especially US data sources with global mapping coverage are available at low cost. The processed remote sensing environmental correlates can then be integrated into spatial disease or host-pathogen spread models. Spread or distribution modelling of vector-borne diseases is yet a challenge of modern epidemiology (Ostfeld et al., 2005) and requires the availability of quality environmental data.

2.1 Recent developments in the creation of ecological indicators from space for epidemiological applications

Risk prediction of exposure to vector-borne diseases is based on biotic (e.g. tick and host abundance) and abiotic variables (climatic indices, energy budget and weather). In order to develop a risk mapping methodology for emerging vector-borne diseases, numerous scientists have used remote sensing data to enhance their GIS databases. Kitron (1998) and Daniel et al. (2004) reviewed the application of GIS, GPS, satellite imagery, and spatial statistics to vector-borne diseases. Tatem et al. (2004) reviewed the usability of new sensors on the Terra and Aqua satellites. Daniel et al. (1999) used LANDSAT TM5 data to predict *I. ricinus* abundance habitats for risk assessment of tick-borne encephalitis (TBE). Estrada-Peña (2002) used discriminant analysis to show that the increase in winter temperatures and in vegetation vitality is the key to habitats switching from unsuitable to suitable for tick survival. Eisen et al. (2005) used LANDSAT-TM5 NDVI of four seasons to predict habitat for exposure to *B. burgdorferi*-infected nymphs where humans are at risk for Lyme disease in the far-western United States. Purse et al. (2004) used 40 temporally Fourier-processed remotely sensed variables along with other GIS variables to develop climatic models for prediction of the distribution of the main European bluetongue virus

vector *Culicoides*. Randolph and Rogers (2002) linked phylogenetic trees of organisms generated from molecular biological analysis to satellites data in order to characterise the distribution of tick-borne flaviviruses from western Europe. Thomson and Connor (2000) reviewed remote sensing-based methods in combination with GIS for the analysis of arthropod pests and vectors of diseases affecting humans and livestock. An extensive literature review of remote sensing use in public health is found in Herbreteau et al. (2005). They reviewed the application of satellite-based indices for various disease-vector systems and discussed the relevance of these indicators.

In complex terrain like the Central European Alps, meteorological stations and ground surveys are usually sparsely and/or irregularly distributed (Stahl et al., 2006) and often favour agricultural areas. The application of traditional geospatial interpolation methods in complex terrain remains challenging (Steinacker et al., 2006) and difficult to optimize. An alternative data source is remote sensing; in fact, the integration of satellite data into epidemiological research significantly enhances the spatio-temporal resolution (Hess et al., 2002). The aim is to reach higher quality of extracted ecological indicators through the improved data availability provided by remote sensing (Kerr and Ostrovsky, 2003; Hais and Kučera, 2009). Indicators based on high temporal resolution data are crucial for the analysis and the understanding of disease patterns. These indicators can currently be generated on a global scale from optical/thermal remote sensing data (with the exception of cloud-dominated areas). Remote sensing data at medium spatial resolution (MRRS) can even be done even with a low cost. The quality of ecological indicators, especially in complex terrain, is determined by thorough pre- and postprocessing of the data in order to minimise artefacts in the resulting maps.

A series of epidemiological studies has been performed using the two main families of remote sensing platforms, i.e., geostationary satellites (geosynchronous orbit; repeated data acquisition in the range of minutes possible) which are "fixed" over a certain part of the earth and the polar orbiting satellites which repeatedly capture the entire earth in strips (repeat-cycle between 0.5 days to 16 days). The polar orbiting satellites are typically sun-synchronous so that the orbital pass occurs at the same local time of day.

The following selection of studies which integrate remote sensing into epidemiological applications is restricted to some satellites with carry thermal channel(s) as a payload (in parentheses the spatial resolution of thermal channel(s) and the revisit time are given). The studies are not necessarily using the thermal channel but at least the indicated sensor:

- Geostationary satellites (partial global coverage, low resolution remote sensing, LRRS):

    - *Meteosat* (focus on Europe; 3km, 15 minutes) used in Hay et al. (1996); Hay (2000); Rogers et al. (2002): among other indicators Meteosat cold-cloud duration (CCD) to estimate rainfall in Africa;
    - *GOES* (focus on Northern America; 4/8km, 30 minutes) proposed in Bernardi (2001): Meteosat/GOES cold-cloud duration (CCD) for Africa;

- Polar orbiting satellites (full global coverage):

    - Medium resolution remote sensing (MRRS):
        * *NOAA AVHRR* (1100 m, daily) used in Hay et al. (1996); Estrada-Peña (1999a); Randolph (2000); Rogers et al. (2002); Hay et al. (2006): Remote sensing as

source for surrogate variables; Vegetation indices and LST maps to characterize *Ixodes ricinus* tick habitats in the western Palearctic; Autumnal cooling derived from LST to assess life-stage synchrony among ticks in TBE foci (comparison of discriminant analysis, logistic regression and tree-based classifications); Middle infrared, LST and vegetation index derived to assess *Anopheles gambiae* complex habitats in Africa; Production of a data set of ecological indicator time series relevant to epidemiological applications including LST, and vegetation index;

* *Terra/Aster MODIS* (1000 m, daily) used in Rizzoli et al. (2007a); Xiao et al. (2007); Altobelli et al. (2008); Carpi et al. (2008): Autumnal cooling derived from LST to assess life-stage synchrony among *Ixodes ricinus* ticks in TBE foci in a part of Northern Italy; LST, Land Surface Water Index and vegetation index to map potential present distribution of Lyme borreliosis in a part of Northern Italy; *Ixodes ricinus* tick infestation on roe deer and co-feeding assessment along with autumnal cooling from LST;

– High resolution remote sensing (HRRS):

* *LANDSAT TM5* & *ETM+* (120/60 m, 16 days) used in Ogden et al. (2006); Allen and Shellito (2008); Brown et al. (2008): Habitat suitability analysis for *Ixodes scapularis* in southeastern Canada; Abundance and patterns of mosquito vectors of West Nile virus in Virginia, USA; Prediction of larval mosquito presence in Connecticut (USA) wetlands;

* *Terra ASTER* (90 m, 16 days) used in Brown et al. (2008): Prediction of larval mosquito presence in Connecticut (USA) wetlands.

A detailed review of surveillance of arthropod vector-borne infectious diseases using remote sensing techniques is given in Kalluri et al. (2007).

The new multitemporal remote sensing technologies allow a creation of ecological indicators from space at unprecedented resolution. While only 10 years ago a "finer" spatial resolution was commonly defined as 0.5 ° pixel resolution (see New et al. 1999), which was later improved to 10 arc-minutes (New et al., 2002), today's MRRS satellite platforms deliver spatial resolutions from 250 m to 1000 m (naturally not providing all types of climatic data). The optimal match of temporal and spatial resolution is currently MODIS, which is flown on the Terra and Aqua satellites. Hence this thesis focuses on the reconstruction of MODIS time series, in particular on the Land Surface Temperature (LST).

The validation of remotely sensed variables is a typical challenge of this type of analysis. For example, vegetation indices and snow cover extent maps are hard to compare with ground truth data as these variables are typically not monitored systematically over large areas. However, validation can be more easily done for land surface temperatures (LST), since temperature is more widely and continuously measured. While LST data are not directly comparable to air temperatures, which are measured at 2 m above ground, it has been shown that general temperature profile/patterns are closely correlated (Colombi et al., 2007; Vancutsem et al., 2010). In this study, the obtained root mean square error (RMSE) was approximately 2 °C using filtered but not further postprocessed daily MODIS LST data (Colombi et al., 2007). Clearly, instantaneous LST measurements will deviate from a related air temperature measurement but the lower resolution of 1000 m pixel size of MODIS LST might average out effects of heterogeneous

MODIS V005 products	*Spatial Resolution*	*Temporal Resolution*	*Purpose*	*Thesis Section*
MOD11A1, MYD11A1	1000 m x 1000 m	4 maps/day	LST daily data (day/night)	*3.2 Processing & reconstruction of daily LST maps*
MOD13Q1	250 m x 250 m	16 days	EVI/NDVI 16 days composite	*not considered*
MOD09GHK, MYD09GHK	500 m x 500 m	daily	Surface Reflectance Daily	*not considered*
MOD10A2, MYD10A2	500 m x 500 m	8 days	Snow cover 8 days composite	*not considered, see Endrizzi et al. (2005)*

Table 2.1: List of MODIS V005 products with relevance to landscape epidemiological studies (MOD prefix indicates Terra satellite, MYD prefix Aqua satellite)

landcover on temperature. So far no systematic studies are found which properly reconstruct filtered MODIS LST data in order to provide a continuous multi-annual time series.

It was found that satellite based indicators are sometimes even more suitable for epidemiological applications than traditional meteorology-based methods; for example, it has been shown that linking air temperatures from meteorological stations to tick development significantly overestimates the development cycles (Randolph, 2004b). In contrast, satellite based LST data appeared to be a valid proxy for analysing the temperature profile in relation to tick activity.

2.1.1   Data products from MODIS sensor time series

Recent polar-orbiting satellite systems, especially the Terra and Aqua satellites with their MODIS sensors onboard, significantly improve the potential and availability of scientific data for epidemiological applications. The orbit of Terra around the Earth is scheduled to pass from north to south across the equator in the morning, while Aqua passes in reverse direction from south to north over the equator in the afternoon. Terra is in a sun-synchronous orbit with a delay of 30 minutes with respect to LANDSAT-7. The further orbital parameters are equal to those of LANDSAT-7. Terra overpasses at 10:30hs and 22:30hs local solar time, while Aqua overpasses at 01:30hs and 13:30hs local solar time (Wan et al., 2004). Due to this time pattern, MODIS data are available four times a day.

MODIS is a whisk-broom sensor with 36 channels ranging from visible to thermal-infrared (Justice et al., 2002). Data are delivered at 250 m (Red, Near Infrared), 500 m (Mid Infrared) and 1000 m resolution (Thermal Infrared). MODIS can be considered as a much enhanced successor of the AVHRR instrument onboard the NOAA series of satellites. MODIS improves upon the performance of AVHRR by providing both higher spatial resolution and greater spectral resolution. Several of the numerous MODIS data products are of epidemiological relevance (see also Tab. 2.1)[1]:

- MODIS Land Surface Temperature and Emissivity products (LST/E; MOD11A1 daily 1000 m from Terra satellite and MYD11A1 from Aqua satellite). These raster maps contain land surface temperatures and emissivity values (Wan, 1999, 2003);

---

[1]MODIS Products Table, `https://lpdaac.usgs.gov/lpdaac/products/modis_products_table`

- MODIS Normalized Difference Vegetation Index (NDVI) and Enhanced Difference Vegetation Index (EVI) which are used to monitor the phenological status of vegetation (MOD13Q1 16-Day L3 Global 250 m, Huete et al. (1999, 2002));
- MODIS Snow and ice maps which describe the extent and persistence of snow and ice cover (MOD10A2 Eight-day 500 m, Hall et al. (2002));
- MODIS Surface Reflectance maps which describe reflected radiation in the visible and infrared spectrum (MOD09GQ daily 250 m, Vermote and Vermeulen (1999)). They can be used to calculate a wetness index.

2.1.2   GIS based time series processing of satellite data to derive ecological indicators related to epidemiology

A GIS may be used to answer questions of environmental conditions, locations and related to time series also questions of trends and patterns. Furthermore, modelling/scenario aspects can be addressed with respect to future conditions (definition adapted from Bernardi (2001)). Remote sensing is a rapidly advancing technology for gathering environmental data and hence of major interest for epidemiological problems. The spread of many diseases is driven by host-pathogen systems which are susceptible to environmental changes. GIS have been widely used along with remote sensing to study the spatial and temporal patterns of diseases (Glass et al., 1995; Clarke et al., 1996; Dale et al., 1998; Curran, 2001; Hay, 2000; Randolph, 2000; Kobayashi et al., 2002; Rogers and Randolph, 2003; Hay et al., 2006; Kalluri et al., 2007; Estrada-Peña, 2008). GIS and remote sensing software have been more and more converging over the last decade since both software families are based on spatial data analysis.

For MODIS time series, the first software developments have already been carried out to support reconstruction and analysis of time series of the MODIS Land Surface Temperature data (Neteler, 2005; Hay et al., 2006) and vegetation indices data (Beck et al., 2006; Colditz et al., 2006). These approaches address the maintenance of the entire annual time series or the description of the time series through a fitted characteristic function (with the aim of data compression). Seasonal differences between different years are maintained. Time series of these MODIS products allow the derivation of many indicators, that can be used to improve predictive epidemiological risk modelling (Rizzoli et al., 2007a; Carpi et al., 2008).

A special branch is the derivation of environmental indices from Temporal Fourier Analysis (TFA) of satellite imagery where multi-annual data are aggregated by a Fourier transform to find temperature or vegetation patterns (Rogers et al., 1996; McPherson et al., 2004; Purse et al., 2004; Wang et al., 2005; Hay et al., 2006; Kalluri et al., 2007; Scharlemann et al., 2008). The Temporal Fourier analysis (TFA) delivers a set of sine curves (harmonics), which are of different frequencies, amplitudes and phases. The set of all curves sums up to the original time series signal (Rogers et al., 1996). However, inter-annual variations are lost in this approach since multi-annual data are aggregated. The application to MODIS data can introduce errors of up to 30 % in the estimation of the amplitudes and phases of the Fourier harmonics (Scharlemann et al., 2008).

A central problem of optical/thermal satellite data is cloud contamination which hinders a continuous observation of an area of interest. For any kind of time series analysis it is ideal to work with complete maps. In thermal remote sensing, when deriving climatic parameters from LST

time series, the reconstruction of the missing pixel areas is desired. With regard to LST data, despite a series of filters applied by the data providers (e.g. NASA for MODIS data) to filter clouds in the LST products, outliers still remain. They originate from undetected clouds which introduce very low temperatures in the LST maps and reprojection artifacts.

It is important to appropriately maintain metadata in the GIS based data management of remote sensing data. They are not only needed to correctly integrate satellite/airborne data with other GIS data but also to be able to make data available through online geodata catalogues[2]. Since time series processing typically results in thousands of files, a catalogue based management for the end user is desired. Through OGC Web Services, both metadata and data can be made available.

2.1.3 Satellite data derived indicators relevant to vector-borne diseases

From a geographical point of view, it is interesting to observe that diseases like Lyme disease and tick-borne encephalitis show different epidemiological and spatial patterns while being transmitted by the same vector (Randolph, 2001a,b). Many ecological and epidemiological questions are still unanswered at a regional or local scale (Kahl et al., 2002; Gern and Humair, 2002) such as the abundance of the different vector species in areas of high microclimatic and host presence variability. This applies in particular to complex terrain. Since the infectivity of a host varies between a few days and life-time, spatio-temporal patterns are relevant for disease transmission. Special pathogen transmission, e.g. the co-feeding between larval and nymphal ticks on the same host (Labuda et al., 1997; Randolph et al., 1999) increase the complexity of the problem. Raw and even preprocessed satellite data are usually of limited interest to landscape epidemiological applications (Herbreteau et al., 2007). Satellite data become relevant when being aggregated as time series; especially the new MODIS sensor leads to an unprecedented data quality. The creation of ecological indicators from MRRS satellite data time series have been yet rarely used for landscape epidemiological studies (Beck et al., 2000; Tatem et al., 2004; Herbreteau et al., 2005). One reason is the complex processing of data originating from AVHRR (the only long term MRRS data source), another reason the unavailability of the required computational resources. These problems have been addressed with the advent of MODIS and the nonlinear increase of computational power.

The following subset of indicators which can be generated from Land Surface Temperature data is regularly requested and used in research projects:

- identification of years with annual temperature higher than long(er)-term average (drought risk; longer period over minimal threshold for development/moulting);
- calculation of daytime LST minimum, and of annual LST amplitude;
- identification of colder-than-usual winters (winter survival) or warmer-than-usual winters (rodents reproduction);
- mean winter temperatures (overwintering of hosts, vectors and parasites);
- number of mild winter days (above 7 °C);

---

[2]Catalogue software GeoNetwork, `http://www.osgeo.org/geonetwork`

- gradient of spring temperature rise ("spring warming", ticks synchrony among different life stages) and autumn decrease ("autumnal cooling", may trigger behavioural diapause in ticks);
- higher-/colder-than-average summer temperatures (drought risk); identification of droughts in ticks questing period;
- identification of special temperature conditions (may trigger tree masting which is of relevance for rodents);
- shift of seasons throughout the year including shortening/lengthening of seasons (influences life cycle);
- calculation of seasonal gaps between 7 °C (tick nymphs active) and 10 °C (tick larvae active);
- coincidence of raised summer temperatures with lowered summer precipitation (leads, for example, to desiccation of ticks);
- summer temperatures high enough to complete moulting before onset of winter (based on degree days);
- extended spring and autumn seasons (more days with minimum temperatures not lower than 5-8 °C).

The calculation of these indicators is described in Section 3.7.

2.1.4 Existing work related to the thesis

MODIS Land Surface Temperature map processing and applications   Tsetse fly habitat seasonality was assessed on a continental scale with Temporal Fourier Analysis (TFA) applied to AVHRR satellite maps (Rogers et al., 1996). The derived aggregated indicator maps included among others temperature phase, amplitude, mean, minimum, maximum and range, and were calculated from a time series of 1987-1992. This Temporal Fourier Analysis technique was later expanded to MODIS LST 8-day (MOD11A2) composites by Scharlemann et al. (2008), aggregating data from 2001-2005 into a set of indicator maps. In this thesis, instead of that daily MODIS LST data are used (MOD11A1 and MYD11A1).

Another way to analyse and to reconstruct time series was performed in the time domain by applying non-linear least squares fits of asymmetric Gaussian model functions (Jönsson and Eklundh, 2002). Colditz et al. (2006) used splines and polynomial fits for time series. Both approaches were developed for vegetation index data but not for temperature time series.

Goetz et al. (2000) proposed a method to derive air temperature from combined vegetation and LST data based on the AVHRR satellite sensor. Colombi et al. (2007) used filtered, but not reconstructed daily MODIS LST maps and compared them to air temperature measurements. They found a reasonable agreement with a root mean square error of approximately 2 °C. Vancutsem et al. (2010) used both 8-day (MOD11A2, MYD11A2) and daily LST data (only MYD11A1) in order to compare them with air temperature measurements. However, also here only filtered but not reconstructed data were used which still contained cloud contamination errors as stated by the authors.

Application of satellite time series in epidemiology   While the creation and application of satellite based meteorological surrogate variables is widely documented in the literature (Hay et al., 1996; Estrada-Peña, 1999a; Hay and Lennon, 1999; Thomson and Connor, 2000; Randolph et al., 2000; Randolph, 2000; Estrada-Peña, 2002; Green and Hay, 2002; Purse et al., 2004; Aplin, 2005; Carpi et al., 2008), long term reconstructed time series from satellites at daily resolution have not yet been proposed and applied.

Splines interpolation used to spatialise meteorological data   Splines are commonly used for the interpolation of various climate variables including regions with complex topography (Hutchinson, 1995; New et al., 1999). Typically 2D-splines are used, but Hofierka et al. (2002) and Suprit and Shankar (2008) used a volumetric implementation of regularised splines with tension. In all mentioned studies precipitation data were interpolated in order to obtain maps. Scharlemann et al. (2008) used cubic 2D-splines in conjunction with Temporal Fourier Analysis in order to fit time series.

Haylock et al. (2008) used a mixed approach of splines and kriging in order to provide a European daily map time series data set for precipitation and temperature for the period 1950-2006. No existing work related to volumetric (3D) interpolation of temperature data was found.

Rolland (2003) studied (unrelated to interpolation) lapse rates of minimum, mean, and maximum air temperatures in the Trentino-South Tyrol region, finding lapse rates from -0.40 °C/100 m to -0.75 °C/100 m (monthly values).

Climatic indicators extraction from MODIS LST   Hassan et al. (2007) used filtered but not reconstructed 8-day MODIS LST maps to produce growing degree day (GDD) maps. In this thesis, GDD maps were produced from reconstructed daily MODIS LST data.

Ticks and temperature   Temperature data from satellites are gaining interest as surrogates of meteorological station data because a continuous field rather than point measurements is observed. LST data have already been used in tick-borne encephalitis studies (Randolph et al., 2000; Rizzoli et al., 2007a; Carpi et al., 2008) but so far with original MODIS LST data not being void-filled.

Mosquitoes and temperature   The European Centre for Disease Prevention and Control (2009) predicted the *Aedes albopictus* distribution in Europe based on temperature derived variables including MODIS LST data which were subjected to Temporal Fourier Analysis.

Figure 2.1 shows the potential distribution of four West Nile virus-carrying mosquito species in the United States. The distribution was predicted using Temporal Fourier processed satellite derived environmental data (Kalluri et al., 2007).

So far, no existing work has been found in which reconstructed daily MODIS LST data were used to produce a generic temperature time series, nor to apply them in distribution modelling of ectoparasites.
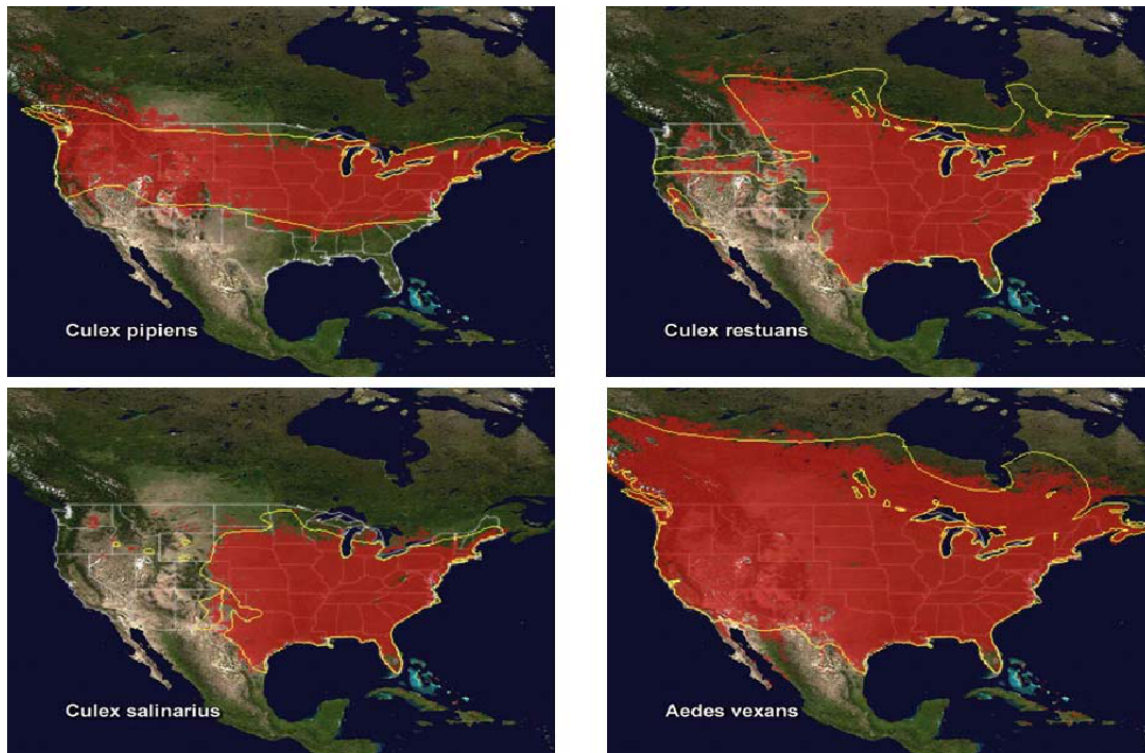
doi:10.1371/journal.ppat.0030116.g002

Figure 2.1: **Maps showing the potential distribution of four species of mosquitoes in the United States**
Distribution predicted using satellite derived environmental data is in red, and recorded distribution is outlined in yellow. Cited from Kalluri et al. (2007).

2.2 Methodological aims of the thesis

The goals of this thesis are directly linked to the problems indicated earlier in this chapter. In a situation of increasing disease vector spread in Europe and emerging infectious diseases, new approaches for the creation of ecological indicators from geospatial data are needed. New satellite based sensors have been used yet under their potential. The thesis aims at closing the gap between lack of detailed temperature maps (with focus on areas with complex terrain) and the availability of medium spatial resolution but high temporal resolution land surface temperature satellite data. Since incomplete maps (cloud contamination, bad pixels, etc.) are difficult to use in GIS applications, map reconstruction is needed to render the satellite data useful. Existing publications are based on 8-day aggregated observations and are aggregated multi-annually. To be able to capture short-term or inter-seasonal variations, instead of that daily data need to be used. However, a complete, reconstructed LST time series has not been available so far.

The overall aim of this thesis is the creation of a completely reconstructed time series of daily MODIS LST maps and its application in two case studies related to the assessment of ticks and mosquito disease vectors.

The related sub-goals can be split into different aims:

Aim 1: Creation of a completely reconstructed time series of daily MODIS LST maps   The spatio-temporal reconstruction of all available MODIS LST maps for the study region shall overcome the lack of consistent temperature time series maps which are an obstacle in epidemiological modelling:

1. The scope is to substitute the commonly used maps obtained from interpolated meteorological point data with reconstructed MODIS LST satellite maps. Maps of sufficient quality need to be produced from the original MODIS LST maps.
2. The implementation of the MODIS LST map reconstruction shall be done in a GIS framework for integration with existing spatial data in the reconstruction process.
3. The quality of the reconstructed MODIS LST has to be verified against meteorological time series and other remotely sensed thermal maps.

Aim 2: Deriving climatic parameters from reconstructed LST time series   Since daily indicators are of limited use in epidemiology, the reconstructed MODIS LST maps need to be aggregated to periodical indicators (16-days, monthly, seasonally, annually) in the time domain:

1. The aim is to develop aggregated temperature indicators from MODIS LST data which are comparable in quality to related indicators from meteorological data.
2. Interannual indicator comparisons shall identify differences in winter minimum temperatures (in order to assess disease vector winter survival), spring arrival (which corresponds to ticks or mosquito activity onset), or seasonal thresholds of growing degree days (indicator for insect life stage completion).

Aim 3: Case studies – application of the reconstructed LST time series   In the literature, no high temporal resolution LST time series have been used so far to disease vector distribution modelling. The aim is to apply the general purpose time series and the more specific indicator maps produced in this thesis in tick and mosquito case studies:

1. The developed approach delivers meaningful input variables (maps) for the assessment of the disease vector distribution.
2. Integration of remotely sensed time series in a GIS framework shall better support the spatial analysis of disease vector distribution.
3. The reconstructed MODIS LST maps shall deliver more detailed disease vector distribution as they are expected to reflect microhabitats other than classical methods based on interpolation of meteo-station data.

GIS based map reconstruction   The huge amount of data (to date more than 11000 MODIS maps have been collected for each MODIS map tile) requires the automation of data processing. The thesis covers the entire workflow from processing and reconstruction of daily MODIS LST maps to deriving climatic parameters from reconstructed LST time series to the application of the reconstructed LST time series in the two case studies (ticks and mosquitoes).

3 Concepts, methods and materials

3.1   Remote sensing of Land Surface Temperatures from space

Land Surface Temperature (LST) is derived from measurements of the radiation emitted by the land surface. It is observed for example by MODIS sensors (Wan et al., 2004). In principle, the calculation of the LST is based on Planck's law which describes the spectral radiance at all wavelengths from a black body at a certain temperature (Wan, 1999). The effects of surface emissivity (lower than 1 for a non-perfect Black Body), and atmospheric effects must be taken into account. The latter effect lowers the estimated surface temperature and needs to be corrected with appropriate algorithms.

MODIS Land Surface Temperature and Emissivity products (LST/E; MOD11A1 from Terra satellite and MYD11A1 from Aqua satellite) map land surface temperatures and emissivity values ideally under clear-sky conditions. The underlying algorithms use other MODIS data and further auxiliary maps for input, including geolocation, radiance, cloud masking, atmospheric temperature, water vapour, snow, and land cover. Temperatures are provided in Kelvin. The retrieval of LST from MODIS is based on two methods: one method is the generalized multi-channel method (split-window, Wan and Dozier (1996)) which uses two thermal channels with an empirical linear function to calculate LST (as result, the LST level 2 product MOD11_L2 and level 3 MOD11A1 are generated, the latter is used in this thesis). The degree of atmospheric absorption is known for the spectral bands covered by the split-window channels, hence the inverted Planck function will deliver the ground surface brightness temperature. It requires knowledge about emissivity of observed object, i.e. a precise land-use/land-cover maps to estimate the spatially heterogeneous emissivities is needed. The second method is the physics-based day/night LST method used to generate the LST level 3 product MOD11B1 (Wan, 2003; Wan et al., 2004). It is based on pairs of daytime and nighttime MODIS data.

The MODIS LST algorithm is aimed at reaching an accuracy better than 1 Kelvin ($\pm$ 0.7 K standard-deviation) for areas with known emissivities in the range from -10 °C to 50 °C (Wan, 1999; Wan et al., 2004; Wan, 2008).

In theory, also near surface air temperatures could be estimated by studying the relationship between vegetation index and LST (NDVI/T_s slopes, the TvX approach) (Goetz et al., 2000; Kawashima et al., 2000). However, in this thesis this method was not tested since land surface temperature is preferred over near-surface air temperature as surrogate variable in many epidemiological applications (Hay et al., 1996; Hay and Lennon, 1999; Green and Hay, 2002). Furthermore, no reconstructed vegetation index maps were available in the framework of this thesis; the processing of MODIS EVI was out of its scope.
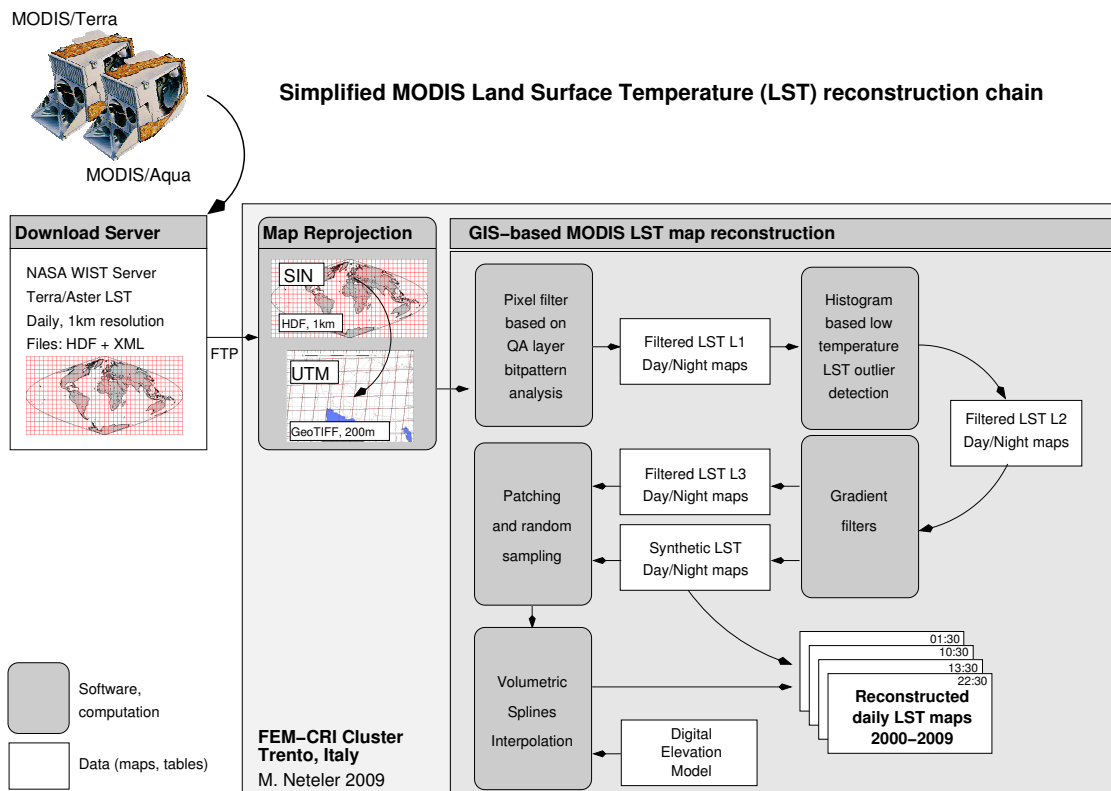
Figure 3.1: Simplified sketch of MODIS LST reconstruction processing chain
(for detailed version, see Figure 3.4)

3.1.1   MODIS LST data availability

MODIS data sets are provided besides "Base Level Swath Data" as "gridded data". Grid data are projected in equal-area Sinusoidal projection (SIN from MODIS product level V004 onwards) and provided in HDF data format.[1] In this work, the new MODIS product level V005 data was used. This level offers significantly improved data quality compared to previous levels, especially for inland water pixels (Wan, 2003, 2008) and other, product specific improvements.[2] MODIS data are delivered in the HDF data format, additionally a XML file is provided with metadata (of interest are the fields "RangeBeginningTime", "RangeEndingTime", "QAPercentCloudCover", "QAPercentMissingData", "DayNightFlag", "PGEVersion"). Table 2.1 lists some of the over 40 available MODIS products which are relevant to eco-health applications.

3.1.2   MODIS LST data general GIS based processing

The scope was to develop a self-contained LST reconstruction algorithm which does not depend on meteorological data since they are often unavailable. The overall simplified procedure is shown in Figure 3.1. For a detailed view, see Figure 3.4. The procedure includes the reprojection of the MODIS LST maps, the application of the accompanying quality assessment map layer to filter out invalid pixels, and the application of several histogram and gradient based outlier

---

[1]MODIS data order through the NASA EOS Data Gateway, `http://edcimswww.cr.usgs.gov/pub/imswelcome/`
[2]MODIS product level V005 changes,
`http://modland.nascom.nasa.gov/cgi-bin/QA_WWW/newPage.cgi?fileName=MODLAND_C005_changes`

filters. From each outlier filtered LST map the temperature gradient is calculated if a sufficient number of valid pixels is available in the map. From the related gradient, a synthetic map is generated and patched into the no-data map areas if present. Then random sampling is performed to finally obtain a smooth map in the subsequent volumetric splines interpolation process which uses the elevation model as additional variable. If no sufficient number of pixels is available in the filtered LST map, instead a purely synthetic map is generated based on the 16-day period mean gradient model which was derived earlier. This approach is applied to all available MODIS LST maps from Aqua and Terra satellites for the study area.

In the following sections, these steps are described in greater detail.

Reprojection of MODIS LST maps

The "MODIS Reprojection Tool V4.0" software (MRT, U.S. Geological Survey (2008)) has been used to reproject the original Sinusoidal projection (SIN) to the Universal Transverse Mercator projection (UTM Zone 32N, WGS84 ellipsoid, EPSG code 32632). MRT allows for geographical subsetting, and it exports the resulting maps to standard GIS data formats such as GeoTIFF. The MRT software supports nearest neighbour, bilinear, and cubic convolution resampling. In this work, nearest neighbour (NN) resampling was chosen for two reasons: only NN is able to maintain the bit-pattern encoded structure of the quality maps during resampling as it does not interpolate between existing bit values. Additionally, tests with the bilinear and cubic convolution (CC) resampling revealed that artifacts were introduced in the resulting maps. Especially CC tends to overshoot at cloud mask boundaries (too high values are introduced due to numerical instability in the underlying MRT algorithm). To minimise data loss during the reprojection, spatial oversampling was performed to increase the target raster cell resolution: the LST data with nominal resolution of 1000 m x 1000 m were resampled at 200 m x 200 m resolution to reduce artifacts and pixel shifts due to the unavoidable use of the NN resampling method. Figure 3.2 shows resolution differences and shifts for a synthetic LST map. The upper map (northern part of the Garda lake, Italy) shows in orange the MODIS tiles reprojected from sinusoidal projection (Sanson-Flamsteed)[3] to UTM32/WGS84 at 1000 m x 1000 m resolution, and in gray a rectangular UTM grid at the same resolution which corresponds to the target raster map. To minimise data artifacts (esp. caused by pixel shifts), spatial oversampling at 200 m x 200 m resolution was performed. The second map below shows a zoomed detail, in orange again the MODIS tiles reprojected from sinusoidal projection and in gray the target pixels in UTM. Selected pixels are highlighted to illustrate the positive effect how higher resolution resampling when using the NN method. The increased resolution is furthermore supported in case of the LST maps by the use of higher resolution auxiliary maps (elevation model) during the map reconstruction process as illustrated below.

MODIS quality assessment layer

Before publication by NASA, all MODIS products are subjected to an automated Quality Assessment (QA; Justice et al. (2002); Roy et al. (2002)). The QA information is provided as separate map layer in the HDF file of the individual MODIS product indicating pixelwise the quality status through a bitpattern (clear pixel, cloud/cirrus/aerosol contaminated, etc.). This quality assess-

---

[3]MODIS tiles map in sinusoidal projection, `http://gis.fem-environment.eu/modis-sinusoidal-gis-files`
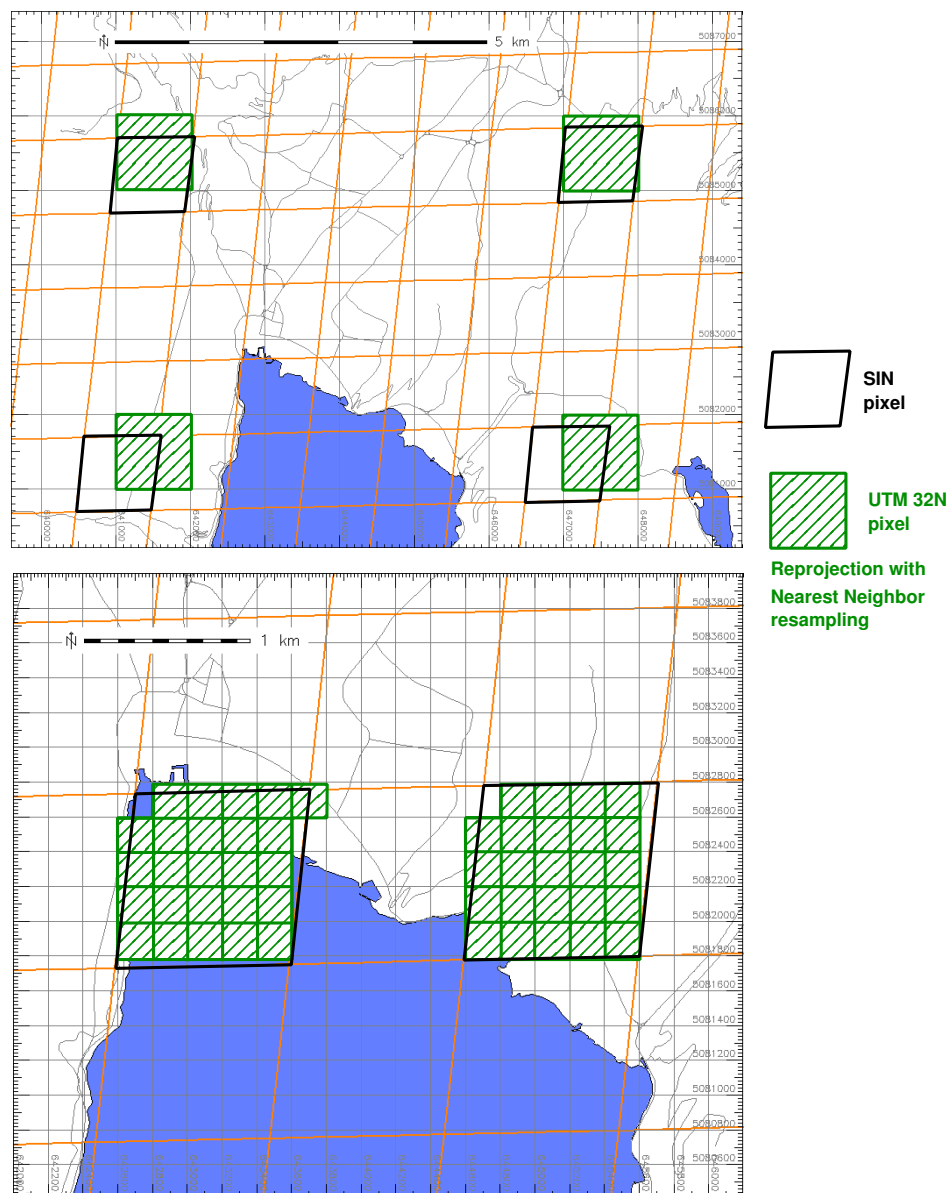
Figure 3.2: **Artefact minimisation through reprojection to higher resolution (synthetic LST example, Northern Garda lake, Italy)**
The upper map shows in orange the MODIS LST pixel grids originally in Sinusoidal projection (here reprojected to UTM32/WGS84) at 1 km^2 resolution, and in gray the UTM32 pixel grid at the same resolution which corresponds to the target raster map, the lower map a zoomed detail with the UTM grid at 200 m x 200 m resolution. Selected pixels are highlighted to illustrate the positive effect how higher resolution resampling when using Nearest Neighbor (NN) resampling. For explanations, see text.

ment is giving added value to the MODIS end users since the user can decide at which level of quality degradation (cloud, aerosol, etc.) s/he wants to reject a pixel by applying a filter rule (raster map algebra).

However, despite NASA's quality assessment, further MODIS data outlier filtering is needed at least for the Land Surface Temperature map product (Neteler (2005); Rizzoli et al. (2007a); Carpi et al. (2008), see Section 3.2.1).

Import of MODIS LST maps (MOD11A1/MYD11A1) into the GIS

The MODIS data are imported into GRASS GIS V6.4.0[4] through batch jobs, i.e., a Unix (Linux) shell script was prepared which generated the control files for the MODIS Reprojection Tool in order to define the target projected and the map layers of interest to be imported from the MODIS HDF file into the GIS. The script then executed MRT in batch mode in order to reproject the data (from Sinusoidal – SIN – projection to UTM32/WGS84) and to import both the LST data layers and the QA layer (eventually, these layers were imported via temporary GeoTIFF file with `r.in.gdal` command into GRASS by this script).

Land Surface Temperature and Emissivity maps are available as MOD11A1 product from Terra satellite and MYD11A1 product from Aqua satellite. For the map reprojection from the original Sinusoidal to UTM32N/WGS64 projection the "nearest neighbor" resampling method was selected in the MRT software. Relevant metadata extracted from the accompanying XML file included "RangeBeginningDate", "RangeBeginningTime", "RangeEndingTime", "DayNightFlag", "QAPercentCloudCover", "QAPercentMissingData", and "PGEVersion" (Product Generation Executable which refers to the underlying algorithm version number). Especially "DayNightFlag" and "QAPercentCloudCover" were relevant for the postprocessing as described below.

For the LST maps, pixels with the following errors indicated in the QA bitmap layer[5] were rejected: "clouds", "other error", "cirrus cloud", "missing pixel", "poor quality", "Average emissivity error > 0.04", "LST error 2K-3K", and "LST error > 3K". The bit patterns of interest were combined into logical conditions and applied to the LST map using map algebra. The maps are originally provided in Kelvin and were transformed to degree Celsius. To each resulting filtered LST map a temperature color table was assigned and the metadata (as extracted from the XML file) stored as GIS metadata for each map (`r.bitpattern`, `r.mapcalc`, `r.colors`, and `r.support` command into GRASS).

3.2 Processing and reconstruction of daily LST maps

As listed in Section 2.1.3, a series of indicators with relevance to vector-borne diseases are of interest to be derived from remotely sensed land surface temperatures. While the available MODIS data are already provided as high level products, the LST data have yet to undergo further processing and reconstruction before being readily usable in epidemiological and other applications.

3.2.1 Histogram based MODIS LST data low range temperature outlier elimination

A central problem of optical/thermal satellite data is cloud contamination as clouds hinder observation of land and sea surfaces. In the case of LST maps, in cloud covered areas the land/sea surface temperatures are simply unavailable since the cloud top temperatures are measured instead. In case of a thin cloud cover (cirrus clouds, etc.), cloud detection is rather difficult (Ackerman et al.). Statistically, more cloud contaminations are found in night-time LST maps

---

[4]GRASS GIS 6.4.0, `http://grass.osgeo.org`

[5]MODIS LST QA bitmap flags, `http://igskmncnwb001.cr.usgs.gov/modis/qa/mod11a1_qa_v5.asp`
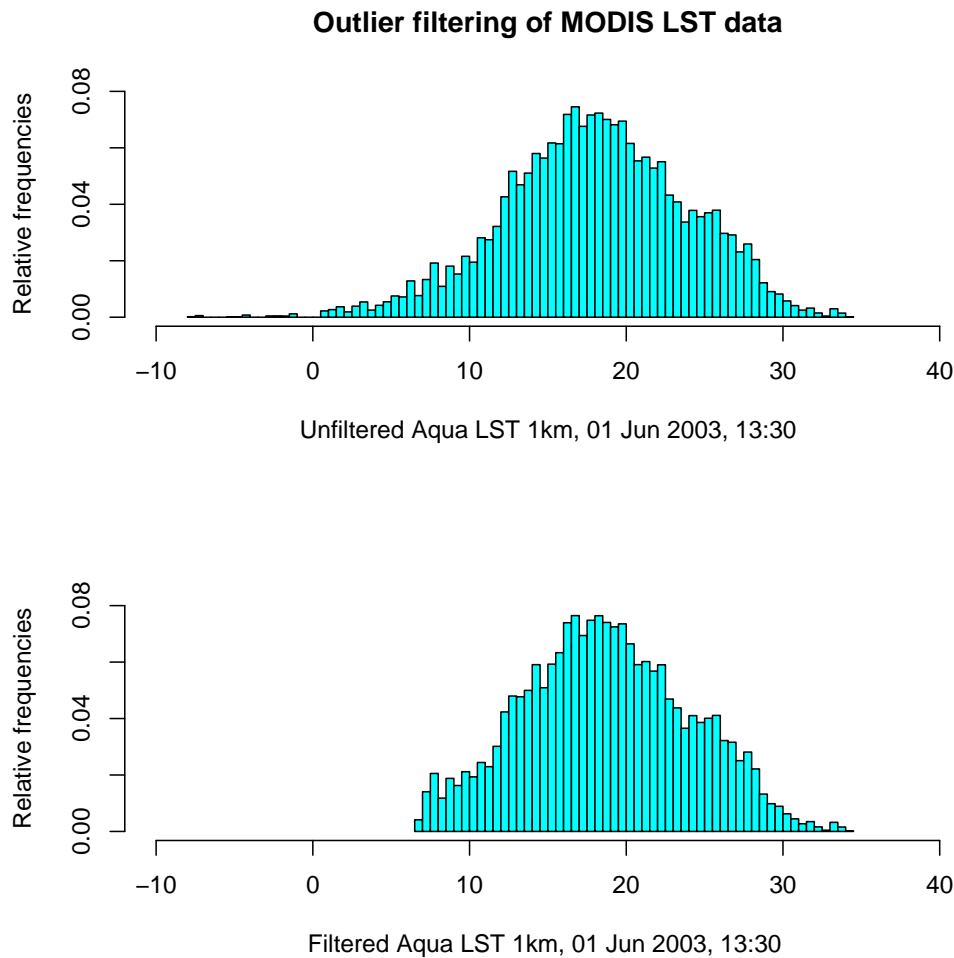
Figure 3.3: **Histogram based outlier filtering in MODIS LST data of an Trentino/Belluno/Bolzano Provinces (Italy) coverage, 1st June 2003**
Some undetected clouds introduce low temperature pixels (upper graph) which are detected and filtered out (lower graph) based on the monthly mean lower boundaries. The upper temperature range remains untouched.

because only thermal infrared (TIR) band data can be used at night in the spectral tests needed for the cloud mask production. During daytime also other channels are usable. Most cloud-contaminated LST pixels which remain undetected by the NASA LST map production algorithms appear to occur near cloudy areas, i.e. at the fringes of cloud fields (Neteler, 2005; Rizzoli et al., 2007a).

Outliers in MODIS V005 LST data typically appear only in the negative degrees Celsius range as they are usually caused by undetected clouds. To overcome this problem, a post-import outlier detector was developed in this thesis and applied in order to eliminate remaining cloud-contaminated pixels. The detector is based on an image-based histogram analysis to find and remove pixels which show unusually low LST values (Neteler, 2005). The outlier detection is only applied to the lower temperature range (since high temperature outliers are uncommon). It is based on the R boxplot algorithm (R Development Core Team, 2006):

$$lower\_boundary = 1st\_Quartile - 1.5(3rd\_Quartile - 1st\_Quartile) \qquad (3.1)$$

Only LST maps with a sufficient number of pixels are used in this calculation to avoid that a few pixels badly influence the overall outlier statistics. A minimum availability of at least 25 % valid LST pixels (i.e., after QA map filtering applied) per map was chosen. For each map, the above equation was determined by calculating the univariate statistics of the map (`r.univar` command in GRASS). Then on a monthly basis, the mean lower boundary value was calculated and used as a filter threshold. If the entire month was below the minimum number of valid LST pixels, a fixed mean lower boundary value was set to -20 °C. Then all LST maps of a month were filtered with the mean lower boundary threshold by setting pixels below the threshold to Null.

The procedure was implemented in Unix (Linux) shell scripts. It loops over all available Terra and Aqua scenes separately and within this loop it processed separately the day and night overpasses. This separation was chosen for two reasons: data from Terra are available for a longer period; additionally, missing data (arising from cloud coverage etc.) would lead in a single pass processing to undesired shifts of the daily minimum and maximum in case of maps lacking. Doing the calculations constrained to time phases of the day/night reduces significantly the error rate when calculating the lower boundary threshold.

Figure 3.3 shows the histogram of a selected MODIS LST daytime scene before and after application of the histogram based outlier detector. Subsequently, individual post-processed MODIS images may contain areas devoid of data due to the previous filtering (note that no-data areas in high altitudes which are covered by snow and ice were not considered as these areas are not relevant for eco-epidemiological studies).

3.2.2 Temperature gradient based LST map reconstruction with volumetric splines interpolation

General approach

As described above, the quality controlled and outlier filtered LST map are partially devoid of data. For the preparation of ecological indicators this is an obstacle since Null (no data) propagation would have to be carefully considered in further data aggregation. To overcome the problem, a void-filling algorithm has been implemented to reconstruct the LST maps. Despite the previously applied histogram based outlier filter, several additional filters have to be applied to the data and the models used for map reconstruction which are outlined below.

In general, we have the observations (x_1, y_1, z_1, w_1), ... (x_n, y_n, z_n, w_n) where $0...n$ observations of w are void. The goal is to obtain $w = w(x, y, z)$ on a regular grid. In the proposed approach voxels are used, i.e., raster volume pixels of (x, y, z). Since the desired result is a map in 2D space, the resulting $w(x, y, z)$ values are transformed using the (x, y, z) points of the digital elevation model (DEM) and written out as 2D map to (x, y, w). The estimation of $w(x, y, z)$ requires the fitting of a model "temperature change versus elevation change" which is based on the available LST observations and a related temperature gradient. The developed algorithm is using the concept of temperature gradient (i.e, the decrease of temperature with altitude) as a foundation for the reconstruction. The adiabatic lapse rate which determines the gradient is calculated with linear regression applied to the individual LST/elevation maps, i.e. all LST maps

with a statistically significant number of available pixels. Since air temperature is not involved, this lapse rate can be considered as a special "MODIS LST lapse rate" which is a mixture of soil (surface) temperature and near-surface temperature.

Preliminary temperature gradients are generated for each of the LST maps with less than 10 % of no data pixels. In the case that too low a number of valid pixels is found, all gradient parameters (i.e., the linear regression formula) are set to zero; these gradients are subsequently removed in a later step from the set of valid gradients. For the study area, 11179 available maps were processed for the period of 3/2000-2/2009. All LST maps were then filtered again based on the 1st and 3rd quartiles of the intercepts and slopes of the 16-day period mean gradients to identify and remove remaining LST outliers (compare Fig. 3.7). From the filtered maps the final set of gradients was generated, defining again a minimum of 10 % of valid LST pixels per map to maintain statistical significance. The statistics are done separately for each overpass (01:30, 10:30, 13:30, 22:30). The resulting set of final 16-day period mean gradients is taken to generate for each LST map an accompanying synthetic LST map which is used to fill holes in the actual LST maps. Rather than interpolating over map holes it was deemed to be better to fill these holes with typical values for a given 16-day period/overpass time in order to stabilise the interpolation (see Fig. 3.8 for the procedure). To avoid artifacts at the confluence of actual and synthetic maps, a random sampling approach was selected to extract 10 % of the pixels as samples from each patched map for the interpolation step.

Finally, for each map a volumetric splines interpolation was performed with these randomly sampled points. Each resulting 200 m resolution LST map was extracted from the interpolated volume using the 200 m DEM. By processing all available data, a completely reconstructed LST time series has been produced. The overall flowchart of the developed MODIS Land Surface Temperature (LST) map reconstruction chain is shown in Figure 3.4. The detailed approach is now discussed in four parts.

Part 1: Temperature gradient creation and outlier detection

Creating an appropriate DEM for the temperature gradient correction   The spatial resolution of the digital elevation model (DEM) needs to match the increased LST map resolution produced in the initial reprojection step with oversampling (MODIS Reprojection Tool, see Section 3.1.2). A higher resolution DEM needs to be properly downsampled to the target resolution, here to 200 m x 200 m.

Since 200 m pixel length was chosen as target resolution of the LST map, an appropriate DEM had to be prepared. Here, the Italian 20m DEM was downsampled to 200 m pixel resolution using a weighted pixel aggregation to minimise the error. The GRASS command `r.resamp.stats` was used which resamples raster map layers to a coarser grid using aggregation with weight according to area: this aggregation, the values from all input cells which intersect the output cell are weighted according to the proportion of the source cell which lies inside the output cell.

Creation of a preliminary set of temperature gradients   From each of the previously filtered LST maps a set of preliminary temperature gradients was extracted along with the number of total valid pixels per map (hence, 11179 gradients). Tests with a LST map reconstruction based on these gradients regardless the number of valid pixels showed that maps with few pixels
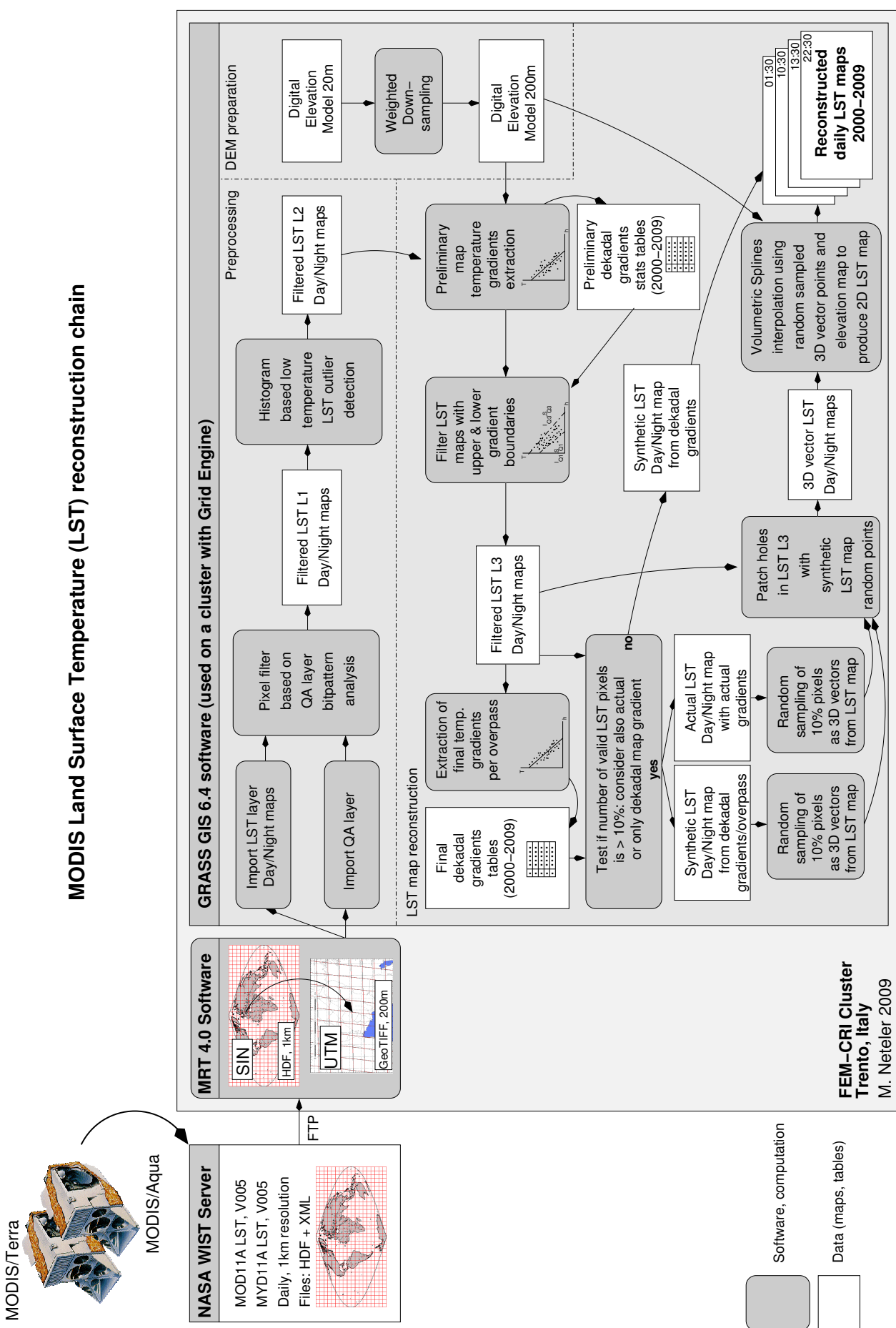
Figure 3.4: Flowchart of MODIS Land Surface Temperature (LST) map reconstruction chain
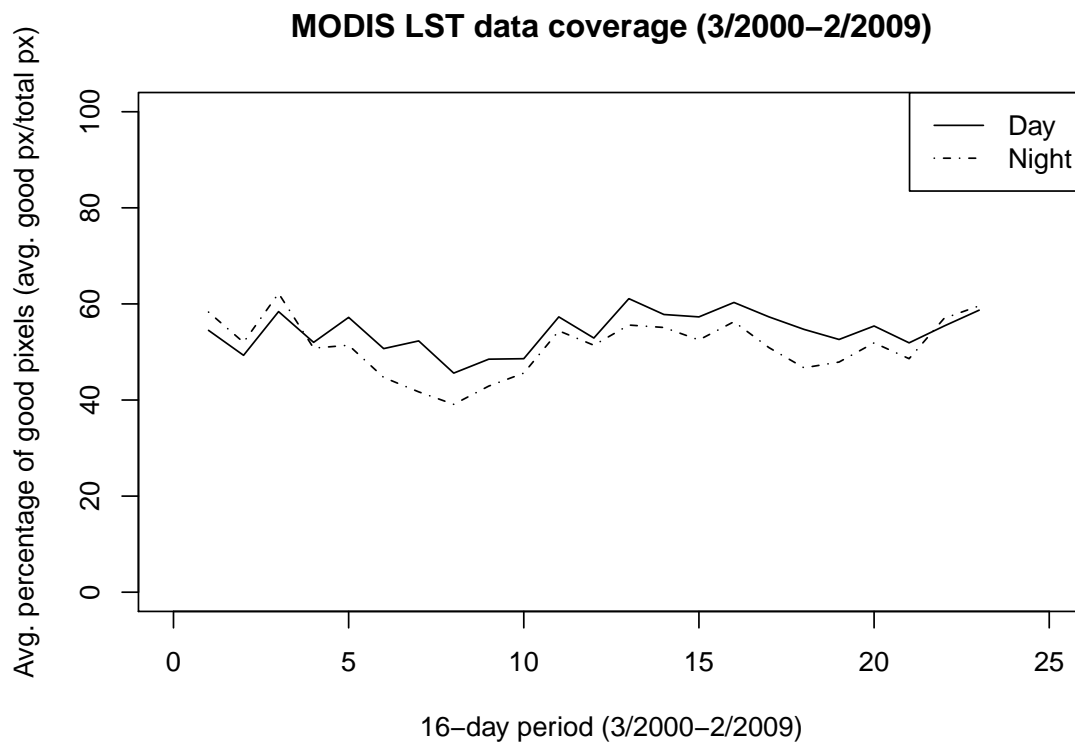
Figure 3.5: **Average percentage of valid pixels in outlier filtered MODIS LST time series maps aggregated to 16-day period**
The graph shows the average percentage of good pixels and total pixels separately for the day and night overpasses. Included are all available maps from 3/2000-2/2009 with maps rejected which contain less than 10 % of valid pixels; spatial extent is three Northern Italian provinces (TN, BZ, BL), based on 11179 LST maps.

caused, as expected, invalid gradients and unusable reconstructed LST maps. As a solution to this problem, a minimum threshold for the number of valid LST pixels per map was established. While a value of $>= 25$ % valid pixels too many maps were rejected; good results were yielded with a $>= 10$ % threshold as a compromise between acceptable gradient quality and low map rejection rate. This relatively low rejection value is a relaxed condition with respect to the 25 % threshold as used earlier in the post-import filter (see Section 3.2.1). Maps with less than 10 % of valid pixels are made invalid (completely no-data) in this step as their statistical significance is not sufficient.

The analysis of the average percentage of valid LST pixels has been done on aggregated rather than individual map statistics. Since usually aggregated data are relevant to epidemiological applications, the 11179 individual gradients were aggregated to 16-day period (in agreement to the epidemiologically relevant MODIS vegetation index product, see Tab. 2.1). Fig. 3.5 shows the average percentage of valid pixels (average good pixels/total pixels) separately for day and night overpasses.

Surprisingly, during the winter period the average percentage of valid pixels with respect to the total amount of pixels is higher than in the daytime overpass in the three Northern Italian provinces (TN, BZ, BL).

Split of LST time series to extract preliminary 16-day period mean gradients In order
to minimise effects of missing data on the temperature gradients models which are used to
eventually reconstruct the LST maps, the temperature gradients are aggregated (i.e., grouped)
by taking data from all available years for the given period. Tests with LST data aggregated at
monthly level have shown that too much of the sub-seasonal differences would be removed by
averaging at that temporal resolution. In contrast, weekly grouping is too prone to capture a too
high percentage of no-data maps which would badly influences the statistics (e.g., in the case of
a passage of low-pressure area which lasts several days).

Fig. 3.6 shows effects of different gradient aggregations and differences between fil-
tered/unfiltered gradients on the aggregation. It can be seen that the $y\_intercept$ quartiles
show the expected correlation to day length and solar radiation with a mimimum in winter
and maximum in summer. Opposed to that, the $slope$ quartiles (ranging from -0.3 °C/100 m to
0.97 °C/100 m in the filtered data set) show for the day satellite overpasses a peak in spring time
and a relative minimum in summer. The night curves are closer to the pattern of the $y\_intercept$
quartiles with very low values in winter.

As a compromise it was decided to perform periodical splits of the LST time series rather than
doing monthly aggregation. As mentioned before, a 16-day period length was selected. The
splits are performed on all available multi-annual gradients to group them in 16 day chunks
throughout the course of the year.

Quality assessment of gradients to remove gradient outliers To avoid unusually steep or
even inverted temperature gradients (originating from LST maps which passed the previous
filter) being included, the gradients selected for each 16-day period were statistically analysed
and filtered for outliers. For each 16-day period, they were analysed with five-number summary
(minimum, 1st quartile, mean, 3rd quartile, maximum) in order to obtain quality measures for
the identification of representative gradients for a given 16-day period. The statistics are done
separately for each overpass (01:30, 10:30, 13:30, 22:30).

Tests with MODIS V005 LST time series revealed that especially in the night overpasses still un-
detected cloud pixels remain despite the previously applied histogram based outlier filter. These
outliers would lead to degraded quality in the LST reconstruction. It was necessary to implement
a subsequent second filter based on temperature gradient quartiles in order to identify outliers
which are outside the range of the gradient range representative for a given 16-day period.

To obtain these representative gradients, the gradients of all available years for each 16-day
period were statistically analysed to find the 1st and 3rd quartiles for $y\_intercept$ (I_{Q1}, I_{Q3}) and
$slope$ of the gradients (S_{Q1}, S_{Q3}) in each 16-day period. The differences between statistically
valid and invalid gradients is shown in Fig. 3.7. The validity boundaries are found by the
following calculations (after R boxplot algorithm, R Development Core Team (2006)):

$$
\begin{aligned}
lower\_boundary &= 1st\_Quartile - 1.5 * (3rd\_Quartile - 1st\_Quartile) \\
upper\_boundary &= 3st\_Quartile + 1.5 * (3rd\_Quartile - 1st\_Quartile)
\end{aligned}
\tag{3.2}
$$

The formulae are applied to both the $y\_intercept$ and $slope$ parameters as global statistics to all
$y\_intercepts$ and $slopes$ of a 16-day period. Fig. 3.7 illustrates that still unacceptable gradients
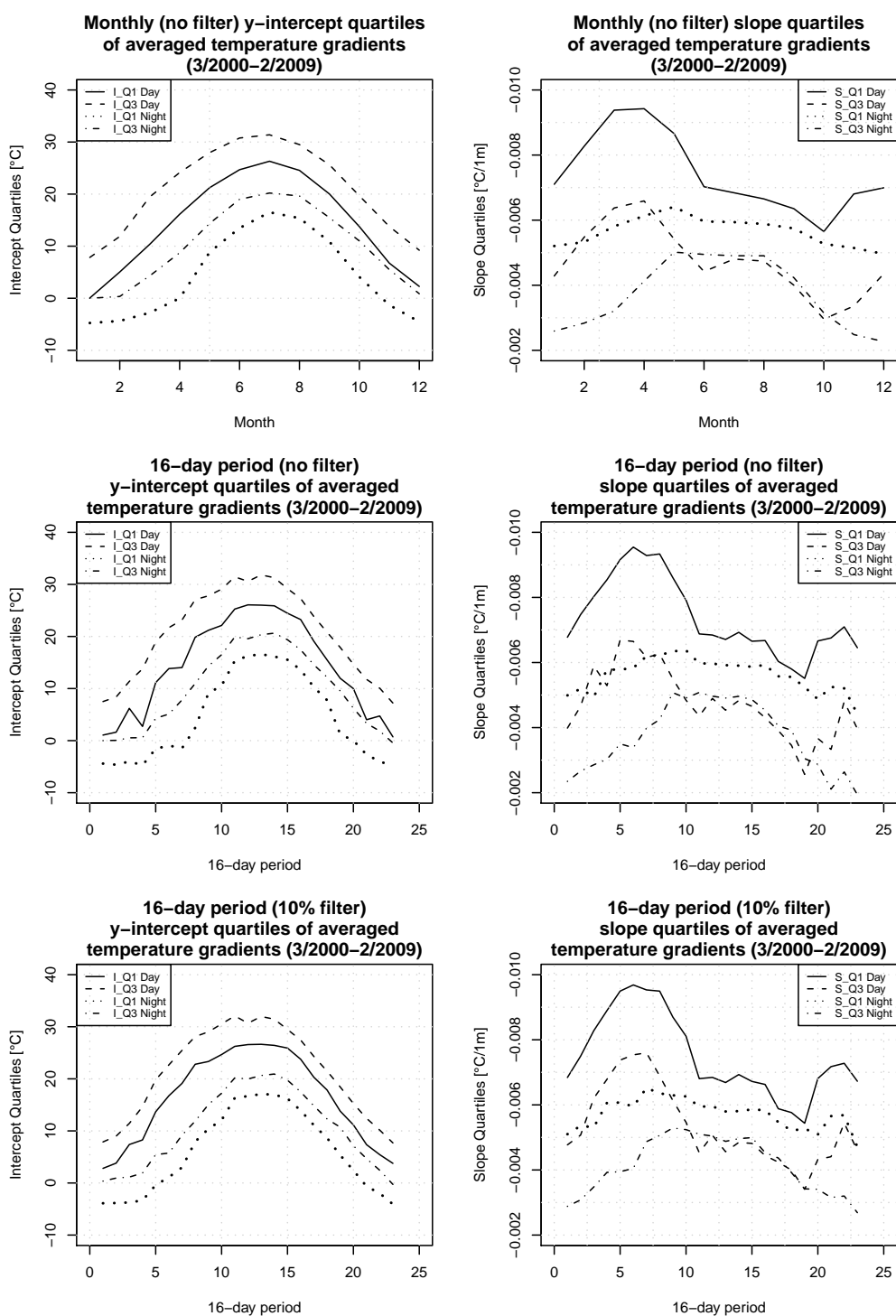
Figure 3.6: Temperature gradient time series of MODIS LST maps and 200 m DEM (based on 11179 LST maps from 3/2000 to 2/2009)

The temperature gradients are shown separately as intercept curves (left) and slope curves (right, with a range from -0.3 °C/100 m to 0.97 °C/100 m in the filtered data set). While the monthly aggregation shows smooth curves without special differences in seasonality, the unfiltered 16-day period curves show significant outliers to the negative range in late and early winter. The 16-day period curve is only based on maps with more than 10 % of valid LST map pixels. This 16-day period length is a compromise between curve smoothness (i.e., outlier minimisation) and maintenance of seasonal patterns.
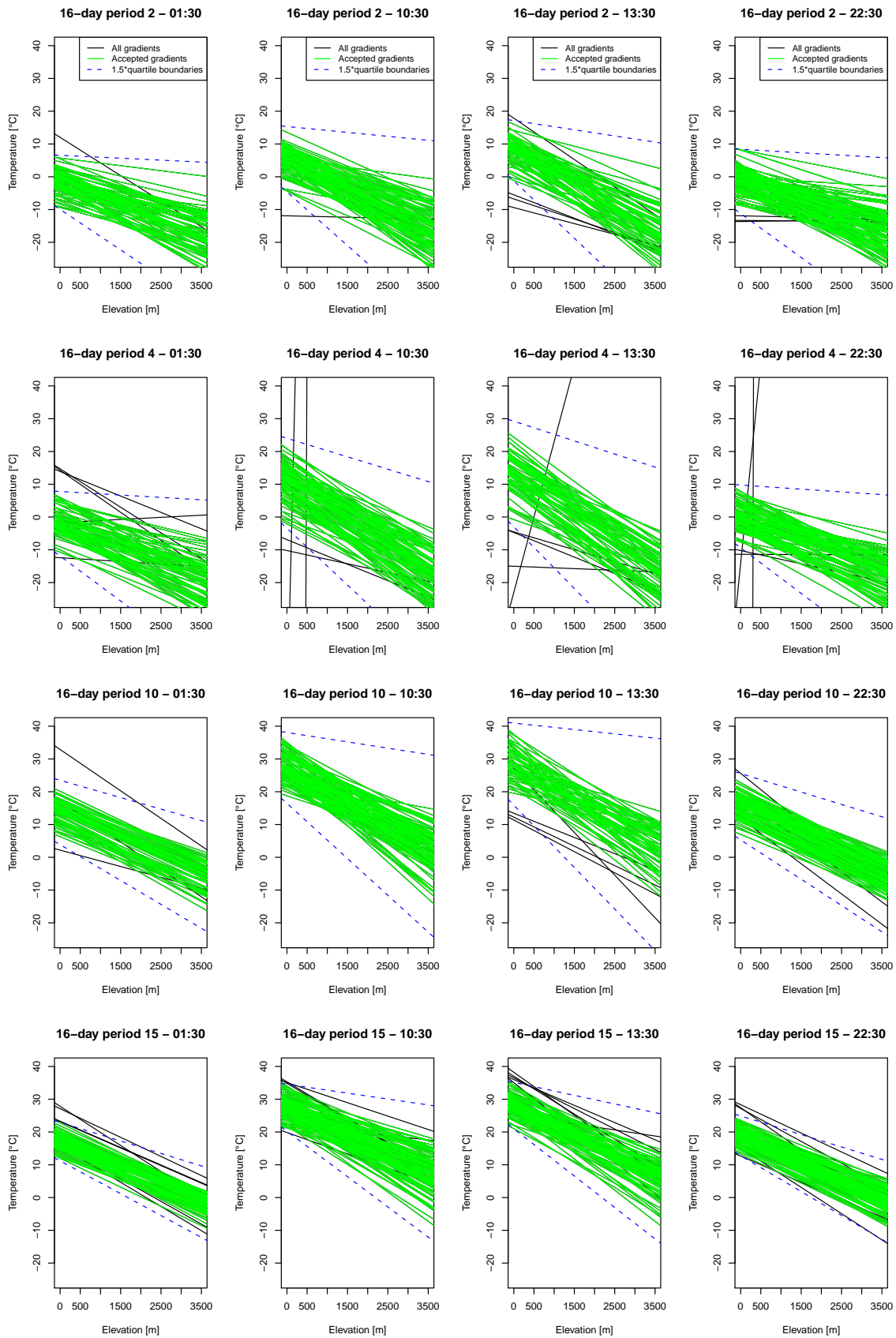
Figure 3.7: **Gradient plots: Valid (green) and invalid (black) gradients plotted for selected 16-day period (3/2000-2/2009)**
The gradient plots are shown as an illustration for gradient-based outlier detection of each overpass. In the subsequent filtering of the LST maps only pixels which are within the valid gradient quartile boundaries are accepted (green lines) to avoid that maps with statistically significant (due to sufficient number of pixels) but incorrect gradients are incorrectly accepted as valid.

(black color) were present which bypassed the previously applied LST filters (QA and histogram based) but which could identified by this gradients quality assessment. Remaining gradients (green color) are defining the range of LST-elevation relationships considered to be valid.

LST map filtering based on quartile boundaries of representative temperature gradients
The 16-day period $y\_\mathrm{intercept}$ and *slope* quartile boundaries computed above are used to filter all LST maps again in oder to eliminate remaining outliers which deviate significantly from the typical LST-elevation variable space in a given 16-day period of the year. I.e., all pixels outside of the I_{Q1}–S_{Q1} and I_{Q3}–S_{Q3} variable space are rejected in this filter. This removes remaining cloud pixels as well as pixels of large water bodies (e.g., Garda lake) in winter time which are relatively warmer and which would hence disturb the statistics of the land pixels.

In order to keep the notion of "lapse rates" also for MODIS LST data, a physical connection was imposed to keep the gradient slope within reasonable limits. The conventional air lapse rates are -0.51 °C/100 m for humid air, and -0.99 °C/100 m for dry-adiabatic air. In a study in Trentino-South Tyrol, Rolland (2003) found similar values (-0.40 °C/100 m to -0.75 °C/100 m, monthly values) in measured meteorological data.

In this thesis, it must be noted that the "lapse rates" are indeed special "MODIS lapse rates" for land surface temperature. Like air lapse rate, the LST decreases with altitude due to the surface-atmosphere energy flow. On the basis of the air lapse rates, the following limits were defined for MODIS LST data: "humid" land surface gradient with -0.02 °C/100 m, and "dry-adiabatic" land surface gradient with -0.95 °C/100 m. The former threshold value avoids to accept thermal inversion in the MODIS LST gradients but is yet tolerant enough to permit very shallow gradients as found in some LST maps (close to "isothermal" conditions). The right column graphs in Figure 3.6 show the gradient variation over the months (data aggregated over several years) and its range (note the different y-scale; range between -0.02 °C/100 m and -0.95 °C/100 m).

Since the procedure of map filtering is time consuming, the maps were processed in parallel on the 128-nodes FEM-CRI cluster[6].

Creation of the final set of temperature gradients   From each of the LST maps previously filtered for several times, the final temperature gradients are extracted by linear regression along with the number of total valid pixels per map. Again, as described in paragraph 3.2.2 a minimum threshold of 10 % is applied, i.e. maps with less than 10 % of valid pixels are in this step made invalid (completely no-data) as their statistical significance is not sufficient.

Split of LST time series to extract preliminary 16-day period gradients   The final set of gradients is split into 16-day period sets, separately for each overpass time. By aggregation to this period length over the years 2000-2009 the representative 16-day period mean gradients are obtained.

---

[6]FEM-CRI cluster description, `http://gis.fem-environment.eu/cluster`

Part 2: Synthetic LST maps creation based on actual map or 16-day period mean gradient

Since parts of a LST map or even the entire map may be devoid of valid pixels, statistical support for a more reasonable reconstruction of the LST time series is necessary. To overcome the problem, an accompanying synthetic LST map has been generated for each filtered MODIS LST map using its temperature gradient (*dgrad*) given that sufficient valid LST pixels are present (10 % threshold). If not, the related 16-day period mean gradient is selected from the list of all valid gradients and used in the creation of the synthetic LST map.

It was verified if it was necessary to correct for exposure in order to better take north/south orientation of slopes in the day overpass into account. For this, a cosine correction (Teillet et al., 1982) to simulate exposure effects in daytime overpasses was initially considered in order to render southern exposed slopes warmer and northern exposed slopes colder than the average temperature. But it turned out to be impossible to sufficiently quantify the required "LST signal modulation" effect of the exposure on the synthetic LST maps according to slope and exposition. The reason is that no "ideal" mountain was found in the study area with sufficiently homogeneous landuse/landcover to estimate the effect of the exposition on the LST, in order to define a transfer function for the synthetic model. Indeed, the analysis of more than 11000 filtered LST maps to statistically assess the differences between north and south exposed sloped did not reveal a significant pattern which could be readily integrated into the gradient model. A reason may be the low original resolution of 1000 m which averages out some terrain effects. Some examples for the impact of direct sunlight on slopes are shown in Figures 5.8 and 5.9. Additionally, in case of LST pixel reconstruction, the missing pixels are typically cloud or fog contaminated which indicates that no direct sunshine was involved, leading to only low differences between northern and southern exposed slopes.

Hence, for each day phase and overpass, a related synthetic LST map *lst_*synthetic is calculated based on the following rules

- if more than 10 % of valid pixels are present in the LST map, the actual map gradient is extracted from the map through linear regression and used to generate a new synthetic LST map, using

$$\text{lst\_synthetic} \quad = \quad \text{agrad}_{y\_\text{intercept}} + \text{agrad}_{\text{slope}} * \text{DEM} \tag{3.3}$$

- if the LST map is statistically not significant since only a few valid pixels are found, the related 16-day period temperature gradient is selected from the gradients table and used instead as

$$\text{lst\_synthetic} \quad = \quad \text{dgrad}_{y\_\text{intercept}} + \text{dgrad}_{\text{slope}} * \text{DEM} \tag{3.4}$$

with:

    $agrad_{y\_\text{intercept}}$: actual temperature gradient parameter [-],

    $agrad_{\text{slope}}$: actual temperature gradient parameter [-],

    $dgrad_{y\_\text{intercept}}$: 16-day period temperature gradient parameter [-],

    $dgrad_{\text{slope}}$: 16-day period temperature gradient parameter [-],

    DEM: elevation [m],
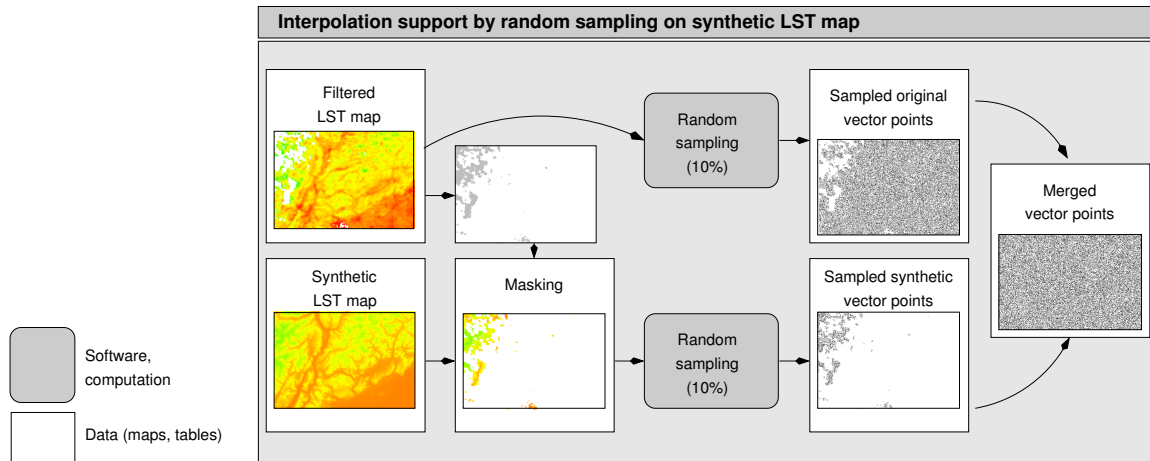
Figure 3.8: **LST map random sampling**
Random sampling sub-procedure in order to obtain balanced input for the LST map interpolation

In this study more than 11000 synthetic LST maps were generated using this set of rules. In case that no valid actual gradient was found, the synthetic LST map based on the typical 16-day period gradient became the final LST map. Otherwise the procedure continued as described below.

Part 3: 3D vector point random sampling and map patching

In general, two problems emerge: The filtered LST maps may still contain artifacts like locally disturbed pixels or other artifacts introduced through the SIN to UTM reprojection. Additionally, it is expected that a synthetic LST map differ to some extent at most joint borders to its related actual LST map – especially when it is based on a 16-day period average gradient which is not necessarily close to the actual gradient. To overcome this problem, random sampling has been included in the procedure (see Fig. 3.8 for the procedure). It is performed on both the actual (filtered) and the synthetic LST maps to reduce these artifacts in the subsequent interpolation process. Additionally, the volumetric splines interpolator requires 3D vector points input (see below).

In detail, the maps are randomly sampled through extraction of 10 % of their pixels. First the 10 % of LST pixels are sampled from the valid MODIS LST maps, then these valid LST pixels are made invisible through a MASK (`r.mask`); in the remaining areas (i.e., no-data area in LST map), random sampling is performed on the accompanying synthetic LST map (`r.random`). Both vector maps are then patched together (`v.patch`) in order to obtain a complete map of random samples for the subsequent volumetric interpolation.

Part 4: Volumetric spline interpolation based LST map reconstruction

For the interpolation part of the LST reconstruction procedure a splines method was chosen. Splines are based on a physical model (TPS: thin plate splines; model of the bending energy of a thin metal plate) with flexibility provided by change of elastic properties of the interpolation function (Mitas and Mitasova, 1999). The underlying concept of the splines function is that it should pass through or close to the data points while trying to remain as smooth as possible.

Hence it is also called variational approach in contrast to (geo)statistical approaches like kriging. Splines proved to be rather successful for modelling physical phenomena from processes which minimise energy. They provide enough flexibility for local geometry analysis, which is often used as input to various process-based models (Mitas and Mitasova, 1999).

The splines implementation used here is the RST function (Regularised Splines with Tension, Mitasova and Mitas (1993); Mitasova and Hofierka (1993)); it has been implemented in a volumetric form in GRASS GIS as `v.vol.rst` module. The RST function minimises a specific measure of surface smoothness and simulates a flexible sheet forced to pass through the data points while minimising its energy (Mitas and Mitasova, 1999). The properties of this function can be controlled by the *tension* and *smoothing* parameters. The tension parameter controls the distance over which each given point influences the resulting volume (i.e, with very high tension, each point influences only its close neighborhood and the volume describes rapidly the trend between the input 3D data points). In the 2D thin metal plate model this corresponds to the stiffness of the surface (stiff or elastic). With higher values of tension overshoots can be avoided which may appear in volumes with rapid change of gradient. The smoothness parameter controls how much the interpolation function is allowed to deviate from the given 3D points (Neteler and Mitasova, 2008). It is relevant especially for noisy data. With a low smoothness parameter the interpolation function will pass close to the data points (with smooth=0 exactly through the data points) while a high smoothness value permits for larger deviations. Smoothness is important when using a low tension value because it prevents overshoots of the interpolation function.

Splines have been used extensively in the interpolation of various climate variables including regions with complex topography (among others, Hutchinson (1995); Hofierka et al. (2002); Suprit and Shankar (2008)). Splines are robust in areas with sparse or irregularly spaced data points (New et al., 1999).

The above described volumetric implementation of RST (Vol-RST) was selected as method to reinterpolate the MODIS land surface temperatures. Vol-RST interpolates the temperatures in a 3D space described by voxels (volume pixels) with elevation as the third dimension. An interpolated LST value depends on the horizontal position as well as vertically on the elevation. As shown in many cases, the elevation is an important covariate for the description of temperatures in rugged terrain (e.g, Hofierka et al. (2002)). In the alpine study area is is of particular relevance since the available meteorological stations are not well distributed over the terrain but moreover concentrated in the agricultural areas at lower altitudes (see Section 3.4.3).

To accelerate the volumetric RST interpolation, a single layer volume (3D region) was defined in GRASS (all calculations were performed UTM32/WGS84 projection), i.e. a volume was defined with only one vertical layer (-10 m to 4000 m). From the volume a 2D map was subsequently extracted. To reconstruct a LST map, the previously patched 3D vector points map was used in the volumetric interpolation along with the DEM as auxiliary variable. The following settings have been stabilised for the RST algorithm (`v.vol.rst`):

- $tension = 20$: found by performing a cross-validation analysis of RST parameters, selected was eventually the half of default value;
- $zmult = 10$: Rescaling of z-coordinates is needed when the distances in vertical direction are much smaller than the horizontal distances. In this case, the value of *zmult* should

be selected so that the vertical (mean avg. temperatur: 12 °C) and horizontal distances (here: 200 m) have about the same magnitude;

- $dmin = 2000$: the smaller *dmin* (minimum distance, in map units), the more points are considered, and the higher *segmax* must be;

- $segmax = 6000$: set high for no segmentation (along with *npmax* which is set to same value to avoid segmentation); in the processing it is gradually increased in case of being too low to contain all input 3D vector points but aiming at keeping the memory consumption of `v.vol.rst` low;

- $npmin = 300$: minimum number of points taken for interpolation;

- $npmax = 6000$: set to same value of *segmax* in order to avoid segmentation; gradually increased along with *segmax* during the processing;

- $smooth = 0.2$: smoothing, i.e. possible deviation from data points during splines fitting, twice the default value.

Segmentation was disabled in order to avoid visible connection of segments. Due to increased availability of computer memory segmentation can often be avoided although this approach is penalised by longer computations.

After the volumetric splines interpolation, in order to obtain the resulting 2D LST map, the temporarily created RST volume is intersected with the terrain surface (DEM, Neteler and Mitasova (2008)). Finally, map metadata are written out which include the interpolation parameters.

The resulting LST map is either based on the actual (filtered) land surface temperature gradient or, in case of lack of valid pixels, on the 16-day period land surface temperature gradient.

A few disadvantages are reported in the literature for splines: the lack of direct error mapping (as for example provided by kriging) as well as the sometimes overly smoothing effects which can result from splines (Burrough and McDonnell, 1998). While the second aspect is hard to judge in terms of LST map reconstruction, the errors can be assessed to some extent through calculating the pixel differences between LST map generated from the actual map gradient to that of the 16-day period gradient (see Section 3.5).

Remarks about kriging   An interpolation technique commonly used in geosciences is kriging. Kriging assumes spatial dependence of random variations and uses the modelled dependence along with statistical techniques to describe the distribution of a geographic phenomenon. With kriging data (drift, covariance) and statistical criteria (unbiasedness and minimum variance) data are analysed for predictions (Mitas and Mitasova, 1999). A problem of the kriging method is that subjective decisions are necessary (Journel, 1996) such as judgement about stationarity, choice of function for theoretical variogram, etc. (Mitas and Mitasova, 1999). It was demonstrated by several authors (e.g., Wahba (1990); Cressie (1993)) that splines are formally equivalent to universal kriging with the choice of the covariance function determined by the smoothness seminorm (also called roughness penalty, Neteler and Mitasova (2008)). Therefore, many of the geostatistical concepts can be exploited within the spline framework. In contrast with kriging, no spatial stationarity across the map is assumed (Hargrove, 1997).

Surfaces generated with kriging are defined by minimizing the variance of the error of estimation, which is normally dependent on a preliminary variogram analysis (New et al., 1999). Instead, splines do not require prior estimation of the spatial autocovariance structure (Suprit

and Shankar, 2008) which results as main advantage (also in terms of the more than 11000 maps to be processed for this thesis). Haylock et al. (2008) used a mixed approach of splines and kriging.

Since splines were giving more advantages for the purpose of this thesis, kriging was not chosen for the LST map reconstruction.

3.3 Constraints, limitations, and assumptions

In case of (partial) cloud coverage or other reasons which lead to few valid pixels in a LST map no statistically significant gradient can be generated from the map. Instead, the failover algorithm (see Section 3.2.2) replaces missing pixel values by a 16-day period temperature average gradient based on all available years for that specific 16-day period. However, in case of long periods of cloud coverage in the observed area, the pixel(s) are hence completely synthetically generated by the failover algorithm which leads to non-significance of the observations in that period. A future solution might consider a failover model based on meteorological observations to statistically better support the LST map reconstruction in those cases.

The use of global temperature gradients assumes that the geomorphological composition of the study area is homogeneous. In this study, this condition was fulfilled (see geomorphometrical parameters in Chapter 4). Alternatively, in heterogeneous geomorphological areas local gradients might be applied using a masking approach to subdivide a large study area into homogeneous parts. For example, in New et al. (1999) a tiling approach was used.

The 16-day period gradients which are used as failover in case of too high cloud contamination/pixel errors are clearly only based on days with low cloud contamination and cloud-free image scenes. It is yet unclear if this causes an overestimation of the Land Surface Temperatures or if the positive and negative effects are averaged out (since night images will report temperatures with low peaks). Within this thesis no method was found to retrieve LST from the raw MODIS data in case of cloud coverage. A future solution might be to search for adjacent days with low/no cloud coverage to better understand the statistical relevance.

The original resolution of nominally 1000 m x 1000 m was oversampled to 200 m x 200 m in the reprojection process. Since the temperature gradient is based on a true 200 m x 200 m DEM, additional information is added to support a higher than 1000 m x 1000 m LST map resolution which was assumed to be acceptable.

In winter periods, atmospheric thermal inversion is a common phenomenon in the valleys which is completely ignored by the assumption of linear temperature gradients. However, is it unclear how an atmospheric thermal inversion is reflected by Land Surface Temperatures since the surface response is slower than a change of atmospheric temperatures when an inversion occurs.

In the calculation of aggregates, the different daytime and nighttime lengths throughout the years have been ignored which may have a limited effect on the results.

Technical constraints (data management) The *Ext3* filesystem which was used on the FEM-CRI cluster does not permit to store more than 32000 subdirectories in a directory. GRASS GIS stores the files related to a raster map into five subdirectories. Hence, the storage of the more than 11000 MODIS LST maps (i.e., 55000 subdirectories) required a split into five years chunks

which is easily done with GRASS "mapsets".

The data storage was shared via NFS on the FEM-CRI cluster. Due to the large amount of data processed in parallel (128 nodes cluster) it was necessary to tune the internal network protocol to use "jumbo-frames", i.e. extra long TCP/IP packages to avoid a saturation of the 10GiB/s internal cluster network due to the large amount of files to be processed.

For the time series processing of annual measure from MODIS LST, the limit of open files per process was reached (64bit Linux: 1024 files; `ulimit -n`) since 1460 MODIS files are available per year after July 2002. To overcome this problem, the `nofile` parameter was set to 1500 in the `/etc/security/limits.conf` file.

3.4   GIS, meteorological data and disease vector data

3.4.1   GIS data availability

A set of official GIS maps was obtained for the study area, in particular:

- digital elevation models (DEM: raster map, at pixel resolution of 1m for Trentino, and 20m for Belluno and Bolzano). These DEMs were postprocessed and used to calculate the temperature gradients (see Section 3.2.2);
- political boundary maps of provinces (vector maps) including municipalities, rivers and lakes;
- map of larger lakes from the OpenStreetMap.org project.

3.4.2   Meteorological data availability

The availability of meteorological observation which can be readily integrated into epidemiological applications is limited in Europe as obtaining these data is typically cost and work intensive. Low cost/gratis meteorological data for Europe are even for research purposes rarely available and limited to either a small set of stations or a short time series. Datasets of some stations are available for Italy and other countries from the *European Climate Assessment & Dataset* project (ECA&D[7]), however, for this thesis they were considered as spatially too distant from the field sites of the EDEN and RISKTIGER projects. The same applies to the station time series from *Global Surface summary Of day Data* climatic data (GSOD compiled by NOAA[8]). The data used in this thesis are listed below:

Data for the Autonomous Province of Trento   For the Trentino Province, data from two providers were available: Meteotrentino (`http://www.meteotrentino.it`, daily data available online, data are to unknown extent validated but not homogenised).[9] Furthermore, data from the Fondazione Edmund Mach–Centro Trasferimento Tecnologico (FEM-CTT, formerly IASMA, `http://meteo.iasma.it/meteo/`, hourly data internally available, unvalidated, timestamps indicate local solar time) were used. The list of selected stations is given in Tab. 3.4.2.

---

[7]ECA&D Web site, `http://eca.knmi.nl/`

[8]GSOD Web site, `http://www.ncdc.noaa.gov/cgi-bin/res40.pl?page=gsod.html`

[9]Meteotrentino data download, `http://www.meteotrentino.it/AspWeb/Monitoraggi/monitoraggi.asp?ID=3`

Station name	East UTM32	North UTM32	Altitude [m]	East LL/WGS84	North LL/WGS84
Arco	646359	5085826	84	10.887125	45.910415
Arsio	661091	5143503	802	11.096574	46.425874
Avio	651263	5066650	145	10.944304	45.736861
Borgo Valsugana	691490	5102049	415	11.475048	46.045214
Cavedine	653432	5094290	561	10.980978	45.985015
Cunevo	657004	5127631	559	11.038102	46.284085
Malga Flavona	648877	5120386	2002	10.930380	46.220750
Paneveggio	711551	5132109	1538	11.747483	46.309536
Passo Tonale	623056	5124456	1876	10.596779	46.262527
Rabbi	639036	5141389	1400	10.809065	46.411768
S. Michele a/A	664707	5117303	207	11.134420	46.189375
S. Orsola	676700	5106889	770	11.285832	46.092718
Storo	621314	5078210	385	10.562406	45.846769
Terlago	658180	5105820	425	11.046065	46.087641
Trento Sud	664585	5098672	187	11.126386	46.021841

Table 3.1: List of 15 selected meteorological stations in the Province of Trento with instantaneous meteorological measurement (data source: FEM-CTT)

The univariate statistics of the altitude distribution of the selected FEM-CTT stations are as follows for the selected stations (n=15): minimum: 84.2 m, maximum: 2001.9 m, range: 1917.7 m, mean: 757.0 m, and population standard deviation: 617.8 m. The selection aims at better representing the altitudes found in Trentino as well as giving a good spatial representation for the terrain. The stations are used to statistically compare MODIS LST values to meteorological measurements (see Chapter 5 for results).

Data for the Autonomous Province of Bolzano   For the Bolzano Province, data for the Bolzano station were obtained from the Hydrographical Service of the province (`http://www.provincia.bz.it/meteo/`, data available upon request). The station coordinates are: 11.31395E, 46.50041N, 243 m a.s.l.; in UTM32/WGS84: 677550E, 5152250N.

Data for the Province of Belluno   Due to the costs involved in obtaining meteorological data from Meteo Belluno, only a single time series could be acquired on behalf of the EDEN project (station Agordo, 12.03227083E, 46.27678972N, 622 m a.s.l.; UTM32/WGS84: 733617E, 5129271N). The time series includes daily data from 1956-2004. Due to the lack of distributed meteorological stations it was not possible in this thesis to spatially interpolate meteorological maps based on station data. For the Belluno Province data from ARPAV – Centro Valanghe di Arabba (`http://www.arpa.veneto.it/datirete.htm`, data available for payment.

More interesting for this thesis were the field measurements of meteorological conditions done during tick sampling in Belluno (2000-2007, see details below in Section 3.4.4). A subset of these data was used for comparison with LST map values.

Data set	Min.	1st Qu.	Median	Mean	3rd Qu.	Max.
Elevation model (200 m)	54.3	900.7	1382.0	1402.0	1878.0	3708.0
FEM (former IASMA)	73.2	207.0	527.5	734.5	994.8	2971.0
Meteotrentino (PAT)	82.6	608.0	908.0	1049.0	1470.0	2971.0

Table 3.2: **Representativeness of the available Trentino meteorological stations with respect to the territorial elevation distribution**
Results of the five-number summary (minimum, 1st quartile, mean, 3rd quartile, maximum) statistics of Trentino DEM (analysed at 200 m downsampled resolution) and meteo-stations altitudes to assess the representativeness of the available Trentino meteorological stations with respect to the territorial elevation distribution. A few stations are shared among the meteo data providers. Heights in [m].

3.4.3   Assessment of territorial representativeness of meteorological stations with respect to the elevation distribution in complex terrain

The overall goal of obtaining a continuous temperature field from point observations or incomplete raster surfaces is reached by using interpolation. Interpolation predicts values at unsampled sites from measurements made in relative adjacency. An ideal interpolation requires well distributed data points from which to interpolate which are commonly unavailable. Moreover, data points are often sparse and unevenly distributed.

In terms of temperature map spatialisation from meteorological stations, these stations should be ideally placed corresponding to the elevation distribution (histogram) in order to obtain measurements in all altitudes. However, this is commonly not the case since a predominant driver for the placement of meteorological stations is agriculture which is typically linked to limited terrain slope and as well as valley floors at low altitudes.

A statistical analysis for the meteorological stations available in Trentino (data sources: Meteotrentino (PAT) and Fondazione Mach (FEM, former IASMA) is shown in Tab. 3.4.3. High altitudes are not well represented but may be even less interesting in disease vector distribution modelling. The mean altitude of the meteorological stations and of the elevation differ significantly, as do the 1st and 3rd quartiles. From the results of the five-number summary (minimum, 1st quartile, mean, 3rd quartile, maximum) statistics and Wilcoxon tests of the distributions of the meteorological stations versus elevation (FEM vs. DEM: W=11193704, p-value < 2.2e-16; PAT vs. DEM: W=17652608, p-value=6.088e-13) the distribution of the available Trentino meteorological stations cannot be considered as representative for the entire provincal territory.

Hence, an interpolation only based on the meteorological stations would potentially lead to skewed results unless auxiliary data sources are used. Fig. 3.9 shows the histograms of the stations of Meteotrentino (in red) and Fondazione Mach-CTT (formerly IASMA, in blue) in contrast to the elevation distribution (in green). Related data of the provinces Bolzano and Belluno are not shown here but the terrain composition and organisation of meteo-stations is similar.

Microclimatic conditions are especially difficult to obtain from interpolation of meteorological station data. Much better spatial support is gained from satellite data which are by definition spatialised: under ideal conditions, a complete map coverage is taken per satellite overpass; with increasing cloud presence fewer valid LST pixels are available (compare also Fig. 3.5). Still the number of valid pixels is typically much higher than the number of meteorological stations.

3.4.4 Disease vector data: Belluno ticks data and Trentino/Belluno mosquito data

ULSS 2 Feltre (Belluno), ticks sampling   Tick field data have been obtained for a series of years in the Province of Belluno from the Bulletin of ULSS 2 Feltre, Belluno (Unità Locale Socio Sanitaria)[10]. In a series of provincial tick campaigns, ticks were collected for the years 2000 to 2007. In the years 2000-2001, over 200 sites were sampled (in the year 2000 with 14 sites and 2001 with 206 sites). These data include results of tick pathogen analysis (5987 ticks in total). In the following years (2002-2007), the campaign was continued only in area of the Municipality of Feltre. These ticks were not further analysed for pathogens but they can be considered as presence/absence data (Piccolin et al., 2001, 2006; Furlanello et al., 2002). The records are geocoded and contain additional environmental data: atmospheric conditions (descriptive), altitude, vegetation type (descriptive), and observed fauna (species). The atmospheric conditions are especially valuable for comparison with MODIS data since no distributed meteorological station data for Belluno were accessible (since they were too costly to obtain). A few sites have been incorrectly geocoded (IDs: 87-90, probably more) and refer to places outside of the Belluno province.

---

[10]ULSS 2 Feltre, "Il Bollettino delle zecche", `http://www.ulssfeltre.veneto.it/Piani/Zecche/index.html`
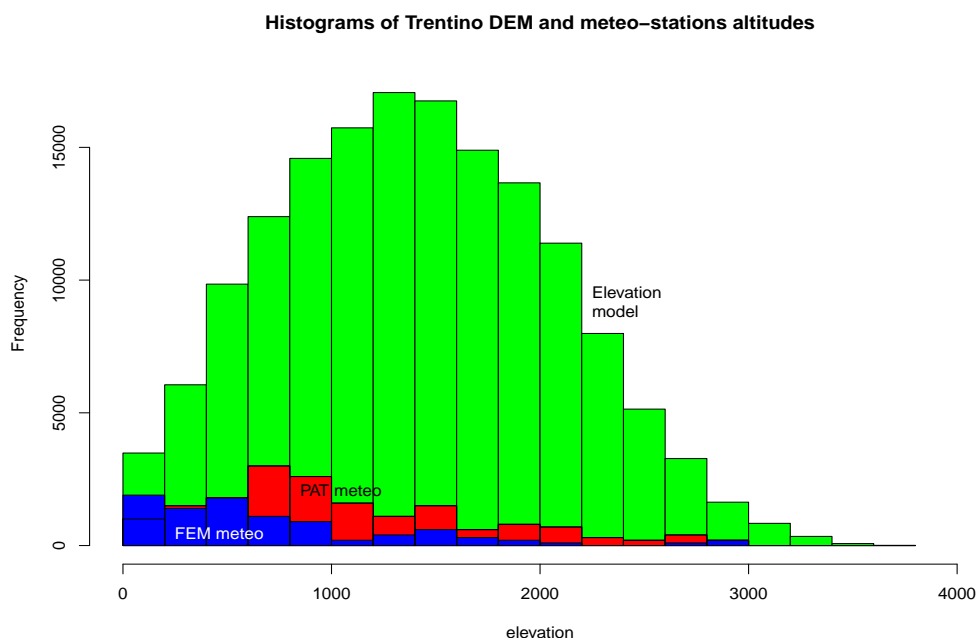
Figure 3.9: **Histograms of Trentino DEM and meteo-stations altitudes**
Histograms of Trentino DEM (analysed at 200 m resolution; green) and meteo-stations altitudes (Meteotrentino: red; Fondazione Mach-CTT: blue; the frequencies of the meteo-stations have been multiplied by 100 to improve visibility in the histogram) to assess the representativeness of the available Trentino meteorological stations with respect to the territorial elevation distribution. A few stations are shared among the two meteo data providers.

EDEN tick sampling for Belluno   In the EDEN EU project, a series of sites are maintained for tick sampling. The site selected for this thesis is located in Candaten (Belluno, Italy; EDEN site IT4; UTM32/WGS84: 741521E, 5122255N; Lat-Long: 12.131115E, 46.2109709N, altitude: 530 m a.s.l.), The incidence rates (per 100,000 inhabitants) of human TBE cases recorded in 2006 in the Belluno province was 3.71 (Rizzoli et al., 2009). Ticks were collected from the vegetation by dragging a 1m^2 white blanket along transects of 100 m from March to November for the years 2006-2009. All ticks were microscopically identified by species and life stage using reference keys developed by Manilla (1998). Together with the tick data from ULSS 2 Feltre a longer time series is obtained. The sampling site Candaten is at the floor of a narrow river valley. This valley is almost completely occupied by the river bed of a torrential river (torrente Cordevole), with scree, alpine meadows, and small patches of broadleaved trees.

RISKTIGER mosquito sampling   The *Aedes albopictus* mosquito data have been collected for the RISKTIGER in the Province of Trento in summer and autumn 2008 to assess the potential distributional area with oviposition traps (ovitraps, Roiz et al. (in press)). In total, 118 sample stations were positioned along the roads at a distance of more than 500 m northwards and southwards of the "hot spots" of known distribution (Rovereto, Arco and Riva area). They were placed in sheltered sites shaded by vegetation. The locations of the traps were recorded with GPS (GeoExplorer 2005 series, Trimble). Ovitraps were checked for the presence of mosquito eggs in the year 2008 from the first week of August to November. Whenever for an ovitrap eggs were identified as *Ae. albopictus* eggs using a stereo-microscope and furthermore developed as larva in the FEM-CRI laboratory, the related ovitrap was removed (Roiz D., pers. comm.). The detection of the *Ae. albopictus* presence was sufficient for the scope of the study. For this thesis, only ovitrap data aggregated at municipality level were used.

Further recordings from the Rovereto area (Ferrarese, 2003) and Belluno (S. Martini, pers. comm.) were also integrated into the study.

3.5   Quality assessment of the reconstructed MODIS LST time series

Despite the lack of spatial representativeness and also the difficulty of directly comparing land surface temperatures to air temperatures (measured 2 m above ground), it was deemed appropriate to document not only comparisons with instantaneous meteorological measurements but also to compare trends.

3.5.1   Cross-check of Land Surface Temperature against elevation

A LST map represents the pixelwise measured surface temperatures. A (almost) complete map should show a certain independence from the elevation in complex terrain since the exposure of slopes comes into play. Since the LST map reconstruction proposed in this thesis is based on a linear gradient model (elevation-temperature lapse rate), it is most interesting to understand how strong the influence of the elevation on the temperature pattern in partially or un-reconstructed maps really is. Ideally, there is a certain independence since southern exposed slopes are expected to be warmer than northern exposed slopes. In order to validate this, a cross-check with contour lines has been done. It has been performed in selected zones:

- South-north exposed slopes: Valsugana (Trentino; 11.460E, 46.042N);
- East-West exposed slopes: Val di Non (Trentino; 11.069E, 46.305N);
- river plains with similar altitude: surroundings of Mezzocorona (Trentino; 11.125E, 46.209N) in contrast to Riva del Garda-Arco (Trentino; 10.865E, 45.907N; strongly influenced by Garda lake);

The results are presented in Section 5.2.1.

3.5.2   Comparison with meteorological measurements of air temperature

A set of meteorological stations was selected for the comparison of LST to air temperature which cover parts of the relevant areas of the study area:

- instantaneous hourly data: FEM-CTT (Trentino) stations as listed in Tab. 3.4.2;
- field measurements during tick sampling campaigns in Belluno (ULSS 2 Feltre and EDEN data).

For results of the following paragraphs, see Section 5.2.2.

Comparison with instantaneous meteorological measurements   Given the regular overpasses of the Aqua and Terra satellites[11], it is possible to compare LST maps to instantaneous meteorological measurements for the pixels which contain a meteorological station. The overpass sequence is: Aqua at 01:30, Terra at 10:30, Aqua at 13:30, and Terra 22:30 local solar time (Wan et al., 2004). Hence, from the LST maps timestamps the corresponding meteorological observation can be extracted from the station database. For each station, up to four daily observations can be compared.

Additionally, the Belluno tick sampling records contain measurements of weather conditions during the tick collection (see Section 3.4.4). These are used as well to cross-check LST data derived from satellite observations (see Section 3.4). Since a sufficient number of field measurements was available, a subset was extracted which had a timestamp close to the moment of the satellite overpasses.

Despite direct comparisons, the collection of LST-meteo pairs can be subjected to correlation analysis. For different time periods (day, month, year), correlation plots with y (t_{air}) and x (LST) can be created and analysed.

Comparison of 16-day period, monthly and annual averages   Besides direct comparison and correlation plots, a comparison of 16-day period, monthly and annual averages is of interest to identify similarities or systematic differences.

For the above indicated stations 16-day period, monthly, and annual averages were elaborated.

Comparison of short term trends   Besides comparison with instantaneous measurements also short term trends are of interest. A set of indicators can be used to compare aggregated MODIS LST maps to the corresponding meteorological time series for meteo-station pixels (relevant

---

[11]Satellite Overpass Predictor, `http://earthobservatory.nasa.gov/MissionControl/overpass.php`

to *Ixodes ricinus* and *Ae. albopictus*): Trend of monthly average temperatures in summer and winter and the comparison of spring temperature increase gradient ("warming") and autumnal temperature decrease gradient ("cooling").

3.6 Comparison with LANDSAT-TM thermal maps

Thermal radiation (TIR) is the surface emitted radiation. LANDSAT 5 and 7 satellites offers the capability of detecting emitted thermal energy from the Earth's surface at the resolution of 60 metres every 16 days. It is detected in the spectral range of 10.40-12.50 μm (LANDSAT band-6, registered in both low and high gain mode).[12] Data are available from the USGS Web site `http://landsat.usgs.gov/`.

To use these data, a conversion of the pixel data values (DN, digital numbers) from the 8bit range into meaningful temperature values using a calibration equation has to be done. The image file headers carries the required metadata (gain, offset). First the digital numbers (DN) are converted to spectral radiances (L):

$$L = \text{gain} * \text{DN} + \text{offset} \tag{3.5}$$

Then these spectral radiances are converted to absolute temperatures:

$$T = \frac{K_2}{ln(K_1/L + 1))} \tag{3.6}$$

where:

T: Effective at-satellite temperature $[K]$

K_2: Calibration constant, for LANDSAT 5: 1260.56 (LANDSAT 7: 1282.71) $[K]$

K_1: Calibration constant, for LANDSAT 5: 607.76 (LANDSAT 7: 666.09) $[W/(m^2sr\mu m)]$

L: Spectral radiance $[W/(m^2sr\mu m)]$

and finally converted to degree Celsius by subtracting the value 273.15 from T.

To better match the reconstructed MODIS LST maps, the postprocessed LANDSAT thermal maps were downsampled to 200 m pixel resolution using weighted pixel aggregation to minimise the error.

Then, for each MODIS-LANDSAT map pair the spatial and statistical (univariate, histogram) differences can be assessed. Small deviations are expected for two reasons: the spectral range coverage is not identical (but close) and the overpass time of LANDSAT 5 is circa at 9:30hs (LANDSAT 7 at 10:00hs) local solar time, 60 minutes earlier than Terra.

The results are presented in Section 5.2.3.

3.7 Climatic parameters derived from reconstructed LST time series

In Section 2.1.3, a series of indicators have been introduced to perform comparisons between MODIS LST maps and meteorological measurements including climatic parameters with relevance to epidemiological studies which can be derived from MODIS LST time series.

---

[12]LANDSAT 7 mission, `http://landsat.usgs.gov/about_landsat7.php`

3.7.1 Indices: Saturation deficit from datalogger and from daily MODIS LST maps

Questing ticks (host seeking ticks) are highly dependend on the actual temperature-humidity patterns (see Section 1.1.1). Hence, the saturation deficit can be used as indicator for an estimation of the decline in tick activity in early summer months (Knap et al., 2009).

For a limited number of sites in Belluno it was possible to calculate the saturation deficit (vapour pressure deficit, VPD) since also the relative humidity was measured in the same moment. In the saturation deficit fomula (Perret et al., 2000) both the temperature measurements from datalogger (Temp$_{logger}$) as well as those from reconstructed daily MODIS LST maps (Temp$_{LST}$) were used. The relative humidity (rH) values from the datalogger was applied in both cases:

$$
\begin{aligned}
\text{VPD}_{\text{logger}} &= (1 - \text{rH}/100) * 4.9463 * e^{(0.0621 * \text{Temp}_{\text{logger}})} \quad (3.7) \\
\text{VPD}_{\text{LST}} &= (1 - \text{rH}/100) * 4.9463 * e^{(0.0621 * \text{Temp}_{\text{LST}})} \quad (3.8)
\end{aligned}
$$

While this usage of MODIS LST yet requires in-situ measurements of relative humidity, in future a purely satellite based solution shall be developed which is ideally only based on MODIS data. For existing approaches, see Green and Hay (2002) and Hashimoto et al. (2008) which are based on simple regression models (based on 8-day MODIS LST data) on saturation deficit and saturation vapor pressure at the mean daily LST estimated from satellite data with:

$$
\text{VPD} = 0.668 e^*(LST) - 0.015 T_{ltm} - 0.278 \quad (3.9)
$$

where $e^*(LST)$ is saturation vapor pressure at the mean daily LST estimated from satellite data and T_{ltm} is long-term mean air temperature. However, this relationship has not beed addressed in this thesis and is left to future research.

Results of the air temperature substitution measured in the field with MODIS LST are shown in Section 5.3.1.

3.7.2 Indices: Aggregated daily/monthly/annual indices and BIOCLIM variables

Numerous map based indices can be derived from the reconstructed daily LST time series by time series aggregation. In particular, daily/monthly/annual mean value maps of minimum/mean/maximum are relevant ecological indicators. Inputs are the four daily MODIS LST observations from the reconstructed LST data set which can be easily aggregated in a GIS framework. Results are shown in Section 5.3.2.

Furthermore, the BIOCLIM set of variables can be considered which has been used in a series of studies. The following list shows selected temperature based indicators of the WORLD-CLIM/BIOCLIM data set[13] were considered (Hijmans et al., 2005):

- BIO1 = Annual Mean Temperature;
- BIO2 = Mean Diurnal Range (Mean of monthly (max temp - min temp));

---

[13]WORLDCLIM/BIOCLIM data set `http://www.worldclim.org/bioclim.htm`

- BIO3 = Isothermality (BIO2/BIO7 * 100);
- BIO4 = Temperature Seasonality (standard deviation *100);
- BIO5 = Max Temperature of Warmest Month;
- BIO6 = Min Temperature of Coldest Month;
- BIO7 = Temperature Annual Range (BIO5-BIO6);
- BIO10 = Mean Temperature of Warmest Quarter;
- BIO11 = Mean Temperature of Coldest Quarter.

Since the calculation of these variables is rather straightforward with daily LST maps, results are not shown in this thesis.

Deriving Diurnal Temperature Range (DTR) and Monthly Mean Temperature Range (MMTR) from daily minimum/maximum temperatures

The diurnal temperature range (DTR) is the difference between daytime maximum and night-time minimum temperatures. Studies of global climatic change have shown that differential changes in daily maximum and minimum temperatures result in a narrowing of the DTR (Easterling et al., 1997).
In theory, DTR can be easily obtained from MODIS LST maps by searching pixelwise the minimum and maximum of the four daily map coverages and calculating the range. In practice, no-data pixels (due to clouds or those not satisfying the quality requirements) would be leading to wrong calculations, since the true minima and maxima can be missed. To overcome this problem, the reconstructed MODIS LST data were used here, although they may not perfectly reflect the true minima and maxima since the satellite overpass times do not coincide with the daily minimum and maximum temperatures (the closest overpass to the daily maximum is at 13:30 and the closest overpass to the daily minimum is at 01:30). Especially the night overpass is missing the daily minimum. Accepting this, from DTR maps it is possible to derive monthly mean temperature range (MMTR) maps.
Results are shown in Section 5.3.2.

Growing degree days (GDD)

Growing degree days (GDD) are a simple temperature-based index which is mostly used in phenology to predict for example flowering of plants or insect moulting (Pasotti et al., 2006). GDD is based on the idea that the development of for example a plant will occur only when the temperature exceeds a specific base temperature (T_{base}) for a certain number of days. This base temperature is species specific (e.g., 10 °C). GDD estimate the heat accumulation with a simple formula by taking the daily mean temperature (sometimes simply derived from the maximum and minimum temperatures) minus the base temperature:

$$GDD = T_{\mathrm{mean}} - T_{\mathrm{base}} \approx \frac{T_{\mathrm{max}} + T_{\mathrm{min}}}{2} - T_{\mathrm{base}} \qquad (3.10)$$

GDDs are calculated year-wise from the winter minimum, e.g. the 1st January of a year. Before calculating the average, any temperature below T_{base} is set to T_{base}. Also a maximum temperature is defined: usually values exceeding 30 °C are set to 30 °C as typically no further increase of the plants or insects growth rate is expected above that temperature.

The usage of MODIS LST data as a temperature data source assumes that the LST is close to air temperature. However, a fundamental problem arises when performing GDD calculation from MODIS LST maps rather than hourly based meteorological observations: since the reconstructed MODIS LST maps cover only four timestamps per day (at the known overpass times), the daily minimum and maximum values are not hit. A solution to this problem would be a curve fitting to describe the daily LST progression as a function (e.g., a shifted splines curve). This elaboration was not considered in this thesis. A remaining question is the error with direct MODIS LST GDD calculations since the maximum is lower and the minimum is higher which may compensate to some extent the lack of the true maximum and minimum. A verification is subject to future research. In a study based on the 8-day MODIS LST product, the GDD values were systematically overestimated (by 511 GDD for compared to Canadian meteo stations) (Hassan et al., 2007). Results based on daily MODIS LST are presented in Section 5.3.2, some discussion of GDD applied to mosquitoes is also found in Section 7.1.1.

Exceptional warm/cold seasons

Using temperature thresholding over multi-annual temperature averages, exceptional warm/cold seasons can be easily identified. If the number of events (i.e., pixels over or under a threshold) is significant over a time period, the season can be defined as outlier. In mountainous areas, an exceptional season is not necessarily found evenly distributed over the terrain.
Results are presented in Section 5.3.2.

3.7.3 Indices: Intra-annual short term trends

Aggregation of daily MODIS LST maps over several months allows the intra-annual short term trends to be determined; for example, the spring temperature increase gradient ("warming") and autumnal temperature decrease gradient ("cooling"). The latter has been already used in tick-borne encephalitis studies (Randolph et al., 2000; Rizzoli et al., 2007a; Carpi et al., 2008) (see also Section 1.1.1).

Autumnal cooling, spring warming   The decrease of the temperature in autumn ("autumnal cooling") is assessed with the year-wise linear regression of the monthly LST mean values of August, September and October. In addition, the annual maximum of the monthly mean LST values per pixel is selected. The cooling rate is the relationship between this monthly temperature decrease and the maximum LST value. Linear regression was chosen to take the mean temperature of September into account as the behavioural diapause of the tick is driven by temperature characteristics of all autumnal months, not only the difference in temperature between August and October: in case of a relatively warm September this leads to delayed autumnal cooling while a relatively cold September leads to increased autumnal cooling.
The spring warming rate calculation is done likewise: February, March and April monthly LST mean values are subjected to linear regression with the winter minimum temperature as a difference value.
Results are shown in Section 5.3.3.

4 Study area: Trentino, Bolzano and Belluno provinces

The area under study is situated in the central-eastern Alps in Northern Italy (see Fig. 4.2). The relevant provinces for this study are the Autonomous Provinces of Trento (Trentino) and Bolzano and the Province of Belluno. The study area was selected in a way that the Autonomous Province of Trento and the Province of Belluno were completely covered as well as the parts with lower elevation of the Autonomous Province of Bolzano (in order to reduce the computational time of the LST map reprocessing; no ticks nor mosquitoes are expected in high altitudes). The study region (see red box in Fig. 4.2) covers an area of 24,240 km^2 (120*202 km^2) with the boundaries: north latitude: 46:45:00N, south latitude: 45:36:50N, west longitude: 10:06:33E, and east longitude: 12:46:30E. The center coordinates are 11:26:31E and 46:10:55N. See Figure 4.1 for an overview map.

The geological upfolding of the Alps began at the turn of the Jurassic to the Cretaceous period and concluded about 30 to 35 million years ago in the Tertiary. The landscape was significantly modified during the Quaternary by Alpine glaciation. The river valleys have been eroded since then to relatively low elevations (a few hundred metres a.s.l.), surrounded by mountains in the range of 1,500-3,000 m a.s.l. In the southern Alps, the low altitudes of the valleys and the influence of the Mediterranean basin cause the climate to be much milder than on the surrounding heights.

Climatically, the Alps are affected by the European circulation as well as affecting it. The Alps are a barrier for air masses, leading to elevated precipitation with respect to adjacent areas. In the northern parts fog is a common phenomenon caused by cold air flow which is blocked by transversal mountain ridges. In contrast to that, the cold air flow is not blocked in the southern Alps, leading to significantly warmer temperatures (Locarno, Italy, has 18% more sunshine hours with respect to Zurich, Switzerland; Veit 2002).

The Alps are affected by four main climatic influences: from western directions arrives relatively mild, moist air of the Atlantic; from North cool or cold polar air; from East arrive moreover continental air masses which can be cold and dry in winter and hot in summer; and, from South warm air masses. In summer, thunderstorms are frequent. In winter, temperature inversions can occur in the valleys which may last for several days. In this case, valley floors can be significant colder (5-10 °C) than the slopes (Veit, 2002). The lapse rate is low in winter (0.4 °C/100 m) and higher in summer (0.7 °C/100 m) (Rolland, 2003) and close to the dry-adiabatic lapse rate of 1 °C/100 m in case of south-föhn. In case of inversion, the lapse rate can even become negative. Solar radiation is a driver for the local temperature regimes; radiation typically increases with increasing altitude (clouds and aerosols are limiting factors here). Besides vegetation, altitude and the presence of snow, relief and exposition play a major role in the determination of the

Figure 4.1: Biogeographical regions of the Alps with indication of study area (red box) (scale: 1:7,000,000)

radiation induced temperature pattern. These patterns are of enormous relevance for the spatial distribution of plants and organisms living on the soil surface.

The trans-alpine temperature gradient from north to south is emphasized with respect to the typical gradient in central Europe; the southern Alps are 2-4 °C warmer than the northern Alps (below 1,500 m a.s.l.; Veit 2002). One reason for this is the relative protection of southern parts against northern cold air masses.

While in the eastern Alps the northern and south alpine valleys are humid, the central Alps are dominated by dry-continental valleys. The amount of precipitation is higher in Southern Alps compared with the Northern Alps while it is inverse for the number of days with precipitation (Veit, 2002). The precipitation patterns are driven by luv-lee effects of the relief. Precipitation generally increases with altitude (60-200 mm/100 m) due to higher wind speed on the summits and other factors. Most precipitation in the summer period is caused in Southern Alps by convective thunderstorms and in the Northern Alps by cold fronts. While precipitation is more equally distributed over seasons in the Central Alps, the humid seasons are the summer in the Northern Alps while the winter in the Southern Alps.

The study area is divided by several dominant wide river valleys; the territory of the Autonomous Provinces of Trento and Bolzano is bisected by the Adige river valley from north to south, following the south-easterly drainage pattern in this area. The study area includes the Dolomites as well as foothills of the Alps and also small parts of the Po river plain. The provinces of Belluno, Bolzano and Trento have a very similar general geomorphometrical composition, with the elevation ranging from 65 m to 3,900 m (mean: 1,490 m) and an average slope of 26.2 degrees. Despite the overall similarities, the provinces show strong contrasts over short distances with small river plains, steep walls and high altitude plateaus.

The human population density in the region is low compared to the rest of Italy (498,000 in Bolzano Province, 519,000 in Trento Province and 214,000 in Belluno Province as of 2008). Up to 50% of the population is concentrated in the valley floors which is of relevance to the potential exposure to ectoparasites like ticks and mosquitoes (population below 500 m a.s.l.:
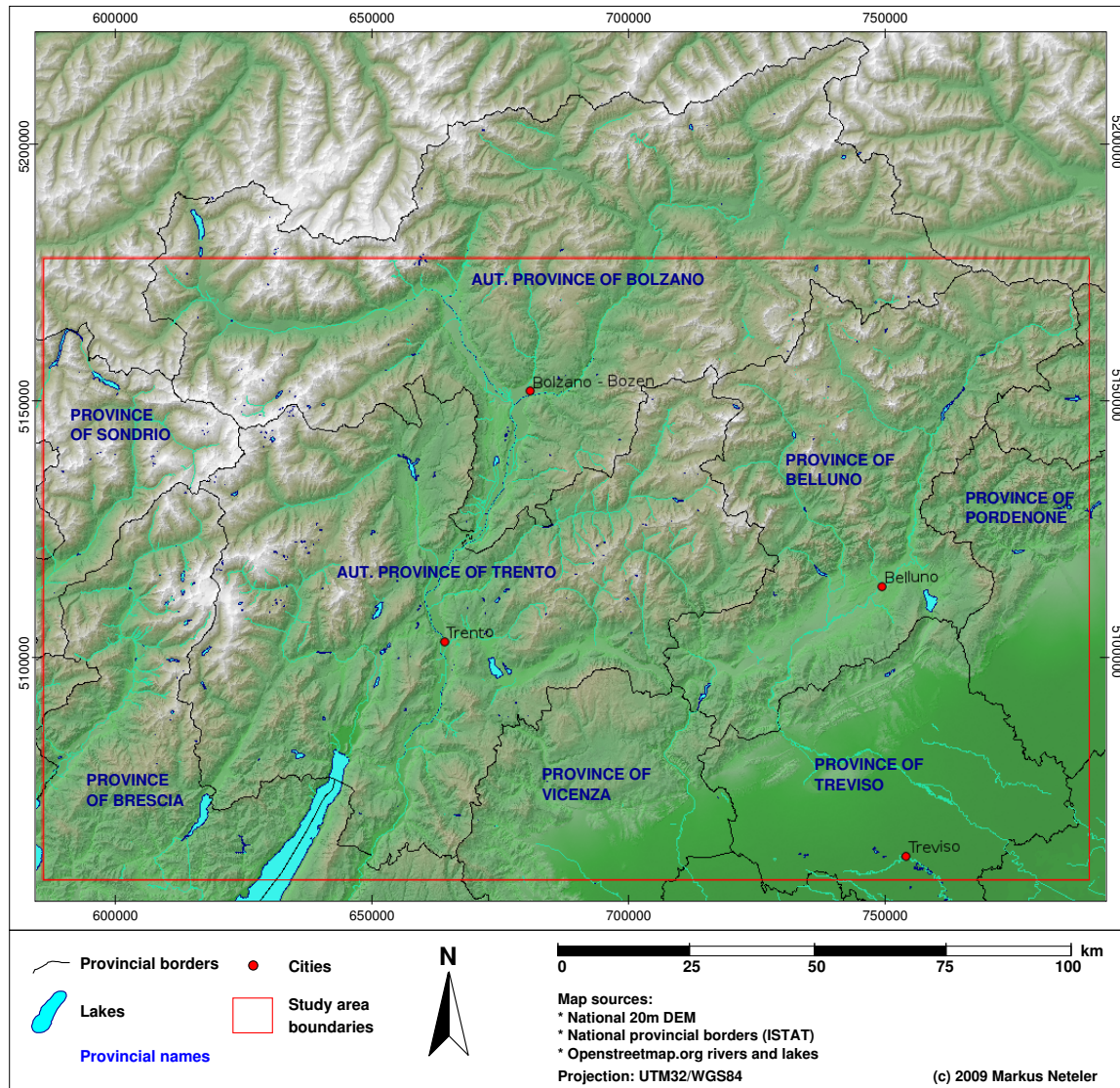
Figure 4.2: Study area in Northern Italy (scale: 1:1,428,000)

Prov. of Trento 57%, Prov. of Bolzano 42%, Prov. of Belluno 61%; author's GIS elaboration of LandScan 2007 map[1]).

The Autonomous Province of Trento can be classified into three distinct areas, driven by annual rainfall, altitude, geology and vegetation structure (Boato et al., 1988). The western part is an alpine area of high altitude. It is characterised by siliceous, igneous, dolomitic and calcareous rocks with a continental/alpine climate and precipitation above 1,100 mm/year (Cattadori et al., 1999). The central area is of lower altitude and consists of mixed sedimentary and calcareous rocks. Due to the influence of the Lake Garda the climate is subcontinental to submediterranean with less than 1,000 mm/year of precipitation. The eastern part is similar to the western part but also with porphyritic rocks. It receives more than 1,000 mm/year of precipitation. About 55% of the Autonomous Province of Trento is covered by coniferous and deciduous forests.

The Autonomous Province of Bolzano has joint borders with Austria and Switzerland and in-

---

[1]Oak Ridge National Laboratory LandScan Italy map, `http://www.cartographic.com/profile/LandScan.asp`

cludes a large part of the Dolomites. While the southern part of the province is characterised by a climate similar to the Aut. Province of Trento, the conditions are becoming more dry-continental northwards.

The typical vegetation of these two provinces is conifer forests (European and silver fir, larch, pine forests). The forest management has faced important philosophical and methodological changes, passing from the pre-19th century concept of a forest as a wood-producer, to that (beginning in the 1960s) of a complex ecosystem and with landscape, requalification, cultural, aesthetic, hydrogeological, soil protection, and biodiversity conservation functions (Rizzoli et al., 2009). The most important change was to adopt the the management of high stand woodlands using an uneven-age model. In northern Italy, especially in the eastern regions, most of the coppices are being converted into high stands forests, except where local communities continue to collect firewood (Rizzoli et al., 2009).

The alpine fauna is in this area more abundant than in many other Italian regions. The chamois and deer are common, as well as marmots, hares, squirrels and many bird species. Lynxes and brown bears were reintroduced into the region several years ago.

The terrain composition of the Province of Belluno is similar to that of the previously described provinces. About 60% of the area is covered by coniferous, deciduous and mixed forests (CORINE Land Cover 2000[2]). The province is crossed by the Piave river.

The valleys of Belluno are classified according to the Köppen-Geiger scheme as "temperate-cold" (Comunità Montana Feltrina, 2006) with continental conditions in the valley bottoms. In the summer relatively hot and in the winter relatively cold temperatures with regular thermal inversions are found. Although protected by pre-alpine mountains to the south, the regime is influenced from the Venetian Po river plane. The meteorological stations Feltre and Monte Avena show a "sub-litoral" pluviometric regime (two maxima and two minima in a year), while the Lamon station shows a more continental pattern close to the "alpine type" with only one peak (Comunità Montana Feltrina, 2006).

The alpine parts of the study area receive less than average rain in the central parts except for the southern mountain ranges. The snow cover is subject to high variability in snow cover duration and quantity.

---

[2]Corine land cover 2000 seamless vector database (CLC2000),
`http://dataservice.eea.europa.eu/dataservice/metadetails.asp?id=950`

5 Results: Land surface temperature time series reconstruction, validation and extraction of climatic parameters

5.1 Reconstructed LST time series maps

As outlined in Section 3.2, the processing and reconstruction of daily LST maps requires a series of steps. Incomplete maps due to cloud contamination or other problems (haze, aerosol, pixel failure, etc.) are turned into complete maps which are much more convenient for GIS based epidemiological applications. The year-wise processed number of MODIS LST maps (current product level V005) is shown in Table 5.1. The values given in the column "Maps processed" is the number of reconstructed maps while "Maps theoretically" indicates the potential number of LST maps as a function of days in the year and operation of the satellites. A few raw LST maps are missing from the NASA archives for unknown reasons, these maps have been treated in this thesis as fully cloud covered maps. In total 11,179 LST maps were processed for the study area with 8,017 maps reconstructed from the actual map gradients and 3,162 maps from a 16-day period model.

5.1.1 Selected reconstructed LST maps

From the more than 11000 LST maps, some selected examples are shown to illustrate the steps of reconstructing the maps and the performance of the approach in different data situations. Results are presented for the four seasons, in different years considering the day and night overpasses. The differences between the original MODIS LST map and the final LST map have been assessed by subtracting pixelwise the final LST map interpolated with volumetric regularised splines with tension (RST), from the raw LST map. For comparison reasons, the same color table was applied to all maps.

Winter The example of a winter MODIS LST daytime map reprocessing is shown in Fig. 5.1. The chosen November day was unusually warm for the season, with a high air temperature daily maximum (air temperature of 16.6 °C was measured in Trento-Sud at 11:00 local solar time, about 30min later than the satellite overpass; in Avio 18.1 °C). This pattern is also reflected in the final RST map. Only small map areas had to be reconstructed, the overall reconstruction process included basically outlier removal and smoothing. For a more detailed comparison between meteorological station measurements and this map, see Tab. A.1.
In Figure 5.2, an example for a map with partial snow cover is shown. In this period, a snow

Figure 5.1: **Winter MODIS LST day map reprocessing (1 Nov 2001, all maps in UTM32/WGS84 metric grid, map scale 1:2,600,000)**
Raw LST map (upper left), map outlier filtered via histogram (upper right), outlier filtered via gradient (central left), volumetric splines reconstructed (RST, central right), differences map between raw and RST map (lower left), scatterplots of raw (black), histogram & gradient filtered (yellow) and RST (green) maps including linear regression gradients (lower right). Reprojection and other artifacts have been smoothed out in the LST map reconstruction process. This day was unusually warm (an air temperature of 16.6 °C was measured in Trento-Sud at 11:00 local solar time; 18.1 °C in Avio) which is reflected in the final RST map. The final gradient (green) results slightly modified with respect to the raw LST map gradient since outliers were removed. See also Fig. 5.10 and Tab. A.1.
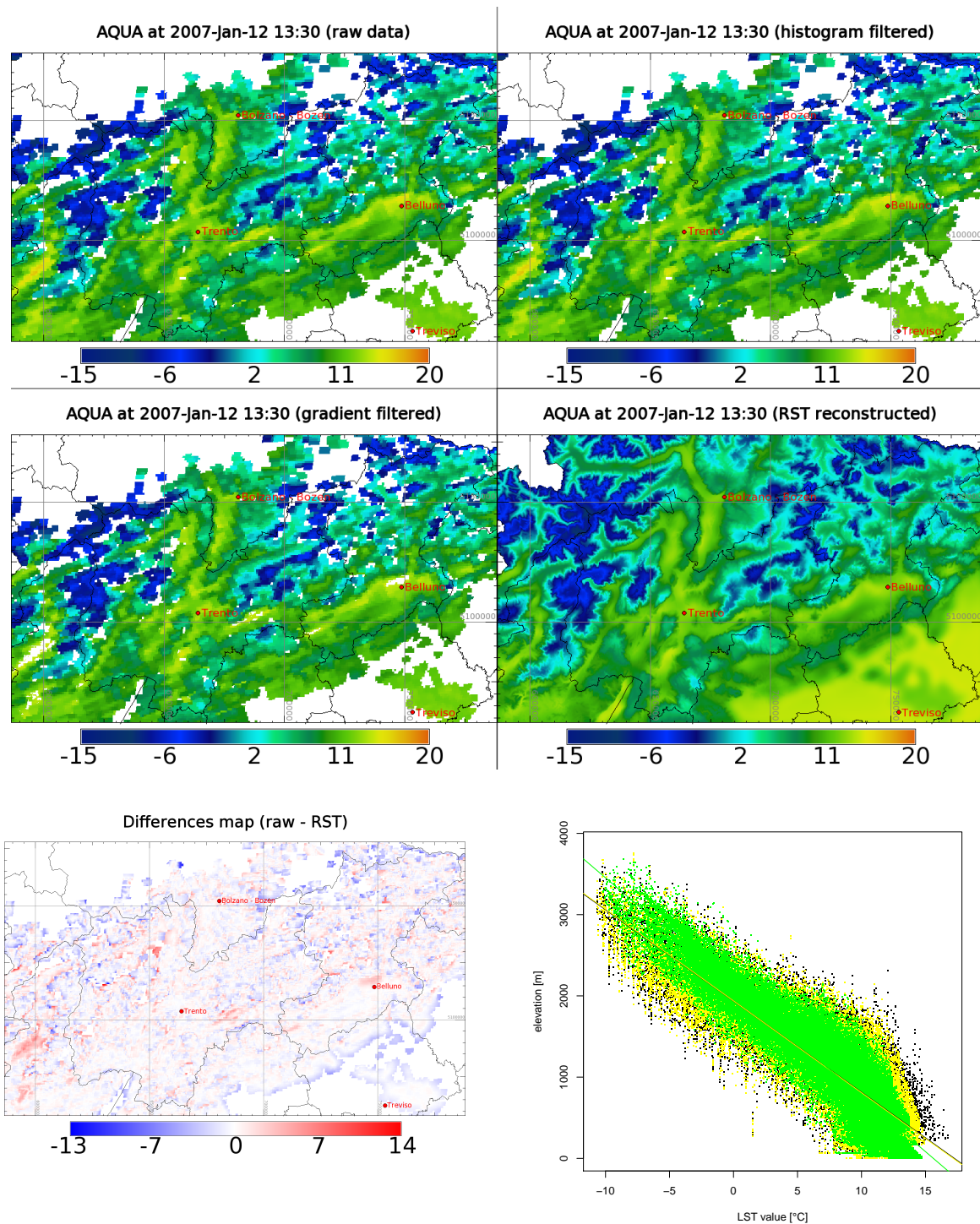
Figure 5.2: **Winter MODIS LST day map reprocessing (12 Jan 2007, all maps in UTM32/WGS84 metric grid, map scale 1:2,600,000)**
Raw LST map (upper left), map outlier filtered via histogram (upper right), outlier filtered via gradient (central left), volumetric splines reconstructed (RST, central right), differences map between raw and RST map (lower left), scatterplots of raw (black), histogram & gradient filtered (yellow) and RST (green) maps including linear regression gradients (lower right). Reprojection and other artifacts have been smoothed out in the LST map reconstruction process. January 2007 was an unusually warm month. Air temperatures of 18.3 °C in Trento-Sud at 11:00 local solar time and 11.2 °C in Arco were recorded. The low temperature areas in higher altitudes are due to snow cover (confirmed for several meteo stations). The final gradient (green) results slightly modified with respect to the raw LST map gradient since outliers were removed. See also Fig. 5.10 and Tab. A.2.

Year	Maps processed	Maps theoretically	Comment
2000	574	622	Terra operative since 24 Feb 2000, data since 6 Mar 2000
2001	692	730	Terra
2002	1021	1100	Terra + Aqua: Aqua operative since 4 Jul 2002, data since 8 Jul 2002
2003	1370	1460	Terra + Aqua fully operative
2004	1462	1464	Terra + Aqua
2005	1460	1460	Terra + Aqua
2006	1460	1460	Terra + Aqua
2007	1444	1460	Terra + Aqua
2008	1454	1464	Terra + Aqua
2009	242	1460	Terra + Aqua (data processed incl. 2/2009)

Table 5.1: **Number of processed MODIS LST V005 subsets per year (MODIS tile h18/v04; period 3/2000 to 2/2009)**
In total 11,179 maps were processed for the study area: 8,017 maps were reconstructed from the actual map gradients and 3,162 maps from a 16-day period model.

cover occurred at higher altitudes (confirmed for Passo Tonale and Folgaria meteorological stations, absent in Andalo)[1] which is reflected in low LST values in these areas. Air temperatures of 18.3 °C was measured in Trento-Sud at 11:00 local solar time; 11.2 °C in Arco. The low temperature areas in higher altitudes are due to snow cover (confirmed for several meteo stations). The final gradient (green) results slightly modified with respect to the raw LST map gradient since outliers were removed. A more precise verification of the snow extent could be done with the MODIS snow products MOD10A1 and MYD10A1 (see Tab. 2.1). January 2007 was an unusually warm month, which is reflected in the elevated temperatures. For a more detailed comparison between meteorological station measurements and this map, see Tab. A.2.

Spring   Figure 5.3 shows a night time spring season map based on a raw LST map with significant void data areas. Despite that, the map gradient derived from the data was still statistically significant due to the pixel distribution in various altitudes (see raw gradient) and could be used to reconstruct the map. The meteorological station of Trento-Sud measured an air temperature of 6.2 °C at 02:00 local solar time; in Arco 6.8 °C. The final LST map values are a few degree Celsius lower than the air temperature, probably due to moisture presence (dew). These differences are even larger elsewhere, see for example Vancutsem et al. (2010). For a more detailed comparison between meteorological station measurements and this map, see Tab. A.3.
Figure 5.4 shows a map with a large range of LST values: here snow at higher altitudes, causing low LST values, which contrast the significantly higher LST values at the valley floors. For this date, instantaneous air temperature measurements are available. They are close to the observed LST values (23:00 local solar time: 14.5 °C at Trento-Sud and 16.4 °C at Arco). The final LST map shows systematically values below the air temperatures (approximately 2-3 °C less). For a more detailed comparison between meteorological station measurements and this map, see Tab. A.4.

---

[1]Meteotrentino – Snow data,
`http://www.meteotrentino.it/AspWeb/Monitoraggi/stations/yeti/Campi_neve/mappa/mappa_neve.asp?ID=141`
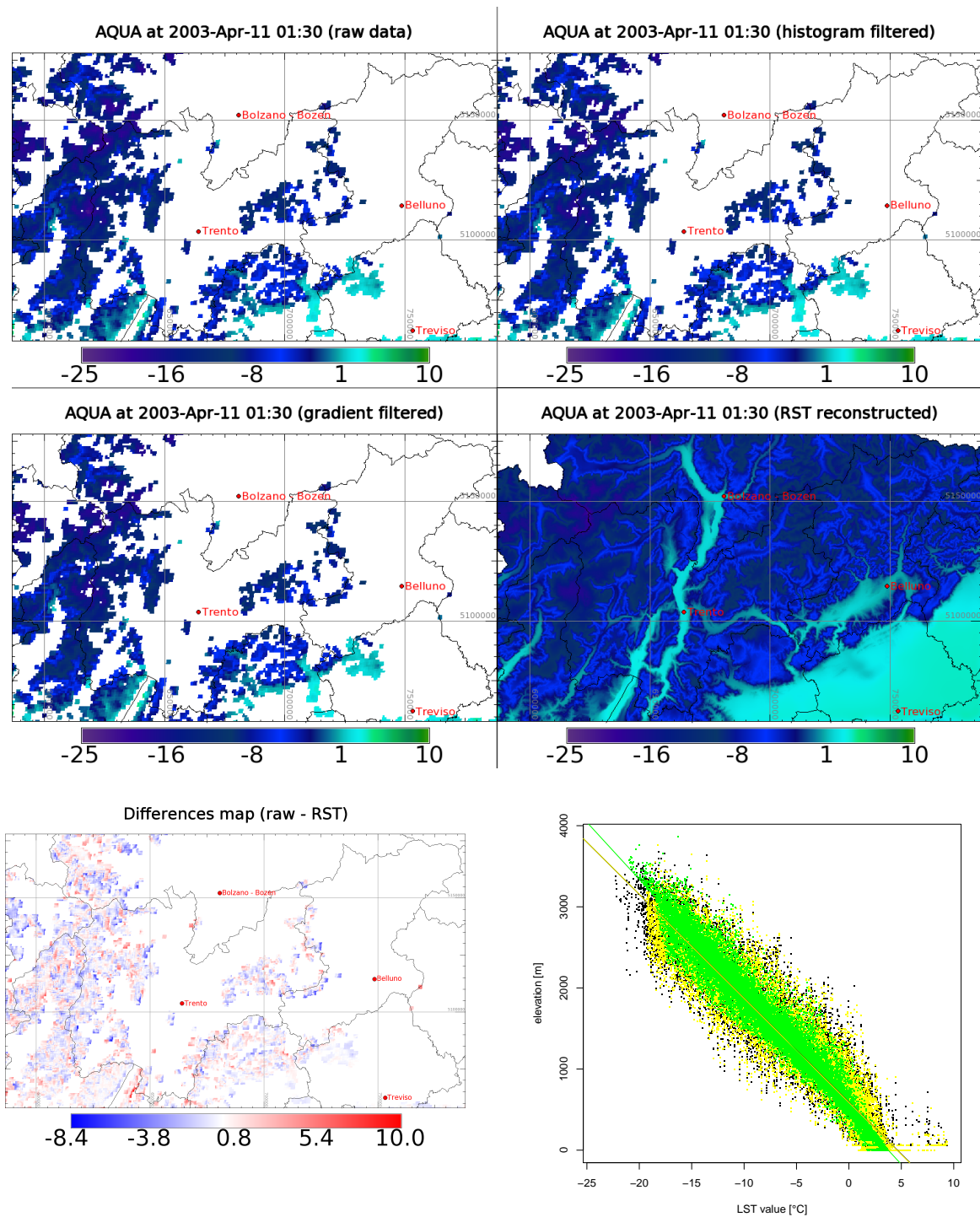
Figure 5.3: **Spring MODIS LST night map reprocessing (11 Apr 2003, all maps in UTM32/WGS84 metric grid, map scale 1:2,600,000)**
Raw LST map (upper left), map outlier filtered via histogram (upper right), outlier filtered via gradient (central left), volumetric splines reconstructed (RST, central right), differences map between raw and RST map (lower left), scatterplots of raw (black), histogram & gradient filtered (yellow) and RST (green) maps including linear regression gradients (lower right). Reprojection and other artifacts have been smoothed out in the LST map reconstruction process. In Trento-Sud an air temperature of 6.2 °C was measured at 02:00 local solar time; 6.8 °C in Arco. The final LST map shows systematically a few degree Celsius less than the air temperature. The final gradient (green) results slightly modified with respect to the raw LST map gradient since outliers were removed. See also Fig. 5.11 and Tab. A.3.
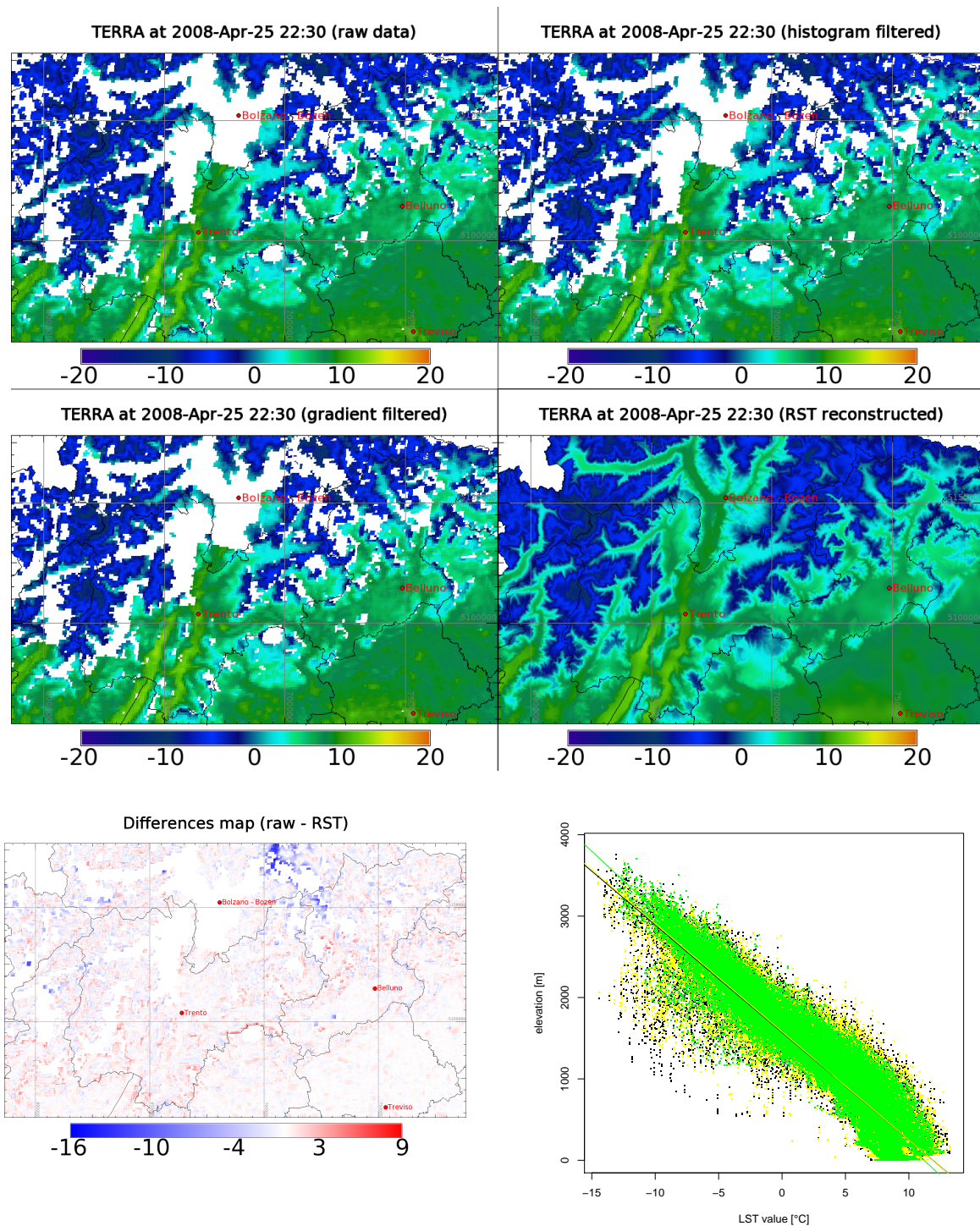
Figure 5.4: **Spring MODIS LST night map reprocessing (25 Apr 2008, all maps in UTM32/WGS84 metric grid, map scale 1:2,600,000)**
Raw LST map (upper left), map outlier filtered via histogram (upper right), outlier filtered via gradient (central left), volumetric splines reconstructed (RST, central right), differences map between raw and RST map (lower left), scatterplots of raw (black), histogram & gradient filtered (yellow) and RST (green) maps including linear regression gradients (lower right). Reprojection and other artifacts have been smoothed out in the LST map reconstruction process. The low temperatures in higher altitudes are due to snow cover which contrast the significantly warmer valley floors. Air temperature of 14.5 °C was reported for Trento-Sud at 23:00 local solar time, about 30min later than the satellite overpass; 16.4 °C in Arco, while the final LST map shows approximately 2 °C less. The final gradient (green) results slightly modified with respect to the raw LST map gradient since outliers were removed. See also Fig. 5.11 and Tab. A.4.
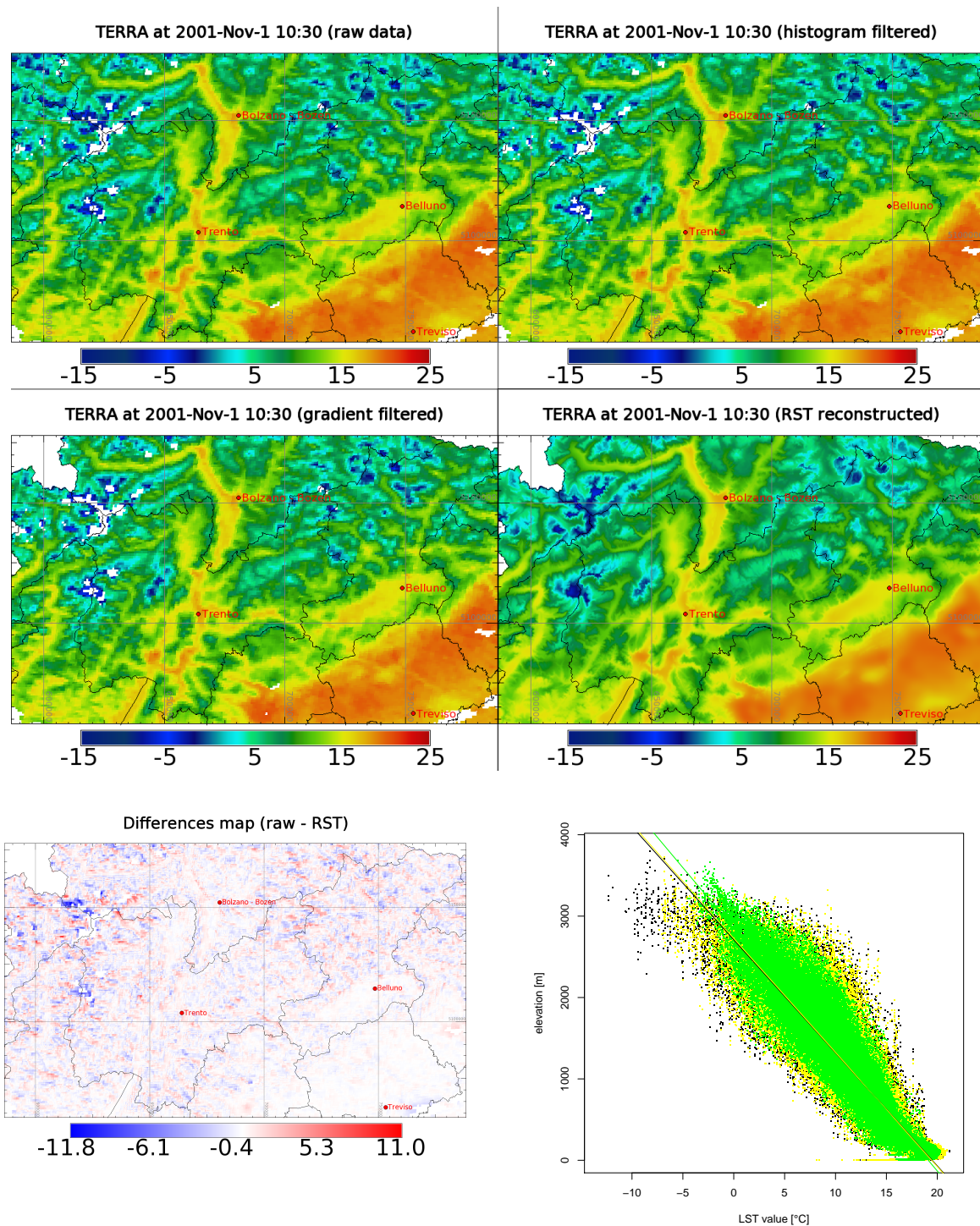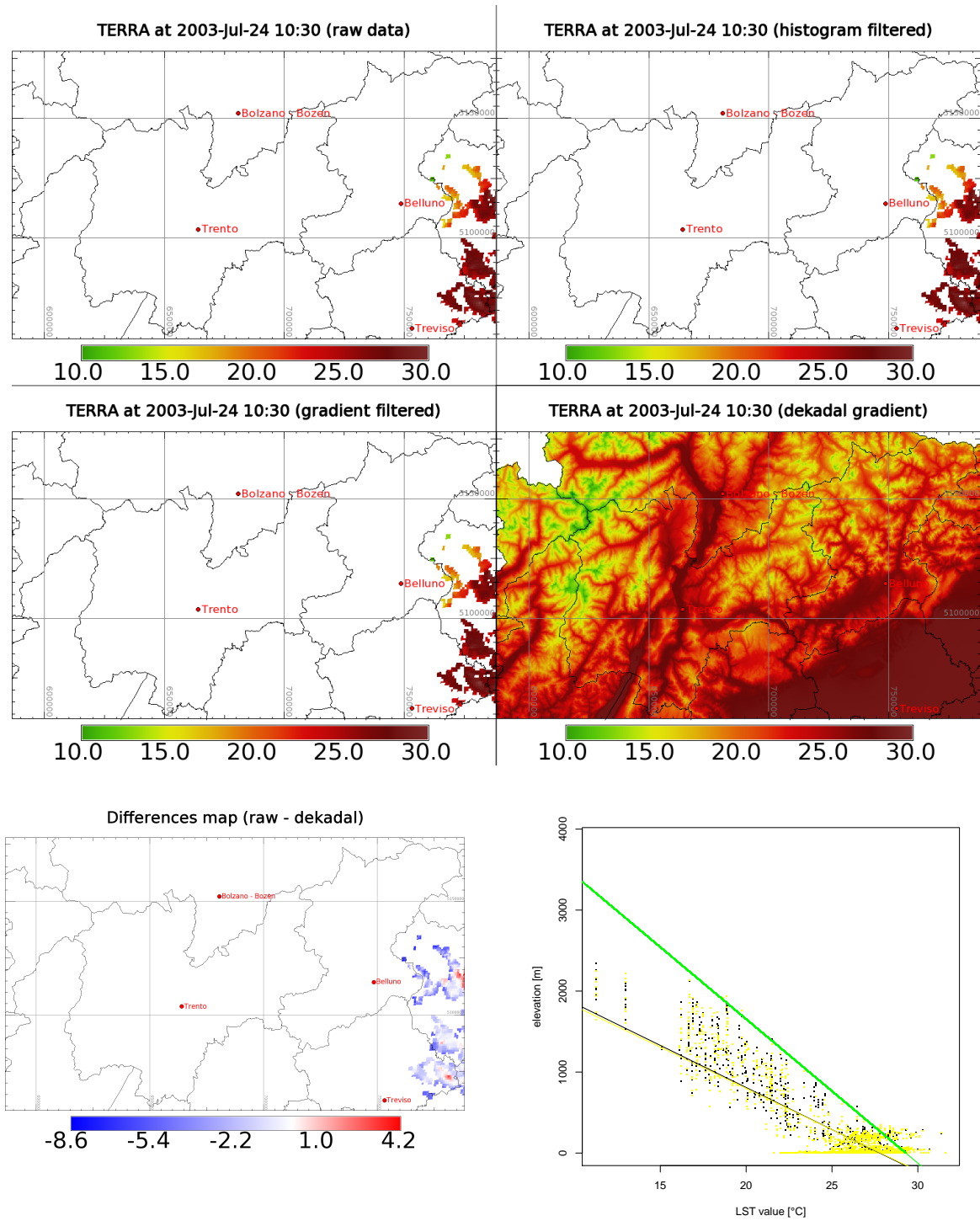
Figure 5.5: **Summer MODIS LST day map reprocessing (24 Jul 2003, all maps in UTM32/WGS84 metric grid, map scale 1:2,600,000)**
Raw LST map (upper left), map outlier filtered via histogram (upper right), outlier filtered via gradient (central left), volumetric splines reconstructed (RST, central right), differences map between raw and RST map (lower left), scatterplots of raw (black), histogram & gradient filtered (yellow) and RST (green) maps including linear regression gradients (lower right). Reprojection and other artifacts have been smoothed out in the LST map reconstruction process. Due to lack of sufficient number of pixels the average gradient of 16-day period no. 13 was used (average of 8 years), no interpolation has been used but the linear 16-day gradient model was applied. Subsequently, the difference map shows a systematic shift to negative temperatures for the available pixels. The final gradient (green, a line) results substantially different with respect to the raw LST map gradient since the 16-day gradient has to be used. See also Fig. 5.12 and Tab. A.5.

Summer   Figure 5.5 presents a map with an insufficient number of valid pixels. For this reason, the average gradient of 16-day period no. 13 was used (based on data of 8 years for this 16-day period). The difference map shows a systematic shift to negative temperatures, since, apparently, the actual temperature was deviating from the 8-years average. While no precipitation was recorded for this day in Trentino[2], cloud coverage prevented Terra/MODIS from recording the LST on ground in most parts of the study area. For this reason, the resulting LST map was not interpolated but is based on the linear 16-day period gradient model. Subsequently, the final gradient (green, a line) results substantially different with respect to the raw LST map gradient. For a more detailed comparison between meteorological station measurements and this map, see Tab. A.5.

Autumn   Finally, an autumn night situation is shown in Figure 5.6. The final LST values are similar to those of meteorological stations. In Trento-Sud air temperature of 5.8 °C was measured at 02:00 local solartime and 8.9 °C in Arco. The Garda lake (south-west in the maps) shows yet elevated water temperatures in this period. The relatively warm Garda lake LST pixels are maintained in the reconstruction process and appear in the lower right quadrant of the scatterplot as well. For a more detailed comparison between meteorological station measurements and this map, see Tab. A.6.

LST data improvements through 1000 m to 200 m spatial resolution increase   As outlined in Section 3.1.2, the spatial oversampling from 1000 m original pixel size to 200 m is performed in the MODIS LST data reprojection step. The spatial support for this increase is gained thanks to the use of the map/16-day period temperature gradient model and a 200 m elevation model in the volumetric splines interpolation step. In correspondence to Figure 3.2, the effects on the final LST map are shown for the Riva del Garda area in Figure 5.7. While the LST pixel are clearly visible in the original map, they become smooth in the final LST map due to the map creation from the gradient model.

[2]Meteotrentino data online, `http://www.meteotrentino.it/AspWeb/Monitoraggi/monitoraggi.asp?ID=3`
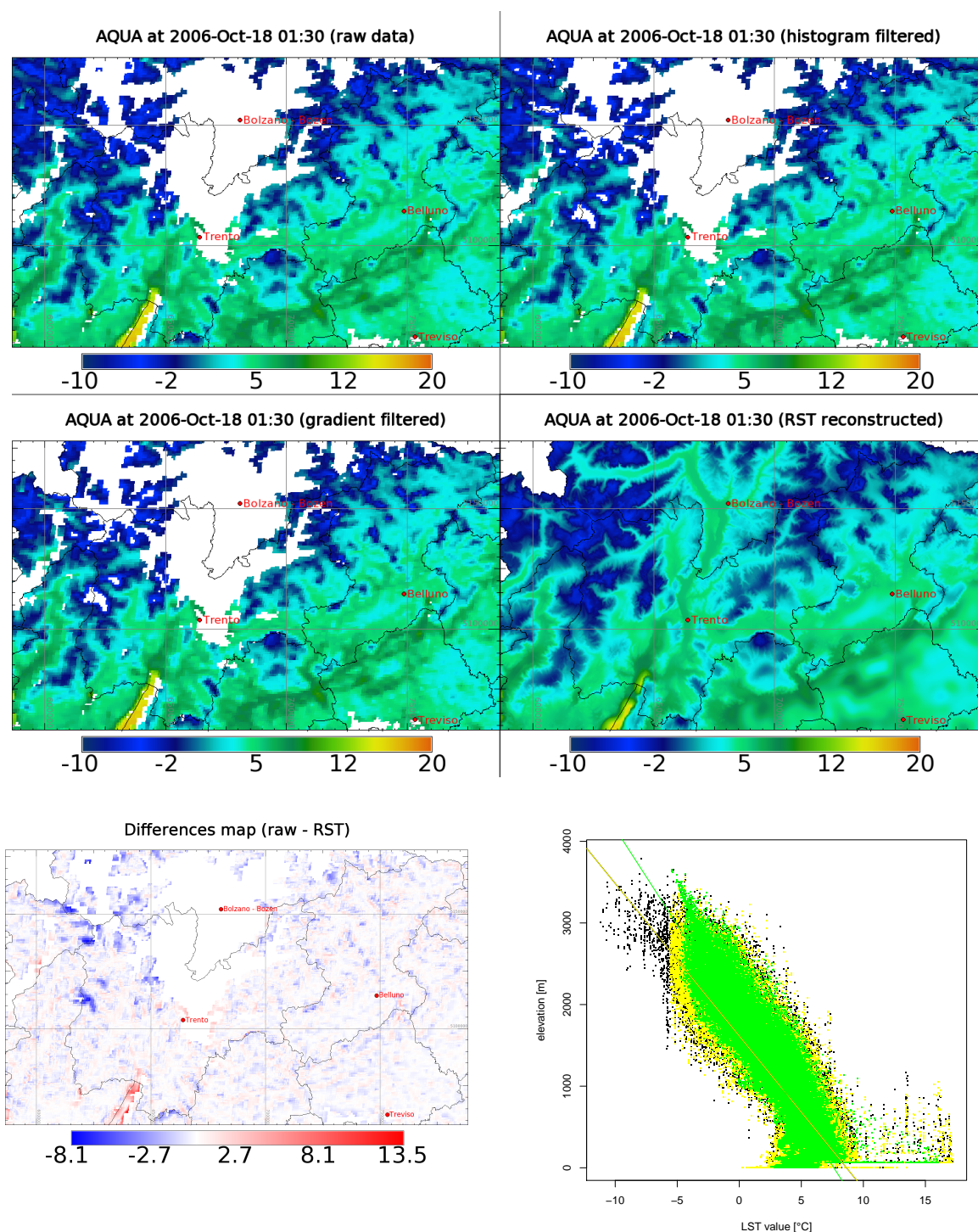
Figure 5.6: **Autumn MODIS LST night map reprocessing (18 Oct 2006, all maps in UTM32/WGS84 metric grid, map scale 1:2,600,000)**
Raw LST map (upper left), map outlier filtered via histogram (upper right), outlier filtered via gradient (central left), volumetric splines reconstructed (RST, central right), differences map between raw and RST map (lower left), scatterplots of raw (black), histogram & gradient filtered (yellow) and RST (green) maps including linear regression gradients (lower right). Reprojection and other artifacts have been smoothed out in the LST map reconstruction process. In Trento-Sud air temperature of 5.8 °C was measured at 02:00 local solar time and 8.9 °C in Arco which is reflected in the final LST map. The Garda lake (south-west in the maps) shows yet elevated water temperatures in autumn. The final gradient (green) results slightly modified with respect to the raw LST map gradient since outliers were removed. The relatively warm Garda lake LST pixels are maintained in the reconstruction process and appear in the lower right quadrant of the scatterplot as well. See also Fig. 5.12 and Tab. A.6.

TERRA at 2001-Nov-1 10:30 (raw data)
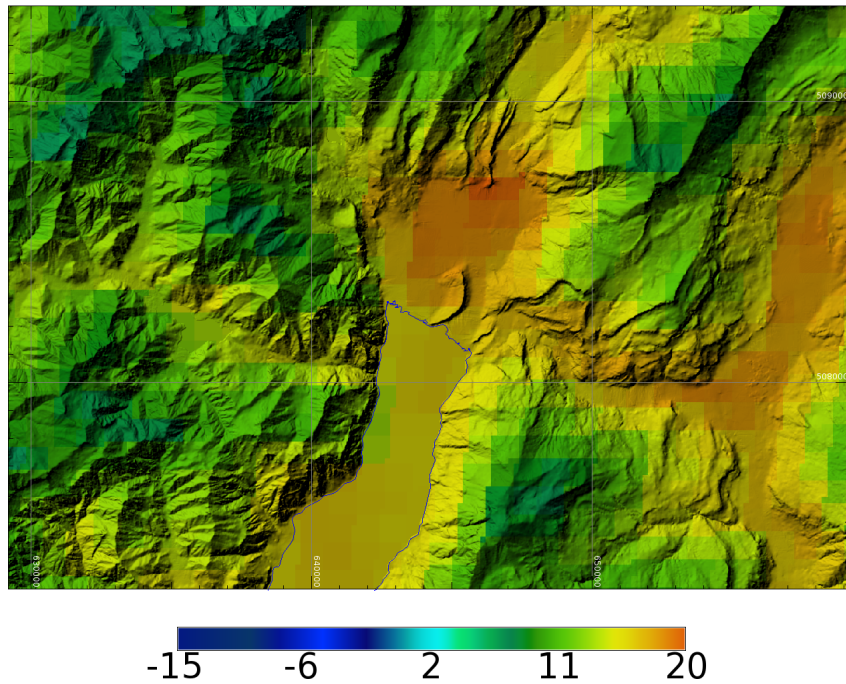
TERRA at 2001-Nov-1 10:30 (RST reconstructed)
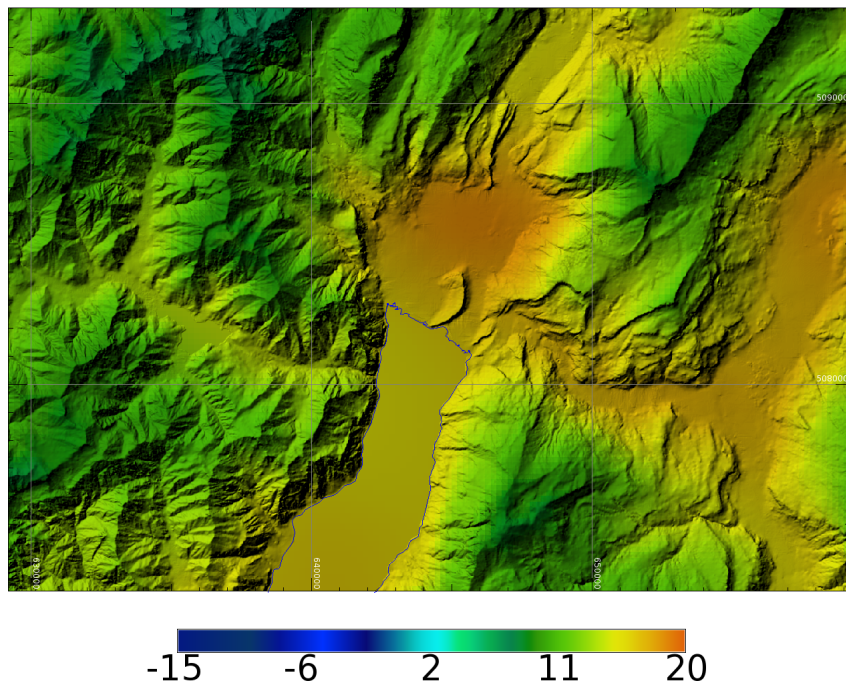
Figure 5.7: **MODIS LST map draped over shaded terrain to illustrate the effect of spatial resolution increase from originally 1000 m pixel size to finally 200 m (UTM32/WGS84 metric grid, map scale 1:25,000)**
The spatial support is gained thanks to the use of the map/16-day period temperature gradient model and a 200 m elevation model in the volumetric splines interpolation step (example: MODIS LST Terra 1 Nov 2008 day (10:30 local solar time), northern part of Garda lake; based on actual map gradient; background map: 20 m DEM). Compare also Fig. 3.2 for the position of the pixels.

5.2 Comparison of reconstructed LST maps to other related data sources

Basically two main resources are available to perform comparisons with MODIS LST maps to 1) time series of instantaneous meteorological observations, and 2) LANDSAT-TM5 or TM7 (ETM+) thermal maps. In this section, a series of tests are provided. But before that a cross-check of LST maps against elevation is performed to assess the variance that is not explained through the temperature-elevation relationship.

5.2.1 Cross-check of LST maps against elevation

As outlined in Section 3.5.1, LST maps contribute to the identification of microclimatic situations in the temperature distribution in (complex) terrain. For the following area, selected as it shows relatively homogeneous landuse/landcover, the relationship of the temperature and elevation has been assessed for South-north exposed slopes in the subarea Eastern Valsugana (Trentino; 11.5993E, 46.02172N).

Figure 5.8 shows that LST does not strictly follow the altitude. Naturally, the southern exposed slopes have higher temperatures than the northern exposed slopes (see SE-quadrant in the map) but not everywhere (map center near Selva). The adjacent structure plays a role as well (shading effects etc). The temperature variance, which remains unexplained by the typical temperature-elevation relationship, is more interesting since it indicates the ability of satellite data to differentiate temperatures over the terrain. This cannot be easily reached when interpolating data from meteorological stations as the commonly used interpolation methods are typically more generalising.

The variance unexplained by the altitude is for example useful to identify microclimatic situations. This ideally requires complete raw LST maps since the more parts of the LST map that have to be reconstructed with the temperature-elevation gradient model, the less details remain as the elevation model is becoming a dominant factor in the reconstruction.

During night time, the situation is rather different: the temperature profile significantly follows the terrain profile (see Figure 5.9). The linear regression gradient shows much more correspondence between temperature and elevation (R^2=0.7758) for the 22:30hs local solar time overpass. Here the LST map corresponds fairly well to the linear model which means that in the case of map reconstruction (i.e., in the case of the use of the 16-day period model) the resulting LST maps is close to the real situation.

5.2.2 Comparison of LST to meteorological time series

To assess the performance of the LST reconstruction, the final LST maps are compared to instantaneous measurements of meteorological stations (for introduction, see Section 3.5.2). For each station, up to four daily observations can be directly compared at 01:30, 10:30, 13:30 and 22:30hs local solar time. The positions of the selected stations are indicated in Tab. 3.4.2 in Section 3.4.2. Furthermore, the Belluno tick sampling contains meteorological information including the air temperature.
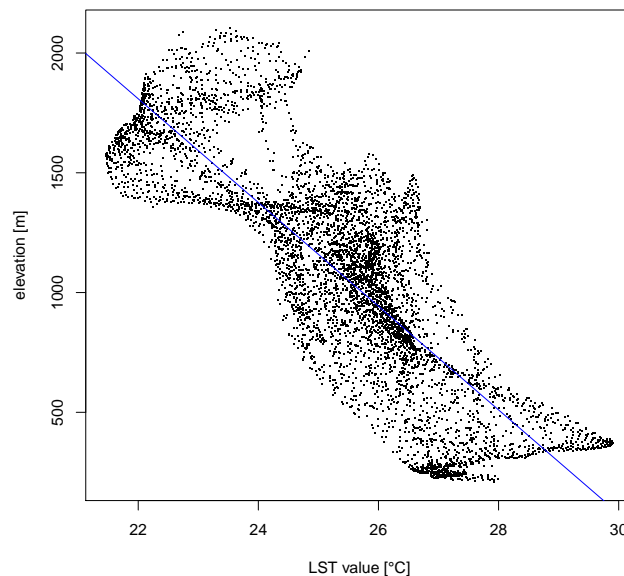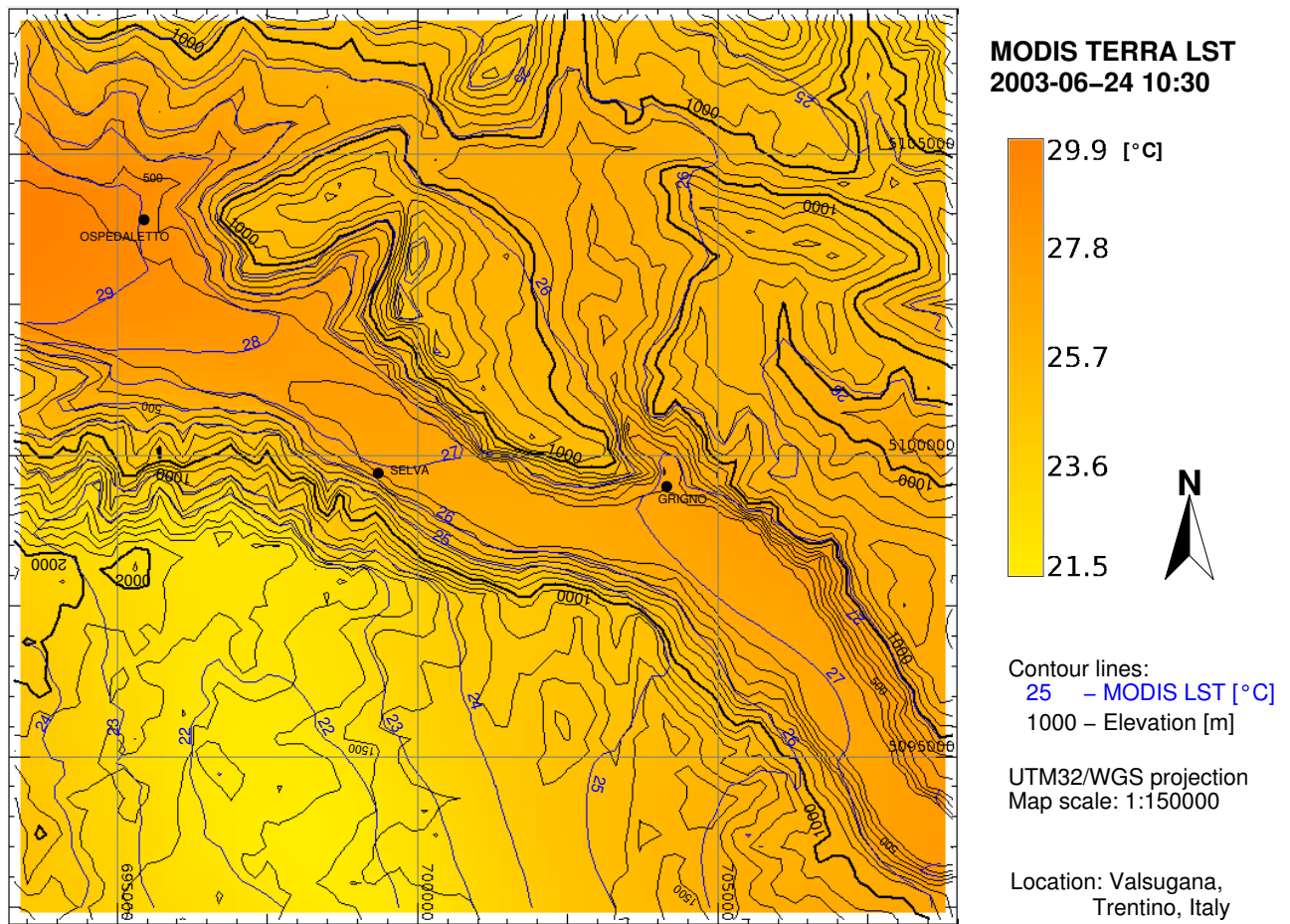
Figure 5.8: **Summer MODIS LST day versus contour lines (map in UTM32/WGS84 metric grid, map scale 1:75,000)**
Reconstructed LST map based on complete raw LST map (upper map) and related LST-elevation scatterplot with linear regression gradient (lower graph). The LST map shows a daytime temperature field pattern (blue contour lines) which is partially independent from the altitude (black contour lines). Not surprisingly, especially the southern exposed slope show higher temperatures than the northern exposed slopes (see SE-quadrant). However, this difference is reduced near Selva (map center). The LST pixels in the scatterplot shows partially strong deviations from the related linear regression gradient (R^2=0.6711) due to the irradiation/exposition differences.
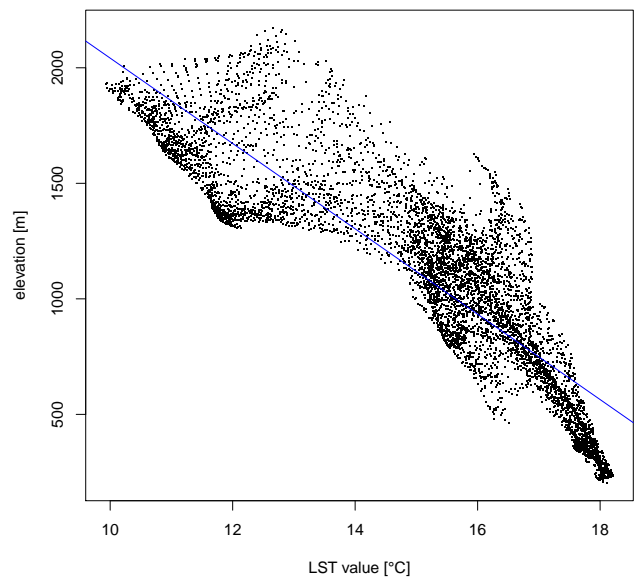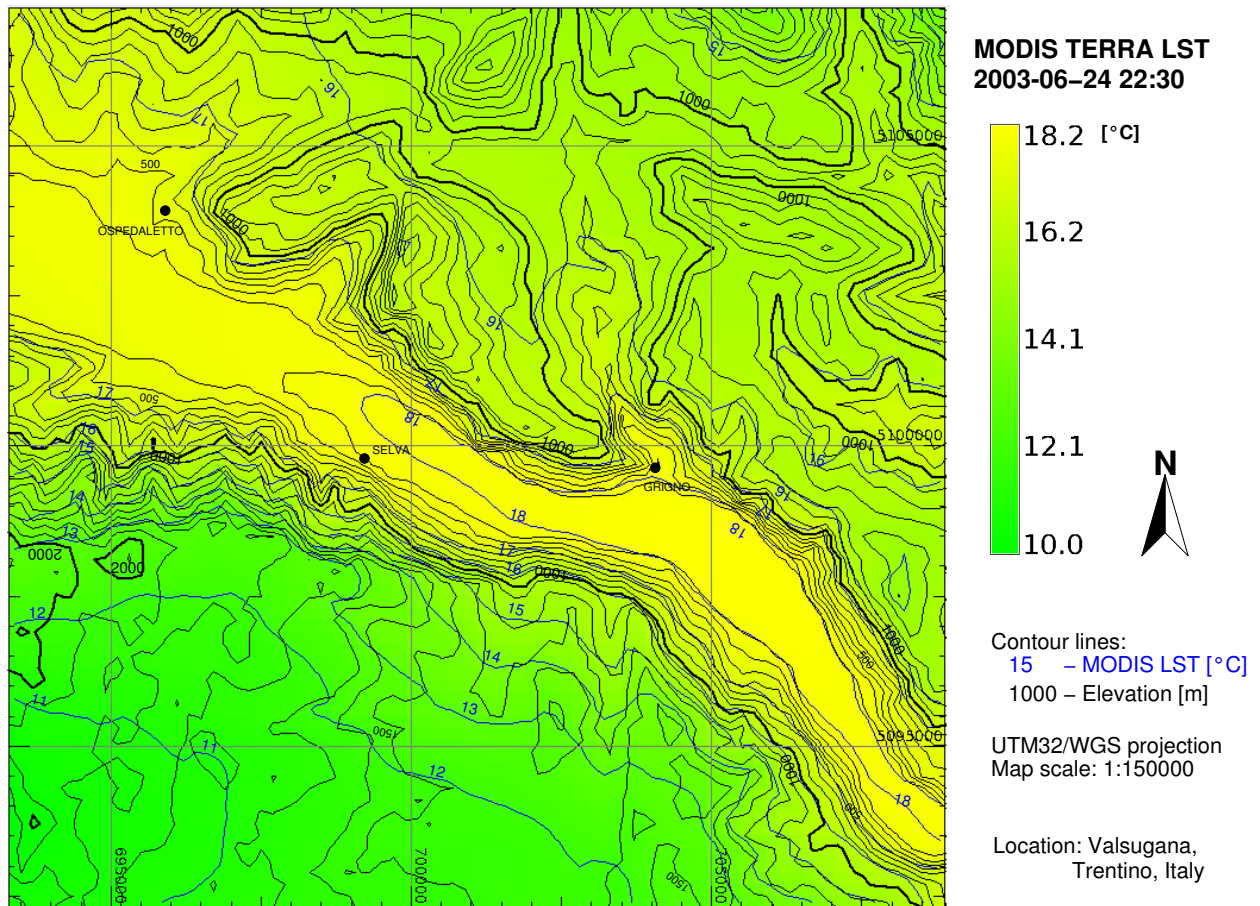
Figure 5.9: **Summer MODIS LST night versus contour lines (map in UTM32/WGS84 metric grid, map scale 1:75,000)**
Reconstructed LST map based on complete raw LST map (upper map) and related LST-elevation scatter-plot with linear regression gradient (lower graph). The LST map shows a nighttime temperature field pattern (blue contour lines) which is mostly dependent on the altitude (black contour lines). The LST pixels in the scatterplot shows limited deviations from the related linear regression gradient (R^2=0.7758) due to the absence of irradiation.
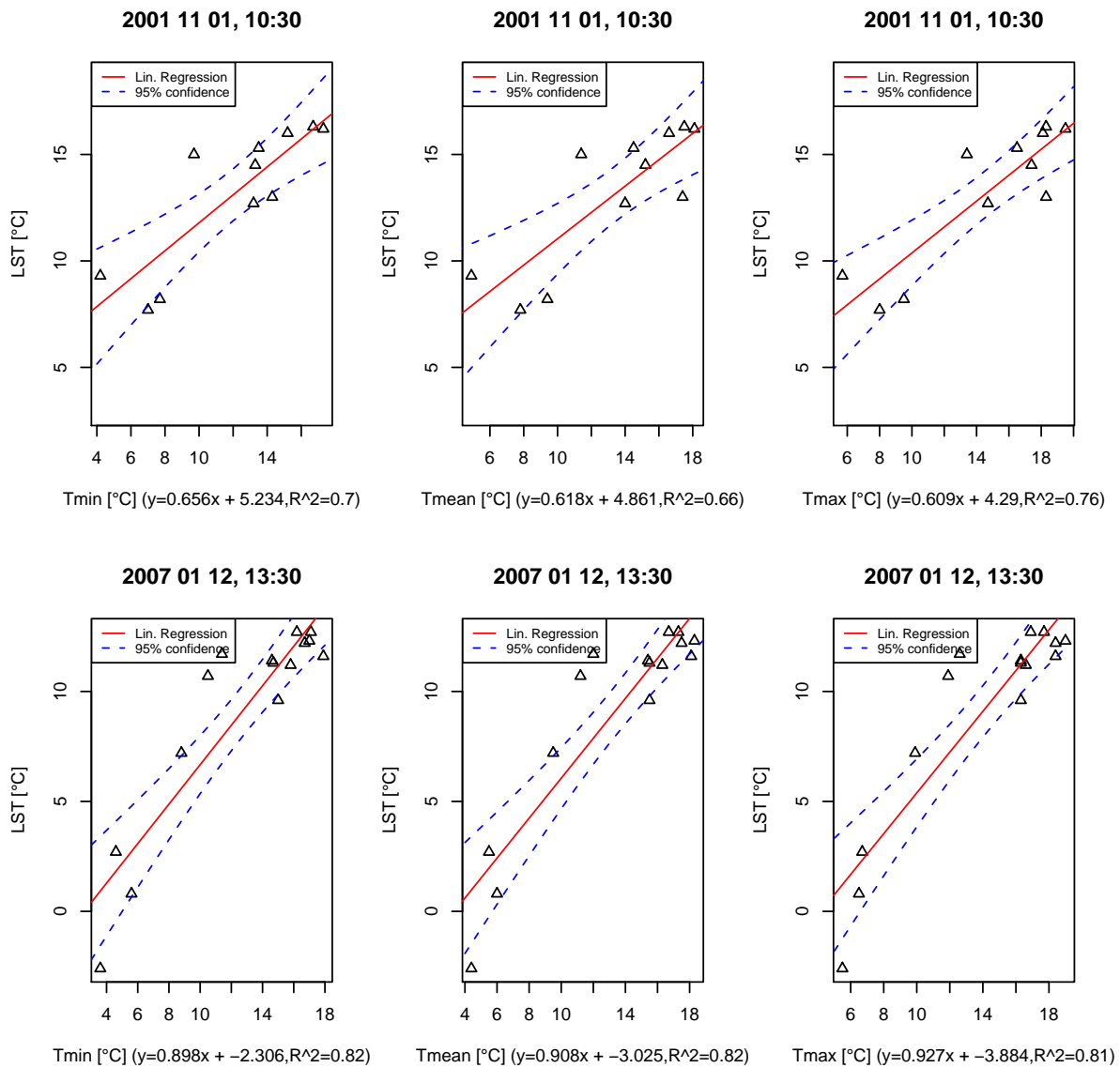
Figure 5.10: **Comparison of air temperature data (at height 2 m) with MODIS LST data from reconstructed LST map**
Upper graphs: Comparison of air temperature data (at height 2 m) with MODIS LST data from reconstructed LST map (10 % void in the filtered map; actual map gradient used) in the position of the stations (date: 1 Nov 2001, air temperatures from 10:00-11:00 local solar time; MODIS LST 10:30). See also LST maps in Figure 5.1 and the original values in Table A.1.
Lower graphs: Comparison of air temperature data (at height 2 m) with MODIS LST data from reconstructed LST map (38 % void in the filtered map; actual map gradient used) in the position of the stations (date: 12 Jan 2007, air temperatures from 13:00-14:00 local solar time; MODIS LST 13:30). See also LST maps in Figure 5.2 and the original values in Table A.2. The stations are listed in Table 3.4.2.

Air temperature data from meteo-stations versus reconstructed MODIS LST data

For the four seasons, selected maps (those presented earlier in Section 5.1) were compared to instantaneous measurements obtained from FEM-CTT stations. The stations are listed in Table 3.4.2 with an elevation range from 84 m a.s.l. (Arco) to 2002 m a.s.l. (Malga Flavona).

Winter   Figure 5.10 shows comparisons between air temperatures (at height 2 m) and MODIS LST daytime data from reconstructed LST map (in the filtered input LST map 10 % were void, see Fig. 5.1 and Tab. A.1) for the position of several stations. Several stations were not functional in that day. No apparent temperature shift between air temperature and LST is observed. It was unusually warm in the beginning of Nov 2001 with air temperatures and LST up to 18 °C.

The analysis of a second winter daytime map to station data is also shown in Figure 5.10 (in the filtered input LST map 38 % were devoid, see Fig. 5.2 and Tab. A.2). January 2007 was unusually warm with air temperatures reaching 18 °C and LST reaching almost 13 °C.

Spring   Figure 5.11 presents a spring time LST night map which has been significantly reconstructed (74 % were void in the filtered input map, see Fig. 5.3 and Tab. A.3). While Tmin and LST are highly correlated (R^2=0.98 for Tmin/LST linear regression), a temperature shift of approximately 3.9 °C is observed with the LST being lower than the air temperature. Despite LST and air temperature are not equal, there is good agreement. This is even more interesting since this LST map originates from a night overpass with typically reduced quality. The lack of 74 % of the pixels seems to contribute marginally to this shift since Tmin and LST are highly correlated.

Figure 5.11 shows as second analysis, another spring LST night map (see also Fig. 5.4 and Tab. A.4) which indicates a similar pattern compared to air temperature than that of 11 Apr 2003 (02:00). However, April 2008 was significantly warmer in the valley floors with respect to April 2003. Snow cover is responsible for the low temperatures at higher altitudes which contrasts with the warm lower altitudes.

Summer   Figure 5.12 shows, in the upper graphs, statistics based on an original LST map (see Fig. 5.5 and Tab. A.5) with an insufficient number of valid pixels (cloud coverage). Due to this, the average gradient of 16-day period no. 13 was used (8-years average for this 16-day period using all available MODIS data). This results in a systematic shift of the temperatures since apparently the actual temperature situation was deviating from the 8-years average (it was actually cooler than the average 16-day period). Due to the use of the 16-day period gradient, R^2 is very high (e.g., R^2=0.95 for Tmin/LST linear regression).

Autumn   The lower graphs in Figure 5.12 are a comparison of air temperature data to LST in autumn (compare also Tab. A.6). It is based on a LST night map with 27 % void in the filtered input map (see Fig. 5.6). Very little shift is observed between air temperature and LST.

Belluno field measurements of air temperature data versus reconstructed MODIS LST data

ULSS 2 Feltre (Belluno) data set   The air temperature data of a series of sites in Belluno (2002-2007) originate from the public ULSS 2 Feltre (Unità Locale Socio Sanitaria) ticks bulletin. The staff recorded meteorological conditions during the ticks dragging (see Section 3.4.4 which are used here to assess the quality of the LST maps).

Figure 5.13 shows boxplots with the differences between air temperature measurements from datalogger versus LST extracted from reconstructed daily MODIS LST maps for the 16 different field sites of the Belluno tick sampling campaigns (43 tick samplings in the period 8/2002-10/2007). While no relevant shift is observed for the LST maps reconstructed from the actual
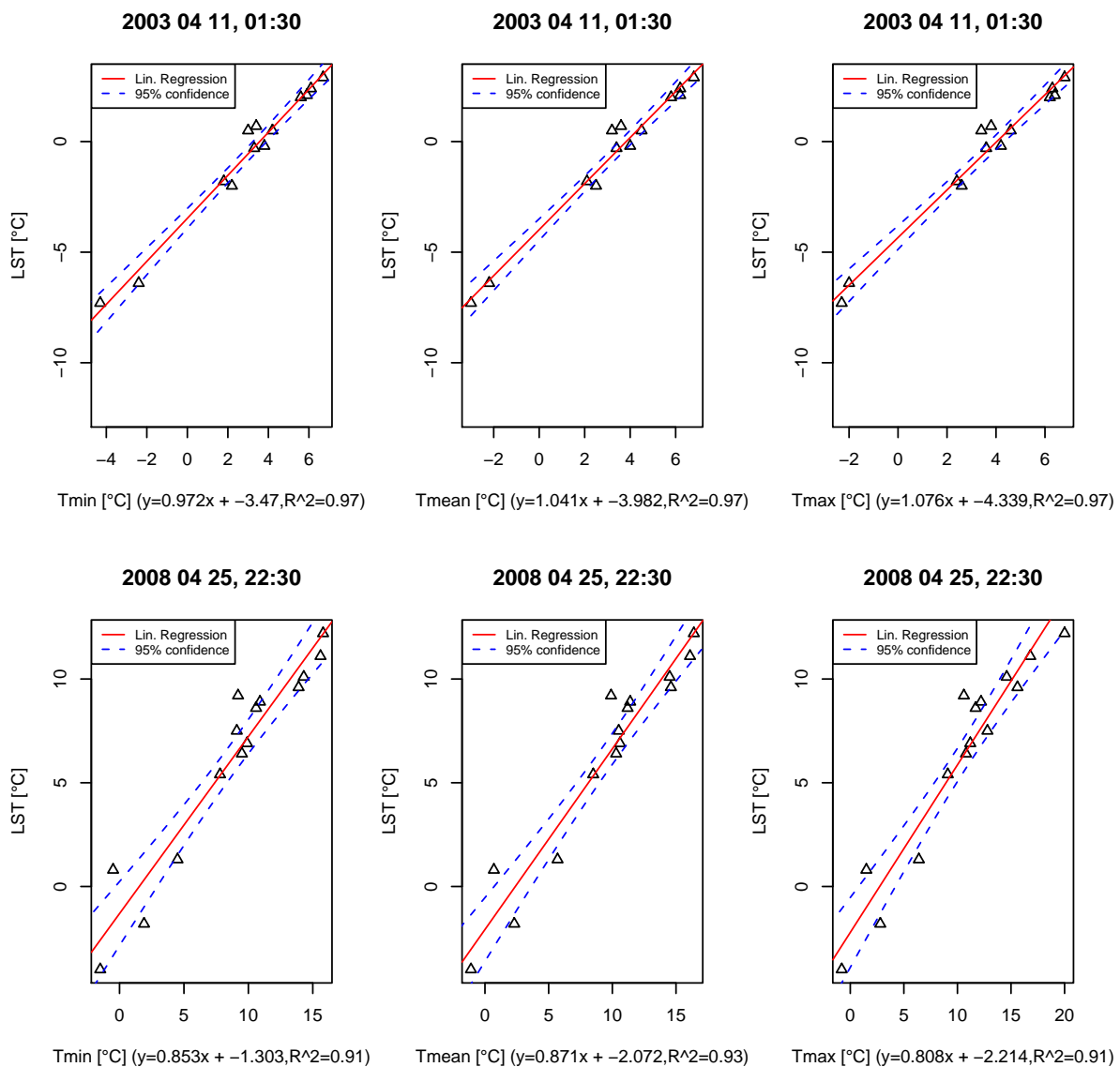
Figure 5.11: **Comparison of air temperature data (at height 2 m) with MODIS LST data from reconstructed LST map**
Upper graphs: Comparison of air temperature data (at height 2m) with MODIS LST data from reconstructed LST map (74 % void in the filtered map; actual map gradient used) in the position of the stations (date: 11 Apr 2003, air temperatures from 01:00-02:00 local solar time; MODIS LST 01:30). See also LST maps in Figure 5.3 and the original values in Table A.3.
Lower graphs: Comparison of air temperature data (at height 2 m) with MODIS LST data from reconstructed LST map (25 % void in the filtered map; actual map gradient used) in the position of the stations (date: 25 Apr 2008, air temperatures from 22:00-23:00 local solar time; MODIS LST 22:30). See also LST maps in Figure 5.4 and the original values in Table A.4. The stations are listed in Table 3.4.2.

map gradients (0.79 °C) there is, not surprisingly, a significant shift for the map based on the 16-day period model (-4.2 °C). The original data are not shown here.

EDEN Candaten IT4 site data set   The EDEN Candaten ticks time series (see Section 3.4.4) contains air temperature measurements for a few tick sampling days. They are compared to the related reconstructed MODIS LST maps in Table 5.2.
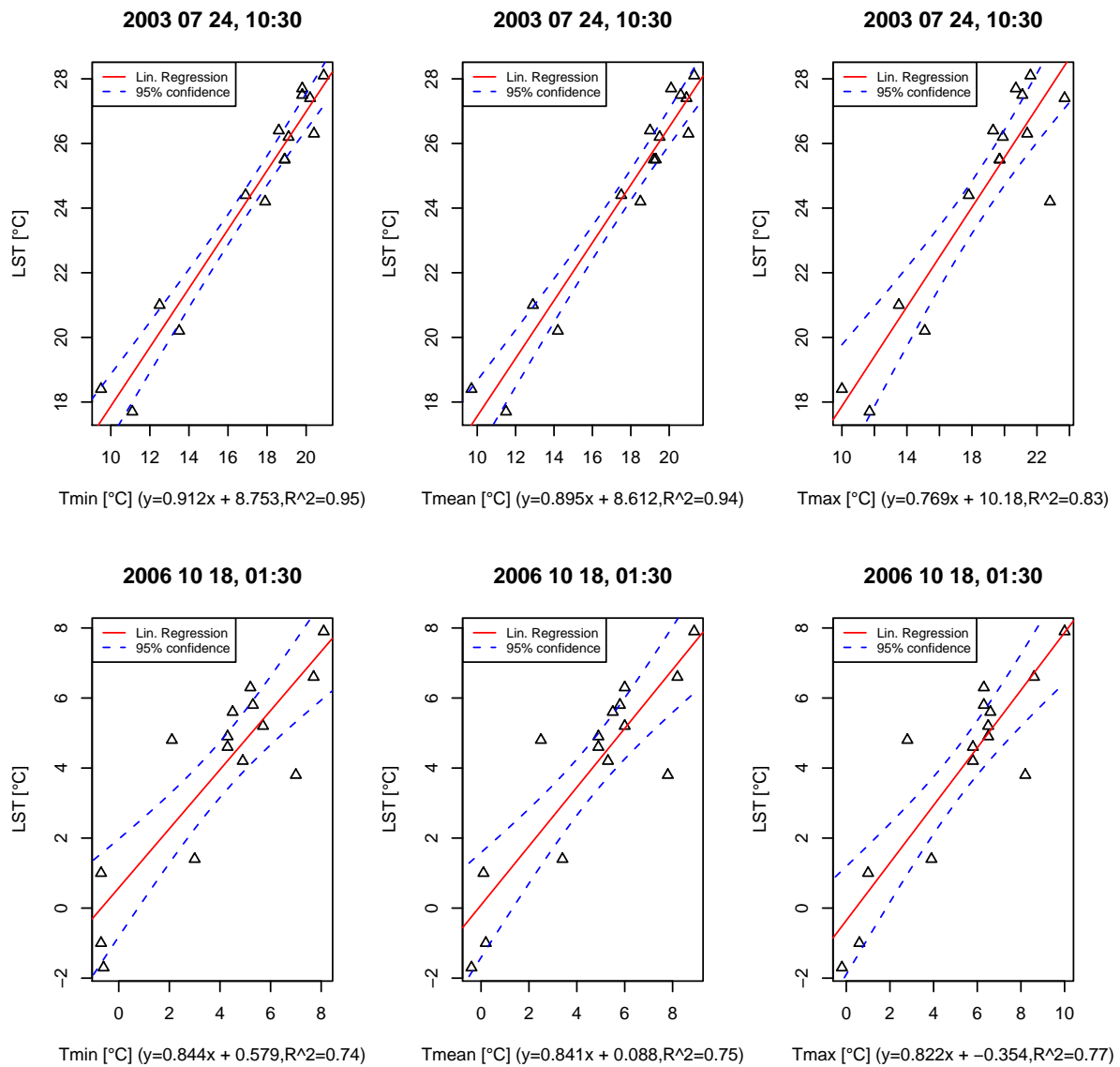
Figure 5.12: **Comparison of air temperature data (at height 2 m) with MODIS LST data from reconstructed LST map**
Upper graphs: Comparison of air temperature data (at height 2 m) with MODIS LST data from reconstructed LST map (96 % void in the filtered map; 16-day period map gradient of 10:30 overpass phase used) in the position of the stations (date: 24 Jul 2003, air temperatures from 10:00-11:00 local solar time; MODIS LST 10:30). The LST map is generated from the 16-day period model since no sufficient number of valid pixels was available. Therefore e.g. Tmin and LST are highly correlated (R^2=0.95 for Tmin/LST linear regression). See also LST maps in Figure 5.5 and the original values in Table A.5.
Lower graphs: Comparison of air temperature data (at height 2 m) with MODIS LST data from reconstructed LST map (27 % void in the filtered map; actual map gradient used) in the position of the stations (date: 18 Oct 2006, air temperatures from 01:00-02:00 local solar time; MODIS LST 01:30). See also LST maps in Figure 5.6 and the original values in Table A.6. The stations are listed in Table 3.4.2.

Table 5.2 shows selected datalogger records of air temperature measured during the tick dragging activities. The datalogger timestamps are indicative, with a potential error of one hour. Besides the 6 Mar 2008 (unexplained deviation of 3.4 °C), the 3 Jun 2008 (unexplained deviation of 2.9 °C) and 6 Nov 2008 (explained deviation due to cloud cover; 16-day period model
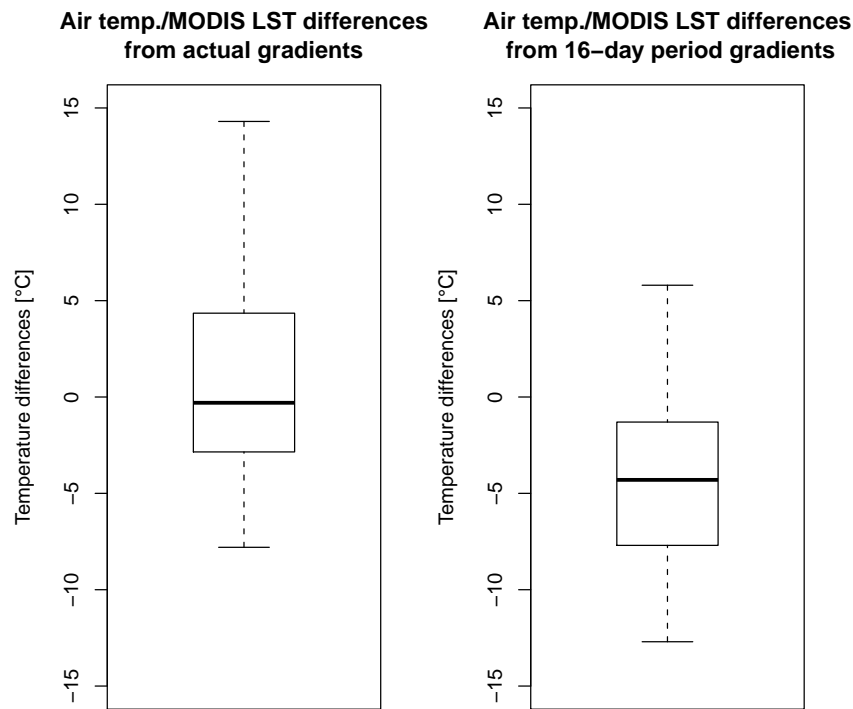
Figure 5.13: **Boxplot of differences between air temperature measurements from datalogger and reconstructed daily MODIS LST maps for 16 different field sites of the Belluno tick sampling campaigns (43 tick samplings in the period 8/2002-10/2007)**
The left boxplot shows LST versus datalogger from actual map statistics while the right graph shows LST versus datalogger from the 16-day period gradient model (insufficient numbers of pixels). While no relevant shift is observed for the LST maps reconstructed from the actual map gradients (0.79 °C) there is a significant shift observed for map based on the 16-day period model (-4.2 °C).

had to be used) which show stronger deviations, most of the comparisons match fairly well (see last differences column: average deviation -0.78 °C).

5.2.3   Comparison of LST to LANDSAT-TM thermal maps

The thermal sensor onboard LANDSAT-TM5 and TM7 (ETM+) including the recent opening of the LANDSAT archives to the public offer the possibility to compare LANDSAT thermal band maps to MODIS LST. As an example, the LANDSAT-TM5 band 6 scene from 30 July 2003 (overpass approximately at 9:30, local solar time) was selected along with MODIS LST from Terra of the same date (overpass approximately at 10:30). The LANDSAT map was recalibrated to degree Celsius (see Section 3.6). For comparison reasons, the LANDSAT map was resampled to 200 m resolution beforehand using a weighted pixel aggregation. The same subarea as in Section 5.2.1 was chosen, which covers a part of the Valsugana area east from Borgo Valsugana (Trentino).
Deviations between maps are expected for three reasons: the spectral range of the sensors is not identical (but close), the overpass time of LANDSAT TM5 is circa 60 minutes earlier than Terra and the resolution of the sensors is quite different (60m versus 1000 m; here 200 m due to the

Date	$T_{datalogger}$	$LST_{01:30}$	$LST_{10:30}$	$LST_{13:30}$	$LST_{22:30}$	Tmin - $LST_{10:30}$
2008-02-07 11:00	7.4	-3.6	7.1	5.3	0.1	0.3
2008-03-06 11:00	5.4	-5.0	8.8	*13.1	*0.7	-3.4
2008-04-03 10:00	13.4	2.0	13.4	16.7	-0.2	0.0
2008-06-03 10:00	18.8	*10.9	21.7	21.1	*11.9	-2.9
2008-08-01 10:00	23.2	14.9	24.9	21.8	19.6	-1.7
2008-09-11 10:00	20.0	11.6	20.0	15.7	16.2	0.0
2008-10-01 10:00	14.5	*6.9	*16.2	*17.8	*8.5	*-1.7
2008-11-06 11:00	12.8	*1.9	*9.6	*10.7	*2.8	*3.2
Average						*-0.78*
StdDev						*2.11*

Table 5.2: **Comparison of datalogger temperature measurements of EDEN site IT4, Candaten (Belluno, Italy) with the related reconstructed MODIS LST maps (all values in [°C])**
Values with * indicate LST map reconstruction from the related 16-day period gradient instead of actual gradient; average and standard deviation include these values EDEN site IT4, Candaten (Belluno, Italy) UTM32: 741521E, 5122255N (12.131115E, 46.2109709N).

reconstruction).

Figure 5.14 shows boxplots with the differences between LANDSAT TM5/thermal band 6 (30 Jul 2003, 9:30) and the related reconstructed daily MODIS LST map (30 Jul 2003, 10:30), small study area East of Borgo Valsugana. A temperature shift is observed for the LST maps reconstructed ($LSAT_{mean}$=19.6 °C versus $MODIS_{mean}$=22.8 °C) due to the different overpass times. Linear regression between both maps revealed slope and intercept which were statistically significant but with a low R^2=0.48. Besides the overpasses being shifted by approximately one hour, also the different spatial resolutions will contribute to the low R^2 value. The resolution of LANDSAT TM5/thermal band 6 is 60 m while the reconstructed MODIS LST maps have 200 m (from originally 1000 m). Furthermore, the terrain is very complex in the analysed subscene which adds to the differences.

Further analysis with other LANDSAT scenes is subject to future research.

5.3 Climatic parameters generated from MODIS time series

An introduction to climatic parameters derived from reconstructed LST time series is given in Section 3.7.2.

5.3.1 Indices: Saturation deficit from datalogger/hygrometer and from daily MODIS LST maps

The saturation deficit is an index of humidity defined by the difference between the saturation vapour pressure and the vapour pressure of a volume of air (also called the drying power of air). The saturation deficit SD can be expressed as (Randolph and Storey, 1999):

$$SD = (1 - \frac{rH}{100}) * 4.9463 * e^{(0.0621*T)} \tag{5.1}$$
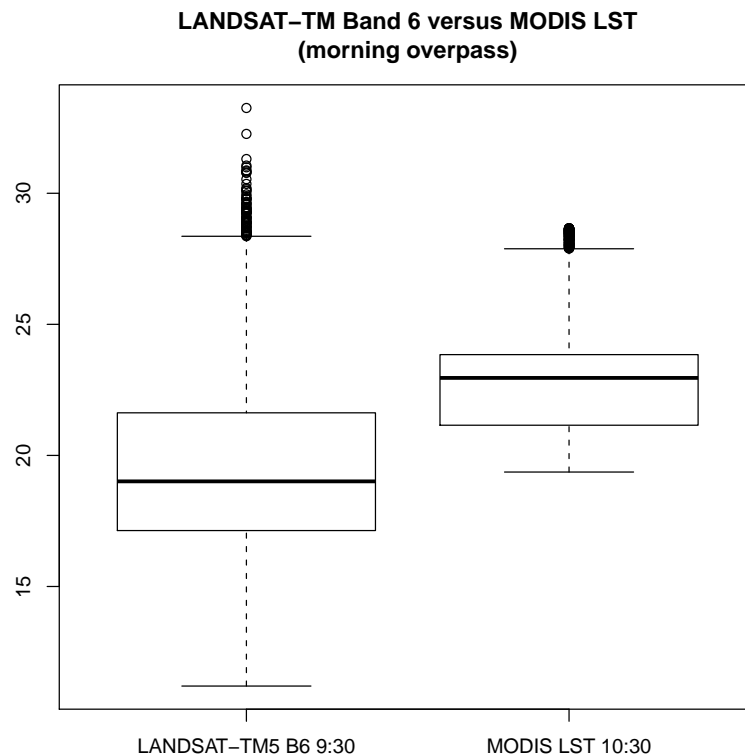
Figure 5.14: **Boxplot of differences between LANDSAT TM5/thermal band 6 (30 Jul 2003, 9:30) and the related reconstructed daily MODIS LST map (30 Jul 2003, 10:30) for a small study area East of Borgo Valsugana**
The LANDSAT map was resampled to 200 m resolution beforehand using a weighted pixel aggregation. A temperature shift is observed for the LST maps reconstructed (LSAT$_{mean}$=19.6 °C versus MODIS$_{mean}$=22.8*C) due to the different overpass times.

with:

  SD: saturation deficit [kPA],

  rH: relative humidity [-],

    T: Temperature [°C].

Saturation deficit is of major interest for assessing the development of tick populations as long-lasting high saturation deficit values may limit tick survival (Gern et al., 2008). High saturation deficit leads to shortened questing periods, also ticks will exhaust their energy reserves faster when moving back to ground from their questing place (top of low vegetation) in order to rehydrate (Gern et al., 2008).

However, mapping of saturation deficit with interpolation from meteorological stations or from field measurements is challenging due to the common unavailability of data (Hashimoto et al., 2008). While the calculation of saturation deficit from MODIS LST (and auxiliary data) was beyond the scope of this thesis, first comparisons with field measurements were carried out.

For a limited number of stations in Belluno the saturation deficit (vapour pressure deficit, VPD) could be calculated since the relative humidity was also measured during the tick sampling campaigns. The saturation deficit formula was applied to both the temperature measurements
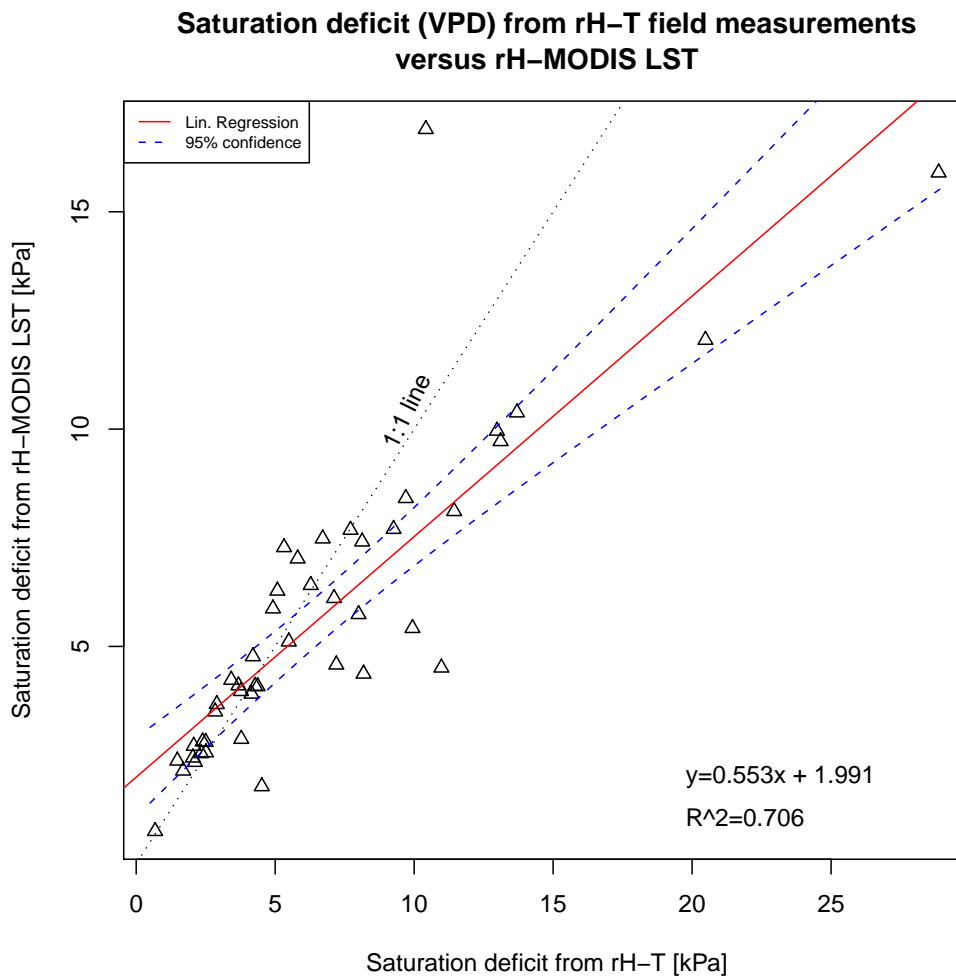
Figure 5.15: **Saturation deficit from field measurements (temperature T and relative humidity rH) versus from LST from reconstructed daily MODIS LST maps for 16 different field sites in Belluno** The data were obtained in the Belluno tick sampling campaigns (43 tick samplings in the period 8/2002-10/2007). Both calculations are based on the same rH measured with hygrometers. Only MODIS LST maps reconstructed from actual gradient used here (16-day period model maps omitted).

from the datalogger as well as the LST values extracted from daily MODIS LST maps at the sampling site positions. In both cases, the relative humidity values from hygrometer were used (see Section 3.7.1 for more theoretical background).

Figure 5.15 shows the saturation deficit for 43 tick samplings in 16 different field sites performed in the period 8/2002 – 10/2007 (data source: ULSS 2 Feltre, Belluno, ticks bulletin; original data not shown). Only MODIS LST, which were reconstructed from actual gradient, have been chosen for this analysis. Since the LST data match well in most cases the observed field temperatures (hygrometer), the linear regression shows a high correlation (R^2-adjusted=0.71). The resulting saturation deficit values are in the same range as those published by Gern et al. (2008). Future research will aim at estimating the saturation deficit completely from satellite data (see Hashimoto et al. (2008) for a proposed approach).
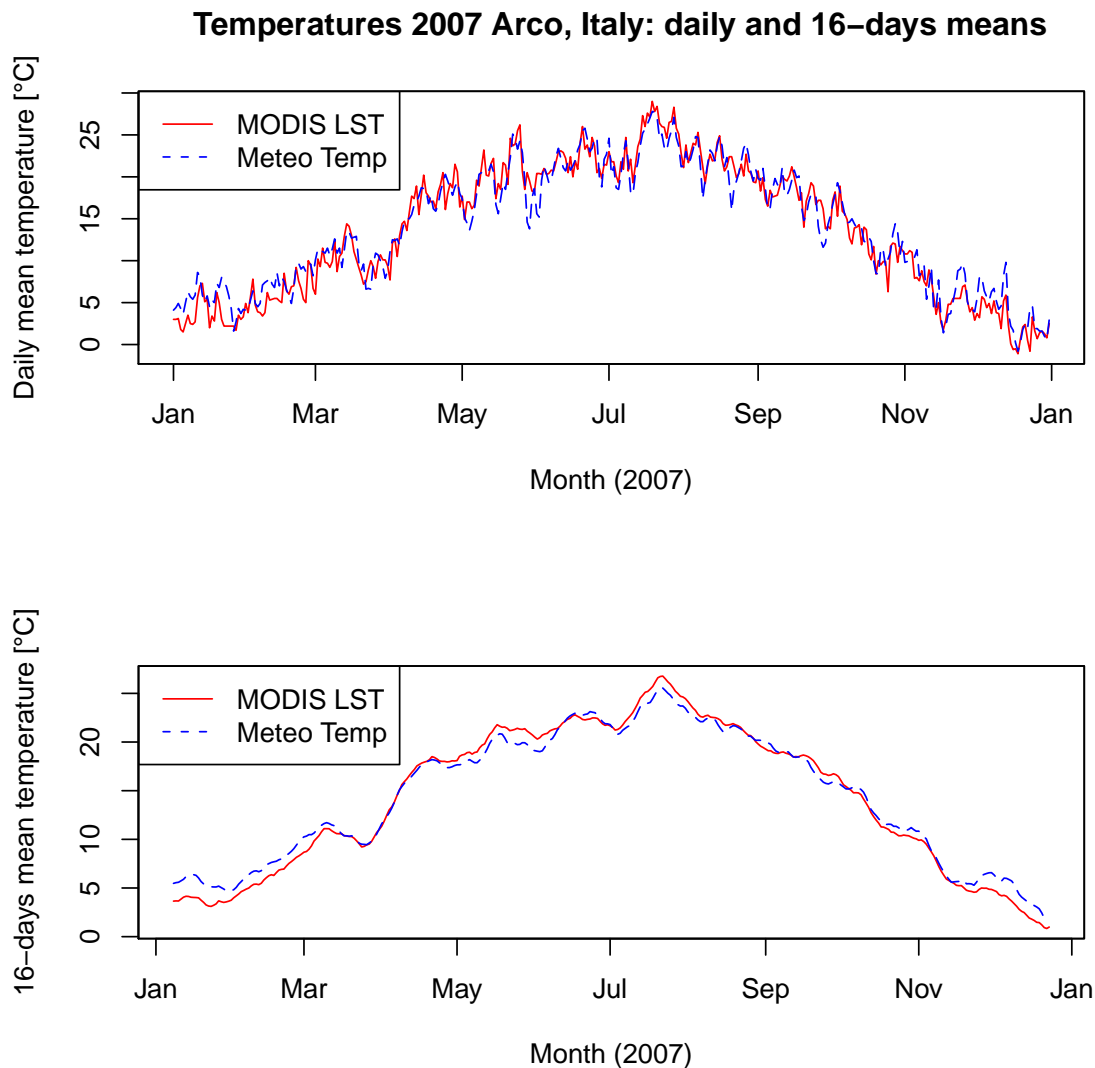
Figure 5.16: **Comparison of daily mean temperature and 16-days aggregated mean temperatures in Arco, Italy**
Time series of the meteorological station (blue dashed) versus MODIS LST values (red) as extracted from 1460 reconstructed Aqua/Terra scenes at the pixel position of the station Arco in Trentino (10.887125E, 45.910415N).

5.3.2   Indices: Aggregated daily/monthly/annual indices

Daily and 16-days aggregated mean temperatures

To analyse the performance of the reconstructed LST data over the time span of one year, the Arco meteorological station was selected (relevant to the RISKTIGER project since many temperature dependent tiger mosquitoes are found there) and daily mean air temperatures were obtained from the FEM-CTT Web site. Additionally, the MODIS LST time series was extracted in this station position for the same period (4 observations per day).
While the daily time series from reconstructed LST data extracted for the pixel position of the Arco meteo-station does not always coincide with the air temperatures time series (also due to

Year	2001	2002	2003	2004	2005	2006	2007	2008
Trento-Sud Tmean	12.4	12.5	13.1	12.2	12.0	12.5	13.1	12.7
Trento-Sud LSTmean	12.0	12.6	12.6	11.9	11.8	12.1	12.7	12.4
Tmean-LSTmean	*0.5*	*-0.1*	*0.5*	*0.3*	*0.2*	*0.4*	*0.4*	*0.3*
Arco Tmean	8.6*	11.8*	13.9	13.1	12.6	13.2	13.9	13.6
Arco LSTmean	13.0	13.5	13.6	12.8	12.7	13.1	13.7	13.1
Tmean-LSTmean	*-4.4**	*-1.7**	*0.3*	*0.3*	*-0.1*	*0.1*	*0.2*	*0.5*

Table 5.3: **Comparison of annual mean temperatures from FEM-CTT Trento-Sud and Arco meteo-stations to related to reconstructed MODIS LST maps (all values in [°C])**
Comparison of annual mean temperatures from FEM-CTT Trento-Sud (11.12639E, 46.02184N, 189 m a.s.l.) and Arco (10.88712E, 45.9104N, 84 m a.s.l.) meteo-stations to related to reconstructed MODIS LST maps. From 7/2002 onwards also the Aqua satellite became operative. The Arco station had many days of outage in 2001 (43 days) and 2002 (244 days) which led to a significant deviation from the typical annual mean temperature (values and derivatives indicated with *). All values given in °C.

the fact that some parts of the LST time series originate from 16-day period gradients rather than actual map gradients), the general temperature profile/pattern is very close when aggregated over several days (see Fig. 5.16). To assess the agreement, a Wilcoxon rank sum test performed on the two 16-day mean temperature curves (meteo station and LST) confirmed that they are statistically not different (W = 63775.5, p-value = 0.6232).

Some differences in the daily data plot can be observed which are less evident in the 16-days aggregated data plot. As a tendency, in winter the LST appears to be lower than air temperature while it is slightly higher in Summer. Analysis of the univariate statistics of the daily (in brackets 16-days aggregated) data shows (all in °C):

- Station Arco: minimum: -0.8 (1.7), median: 14.3 (15.5), mean: 13.9 (14.4), maximum: 27.8 (25.5)
- LST of Arco pixel series: minimum: -1.1 (0.8), median: 14.1 (15.8), mean: 13.7 (14.2), maximum: 29.0 (26.8)

For Trento-Sud (11.12639E, 46.02184N, 189 m a.s.l.) and Arco (10.88712E, 45.9104N, 84 m a.s.l.), the annual mean air temperature time series were obtained from FEM-CTT[3]. Except for the year 2002 (the Aqua satellite is operative from 7/2002 onwards) which had a negative difference, in all years a systematic small positive shift of <= 0.5 °C was observed for Trento-Sud (see Table 5.3). For Arco, except for a stronger difference in 2002, there is no systematic shift. In 2001, the Arco station had 43 days of outage; in 2002, 244 days which leads to a significant deviation from the typical annual mean temperature.

The data show that annual mean temperatures derived from aggregated LST data are very similar to those generated from meteorological stations since individual variations are averaged out. However, the advantage of LST data is that the study area is completely covered (hence, each LST map pixel time series can be considered as "virtual meteorological station" for temperature data).

LST maps of monthly minimum, mean and maximum temperatures

The aggregation of monthly minimum, mean and maximum temperatures from LST maps is fairly straightforward. The maps were generated from time series processing of daily LST maps

---

[3]FEM-CTT pre-calculated meteo tables, `http://meteo.iasma.it/meteo/datimeteo/tabellepronte.php`

Measure (8 ys)	Meteo T_{air}	LST	Meteo - LST
Mean of the monthly minimum January	-2.0	-9.1	7.1
Mean of the monthly minimum August	16.7	12.0	4.7
Mean of the monthly mean January	1.3	0.6	0.7
Mean of the monthly mean August	22.2	21.8	0.4
Mean of the monthly maximum January	6.3	10.2	-3.9
Mean of the monthly maximum August	28.6	32.6	-4.0

Table 5.4: **Comparison of mean air temperature data with MODIS LST data from reconstructed LST maps (3/2000-2/2009) for Trento Sud meteo station (all values in [°C])**
The January values refer to the years 2001-2009; the August values to 2000-2008. While mean values are very close, the minimum and the maximum values deviate significantly. Minimum LST values are lower while maximum LST values are higher with respect to air temperature values.

(3/2000 to 2/2009). Tests revealed that monthly mean maps from MODIS LST are probably not reliable before 7/2002 since MODIS on Aqua became operative only then. The only two daily observations available before 7/2002 apparently introduce a bias (data not shown here).

Table 5.4 shows a comparison of multi-annual means from the Trento Sud station to time series extracted in that position from MODIS LST data from reconstructed LST maps (3/2000-2/2009). Mean values are very close and with less than 1 Kelvin in the range of the MODIS LST precision. However, the minimum and the maximum values deviate significantly. Minimum LST values are lower while maximum LST values are higher with respect to air temperature values. This may be caused by the oversimplification of having only four daily observations as data basis for the mean calculations. In future research, curve fitting may be used to better represent daily minimum and maximum values.

Exceptionally warm/cold seasons   Similar to the calculation of monthly variables, thresholding on three-monthly mean LST maps was carried out to generate maps with "hot spots" concerning exceptionally cold or warm seasons. The following simple aggregation scheme is proposed to obtain the seasons by the following grouping of months (January=1): winter: 12, 1, 2; spring: 3, 4, 5; summer: 6, 7, 8; and autumn: 9, 10, 11.

While results are not shown, it can be reported that the exceptionally warm seasons winter 2006/2007 and summer 2007, and the cold winters 2001/2002 and 2005/2006 were accordingly identifiable in the MODIS LST time series.

Diurnal temperature range (DTR) from daily minimum/maximum temperatures and monthly mean temperature range (MMTR)

Based on daily minimum and maximum temperature LST maps, diurnal temperature range (DTR) maps have been derived (see also Section 3.7.2). To avoid noise and overly details, the more than 3200 DTR maps were aggregated to monthly mean DTR (MMTR, monthly mean temperature range) maps.

As an example, the gradient of MMTR of all available Januaries with four LST observation per day (2003-2009) was analysed to see if a short term trend could be observed. Figure 5.17 shows the pixelwise calculated multi-annual gradient of this variable. The resulting map shows an interesting pattern of an increase of the January monthly mean DTR (MMTR) in the Po river plain, the valley floors and in lower altitudes. On the contrary, in high altitudes a decrease

LST based gradients map of January monthly mean Diurnal Temperature Range (DTR 2001-2009)
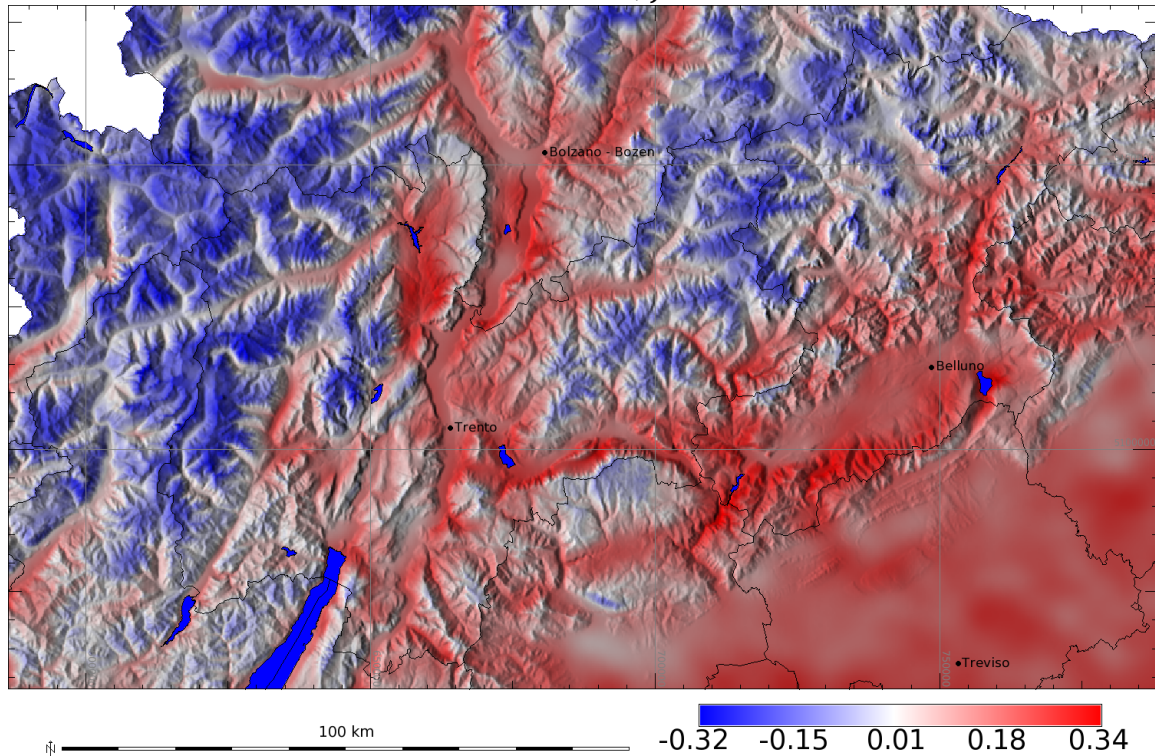
Figure 5.17: **Map of the gradient of the monthly mean DTR (MMTR) from daily reconstructed LST maps of all available January months (2001-2009)**
From the map differential changes result with respect to low and high altitudes resulting in a narrowing of the MMTR in the time period in higher altitudes (blue) and a MMTR widening at low altitudes (red).

was observed. Interestingly, Northern oriented slopes seem to be more affected than Southern oriented slopes. The results are contrary to statements in the literature (e.g. Veit (2002); but it refers to a different decade, annual DTR and a longer period). It needs to be further investigated if DTR maps can be generated from LST data at sufficient quality. However, since the data are aggregated to a trend, systematic underestimation of the minimum and maximum values should be compensated for.

Annual minimum, mean and maximum temperature map from LST maps

Using the stack of 1460 MODIS LST maps, annual mean maps of minimum, mean and maximum LST have be generated for the study area. The resulting maps are not shown here, but for selected stations the annual mean temperatures were extracted in the pixel position of the station:

- Bolzano (11.31395E, 46.50041N), mean annual LST 2003-2008: *12.3 °C* (compared to GHCN 1 data 1981-1990[4]: *12.2 °C*)
- Treviso-Istrana (12.08288E, 45.68487N), LST 2008: *13.7 °C* (compared to GHCN 1 data 1981-1990: *13.3 °C*)

---

[4]GHCN 1 data summaries, `http://www.worldclimate.com/cgi-bin/data.pl?ref=N46E011+1102+16020W`

Year	Arco Met	Arco LST	Borgo Met	Borgo LST	Passo Tonale Met	Passo Tonale LST	San Michele Met	San Michele LST	Trento Sud Met	Trento Sud LST
2001		13.0	11.0	10.7		2.7	12.5	11.8	12.4	12.0
2002		13.5	11.2	11.4		3.7	12.3	12.5	12.5	12.6
2003	13.9	13.6	11.2	11.4		3.1	12.6	12.5	13.1	12.6
2004	13.1	12.8	10.8	10.7	3.2	2.5	12.1	11.9	12.2	11.9
2005	12.6	12.7	10.6	10.5	2.6	2.7	11.6	11.7	12.0	11.8
2006	13.2	13.1	10.8	10.8	3.9	2.9	12.1	12.0	12.5	12.1
2007	13.9	13.7	11.5	11.6	4.6	3.6	12.7	12.6	13.1	12.7
2008	13.6	13.1	10.9	11.2	4.1	2.8	12.1	12.2	12.7	12.4
slope		0.0012	-0.0071	0.0298		-0.0024	-0.0333	0.0190	0.0369	0.0202
offset		13.182	11.0321	10.904		3.011	12.400	12.064	12.396	12.171

Table 5.5: **Comparison of annual mean temperatures and linear regression (gradient slope and offset) from Meteo FEM and MODIS LST in the station pixel positions (all values in [°C])**
The data period is from 2001-2008 (note: until 7/2002 LST only from Terra satellite available). Missing meteo values are cause by station problems. For the station list, see Tab. 3.4.2.

Further long-term annual mean temperatures from meteo-stations were not available for the study area to compare with.

Interannual differences maps between the annual means of 2003 to 2008 (2000 and 2009 are incomplete; 2001 and 2002 do not have 4 observations per day throughout the year) have been calculated as well but are not shown here (see Section 5.3.3 for a trend analysis).

Table 5.5 shows a comparison of annual mean temperatures and linear regression from Meteo FEM and MODIS LST in the station pixel positions (2001-2008). While the annual mean temperatures show generally good agreement, differences are more evident in the linear regression. Despite the heterogeneities, it is evident that even within the sensor groups (meteo or LST) the gradients are differing in sign, i.e. that both increases and decreases of the annual mean temperatures are found.

Growing degree days (GDD)

Growing degree days are a commonly used indicator for the assessment of insect development or also for plant development in agriculture. They can be calculated with some limitations from reconstructed MODIS LST time series (for the theory behind GDD, see Section 3.7.2). The limitations arise from the fact that the MODIS overpass times do not coincide with the daily temperature minimum and maximum. However, mean LST temperatures derived from daily LST maps were shown to sufficiently coincide with mean air temperatures (see Section 5.16).

To compare the annual GDD performance from MODIS to field data, minimum and maximum air temperature data were obtained from FEM-CTT for the years 2003-2008 (10 °C baseline temperature, 30 °C cut-off temperature). For the calculation of the GDD from LST the same values were used. Two years of accumulated GDD curves are shown in Fig. 5.18. While differences are limited, the GDD curves from reconstructed daily MODIS LST are systematically higher in spring time than those calculated from the meteo station, while they coincide in summer and are lower in autumn. Figure 5.19 shows these differences for two years as density plots (station/pixel Trento Sud, years 2003 and 2006). The mean shift is -7.74 GDD (2003) and -16.06 GDD (2006) which is actually less than 5 % of the error obtained in a similar study in Canada, which was

Growing Degree Days from Meteo and MODIS LST
Station/position Trento Sud
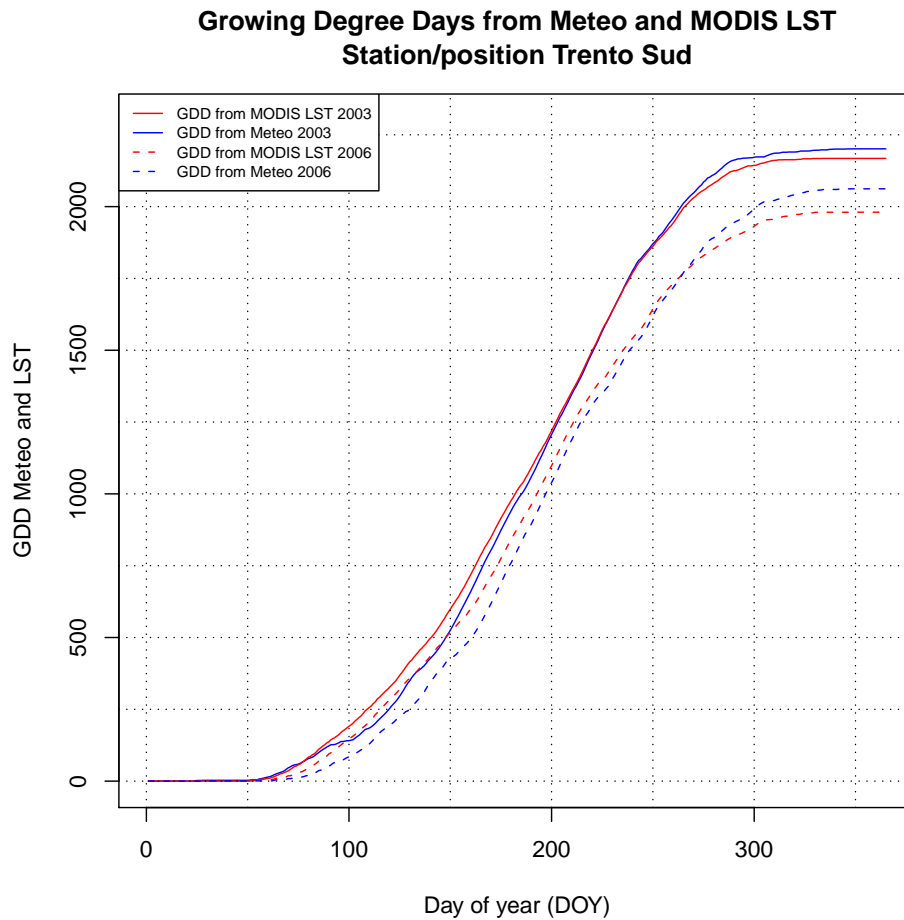
Figure 5.18: **Comparison of accumulated growing degree days curves from FEM-CTT meteo station and MODIS LST for 2003 and 2006**
Time series of the meteorological station (blue dashed) versus MODIS LST values (red) as extracted from 1460 reconstructed Aqua/Terra scenes at the pixel position of the station Trento Sud in Trentino (11.126386E, 46.021841N; baseline temperature 10 °C, cut-off temperature 30 °C). Differences are shown in Fig. 5.19.

based on the 8-day MODIS LST product instead of daily MODIS LST. In the Canadian study, the GDD values were systematically overestimated by 511 GDD (Hassan et al., 2007).

With reconstructed daily MODIS LST the fact that neither the daily night minimum nor the day maximum are well represented is apparently averaged out to some extent.

LST-GDD threshold maps for insect development   Growing degree days threshold maps were used to assess insect development (also used to estimate plant growth and in other domains). For the different insect life stages certain GDD levels need to be reached. The typical GDD maximum for an area can be also used to indicate if a disease vector can survive and establish since all life stages need to be completed.

Accepting the earlier produced LST-GDD maps, threshold maps can be generated by counting pixelwise the number of days needed to reach a certain GDD threshold. Like in the paper of Pasotti et al. (2006), various maps can be generated but in this case from satellite data rather
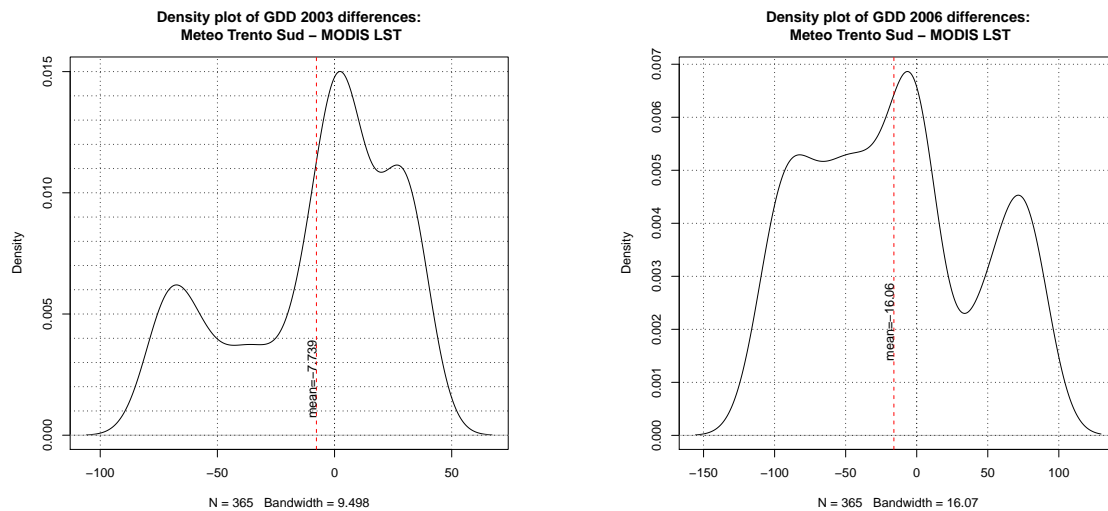
Figure 5.19: **Density plots of differences between accumulated GDDs from meteo station and reconstructed daily MODIS LST (Trento Sud, years 2003 and 2006)**
The mean shift is -7.74 GDDs (2003) and -16.06 (2006). Original curves are shown in Fig. 5.18.

than from interpolated meteorological stations data. It is assumed that MODIS LST based GDD maps better preserve microhabitat-like effects.

Figure 5.20 shows, for two different years, two maps indicating the day of year (DOY) when a certain GDD threshold (here: 440 GDD, compare Pasotti et al. (2006)) was reached. The threshold is reached earlier at the valley floors and in the Po river plain due to the higher radiation, compared to higher altitudes where it is reached later or where it cannot be reached at all. Year 2003 was warmer that 2006 leading to an earlier onset of the threshold and a larger spatial distribution. Compared to GDD interpolation from meteorological stations, microclimatic structures are better represented in the intrinsically spatialised GDD maps from satellite data.

5.3.3   Indices: Intra-annual short term trends: spring warming and autumnal cooling

For cold-blooded parasites like ticks, which are very sensitive to temperature changes and thresholds, the gradients between active and hibernating seasons are of relevance (see also ticks ecology in Section 1.1.1 and introduction to intra-annual short term trends in Section 3.7.3).

Spring warming   To generate spring warming maps, the months of February, March and April were aggregated to daily mean values and compared to the meteorological station of Trento Sud by using a linear regression. Figure 5.21 shows that the two time series are significantly correlated (R^2=0.838 for Tmean-meteo versus LST-mean and almost identical time series regression lines with a gradient difference of 0.001 and an offset difference of 0.1 °C). This means that the reconstructed daily MODIS LST time series is a suitable replacement for meteorological data to assess the spring warming gradient.

The spring warming coefficient is then derived from the relationship of the absolute monthly temperature increase related to the minimum of monthly mean LST in the midwinter period. To simplify the calculations, only the January and February months, when the temperature

Day of year (DOY) for reaching 440 GDD, 2003

Day of year (DOY) for reaching 440 GDD, 2006
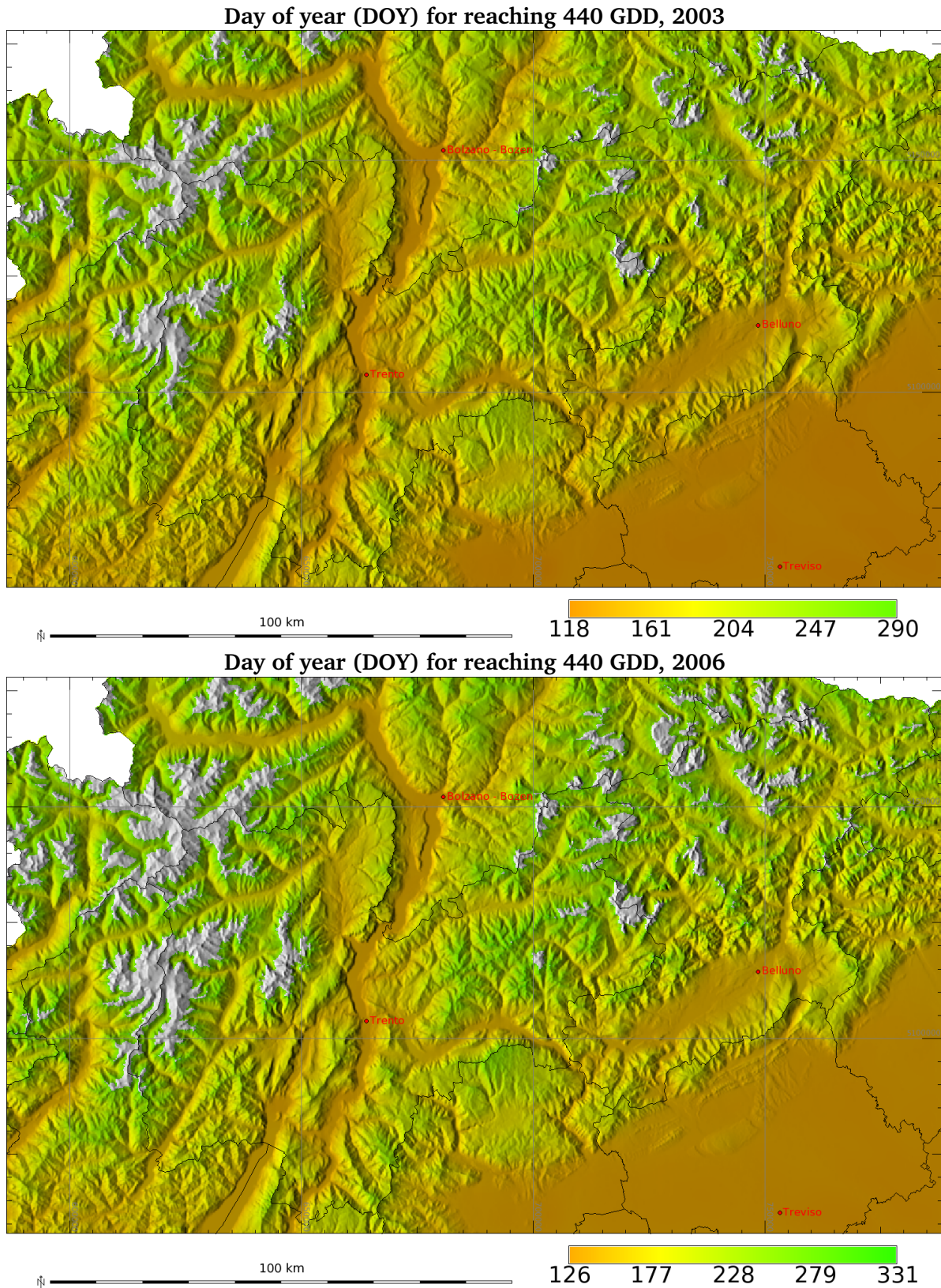
Figure 5.20: **Number of day of the year (DOY) to reach 440 accumulated growing degree days in the years 2003 and 2006**
The GDD baseline temperature is 10 °C, cut-off temperature 30 °C. The 440 GDD threshold is reached earliest in the year at valley floors and the Po river plain, in higher altitudes later or never. Year 2003 was warmer that 2006 leading to an earlier onset of the threshold and a larger spatial distribution. Both maps have a common color table, in uncolored zones the threshold is not reached throughout the year (map scale 1:1,400,000).
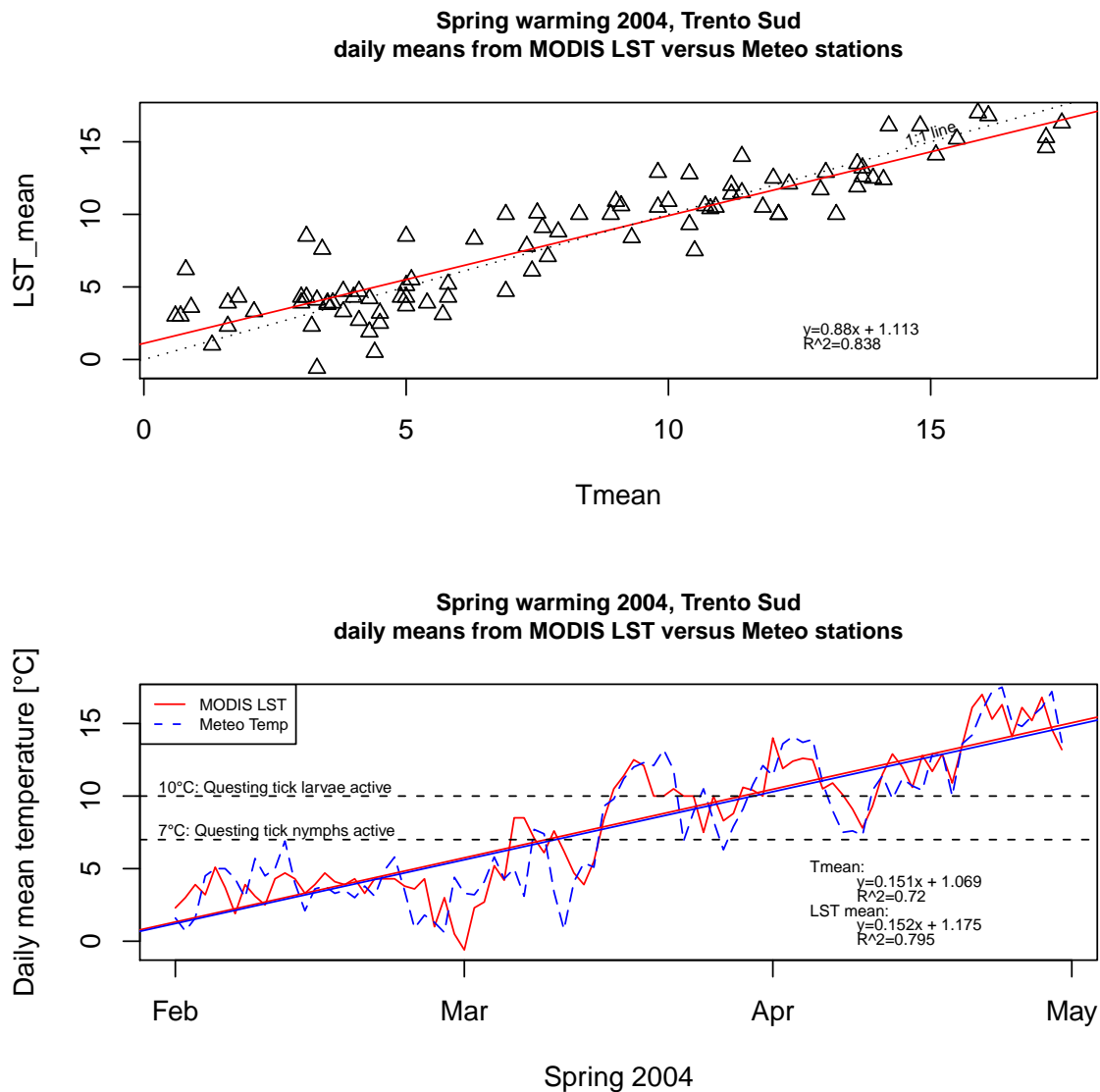
Figure 5.21: **Spring warming of 2004 (February, March and April)**
Comparison between daily mean temperature from meteo station (Trento Sud, 11.126386E, 46.021841N) and the reconstructed daily MODIS LST series in the related pixel position. The upper plot shows the correlation between both measures; the lower plot shows the time series with linear regression to asssess the monthly temperature increase. The two horizontal lines indicate the minimum temperatures when questing ticks start their activity.

minimum typically occurs, were considered. This calculation is performed pixelwise on the LST map stack for each year (2001-2008) to obtain the mapped spring warming coefficients (data not shown here).

Autumnal cooling   The autumnal temperature decline ("cooling") was calculated following the methodology proposed by Randolph et al. (2000) (as outlined in Section 3.7.3). The autumnal temperature decline for the years 2000-2008 was calculated from reconstructed daily MODIS LST time series (period August to October). The autumnal cooling coefficient is the relation of the annual maximum of the monthly mean land surface temperature (LST) level in
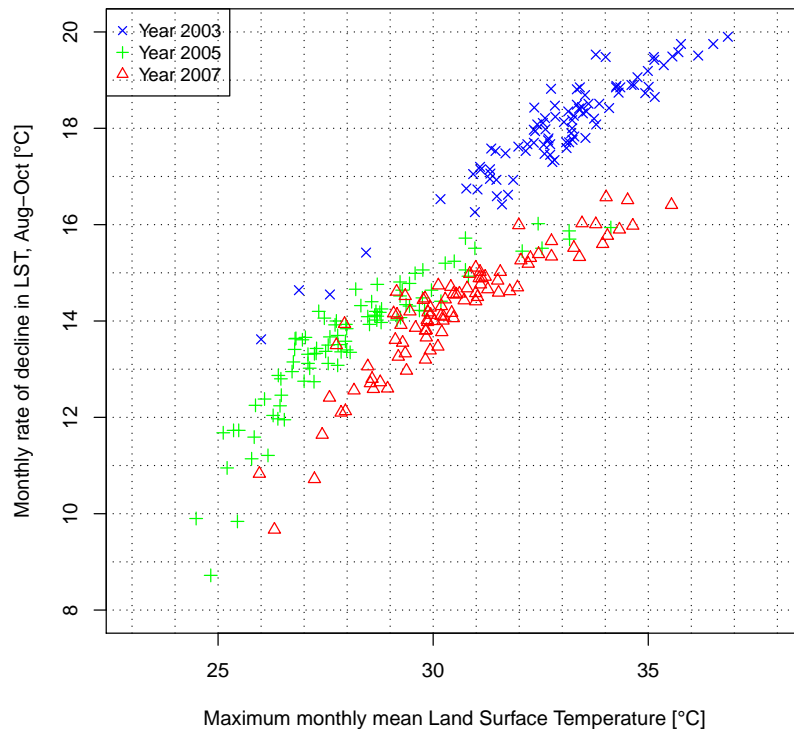
Figure 5.22: **Plot of autumnal "cooling": relationship between absolute monthly LST decline and annual maximum of monthly mean LST in midsummer**
The relationship was obtained for 91 tick sampling sites in Feltre/Belluno; 3 selected years.

midsummer (northern hemisphere) to the temperature decline gradient. As in the other seasons linear regression was applied to the input LST maps.

Figure 5.22 shows a temperature variable plot similar to Fig. 6 in Randolph et al. (2000). These data are further analysed in Section 6.3 in terms of ticks.

5.3.4 Discussion

In this chapter, the reconstructed LST time series maps have been presented together with selected maps to illustrate the quality of the map reconstruction process. To be able to embed these new data sets into existing research, comparisons of reconstructed daily LST maps to other related data sources was shown. Besides the comparison with selected day and night LANDSAT-TM thermal maps, the statistical comparison of LST to meteorological time series is of particular interest. It has been demonstrated that aggregated indicators from reconstructed daily LST maps compare especially well to those derived from meteorological time series.

In the second part of this chapter, a series of climatic parameters generated from MODIS time series has been presented. They comprise aggregated daily/monthly/annual indices, intra-annual short term trends and indicatively also "long" term trends. While there is potential for further indicators, those with relevance to epidemiological applications were presented. These include aggregated daily/monthly and annual means, accumulated growing degree days, daily and monthly temperature range, identification of exceptional periods, spring warming/autumnal

cooling and saturation deficit. Good agreement with the same indicators derived from meteo data was found.

Gray et al. (2009) analysed long term means for tick absence/presence assessment in northern temperate Europe and state that an increase of about 2-3 °C in the average temperature from April to September could result in the establishment of permanent populations of the tick in regions of northern temperate Europe where it is currently absent. Similar considerations may apply also in higher altitudes in mountainous regions in case that a positive long term trend occurs which renders habitats suitable for hosts and vectors.

For obvious reasons, temperature trend analysis is not yet satisfactorily possible when limiting input data to the MODIS sensors. Time series could potentially be expanded with daily AVHRR LST data (starting 1982).

5.3.5   Conclusions

While remote sensing data are nowadays more easily available (especially from US data providers), the important preparation steps are still very time consuming. A major problem of the proposed approach is that it is yet computationally intensive (2 hours per LST map; altogether 22,000 CPU-hours). For future Pan-European maps (collection of indicators) there is a need to either use a segmented approach (this is already implemented in most time intensive `v.vol.rst` command but internally it needs to better attach segments) or to use a substitute for the 3D volumetric splines interpolation with an algorithm of equal quality but significant higher performance. Nonetheless, the processing has been implemented as almost automated procedures which can run on even large grid or cluster infrastructures for parallel computing. The user has to process original MODIS LST data in a few steps, i.e. 1) reprojection and import, 2) histogram based outlier removal using MODIS LST QA layers, 3) linear regression on all maps to calculate preliminary map gradients and quality control of those, 4) second filtering of all prefiltered LST maps, 5) final linear regression to calculate definite map gradients, and 6) volumetric splines based LST map reconstruction. All these steps have been implemented as scripts to minimise user errors during the data processing.

The results show that reconstructed daily LST time series are a valid data set which can substitute in many cases meteorological temperature observations, especially when the distribution of the stations is irregular or sparse. The developed indicators are not only of relevance to epidemiology but can be used in agriculture or forest research as well.

6 Case study 1 – Application of the reconstructed LST time series to tick distribution modelling

As outlined in Section 1.1.1, ticks are transmitting various pathogens and tick-borne diseases are continuously spreading in Europe. This case study analyses a time series of *Ixodes ricinus* tick presence data obtained by dragging (see Section 3.4.4) for the EDEN EU/FP6 project. In particular, the correlation between land surface temperature data, obtained from MODIS, and questing tick activity has been studied.

6.1   Field data and MODIS LST data

Time series of questing tick larvae and nymphs field data were obtained using the dragging technique in two EDEN EU/FP6 project sites (2006-2008). These sites are Candaten (EDEN site IT4; 12.131115E, 46.2109709N, 530 m a.s.l.) and Losego (EDEN site IT5; 12.2891693E, 46.1333335N, 743 m a.s.l.), both located in the Province of Belluno, Italy (see Section 4 for a description of the province). Furthermore, field data from ULSS 2 Feltre were obtained (2002-2007). These have one site in Candaten very close to the EDEN site IT4 site (Candaten ULSS 12.12556E, 46.19925N, 417 m a.s.l.).

Figure 6.1 covers an excerpt of the EDEN ticks database maintained at FEM-CRI. The graph shows the time series of the two selected field sites of Losego and Candaten in Belluno where tick dragging has been regularly performed. A subset, the ticks samples of 2006, was analysed at FEM-CRI for the presence of Tick-borne Encephalitis (TBE) with absence of TBE in questing ticks in Candaten and TBE presence in Losego.

Figure 6.2 shows likewise the appearance of larvae and nymphs in Candaten. There are notable differences in the year 2007 (very warm summer) between the ULSS and the EDEN tick samplings. The larvae peak found in the EDEN site is not seen in the ULSS data.

6.2   Methods

As outlined earlier in this thesis, daily MODIS LST have been reconstructed to obtain a complete time series. For this case study, various environmental variables have been produced by aggregation partial time series. From the resulting maps the various values were extracted in the pixel position of the tick sampling sites (original data not shown here). The resulting variable time series are plotted in Section 6.3.
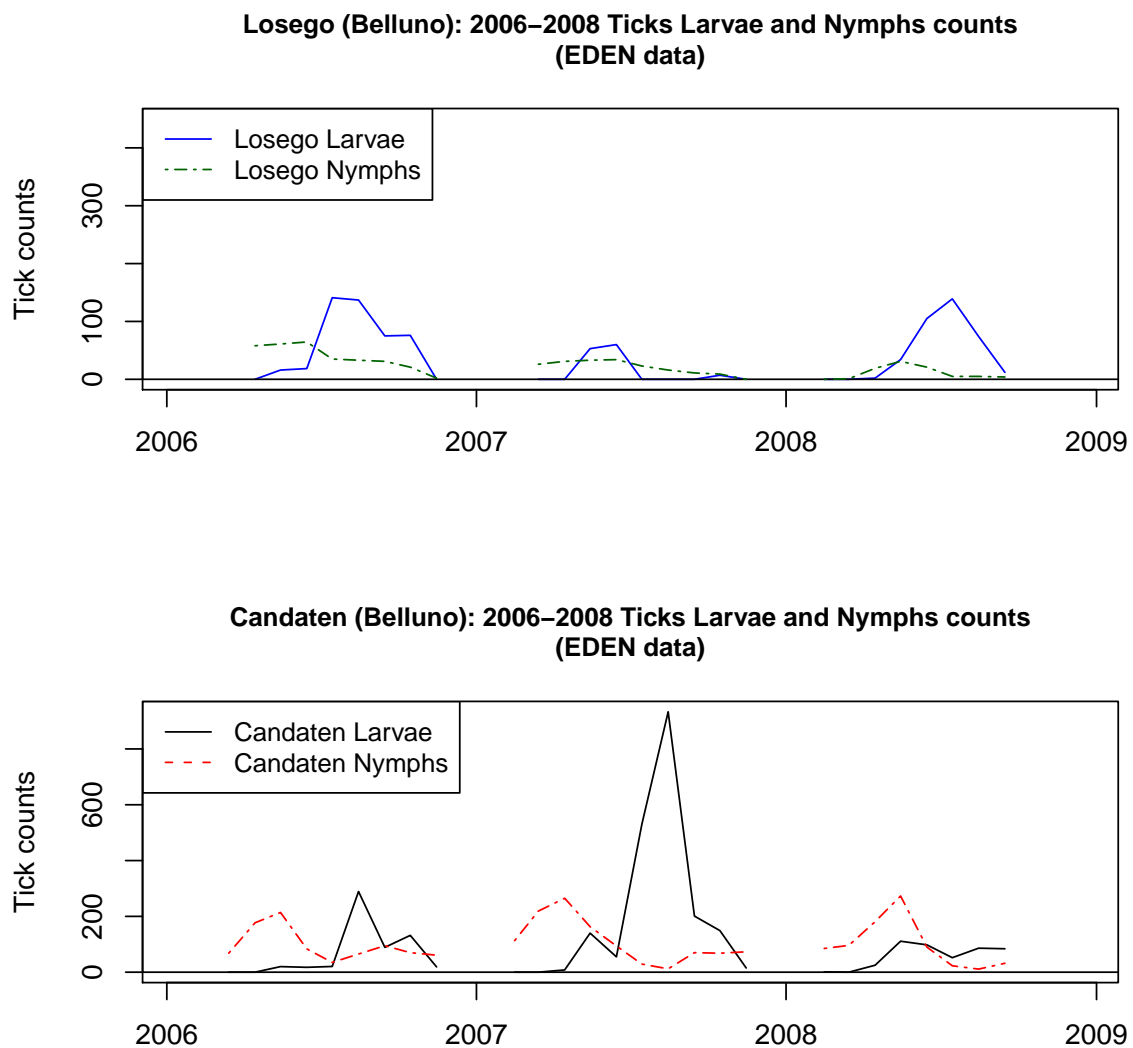
Figure 6.1: **Time series of counts of questing tick larvae and nymphs at Losego and Candaten EDEN tick sampling sites, Belluno, Italy**
The time series of counts of questing tick larvae and nymphs were obtained by dragging at Losego (EDEN site IT5; 12.2891693E, 46.1333335N, 743 m a.s.l.) and Candaten (EDEN site IT4; 12.1351111E, 46.2154583N, 840 m a.s.l.), both located in Belluno, Italy. No tick sampling is performed in the winter months.

16-day period mean LST maps   To reduce potential errors in the LST data, daily reconstructed MODIS LST data were aggregated to 16-day period mean LST maps. For each given 16-day period (23 in total), the average was calculated from the relevant daily maps.

Minimum spring temperature thresholds for nymphs and larvae activation   Based on 16-day period mean LST maps, the timing of the minimum spring temperature thresholds for nymphs and larvae activation can be assessed as the onset of tick activity is also temperature dependent. Using the stack of 16-day period maps, which was ordered by time (23 maps per year with 16-days period length), for each pixel the period number was identified when 7 °C
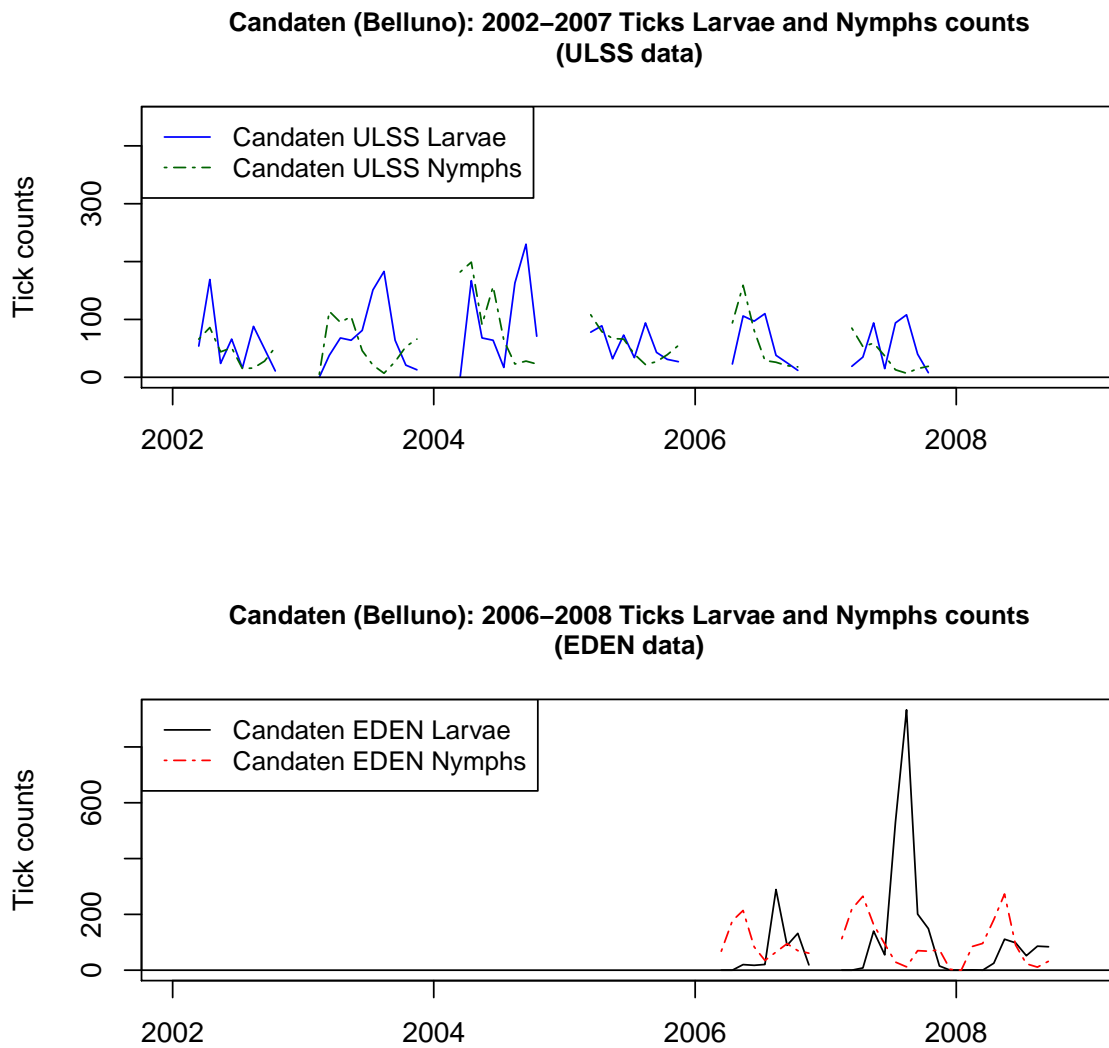
Figure 6.2: **Time series of counts of questing tick larvae and nymphs at Candaten ULSS 2 Feltre and EDEN tick sampling sites, Belluno, Italy**
The ime series of counts of questing tick larvae and nymphs were obtained by dragging at Candaten, Belluno, Italy for several years. The upper graph shows the data obtained from ULSS 2 Feltre; the lower graph shows data from the EDEN tick dragging activities (EDEN site IT4; 12.1351111E, 46.2154583N, 840 m a.s.l.). Both dragging positions are close together. Note the different vertical scales for better curve visibility. No tick sampling is performed in the winter months.

(nymphs) or 10 °C (larvae) mean temperature was reached. As a result, the mapped timing patterns of larvae and nymphs onset in spring was generated with the 16-day period number as pixel value.

Autumnal cooling of the previous year and spring warming of the current year   These parameters are relevant to the tick behaviour since they trigger through tick diapausing in winter a potential synchrony in spring time (see Section 3.7.3 for details). For the years 2001 to 2008 both autumnal cooling (August, September, October) and spring warming (February, March,

April) were calculated from daily MODIS maps. See also Figure 5.21 for an example of a spring warming gradient.

Growing Degree Days   Growing Degree Days were accumulated per year (see Section 3.7.2 for details) as a proxy for the accumulated energy throughout the year. Here they were not thresholded for particular values but simply extracted as time series for the tick sampling sites.

6.3   Results

7 °C and 10 °C temperature threshold for onset of ticks activity   The following 16-day periods were identified for reaching the 7 °C threshold (C: Candaten IT4; L: Losego IT5; 16-day period 1, 2006+2007+2008: 1 Jan to 16 Jan; 16-day period 2, 2006: 17 Jan to 01 Feb):

- Year 2006: C 1, L 2;
- Year 2007: C 1, L 1;
- Year 2008: C 1, L 1.

In 2006, the tick sampling started only in the 6th 16-day period in Candaten (68 nymphs found; Tagliapetra V., pers. comm.), and in Losego in the 7th 16-day period (58 nymphs found); therefore MODIS LST thresholds cannot be compared. In 2007, sampling was started in the 3rd 16-day period (C: 113 nymphs, L: 0), meaning that also here it cannot be verified if 16-day period temperature thresholding can predict the onset of nymphs. In 2008, sampling was performed in the 1st and 3rd 16-day period (C: 85 nymphs found in 3rd 16-day period). The Losego showed low nymphs counts in general and the onset of activity delayed by about one to two months with respect to Candaten.

The following 16-day periods were identified for reaching the 10 °C threshold (16-day period 4, 2006: 18 Feb to 5 Mar; 16-day period 5, 2006: 6 Mar to 21 Mar; 16-day period 1, 2007: 1 Jan to 16 Jan; 16-day period 2, 2008: 17 Jan to 1 Feb):

- Year 2006: C 4, L 5;
- Year 2007: C 1, L 1;
- Year 2008: C 2, L 2.

The reaching of the 10 °C threshold in the first 16-day period of 2007 indicates that this year had an unusually warm winter. The same problem as for the nymphs applies here that sampling was started only later than the potential onset of larvae except for 2008. In Candaten, only the observed larvae onset in 2008 is close to the predicted onset (delayed by one 16-day period). The Losego showed low larvae counts in general and the onset of activity delayed by about two 16-day period with respect to Candaten.

Further aggregated time series   To simplify the interpretation of the various time series, they have been integrated into the previously shown larvae and nymph counts plots. Figure 6.3 shows the following environmental variables derived from MODIS as time series extracted in the pixel position of the field sampling site: autumnal cooling of the previous year overlayed to the current, spring warming of the current year, 16-day period mean LST, and Growing Degree Days. Not shown here are the tick counts from the Candaten/ULSS site (see Fig. 6.2).
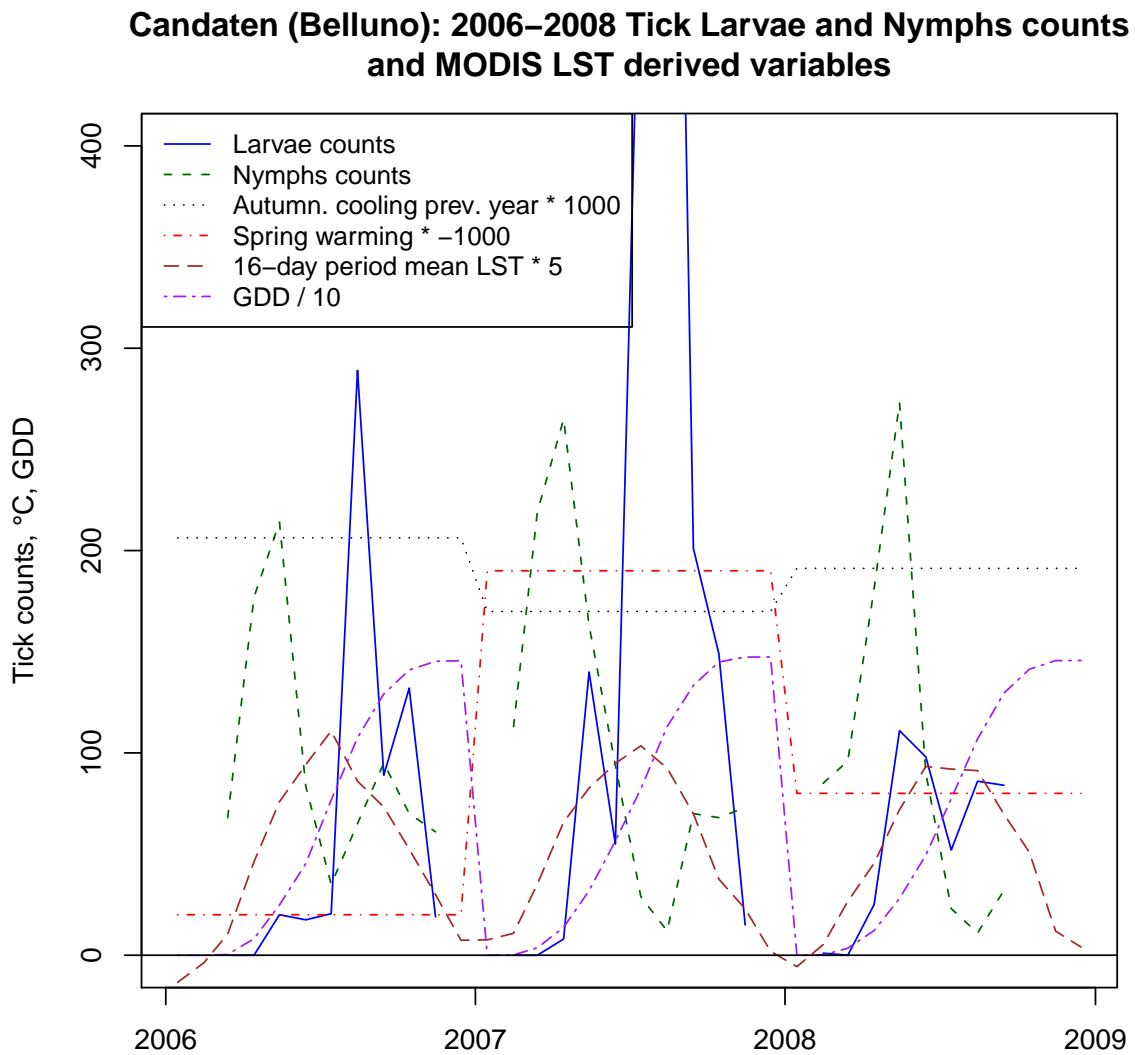
Figure 6.3: **Time series of counts of questing tick larvae and nymphs at Candaten EDEN tick sampling site integrated with environmental variables derived from MODIS LST time series**
The time series of counts of questing tick larvae and nymphs were obtained by dragging at Candaten, Belluno, Italy for three years. Additional curves show environmental variables derived from MODIS LST time series: autumnal cooling of the previous year, spring warming of the current year, 16-day period mean LST (16days), and Growing Degree Days; all these variables have been scaled to match the ticks count scale (see legend for scale factors). The high larvae density is not completely displayed in the graph in order to maintain visibility for the other curves. The tick data were obtained through the EDEN tick dragging activities (EDEN site IT4; 12.1351111E, 46.2154583N, 840 m a.s.l.)

In Candaten (EDEN IT4 site), autumnal cooling of 2005 was highest in the analysed time period. Spring warming was highest in 2007 due to the warm winter 2006/2007. This is also reflected in the 16-day period mean LST series. Growing Degree Days reached unusual high values especially in the first half of the year 2007. Observed larvae counts were high in 2007, possibly due to a combination of several factors since some of the analysed variables show "anomalies" in 2007.

The Losego site (EDEN IT5 site) shows a slightly different pattern (see Fig. 6.4). Autumnal
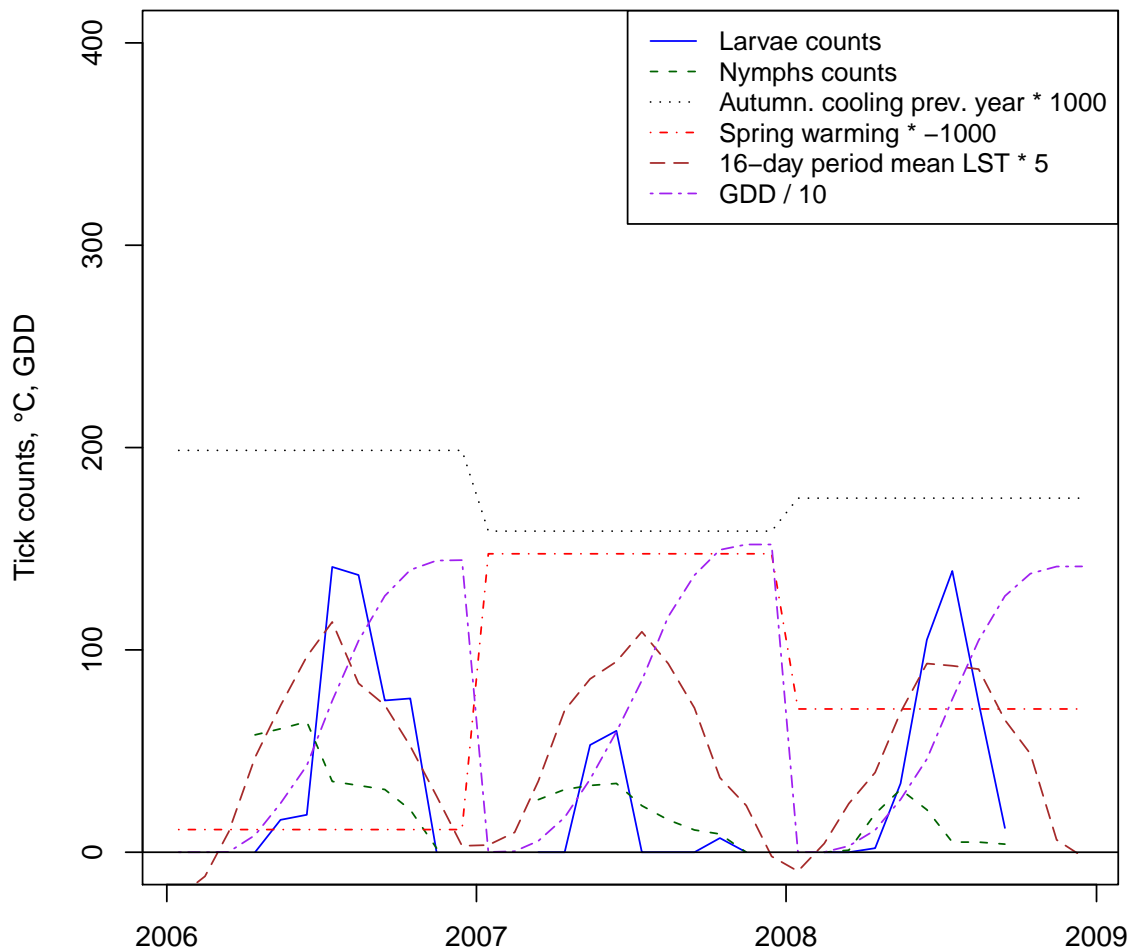
**Figure 6.4: Time series of counts of questing tick larvae and nymphs at Losego EDEN tick sampling
site integrated with environmental variables derived from MODIS LST time series**
The time series of counts of questing tick larvae and nymphs were obtained by dragging at Losego,
Belluno, Italy for three years. Additional curves show environmental variables derived from MODIS LST
time series: autumnal cooling of the previous year, spring warming of the current year, 16-day period
mean LST (16days), and Growing Degree Days; all these variables have been scaled to match the ticks
count scale (see legend for scale factors). The tick data were obtained through the EDEN tick dragging
activities (EDEN site IT5; 12.2891693E, 46.1333335N, 743 m a.s.l.).

cooling in 2005 was also highest in the analysed time period. Spring warming was highest in
2007 due to the warm winter 2006/2007 but relatively higher than in the Candaten site. Also
here, the 16-day period mean LST series reflects the warm winter 2006/2007. Growing Degree
Days is comparable to Candaten in the curve form, but is generally higher. In Losego, no special
peak of larvae or nymphs counts is visible.

An interesting year with respect to tick-borne diseases was 2006: in Cavedine no TBE was found
in questing ticks, but a very high density of ticks was observed in contrast to Losego where

TBE was found despite low ticks density (Carpi G., pers. comm.). From the Losego time series (Fig. 6.1) it appears that some synchrony between the larvae and nymph life stages may have occurred in 2006, while they were rather disconnected at the same time in Candaten. However, it is statistically unclear if this synchrony was triggered by autumnal cooling of the previous year 2005 (see Figure 6.4 and Figure 6.3, cooling of year-1 superimposed to actual year). However, it can be stated that cooling had the highest rate in 2005 throughout the period from 2005 to 2007 (superimposed in the graphs to 2006-2008).

6.3.1 Discussion

In this case study it was not possible to find a reasonable model which could be used to produce a map of tick distribution time series for the different life stages. Time series plotting, correlation analysis on original and grouped data was applied, looking at timing of emergence, synchonisation between life stages, and peaks in tick presence. Some "signals" appear to be within the data, but no clear statistical correlation could be identified. While the indicators have been demonstrated to be valid earlier in this thesis, no clear correlation could be established for the ticks data available for this case study. With respect to tick-borne pathogen infection prevalence data for the EDEN project, only the year 2006 has been analysed so far for the two sites. Other disease data were unavailable. Hence, hypotheses on tick-borne pathogens distribution in relation to temperature derived time series could not be tested, and await a larger tick data time series dataset.

In most cases, finding mathematical functions capable to relate different environmental data would require a number of cases which is sufficient for testing the model and its accuracy and, in case of time series, fulfilling potential discontinuities. As an example, De Beurs and Henebry (2005) suggested both parametric and non-parametric methods for the analysis of discontinuities of time series data which could be implemented once new tick data will become available.

Finally, as a rule of thumb, it should be stressed that finding those climatic data which rule out the spread of tick-borne pathogens through their related vectors is a hard task to deal with, since distinguishing laws from regularities in time series would not directly imply cause and effect relationships (Colyvan and Ginzburg, 2003).

Meanwhile, it is worth noting that the example presented in this thesis represents a first attempt to assess tick phenology (the seasonal evolution of questing tick density over time is called tick phenology, Gern et al. 2008) and distribution directly from daily MODIS LST remote sensing data. This approach will be of great interest in future for a number of environmental tasks including both disease monitoring and management. In this view, remote sensing approaches are dramatically important since they allow for a synoptic view over a large area (Gillanders et al., 2008). For instance, further research steps will include: 1) additional data acquisition on tick-borne diseases, 2) modeling of the relation between remote sensing-based climatic data and field-based disease data, and 3) mapping of disease vectors of an entire study area by applying the achieved model to the climatic data derived from satellite imagery.

6.3.2   Conclusions

A set of variables has been elaborated for the EDEN tick sampling sites with respect to the field sampling dates, using the reconstructed daily MODIS LST data. The variables include autumnal cooling of previous year, spring warming of current year, 16-day period mean LST, growing degree days, and thresholds of 7 °C and 10 °C for nymph and larvae onset of activity). These variables have been cross-checked against the multi-annual tick time series of the two EDEN field sites.

Due to the limited availability of field data, no relevant correlations were found between the various indicators derived from reconstructed daily MODIS LST data and number of ticks. It appears that other environmental factors might be more important to explain the presence/absence of ticks and indirectly also the distribution of tick-borne diseases. However, with the increasing availability of field data it will be possible to refine the proposed approach and to test it against more field sites.

The final aim of the suggested approach is not to replace field based monitoring programs with remote sensing methods, but to help planning disease management in a more efficient way reducing time and costs associated with field based sampling.

7 Case study 2 – Application of the reconstructed LST time series to mosquito-borne disease modelling

The recent rapid spread of *Aedes albopictus* (tiger mosquito), an invasive disease vector is a major health concern in several European countries. Populations of this insect established in Albania and Italy and it is spreading fast in the Balkan countries, France, Greece and Spain. An important environmental factor in the assessment of its distribution is the temperature, which can be assessed from daily satellite data. Further factors are precipitation, the presence of human population to feed on and the existance of small vases or tyres in which small amounts of water accumulate for egg depositing.

Another disease-relevant mosquito species is *Culex pipiens* (house mosquito) which is widely distributed in the world (Vinogradova, 2000). Several species in the *Culex* genus of mosquito are vectors of diseases, like West Nile virus, Japanese and St. Louis encephalitis, avian malaria and others (see also Section 1.1.2). Temperature is also considered here to be relevant for the transmission of certain diseases through *Culex pipiens*.

7.1 Integration of LST remote sensing into mosquito-borne disease modelling

7.1.1 *Culex pipiens* and temperature

The development of *Culex pipiens* mosquitoes, since they are ectotherm animals which depend on the ambient temperature. Warmer temperatures lead to quicker mosquito development (from egg to adult) and accelerates the replication of arboviruses in the mosquito (Dohm et al., 2002). In order to assess the risk of virus transmission such as West Nile virus by *Culex pipiens* in nature, the ambient temperature needs to be considered when evaluating the vector competence of *Culex pipiens* (Dohm et al., 2002).

Paz and Albersheim (2008) analysed temperature time series and West Nile virus (WNV) and found that in Israel heat in the early spring had influence on the vector population increase and on WNV appearance some weeks later. They suggest this relationship as a measure to identify disease risk from high spring temperatures before the disease start to actually spread.

Tachiiri et al. (2006) list the amount of growing degree days (GDD, see Sections 3.7.2 and 5.3.2) to complete the indicated life stages:

- egg: 30 GDD with 7 °C baseline temperature when 3 day mean >= 7 °C;
- larva: 150 GDD with 9 °C baseline temperature when 3 day mean >= 7 °C;
- pupa: 50 GDD with 8 °C baseline temperature when 3 day mean >= 7 °C.

Some criticism on applying the GDD model directly to WNV transmission have been expressed by Kilpatrick et al. (2008). In the opinion of these authors the linear GDD model underestimates the impact of temperature T on WNV transmission and suggest to consider an alternative model which is a fitted function based on T^4, due to the exponential increase with temperature in chemical and molecular processes contributing to viral replication (Kilpatrick et al., 2008).
From reconstructed daily MODIS LST, the GDD maps can be generated and thresholded according to above values. In absence of *Culex pipiens* data, the following case study concentrates on *Aedes albopictus* in the framework of the RISKTIGER project with a similar approach.

7.1.2 *Aedes albopictus* and temperature

Aedes albopictus is an invasive disease vector of increasing importance in Europe and in other places in the world (see 1.1.2). The distribution of *Ae. albopictus* is determined by several environmental variables including winter and summer temperatures. Upon introduction of the *Ae. albopictus* vector in a specific area, its future distribution depends on suitable conditions for its establishment and spread. Besides rainfall (annual precipitation over 500 mm; sufficient summer rainfall), which was not considered here as it is not a limiting factor in northern Italy, the following temperature related environmental conditions are considered to be important:

- *Ae. albopictus* eggs depend on winter temperatures: below a certain temperature threshold the eggs do not survive. Many authors define the threshold of >= 0 °C mean January air temperature as relevant (Knudsen et al., 1996; Kobayashi et al., 2002; Medlock et al., 2006). However, in Japan adult mosquitoes were detected in areas with an even lower mean January temperatures of -2 °C (Kobayashi et al., 2002); other authors report similar negative temperature thresholds elsewhere;
- Summer temperatures are relevant since they influence the speed of development from the immature stages (larva, pupa) to adult mosquitoes. The development rate is optimal when temperatures are between 25 °C and 30 °C (Straetemans, 2008). Low summer temperatures would prolong the time necessary for *Ae. albopictus* larvae to mature into adult mosquitoes. In an European study, different summer temperature thresholds were applied with cutoff temperatures of <15 °C and >30 °C, and an optimum between 20 °C and 25 °C (monthly mean temperatures over July and August, European Centre for Disease Prevention and Control (2009));
- Annual mean temperatures are another ecological indicator used to determinate the areas of adult survival (Medlock et al., 2006; Benedict et al., 2007). The threshold value of 11 °C is a commonly assumed value (Kobayashi et al., 2002);
- Growing Degree Days (GDD) are commonly used as proxy variable of insect development. Typically, a baseline temperature of T_{base}=11 °C (Kobayashi et al., 2002) is applied in *Ae. albopictus* research. A certain amount of GDD must be reached to permit egg hatching in spring, and later to complete larva, pupa development to adult mosquito before egg deposition and the further die-off in autumn;

- The autumnal mean temperature is of relevance for the adult survival and for completion of all life stages. A threshold of mean air temperatures not lower than 10 °C is considered to be relevant (Toma et al., 2003).

As one can see in this list, temperature is an important parameter in the prediction of *Ae. albopictus* distribution and with regard to global change it may also give implications on the future vector spread. European Centre for Disease Prevention and Control (2009) predicted European *Ae. albopictus* distribution based on temperature derived variables.

The aim of this case study is to identify the potential distribution area period by comparing field entomological data to satellite data (MODIS Land Surface Temperature maps). *Ae. albopictus* is currently spreading in the study area in the Trento and Belluno provinces while it is already established in large parts of the Veneto region. In this case study, the focus was on the most important factor, temperature, performed through analysis of *Ae. albopictus* egg winter survival and a distribution assessment through filtered growing degree days. For egg winter survival, the main purpose is to define the correspondence between the known threshold for mean January air temperature and a remotely sensed LST threshold in order to predict the distribution of *Ae. albopictus* at regional scale.

For some parts of the study area, especially in Trentino, absence and presence patterns of *Ae. albopictus* are known from ovitrapping and field surveys (see below). Unfortunately, data from Bolzano and Belluno provinces are absent/scarce and the confirmed vector presence will represent only a fraction of the true distribution of *Ae. albopictus*.

7.2 Survival of *Ae. albopictus* eggs in Trentino/South Tyrol/Belluno: prediction of current and potential mosquito distribution

7.2.1 Field data and daily MODIS LST data

Ae. albopictus presence data were collected at the municipality level for Belluno (Martini S., pers. comm.), Trentino (Roiz D., pers. comm.) with additional data for Rovereto (Ferrarese, 2003) and furthermore from literature for the Veneto and Friuli regions (Drago A., pers. comm.). These data points were geocoded by municipality name, hence the point refers to the barycentre of the municipality and not necessarily to the true position. This will change in future when oviposition trap data from the RISKTIGER project at FEM will be used. For the Bolzano province, *Ae. albopictus* fieldsurvey data were not available.

Reconstructed daily MODIS LST maps were prepared as outlined in the previous chapters and applied in this case study, basically by data aggregation and thresholding.

7.2.2 Capturing winter survival of *Ae. albopictus* eggs with MODIS LST

From the reconstructed daily LST maps, a mean of January LST map was prepared for the study area from all January maps in the period 2001-2009. For each pixel the monthly average of the daily mean temperatures per year for all Januaries (2001-2009) was calculated. The resulting mean LST January map was thresholded for various minimum mean temperatures (0 °C, -1 °C, -2 °C, and -3 °C) to obtain binary threshold maps ("true" if above the threshold,

"false" otherwise). Finally, all threshold maps were integrated into a single map by summing up the number of "true" conditions for each pixel and by a subsequent scoring to classify the frequency of being over the threshold. The goal was to identify > 50% probability of excess of the given minimum threshold with the following classes:

- classes 0, 1, 2, 3, 4: not suitable;
- classes 5, 6: 1 marginally suitable;
- classes 7, 8: 2 moderately suitable;
- class 9: 3 highly suitable.

Results are shown in Section 7.3.1.

7.2.3   Growing Degree Days analysis with autumnal mean temperature threshold

The commonly used indicator variable Growing Degree Days (GDD, see Section 3.7.2) is applied to *Ae. albopictus* typically with a baseline temperature of T_{base}=11 °C (Kobayashi et al., 2002; European Centre for Disease Prevention and Control, 2009). As indicated above, a certain amount of GDD must be reached to permit the completion of the life cycle.

GDD maps were calculated for 2003 to 2008 from reconstructed daily MODIS LST (see Section 5.3.2) in order to spatially assess the required GDD minimum for *Ae. albopictus* survival and establishment. MODIS maps of 2000-2001 were not used since only Terra was available which would lead to skewed GDD values. Likewise in 2002, since Aqua was only started in summer 2002, the resulting GDD maps would have been unreliable.

The created GDD maps were then thresholded for 1,350 GDD to identify the areas where 1,350 GDD are reached throughout the year (value after Kobayashi et al. 2002). As this could happen even in December, the resulting map was filtered again for too low autumnal mean temperature which are a limiting factor for adult survival (Toma et al., 2003). More specifically, LST pixels with autumn mean temperatures of >10 °C were selected as "true", "false" otherwise. For the study area, the monthly mean LST map of October was taken (see Section 5.3.2 for monthly aggregations). Pixels of the 1,350 GDD map were rejected if they had an autumnal mean temperature lower than this autumnal threshold. Effectively, the area which is considered to be suitable for *Ae. albopictus*, was reduced with respect to the pure GDD based distribution map.

Results are shown in Section 7.3.2.

7.3   Results: *Ae. albopictus* distribution maps

7.3.1   Egg winter survival map

For all Januaries from 2001-2009, monthly mean LST maps were created and subsequently individually thresholded for a minimum of 0 °C, -1 °C, -2 °C, and -3 °C. Eventually, the threshold value of -1 °C was selected as the most representative for the distribution of *Ae. albopictus* compared to field sampling. Figure 7.1 shows the spatialised probability classes of the potential areas of egg winter survival along with sites of known *Ae. albopictus* presence. All sites except one were within the predicted distribution area which, in the study area, nonetheless remains

Ae. albopictus egg winter survival distribution maps from thresholded January monthly mean MODIS LST maps (threshold: -1 °C; 2001-2009)
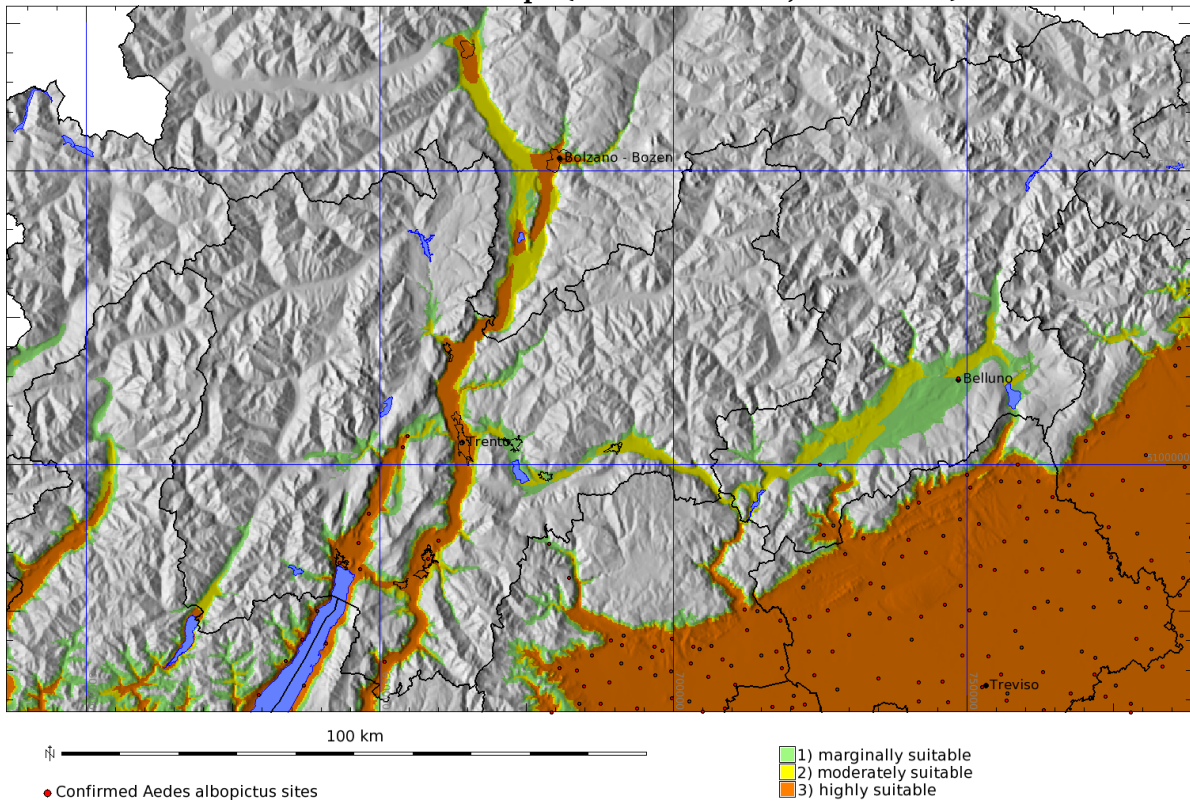
Figure 7.1: **Map of potential *Ae. albopictus* egg winter survival based on January LST monthly mean maps of 2001-2009**
The input maps were individually thresholded for -1 °C and integrated into the resulting map by scoring the number of times the given threshold was reached. Only pixels where in >50% of years the -1 °C threshold was reached are considered, unsuitable areas are grey. For the suitability class definitions, see Section 7.2.2. The sites of known vector presence are overlayed (n=594).

limited to the valley floors and the areas south of the Alps. The resulting map indicates a potential expansion of *Ae. albopictus* within the Adige valley north of Trento; in fact, this species was detected for the first time in the city Trento in 2008 with ovitraps (Roiz et al., in press). A further spread to northern suitable areas, as the city of Bolzano is expected in the near future. In addition, the results suggest that the known minimum mean January air temperature threshold of 0 °C corresponds to -1 °C when using reconstructed daily MODIS LST maps (other threshold maps not shown here).

7.3.2 Distribution prediction through autumnal minimum filtered Growing Degree Days (GDD)

A second approach to predicting the spatial distribution is the use of filtered Growing Degree Days as outlined above. Figure 7.2 shows the areas where 1,350 GDD have been reached throughout the years 2003-2008 with an additional limitation of having an autumnal mean temperature higher or equal to 10 °C. These parameters have been indicated as relevant for *Ae. albopictus* adult survival (Kobayashi et al., 2002). The selected GDD baseline temperature was 11 °C, the cut-off temperature 30 °C. In grey areas either the 1,350 GDD were not reached

Growing degree days/autumnal minimum mean temperature from MODIS LST as predictor for the distribution of *Ae. albopictus* (2003-2008)

● Confirmed Aedes albopictus sites

1) marginally suitable
2) moderately suitable
3) highly suitable
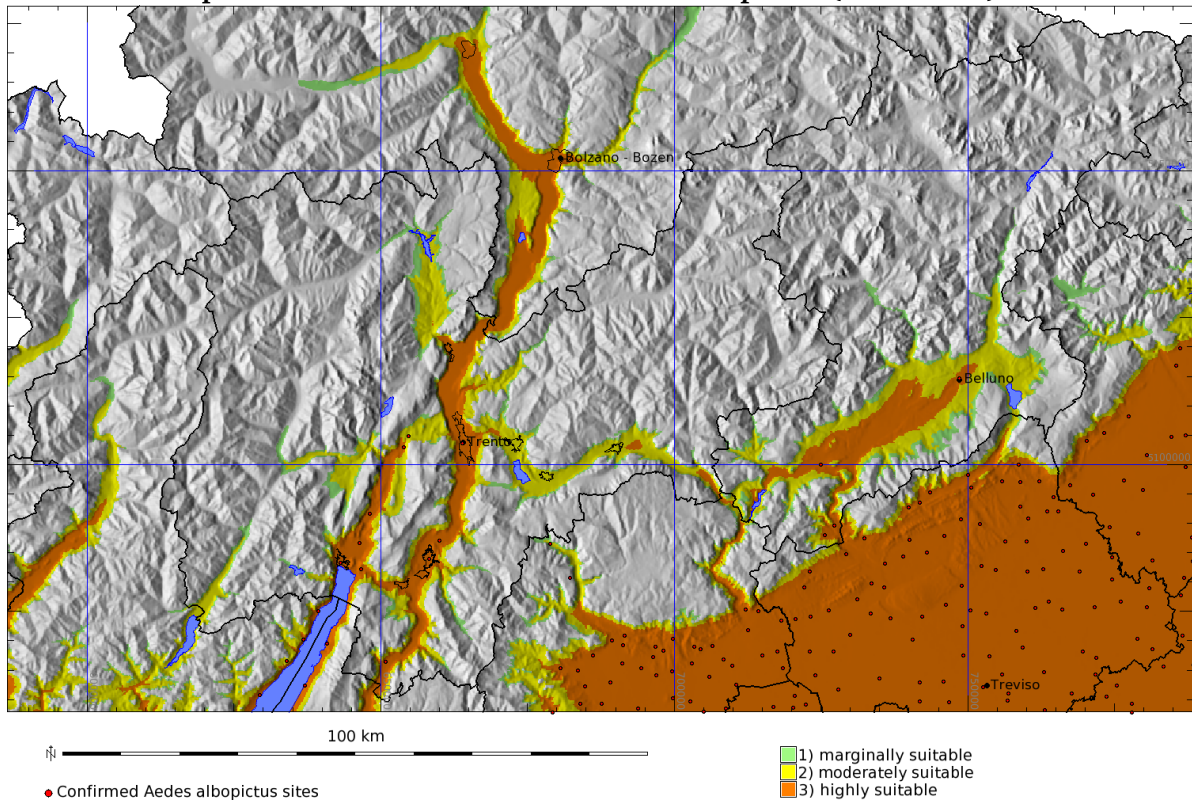
Figure 7.2: **Filtered, accumulated growing degree days (GDD) map of 1,350 GDD from reconstructed daily MODIS LST maps as predictor for the distribution of *Ae. albopictus* (2003-2008)**
In the areas indicated as suitable for *Ae. albopictus* adults, 1350 accumulated growing degree days were reached throughout 2003-2008 before the autumnal monthly mean temperature was falling below 10 °C. As GDD baseline temperature 11 °C was selected with a cut-off temperature of 30 °C. The sites of known vector presence are overlayed (n=594).

in 50% of the years or the autumn was too cold (or both). The sites of known vector presence are overlayed (594 positive municipalities).

7.3.3   Integrated final map of potential distribution map of *Aedes albopictus* based on MODIS LST derived indicators

Figure 7.3 shows the integration of both winter survival and adult survival. Both input maps have been classified as indicated in Section 7.2.2 (classified GDD/autumn map not shown here). The final map is based on a scoring system of these suitability classes which is the pixel-wise summary of the suitability classes of both maps:

- pixel-wise sum 0-3: final class 0 (not suitable);
- pixel-wise sum 4: final class 1 (marginally suitable);
- pixel-wise sum 5: final class 2 (moderately suitable);
- pixel-wise sum 6: final class 3 (highly suitable).

Integrated potential distribution map of *Aedes albopictus* based on classified January threshold map (-1 °C) and classified GDD/autumnal minimum mean temperature
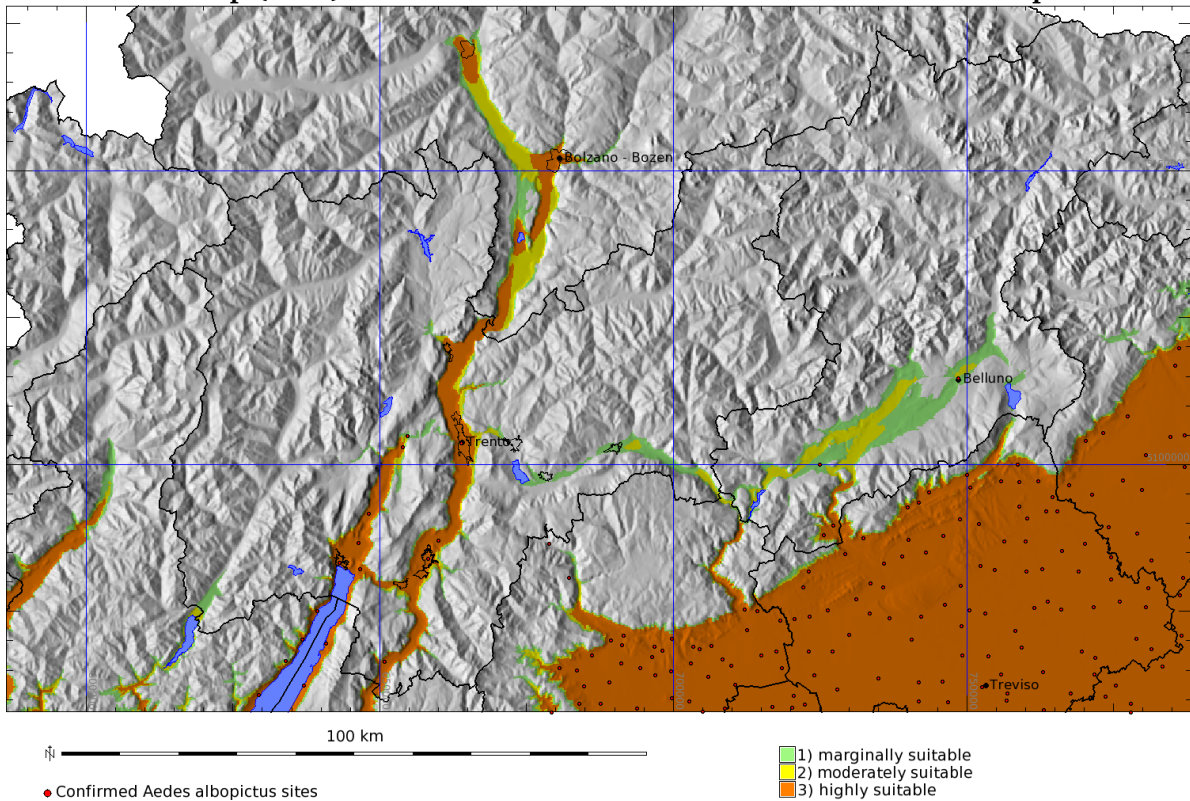
Figure 7.3: **Integrated potential distribution map of *Ae. albopictus* based on MODIS LST derived temperature indicators**
The potential distribution map shows the integrated suitability for egg winter survival and adult survival as three classes, unsuitable areas are grey. For the suitability class definitions, see Section 7.3.3. The sites of known vector presence are overlayed (n=594).

To illustrate the effects of this scoring system, here some examples:

- classes 1/2/3 of winter survival + class 0 of GDD/autumn => sum 3 => not suitable;
- classes 1/2/3 of GDD/autumn + class 0 of winter survival => sum 3 => not suitable;
- classes 3 of winter survival + 1 of GDD => sum 4 => marginally suitable;
- classes 2 of winter survival + 2 of GDD => sum 4 => marginally suitable;
- classes 2 of winter survival + 3 of GDD => sum 5 => moderately suitable;
- classes 3 of winter survival + 3 of GDD => sum 6 => highly suitable;

Overlayed to the final map again all positive municipalities (year 2007) are shown. Only two out of 594 positive municipalities result to be outside of the predicted distribution area of *Ae. albopictus* (false negative error of 0.3%), despite the low spatial precision of the geocoding by municipality name. No false positive municipalities are present.

The Adige valley, the area north of Lake Garda as well as major parts of the Veneto region result to be highly suitable for the vector. Only the basin south-west of Belluno, Valsugana and some northern parts of the Adige valley are moderately or marginally suitable. Altitudes above 800 m are not suitable.

In most of the areas except for the central and northern parts of the Adige valley the presence of *Ae. albopictus* has been confirmed.

7.4   Discussion

The results show that temperature based indicators from reconstructed daily MODIS LST maps are able to discriminate absence and presence of *Aedes albopictus*. The advantage of using reconstructed LST maps is that they are intrinsically spatialised, leading to a differentiated predition which reflects even microhabitats. The two assessment approaches presented here (eggs winter survival map as well as the growing degree day map filtered for minimum autumnal mean temperature) include the areas of known presence of *Ae. albopictus* and show other potentially suitable areas. Interestingly, both distribution maps agree to 89% despite the different approach and the different considered life stages. The adult survival map shows a slightly larger extent than the egg winter survival map.

The spatially overlapping area covers 89% of the two input maps (January temperature threshold and GDD/autumnal means temperature maps). This is caused by the relatively smaller extent of the January temperature threshold map with respect to the other map. Apparently the winter conditions are a more limiting factor than the annual course of temperature profile. This overlap map is subjected to the scoring system in order to obtain suitability classes. From the final, integrated map it can be seen that the resulting area in which *Ae. albopictus* survival is predicted is smaller than the Growing degree days/autumnal minimum mean temperature map due to the limited egg winter survival.

The final map describes the existing areas with vector presence but indicates also potential new area where the vector has not (yet) been detected. Concerning the future expansion of the potential disease vector, it must be stated that while some highly suitable areas (Merano, Bolzano) appear to be disconnected from other areas, there is still the risk of the passive egg transport which can lead to further *Ae. albopictus* dispersal and introduction of the insect in these areas. However, the prediction of the expected future expansion of the vector also depends on the interplay of other factors such as presence of larval habitats, human population density or land cover, and further environmental variables, which were not considered here.

In future research, refinement to assess *Ae. albopictus* habitats can be gained through the integration of additional temperature indicators as outlined in the introduction. Furthermore, the use of additional remote sensing data sources including the MODIS Enhanced Vegetation Index time series will be interesting. To enhance the underlying GIS database, also high spatial resolution data resources as urban vegetation and housing areas (e.g., extracted from classified orthophotos) as well as the distribution of humans from population density maps could be added. Future research may also consider the application of these indicators, with modifications to *Culex pipiens* populations, in order to cover temperature related effects on populations and transmission of diseases.

7.5   Conclusions

In this case study, two approaches of LST data usage for disease vector distribution at a regional scale in Northern Italy have been presented. The calculated two indicator maps (egg winter survival via January temperature thredshold and completion of life stages through growing degree days and autumnal mean temperature) have been integrated into a final potential distribution

map. It coincides with the currently known distribution of *Ae. albopictus* but is covering also new areas in which the mosquito was either not yet detected or not reported. Hence, it is the potentially suitable area which might be colonised in future. These areas are suggested to be included in ongoing and planned monitoring mosquito control campaigns. Since MODIS on Terra and Aqua are a continously monitoring platform, these campaigns can be supported in almost real-time.

The results show that it is possible with postprocessed MODIS LST data, to assess in a rather detailed manner the current and potential distribution of *Ae. albopictus*. The approach deems to be valid with the advantage of avoiding challenging interpolation of meteorological station data, especially in complex terrain.

8 Conclusions and outlook

The availability of new, high temporal resolution satellite data offers fresh opportunities for remote sensing in epidemiological and other fields. The new time series are reducing the gap between high spatial resolution (with typically low temporal resolution) and high temporal resolution (originally with low spatial resolution, although this is now significantly enhanced). Of special interest are the satellites Terra (data available from 3/2000 onwards) and Aqua (data available from 8/2002 onwards). Each day, four global coverages from the MODIS sensors onboard e.g. of Land Surface Temperature (LST) are generated at various resolutions, along with other data (vegetation indices, snow coverage, etc.). The processed MODIS data are usually published less than one week after acquisition on a NASA server.

While the available LST maps time series are already an impressive data source, they suffer from cloud contamination and other pixel problems which leads to no data areas in the LST maps. From the literature no systematic reconstruction of daily LST data is known, only aggregated approaches are found which do not maintain the characteristics of daily changes. This thesis proposes a new approach to overcome this problem. As a result, void data areas are reconstructed using a temperature gradient model which is either based on the actual map statistics (if a sufficient number of pixels is present) or otherwise based on a typical gradient based on 16-day period data aggregation. Like this, even completely missing maps can be synthetically generated to obtain a complete daily LST time series. In total, more than 11,000 maps were reprocessed, through the modelling approach the original LST map resolution of 1,000 m could be increased to 200 m. Not surprisingly, complete time series are of great advantage to facilitate further GIS based analysis.

The typical approach of obtaining temperature maps from meteorological stations is rather challenging for the study area due to its complex terrain (Central European Alps). Meteorological stations and ground surveys are irregularly distributed and favour agricultural zones. In this thesis, it has been shown that reconstructed daily MODIS LST data can be used to substitute aggregated meteorological data for many purposes. An additional advantage is the fact that satellite data are already spatialised; this helps to identify effects of microhabitats which are typically getting lost in classical meteorological data spatial interpolation.

In disease risk modelling, remote sensing has been reported to be underused with respect to existing resources. This may be also caused by unavailability of high temporal resolution data which are of great relevance in epidemiological modelling. The approach proposed in this thesis aims at offering complete data sets at various temporal resolutions (the original daily resolution plus various aggregations including 16-days periods/monthly/annual measures, seasonal anomalies, threshold maps, growing degree days, spring warming and autumnal cooling gradients).

The obtained LST time series and the derived indicators have been applied in two case studies. In the case of the *Ixodes ricinus* distribution and seasonality assessment in Belluno, no clear signal was obtained for the available limited tick data set. Integrating more tick sampling sites may help to better separate signal from noise but at time no more tick data are available.

In the second case study on *Aedes albopictus*, two different derivatives of daily LST maps could be applied successfully to obtain distribution maps of the vector. One is egg winter survival based on January temperature thresholds, the other is a prediction based on growing degree days filtered with an autumnal minimum threshold. Both maps coincide significantly (89% of overlap). This indicates good agreement but yet some variation in the survival of different life stages. Only two out of 594 positive municipalities result outside of the predicted distribution area of *Ae. albopictus* (false negative error of 0.3%). As ectotherm parasites, *Ae. albopictus* is quite susceptible to changes in ambient temperature and hence the use of LST maps it deems appropriate for the vector distribution mapping. Reconstructed MODIS LST data can be accepted as a valid proxy for analysing the temperature profile in relation to mosquito survival.

8.1   Future research

Concerning future improvements of the LST map reconstruction, some limitations will be addressed which are indicated in Section 3.3. To make the obtained time series more general, atmospheric thermal inversion in the winter period needs to be addressed. However, is it unclear how an atmospheric thermal inversion is reflected in the Land Surface Temperatures since the surface response is slower than a change of atmospheric temperatures. This may require ground truth measurements.

In order to be able to transfer the approach to different areas in Europe or elsewhere, the geomorphological composition of the area might be required to be separated into geomorphologically homogeneous subareas to accommodate the fact that global "MODIS LST gradients" (not air temperature gradients) are applied which are bound to the relief type. These separate LST map reconstructions have to be well reconnected then. For larger study areas up to subcontiental size, it is essential to substantially accelerate the LST interpolation part of the algorithm and to make it less computer memory demanding. In this regard, a tiling approach may be helpful. An alternative to be evaluated is a replacement of the spline based interpolation (for example, with co-kriging that supports segmentation).

A more precise estimation of instantaneous air temperatures could be tried with additional MODIS vegetation index maps as suggested in Goetz et al. (2000), Green and Hay (2002), Kawashima et al. (2000), and Colombi et al. (2007). In this thesis some differences were observed between instantaneous meteorological data and LST overpasses. There may be potential to improve this situation.

8.2   Other uses of reconstructed LST time series

The LST time series which have been produced for this thesis are not limited to epidemiological modelling but they are of general purpose. A series of further applications can be anticipated:

In the field of agriculture, growing degree day (GDD) maps are common for the phenological assessment of budburst, flowering and crop maturing. Using MODIS LST based maps provides easy access to spatialised GDD data which are able to take microclimatic effects into account.

Using MODIS LST time series, the shift of the upper forest limits may be assessed, likewise the suitability for the presence of tree (or other plants) species in terms of sensitivity to temperature. In mountaneous areas, in higher altitudes the soil weathering and development is much temperature dependent. Here, MODIS LST can be used to analyse the impact of high(er) surface temperatures while air temperature is commonly lower and less relevant in this regard.

In the vast areas of permafrost where almost no meteorological stations are available, MODIS LST data may be used to determine the duration of the phases over 0 °C and their spatial extent. Global warming appears to shift the permafrost base to north which could be mapped with remote sensing. This could result in a monitoring scheme of an active layer at daily temporal resolution.

A different potential usage can be suggested in the field of production of artificial snow for winter tourism. Artificial snow-making has become the dominant adaptation strategy for the winter tourism industry which requires detailed knowledge about the surface temperature distribution. While MODIS LST data are not instantaneously available if no local receiving station exists (as recently established at EURAG, Bolzano), they are still a reasonable tool for strategic planning.

In an urban context, other uses may include the estimation of cooling degree-days for buildings or for urban heat island analysis as performed in a few studies with NOAA-AVHRR thermal infrared data and MODIS LST (Tran et al., 2006; Stathopoulou et al., 2006).

Bibliography

Ackerman, S. A., Strabala, K. I., Menzel, W. P., Frey, R. A., Moeller, C. C., and Gumley, L. E.Discriminating clear sky from clouds with MODIS. *Journal of Geophysical Research - Atmospheres* **103** (D24): 141–157.

Allen, T. R. and Shellito, B. 2008. Spatial interpolation and image-integrative geostatistical prediction of mosquito vectors for arboviral surveillance. *Geocarto International* **23** (4): 311–325.

Alto, B. W. and Juliano, S. A. 2001a. Precipitation and temperature effects on populations of Aedes albopictus (Diptera: Culicidae): implications for range expansion. *Journal of Medical Entomology* **38** (5): 646–656.

Alto, B. W. and Juliano, S. A. 2001b. Temperature effects on the dynamics of aedes albopictus (diptera: Culicidae) populations in the laboratory. *Journal of medical entomology* **38** (4): 548–556, URL `http://view.ncbi.nlm.nih.gov/pubmed/11476335`.

Altobelli, A., Boemo, B., Mignozzi, K., Bandi, M., Floris, R., Menardi, G., and Cinco, M. 2008. Spatial Lyme borreliosis risk assessment in north-eastern Italy. *International Journal of Medical Microbiology* **298**: 125–128.

Aplin, P. 2005. Remote sensing: ecology. *Progress in Physical Geography* **29** (1): 104–113.

Barbour, A. G. 1998. Fall and rise of Lyme disease and other Ixodes tick-borne infections in North America and Europe. *British Medical Bulletin* **54** (3): 647–658.

Beck, L. R., Lobitz, B. M., and Wood, B. L. 2000. Remote sensing and human health: New sensors and new opportunities. *Emerging Infectious Diseases* **6** (3): 217–227.

Beck, P. S., Atzberger, C., Hogda, K. A., Johansen, B., and Skidmore, A. K. 2006. Improved monitoring of vegetation dynamics at very high latitudes: A new method using MODIS NDVI. *Remote Sensing of Environment* **100** (3): 321–334.

Benedict, M. Q., Levine, R. S., Hawley, W. A., and Lounibos, L. P. 2007. Spread of the tiger: global risk of invasion by the mosquito *Aedes albopictus*. *Vector borne and zoonotic diseases (Larchmont, N.Y.)* **7** (1): 76–85.

Bengis, R. G., Leighton, F. A., Fischer, J. R., Artois, M., Mörner, T., and Tate, C. M. 2004. The role of wildlife in emerging and re-emerging zoonoses. *Revue Scientifique et Technique de l'Office International des Epizooties* **23** (2): 497–511.

Bernardi, M. 2001. Linkages between FAO agroclimatic data resources and the development of GIS models for control of vector-borne diseases. *Acta Tropica* **79** (1): 21–34.

Blanco, J. R. and Oteo, J. A. 2002. Human granulocytic ehrlichiosis in Europe. *Clinical Microbiology and Infection* **8** (12): 763–772.

Boato, S., Arrighetti, A., and Osti, F. 1988. *Parchi e riserve naturali del Trentino*. Temi, Trento.

Bown, K. J., Begon, M., Bennett, M., Woldehiwet, Z., and Ogden, N. H. 2003. Seasonal dynamics of Anaplasma phagocytophila in a rodent-tick (Ixodes trianguliceps) system, United Kingdom. *Emerging Infectious Diseases* **9** (1).

Brown, H., Diukwasser, M., Guan, Y., Caskey, S., and Fish, D. 2008. Comparison of three satellite sensors at three spatial scales to predict larval mosquito presence in Connecticut wetlands. *Remote Sensing of Environment* .

Burrough, P. and McDonnell, R. 1998. *Principles of Geographical Information Systems*. New York: Oxford University Press.

Carpi, G., Cagnacci, F., Neteler, M., and Rizzoli, A. 2008. Tick infestation on roe deer in relation to geographic and remotely sensed climatic variables in a tick-borne encephalitis endemic area. *Epidemiology and Infection* pp. 1416–1424.

Cattadori, I. M., Hudson, P. J., Merler, S., and Rizzoli, A. 1999. Synchrony, scale and temporal dynamics of rock partridge (*Alectoris graeca saxatilis*) populations in the Dolomites. *Journal of Animal Ecology* **68** (3): 540–549.

Chaput, E. K., Meek, J. I., and Heimer, R. 2002. Spatial analysis of human granulocytic ehrlichiosis near Lyme, Connecticut. *Emerging Infectious Diseases* **8** (9): 943–948.

Clarke, K. C., McLafferty, S. L., and Tempalski, B. J. 1996. On epidemiology and geographic information systems: a review and discussion of future directions. *Emerging infectious diseases* **2** (2): 85–92.

Colditz, R., Conrad, C., Wehrmann, T., Schmidt, M., and Dech, S. 2006. Generation and assessment of MODIS time series using quality information. In *Proc. IGARSS, IEEE International Geoscience And Remote Sensing Symposium, Denver, CO*.

Colombi, A., De Michele, C., Pepe, M., and Rampini, A. 2007. Estimation of daily mean air temperature from MODIS LST in Alpine areas. *EARSeL eProceedings* **6** (1): 38–46.

Colyvan, M. and Ginzburg, L. R. 2003. Laws of nature and laws of ecology. *Oikos* pp. 649–653.

Comunità Montana Feltrina 2006. Rapporto sullo stato dell'ambiente. Documento Unico di Programmazione (DOCUP) Obiettivo 2 per gli anni 2000-2006, Misura 4.3 Azione b "Informazione ed educazione ambientale".

Cortinas, M. R., Guerra, M. A., Jones, C. J., and Kitron, U. 2002. Detection, characterization, and prediction of tick-borne disease foci. *International Journal of Medical Microbiology* **291**: 11–20.

Cressie, N. 1993. *Statistics for Spatial Data*. New York: Wiley.

Curran, P. J. 2001. Remote sensing: Using the spatial domain. *Environmental and Ecological Statistics* **8** (4): 331–344.

Dale, P. E., Ritchie, S. A., Territo, B. M., Morris, C. D., Muhar, A., and Kay, B. H. 1998. An overview of remote sensing and GIS for surveillance of mosquito vector habitats and risk assessment. *Journal of Vector Ecology* **23** (1): 54–61.

Daniel, M., Kolár, J., and Zeman, P. 2004. GIS tools for tick and tick-borne disease occurrence. *Parasitology* **129**.

Daniel, M., Kolár, J., Zeman, P., Pavelka, K., and Sádlo, J. 1999. Tick-borne encephalitis and Lyme borreliosis: comparison of habitat risk assessments using satellite data (an experience from the Central Bohemian region of the Czech Republic). *Central European Journal of Public Health* **7** (1): 35–39.

Dennis, D. T. and Hayes, E. B. 2002. Epidemiology of Lyme Borreliosis. In *Lyme Borreliosis: Biology, epidemiology and control* (eds. Gray, J. S., Kahl, O., Lane, R. S., and Stanek, G.). CABI Publishing.

Dohm, D. J., Oguinn, M. L., and Turell, M. J. 2002. Effect of environmental temperature on the ability of Culex pipiens (Diptera: Culicidae) to transmit West Nile Virus. *Journal of Medical Entomology* pp. 221–225.

Donoso, Schädler, R., and Niedrig, M. 2008. Surveillance and outbreak reports. A survey on cases of tick-borne encephalitis in European countries. *Eurosurveillance* **13** (4-6): 1–9, URL `http://www.eurosurveillance.org/ViewArticle.aspx?ArticleId=18848`.

Dumler, J. S., Barbet, A. F., Bekker, C. P., Dasch, G. A., Palmer, G. H., Ray, S. C., Rikihisa, Y., and Rurangirwa, F. R. 2001. Reorganization of genera in the families Rickettsiaceae and Anaplasmataceae in the order Rickettsiales: unification of some species of Ehrlichia with Anaplasma, Cowdria with Ehrlichia and Ehrlichia with Neorickettsia, descriptions of six new species combinations and designation of Ehrlichia equi and 'HGE agent' as subjective synonyms of Ehrlichia phagocytophila. *International Journal of Systematic and Evolutionary Microbiology* **51** (Pt 6): 2145–2165.

Easterling, D. R., Horton, B., Jones, P. D., Peterson, T. C., Karl, T., R., Parker, D. E., Salinger, J. M., Razuvayev, V., Plummer, N., et al. 1997. Maximum and minimum temperature trends for the globe. *Science* **277** (5324): 364–367.

Eisen, R. J., Eisen, L., and Lane, R. S. 2005. Remote sensing (Normalized Difference Vegetation Index) classification of risk versus minimal risk habitats for human exposure to Ixodes pacificus (Acari: ixodidae) nymphs in Mendocino County, California. *Journal of Medical Entomology* **42** (1): 75–81.

Endrizzi, S., Bertoldi, G., Neteler, M., and Rigon, R. 2005. Reproduction of snow melting spatial patterns with the hydrologic model GEOtop. In *Geophysical Research Abstracts; Vienna, Austria, 24-29 April 2005*. European Geophysical Union.

Enserink, M. 2007. Epidemiology: Tropical disease follows mosquitoes to Europe. *Science* **317** (5844): 1485a+.

Eritja, R., Escosa, R., Lucientes, J., Marques, E., Roiz, D., and Ruiz, S. 2005. Worldwide invasion of vector mosquitoes: present European distribution and challenges for Spain. *Biological Invasions* **7** (1): 87+.

Estrada-Peña, A. 2008. Climate, niche, ticks, and models: what they are and how we should interpret them. *Parasitology Research* **103** (S1): 87–95.

Estrada-Peña, A. 1999a. Geostatistics and remote sensing using NOAA-AVHRR satellite imagery as predictive tools in tick distribution and habitat suitability estimations for Boophilus microplus (Acari: Ixodidae) in South America. National Oceanographic and Atmosphere Administration-Advanced Very

High Resolution Radiometer. *Veterinary Parasitology* **81** (1): 73–82.

Estrada-Peña, A. 1999b. Geostatistics as predictive tools to estimate Ixodes ricinus (Acari: Ixodidae) habitat suitability in the western Palearctic from AVHRR satellite imagery. *Experimental and Applied Acarology* **23** (4): 337–349.

Estrada-Peña, A. 2002. Increasing habitat suitability in the United States for the tick that transmits Lyme disease: A remote sensing approach. *Environmental Health Perspectives* **110** (7): 635–640.

Estrada-Peña, A. and Jongejan, F. 1999. Ticks feeding on humans: a review of records on human-biting Ixodoidea with special reference to pathogen transmission. *Experimental and Applied Acarology* **23** (9): 685–715.

European Centre for Disease Prevention and Control 2009. Development of Aedes albopictus risk maps. Technical report, European Centre for Disease Prevention and Control. URL `http://ecdc.europa.eu/en/Activities/Disease_Projects/_ezo/maps.aspx`.

Faulde, M. and Hoffmann, G. 2001. Vorkommen und Verhütung vektorassoziierter Erkrankungen des Menschen in Deutschland unter Berücksichtigung zoonotischer Aspekte. *Bundesgesundheitsblatt - Gesundheitsforschung - Gesundheitsschutz* **44** (2): 116–136.

Ferrarese, U. 2003. Monitoraggio di Aedes albopictus (Skuse)(Diptera, Culicidae) attorno a un focolaio nel comune di Rovereto (Trento). *Annali Museo Civico Rovereto* **19**: 281–295.

Fonseca, D. M., Keyghobadi, N., Malcolm, C. A., Mehmet, C., Schaffner, F., Mogi, M., Fleischer, R. C., and Wilkerson, R. C. 2004. Emerging vectors in the *Culex pipiens* complex. *Science (New York, N.Y.)* **303** (5663): 1535–1538.

Fontenille, D., Failloux, A. B., and Romi, R. 2007. Should we expect Chikungunya and Dengue in southern Europe? In *Emerging pest and vector-borne diseases in Europe* (eds. Takken, W. and Knols, B.), chapter 10, pp. 169–184. Wageningen Academic.

Frumkin, H. 2005. *Environmental Health: From Global to Local (Public Health/Environmental Health)*. Jossey-Bass, 1st edition.

Furlanello, C., Merler, S., Menegon, S., Mancuso, S., and Bertiato, G. 2002. New WEBGIS technologies for geolocation of epidemiological data: an application for the surveillance of the risk of Lyme borrelliosis disease. *Giornale Italiano di Aritmologia e Cardiostimolazione* **5** (1): 241–245.

Gao, B.-C. 1996. NDWI – A Normalized Difference Water Index for remote sensing of vegetation liquid water from space. *Remote Sensing of Environment* **58** (3): 257–266.

Gern, L. and Humair, P. F. 2002. Ecology of Borrelia burgdorferi sensu lato in Europe. In *Lyme Borreliosis: Biology, Epidemiology and Control* (eds. Gray, J., Kahl, O., Lane, R., and Stanek, G.). CABI Publishing.

Gern, L., Morán Cadenas, F., and Burri, C. 2008. Influence of some climatic factors on *Ixodes ricinus* ticks studied along altitudinal gradients in two geographic regions in Switzerland. *International Journal of Medical Microbiology* pp. 55–59.

Gillanders, S. N., Coops, N. C., Wulder, M. A., Gergel, S. E., and Nelson, T. 2008. Multitemporal remote sensing of landscape dynamics and pattern change: describing natural and anthropogenic trends. *Progress in Physical Geography* **32** (5): 503–528.

Glass, G. E., Schwartz, B. S., Morgan, J. M., Johnson, D. T., Noy, P. M., and Israel, E. 1995. Environmental risk factors for Lyme disease identified with geographic information systems. *Americal Journal of Public Health* **85** (7): 944–948.

Goetz, S. J., Prince, S. D., and Small, J. 2000. Advances in satellite remote sensing of environmental variables for epidemiological applications. *Advances in Parasitology* **47**: 289–307.

Gray, J. S. 2001. The biology of Ixodes ticks, with special reference to Ixodes ricinus. In *Proc. Symposium Current Research on Tick-Borne Infections, Kalmar, Sweden*.

Gray, J. S., Dautel, H., Estrada-Peña, A., Kahl, O., and Lindgren, E. 2009. Effects of climate change on ticks and tick-borne diseases in Europe. *Interdisciplinary Perspectives on Infectious Diseases* **2009**.

Green, R. M. and Hay, S. I. 2002. The potential of Pathfinder AVHRR data for providing surrogate climatic variables across Africa and Europe for epidemiological applications. *Remote Sensing of Environment* **79** (2-3): 166–175.

Grunewald, J., Habedank, B., Hartelt, K., Kampen, H., Kimmig, P., Maier, W. A., Naucke, T., Oehme, R., Vollmer, A., Schöler, A., et al. 2003. *Mögliche Auswirkungen von Klimaveränderungen auf die Ausbreitung von primär humanmedizinisch relevanten Krankheitserregern über tierische Vektoren sowie auf die wichtigen Humanparasiten in Deutschland*. 200 61 218/11.UBA-FB 000454. URL `http://www.umweltbundesamt.org/fpdf-k/2291.pdf`.

Haglund, M. 2001. Tick-borne encephalitis (TBE) - an overview. In *Proc. Symposium Current Research on Tick-Borne Infections, Kalmar, Sweden*.

Hais, M. and Kučera, T. 2009. The influence of topography on the forest surface temperature retrieved from landsat tm, etm + and aster thermal channels. *ISPRS Journal of Photogrammetry and Remote Sensing* **64** (6): 585–591.

Hall, D. K., Riggs, G. A., Salomonson, V. V., Digirolamo, N. E., and Bayr, K. J. 2002. MODIS snow-cover products. *Remote Sensing of Environment* **83** (1): 181–194.

Hargrove, W. W. 1997. Interpolation of rainfall in switzerland using a regularized spline with tension. URL http://www.geobabble.org/~hnw/sic97/.

Hashimoto, H., Dungan, J., White, M., Yang, F., Michaelis, A., Running, S., and Nemani, R. 2008. Satellite-based estimation of surface vapor pressure deficits using MODIS land surface temperature data. *Remote Sensing of Environment* **112** (1): 142–155.

Hassan, Q. K., Bourque, C. P., Meng, F. R., and Richards, W. 2007. Spatial mapping of growing degree days: an application of MODIS-based surface temperatures and Enhanced Vegetation Index. *Journal of Applied Remote Sensing* **1** (1): 013511+.

Hawley, W. A. 1988. The biology of *Aedes albopictus*. *Journal of the American Mosquito Control Association* **1**: 1–39.

Hay, S. I. 2000. An overview of remote sensing and geodesy for epidemiology and public health application. *Advances in Parasitology* **47**: 1–35.

Hay, S. I. and Lennon, J. J. 1999. Deriving meteorological variables across Africa for the study and control of vector-borne disease: a comparison of remote sensing and spatial interpolation of climate. *Tropical Medicine & International Health* **4** (1): 58–71.

Hay, S. I., Tatem, A. J., Graham, A. J., Goetz, S. J., and Rogers, D. J. 2006. Global environmental data for mapping infectious disease distribution. *Advances in Parasitology* **62**: 37–77.

Hay, S. I., Tucker, C. J., Rogers, D. J., and Packer, M. J. 1996. Remotely sensed surrogates of meteorological data for the study of the distribution and abundance of arthropod vectors of disease. *Annals of Tropical Medicine and Parasitology* **90** (1): 1–19.

Haylock, M. R., Hofstra, N., Tank, A. M. G. K., Klok, E. J., Jones, P. D., and New, M. 2008. A European daily high-resolution gridded data set of surface temperature and precipitation for 1950-2006. *Journal of Geophysical Research - Atmospheres* **113** (D20): D20119+.

Hendrickx, G., Napala, A., Slingenbergh, J. H., De Deken, R., and Rogers, D. J. 2001. A contribution towards simplifying area-wide tsetse surveys using medium resolution meteorological satellite data. *Bulletin of entomological research* **91** (5): 333–346.

Herbreteau, V., Salem, G., Souris, M., Hugot, J., and Gonzalez, J. 2007. Thirty years of use and improvement of remote sensing, applied to epidemiology: From early promises to lasting frustration. *Health & Place* **13** (2): 400–403.

Herbreteau, V., Salem, G., Souris, M., Hugot, J. P., and Gonzalez, J. P. 2005. Sizing up human health through remote sensing: uses and misuses. *Parassitologia* **47** (1): 63–79.

Hess, G., Randolph, S., Arneberg, P., Chemini, C., Furlanello, C., Harwood, J., Roberts, M., and Swinton, J. 2002. Spatial aspects of disease dynamics. In *The Ecology of Wildlife Diseases* (eds. Hudson, P. J., Rizzoli, A. P., Grenfell, B. T., Heesterbeek, H., and Dobson, A. P.), pp. 102–118. Oxford Univ. Press.

Hijmans, R. J., Cameron, S. E., Parra, J. L., Jones, P. G., and Jarvis, A. 2005. Very high resolution interpolated climate surfaces for global land areas. *International Journal of Climatology* **25** (15): 1965–1978.

Hofierka, J., Parajka, J., Mitasova, H., and Mitas, L. 2002. Multivariate interpolation of precipitation using regularized spline with tension. *Transactions in GIS* **6** (2): 135–150.

Holben, B. 1986. Characteristics of maximum-value composite images from temporal AVHRR data. *International Journal of Remote Sensing* **7**: 1417–1434.

Hubálek, Z. and Halouzka, J. 1999. West Nile fever–a reemerging mosquito-borne viral disease in Europe. *Emerging Infectious Diseases* **5** (5): 643–650.

Hubálek, Z., Lukacova, L., Halouzka, J., Sirucek, P., Januska, J., Precechtelova, J., and Prochazka, P. 2006. Import of West Nile Virus Infection in the Czech Republic. *European Journal of Epidemiology* **21** (4): 323–324.

Hudson, P. J., Rizzoli, A., Rosà, R., Chemini, C., Jones, L. D., and Gould, E. A. 2001. Tick-borne encephalitis virus in northern Italy: molecular analysis, relationships with density and seasonal dynamics of Ixodes ricinus. *Medical and Veterinary Entomology* **15** (3): 304–313.

Huete, A., Didan, K., Miura, T., Rodriguez, E. P., Gao, X., and Ferreira, L. G. 2002. Overview of the radiometric and biophysical performance of the MODIS vegetation indices. *Remote Sensing of Environment* **83** (1-2): 195–213.

Huete, A., Justice, C., and Leeuwen, W. 1999. MODIS vegetation index (MOD 13). Algorithm theoretical

basis document ATBD13. URL http://modis.gsfc.nasa.gov/data/atbd/atbd_mod13.pdf.

Hutchinson, M. F. 1995. Interpolating mean rainfall using thin plate smoothing splines. *International Journal of Geographical Information Science* **9** (4): 385–403.

Jones, C. G., Ostfeld, R. S., Richard, M. P., Schauber, E. M., and Wolff, J. O. 1998. Chain reactions linking acorns to gypsy moth outbreaks and Lyme disease risk. *Science* **279** (5353): 1023–1026.

Jouda, F., Perret, J. L., and Gern, L. 2004. Density of questing Ixodes ricinus nymphs and adults infected by Borrelia burgdorferi sensu lato in Switzerland: spatio-temporal pattern at a regional scale. *Vector-Borne and Zoonotic Diseases* **4** (1): 23–32.

Journel, A. G. 1996. Modelling uncertainty and spatial dependence: Stochastic imaging. *International Journal of Geographical Information Science* **10** (5): 517–522.

Justice, C. O., Townshend, J. R. G., Vermote, E. F., Masuoka, E., Wolfe, R. E., Saleous, N., Roy, D. P., and Morisette, J. T. 2002. An overview of MODIS Land data processing and product status. *Remote Sensing of Environment* **83** (1-2): 3–15.

Justice, C. O., Vermote, E., Townshend, J. R. G., Defries, R., Roy, D. P., Hall, D. K., Salomonson, V. V., Privette, J. L., Riggs, G., Strahler, A., et al. 1998. The moderate resolution imaging spectroradiometer (modis): land remote sensing for global change research. *Geoscience and Remote Sensing, IEEE Transactions on* **36** (4): 1228–1249.

Jönsson, P. and Eklundh, L. 2002. Seasonality extraction by function fitting to time-series of satellite sensor data. *IEEE Transactions on Geoscience and Remote Sensing* **40**: 1824–1832.

Kahl, O., Gern, L., Eisen, L., and Lane, R. S. 2002. Ecological research on Borrelia burgdorferi sensu lato: Terminology and some methodological pitfalls. In *Lyme Borreliosis: Biology, Epidemiology and Control* (eds. Gray, J. S., Kahl, O., Lane, R. S., and Stanek, G.). CABI Publishing.

Kalluri, S., Gilruth, P., Rogers, D., and Szczur, M. 2007. Surveillance of arthropod vector-borne infectious diseases using remote sensing techniques: a review. *PLoS pathogens* **3** (10): 1361–1371.

Kawashima, S., Ishida, T., Minomura, M., and Miwa, T. 2000. Relations between surface temperature and air temperature on a local scale during winter nights. *Journal of Applied Meteorology* **39** (9): 1570–1579.

Kerr, J. T. and Ostrovsky, M. 2003. From space to species: ecological applications for remote sensing. *Trends in Ecology & Evolution* **18** (6): 299–305.

Killilea, M. E., Swei, A., Lane, R. S., Briggs, C. J., and Ostfeld, R. S. 2008. Spatial dynamics of Lyme disease: A review. *EcoHealth* **5** (2): 167–195.

Kilpatrick, A. M., Meola, M. A., Moudy, R. M., and Kramer, L. D. 2008. Temperature, viral genetics, and the transmission of West Nile virus by Culex pipiens mosquitoes. *PLoS pathogens* **4** (6).

Kitron, U. 1998. Landscape ecology and epidemiology of vector-borne diseases: tools for spatial analysis. *Journal of Medical Entomology* **35** (4): 435–445.

Kitron, U., Swanson, J., Crandell, M., Sullivan, P. J., Anderson, J., Garro, R., Haramis, L. D., and Grimstad, P. R. 1998. Introduction of aedes albopictus into a la crosse virus–enzootic site in illinois. *Emerging infectious diseases* **4** (4): 627–630, URL http://view.ncbi.nlm.nih.gov/pubmed/9866739.

Knap, N., Durmiši, E., Saksida, A., Korva, M., Petrovec, M., and Avšič-Županc, T. 2009. Influence of climatic factors on dynamics of questing Ixodes ricinus ticks in Slovenia. *Veterinary Parasitology* p. (in press).

Knudsen, A. B., Romi, R., and Majori, G. 1996. Occurrence and spread in italy of aedes albopictus, with implications for its introduction into other parts of europe. *Journal of the American Mosquito Control Association* **12** (2 Pt 1): 177–183.

Kobayashi, M., Nihei, N., and Kurihara, T. 2002. Analysis of northern distribution of Aedes albopictus (Diptera: Culicidae) in Japan by geographical information system. *Journal of medical entomology* **39** (1): 4–11.

Korenberg, E. I. 2000. Seasonal population dynamics of Ixodes ticks and tick-borne encephalitis virus. *Experimental and Applied Acarology* **24** (9): 665–681.

Korenberg, E. I., Kovalevskii, Y. V., and Gorelova, N. B. 2002. Tick-host-borrelia population interactions: Long-term records in eastern Europe. *Experimental and Applied Acarology* **28** (1 - 4): 225–229.

Kruse, H., Kirkemo, A. M., and Handeland, K. 2004. Wildlife as source of zoonotic infections. *Emerging Infectious Diseases* **10** (12): 2067–2072.

Kuhn, K. G., Campbell-Lendrum, D. H., and Davies, C. R. 2004. Tropical diseases in Europe? How we can learn from the past to predict the future. *EpiNorth Journal* pp. 1–6.

Labuda, M., Kozuch, O., Zuffova, E., Eleckova, E., Hails, R., and Nuttall, P. 1997. Tick-borne encephalitis virus transmission between ticks co-feeding on specific immune natural rodent hosts. *Virology* **235**:

138–143.

Labuda, M. and Nuttall, P. A. 2004. Tick-borne viruses. *Parasitology* **129**.

Manilla, G. 1998. *Fauna d'Italia,* volume 36 of *Acari Ixodida*. Edizioni Calderini, Bologna.

Mantelli, B., Pecchioli, E., Hauffe, H. C., Rosà, R., and Rizzoli, A. 2006. Prevalence of Borrelia burgdorferi s.l. and Anaplasma phagocytophilum in the wood tick Ixodes ricinus in the Province of Trento, Italy. *European Journal of Clinical Microbiology & Infectious Diseases* pp. 1–3.

McPherson, J. M., Jetz, W., and Rogers, D. J. 2004. The effects of species' range sizes on the accuracy of distribution models: ecological phenomenon or statistical artefact? *Journal of Applied Ecology* **41** (5): 811–823.

Mcquiston, J. H., Paddock, C. D., Holman, R. C., and Childs, J. E. 1999. The human ehrlichioses in the United States. *Emerging Infectious Diseases* **5** (5): 635–642.

Medlock, J. M., Avenell, D., Barrass, I., and Leach, S. 2006. Analysis of the potential for survival and seasonal activity of Aedes albopictus (Diptera: Culicidae) in the United Kingdom. *Journal of Vector Ecology* **31** (2): 292–304.

Mitas, L. and Mitasova, H. 1999. Spatial interpolation. In *Geographical Information Systems: Principles, Techniques, Management and Applications* (eds. Longley, P., Goodchild, M. F., Maguire, D. J., and Rhind, D. W.), pp. 481–492. Wiley, 2nd edition.

Mitasova, H. and Hofierka, J. 1993. Interpolation by regularized spline with tension: II. Application to terrain modeling and surface geometry analysis. *Mathematical Geology* **25**: 657–669.

Mitasova, H. and Mitas, L. 1993. Interpolation by regularized spline with tension: I. Theory and implementation. *Mathematical Geology* **25**: 641–655.

Mitchell, C. J. 1995. Geographic spread of Aedes albopictus and potential for involvement in arbovirus cycles in the Mediterranean basin. *Journal of Vector Ecology* **20** (1): 44–58.

Neteler, M. 2005. Time series processing of MODIS satellite data for landscape epidemiological applications. *International Journal of Geoinformatics. Special Issue on FOSS/GRASS 2004 & GIS-IDEAS 2004* **1** (1): 133–138.

Neteler, M. and Mitasova, H. 2008. *Open Source GIS: A GRASS GIS Approach*. Springer, New York, 3rd edition.

New, M., Hulme, M., and Jones, P. 1999. Representing twentieth-century space-time climate variability. Part I: Development of a 1961-90 mean monthly terrestrial climatology. *Journal of Climate* **12** (3): 829–856.

New, M., Lister, D., Hulme, M., and Makin, I. 2002. A high-resolution data set of surface climate over global land areas. *Climate Research* **21** (1): 1–25.

Niedrig, M., Reinhardt, B., Burchard, G. D., Schmitz, H., Tannich, E., Tintelnot, K., Laude, G., Alpers, K., Stark, K., and Mehlhose, J. 2006. *Steckbriefe seltener und importierter Infektionskrankheiten*.

Nurdan, O. 2005. Emerging vector-borne diseases in a changing environment. *Turkish Journal of Biology* **29**: 125–135.

Nuti, M., Serafini, D. A., Bassetti, D., Ghionni, A., Russino, F., Rombolà, P., Macri, G., and Lillini, E. 1998. Ehrlichia infection in Italy. *Emerging Infectious Diseases* **4** (4): 663–665.

Ogden, N. H., Barker, I. K., Beauchamp, G., Brazeau, S., Charron, D. F., Maarouf, A., Morshed, M. G., O'Callaghan, C. J., Thompson, R. A., Waltner-Toews, D., et al. 2006. Investigation of ground level and remote-sensed data for habitat classification and prediction of survival of Ixodes scapularis in habitats of southeastern Canada. *Journal of Medical Entomology* **43** (2): 403–414.

De Beurs, K. M. and Henebry, G. M. 2005. A statistical framework for the analysis of long image time series. *International Journal of Remote Sensing* **26** (8): 1551–1573.

Ostfeld, R., Cepeda, O., Hazler, K., and Miller, M. 1995. Ecology of Lyme disease: Habitat associations of ticks (Ixodes scapularis) in a rural landscape. *Ecological Applications* **5** (2): 353–361.

Ostfeld, R. S. 1997. The ecology of Lyme-disease risk: Complex interactions between seemingly unconnected phenomena determine risk of exposure to this expanding disease. *American Scientist* **85**.

Ostfeld, R. S., Canham, C. D., Oggenfuss, K., Winchcombe, R. J., and Keesing, F. 2006. Climate, deer, rodents, and acorns as determinants of variation in Lyme-disease risk. *PLoS Biology* **4** (6).

Ostfeld, R. S., Glass, G. E., and Keesing, F. 2005. Spatial epidemiology: an emerging (or re-emerging) discipline. *Trends in Ecology and Evolution* **20** (6): 328–336.

Parola, P. 2004. Tick-borne rickettsial diseases: emerging risks in Europe. *Comparative Immunology, Microbiology and Infectious Diseases* **27** (5): 297–304.

Parola, P., Davoust, B., and Raoult, D. 2005. Tick- and flea-borne rickettsial emerging zoonoses. *Veterinary Research* **36** (3): 469–492.

Parola, P. and Raoult, D. 2001. Ticks and tickborne bacterial diseases in humans: an emerging infectious threat. *Clinical Infectious Diseases* **32** (6): 897–928.

Pasotti, L., Maroli, M., Giannetto, S., and Brianti, E. 2006. Agrometeorology and models for the parasite cycle forecast. *Parassitologia* **48** (1-2): 81–83.

Paz, S. and Albersheim, I. 2008. Influence of warming tendency on Culex pipiens population abundance and on the probability of West Nile fever outbreaks (Israeli case study: 2001-2005). *EcoHealth* **5** (1): 40–48.

Perkins, S., Cattadori, I., Tagliapietra, V., Rizzoli, A., and Hudson, P. 2003. Empirical evidence for key hosts in persistence of a tick-borne disease. *International Journal for Parasitology* **33**: 909–917.

Perret, J. L., Guigoz, E., Rais, O., and Gern, L. 2000. Influence of saturation deficit and temperature on Ixodes ricinus tick questing activity in a Lyme borreliosis-endemic area (Switzerland). *Parasitol Res* **86** (7): 554–557.

Piccolin, G., Benedetti, G., Doglioni, C., Lorenzato, C., Mancuso, S., Papa, N., Pitton, L., Ramon, M. C., Zasio, C., and Bertiato, G. 2006. A study of the presence of B. burgdorferi, Anaplasma (previously Ehrlichia) phagocytophilum, Rickettsia, and Babesia in Ixodes ricinus collected within the territory of Belluno, Italy. *Vector-Borne and Zoonotic Diseases* **6** (1): 24–31.

Piccolin, G., Lorenzato, C., Pitton, L., Porta, V., Ramon, M., and Bertiato, G. 2001. La situazione nel Bellunese. La metodologia delle indagini in campo e nel laboratorio. Risultati delle indagini ecologiche ed epidemiologiche delle campagne di raccolta 2000 e 2001. In *Atti del Convegno Interregionale "Le infezioni trasmesse da zecche - problemi epidemiologici e sociosanitari - la situazione nel Bellunese e in Carinzia.*", pp. 35–57.

Piesman, J. and Gern, L. 2004. Lyme borreliosis in Europe and North America. *Parasitology* **129**: S191–S220.

Pilani, R., Caprioglio, A., and Bellini, R. 2004. Surveillance and prevention in Aedes albopictus business: The case of Piedmont region. In *3rd EMCA Workshop, 6-9 October 2004*.

Purse, B. V., Tatem, A. J., Caracappa, S., Rogers, D. J., Mellor, P. S., Baylis, M., and Torina, A. 2004. Modelling the distributions of Culicoides bluetongue virus vectors in Sicily in relation to satellite-derived climate variables. *Medical and Veterinary Entomology* **18** (2): 90–101.

R Development Core Team 2006. *R: A Language and Environment for Statistical Computing*. R Foundation for Statistical Computing, Vienna, Austria.

Randolph, S. E. 2000. Ticks and tick-borne disease systems in space and from space. *Advances in Parasitology* **47**: 217–243.

Randolph, S. E. 2001a. Epidemiological consequenses of tick ecology. In *Proc. Symposium Current Research on Tick-Borne Infections, Kalmar, Sweden*.

Randolph, S. E. 2001b. The shifting landscape of tick-borne zoonoses: Tick-borne encephalitis and Lyme borreliosis in Europe. *Philosophical Transactions of the Royal Society B: Biological Sciences* **356**: 1054–1056.

Randolph, S. E. 2002. Predicting the risk of tick-borne diseases. *International Journal of Medical Microbiology* **291**: 6–10.

Randolph, S. E. 2004a. Evidence that climate change has caused 'emergence' of tick-borne diseases in Europe? *International Journal of Medical Microbiology* **293**: 5–15.

Randolph, S. E. 2004b. Tick ecology: Processes and patterns behind the epidemiological risk posed by ixodid ticks as vectors. *Parasitology* **129**.

Randolph, S. E. 2006. EDEN – Emerging diseases in a changing European environment: tick-borne diseases. *International Journal of Medical Microbiology* **296**: 84–86.

Randolph, S. E., Chemini, C., Furlanello, C., Genchi, C., Hails, R. S., Hudson, P. J., Jones, L. D., Medley, G., Norman, R. A., Rizzoli, A. P., et al. 2002. The ecology of tick-borne infections in wildlife reservoirs. In *The Ecology of Wildlife Diseases* (eds. Hudson, P. J., Rizzoli, A. P., Grenfell, B. T., Heesterbeek, H., and Dobson, A. P.), pp. 119–138. Oxford Univ. Press.

Randolph, S. E., Green, R. M., Peacey, M. F., and Rogers, D. J. 2000. Seasonal synchrony: the key to tick-borne encephalitis foci identified by satellite data. *Parasitology* **121**: 15–23.

Randolph, S. E., Miklisová, D., Lysy, J., Rogers, D. J., and Labuda, M. 1999. Incidence from coincidence: patterns of tick infestations on rodents facilitate transmission of tick-borne encephalitis virus. *Parasitology* **118**: 177–186.

Randolph, S. E. and Rogers, D. J. 2000. Fragile transmission cycles of tick-borne encephalitis virus may be disrupted by predicted climate change. *Proceedings of the Royal Society of London. Series B, Biological sciences* **267** (1454): 1741–1744.

Randolph, S. E. and Rogers, D. J. 2002. Remotely sensed correlates of phylogeny: Tick-borne

flaviviruses. *Experimental and Applied Acarology* **28** (1 - 4): 231–237.

Randolph, S. E. and Storey, K. 1999. Impact of microclimate on immature tick-rodent host interactions (Acari: Ixodidae): implications for parasite transmission. *Journal of Medical Entomology* **36** (6): 741–748.

Reed, K. D., Meece, J. K., Henkel, J. S., and Shukla, S. K. 2003. Birds, migration and emerging zoonoses: West Nile virus, Lyme disease, Influenza A and Enteropathogens. *Clinical Medicine & Research* **1** (1): 5–12.

Rezza, G., Nicoletti, L., Angelini, R., Romi, R., Finarelli, A. C., Panning, M., Cordioli, P., Fortuna, C., Boros, S., Magurano, F., et al. 2007. Infection with chikungunya virus in Italy: an outbreak in a temperate region. *The Lancet* **370** (9602): 1840–1846.

Rizzoli, A., Hauffe, H. C., Tagliapietra, V., Neteler, M., and Rosà, R. 2009. Forest structure and roe deer abundance predict tick-borne encephalitis risk in Italy. *PLoS ONE* **4** (2): e4336+.

Rizzoli, A., Neteler, M., Rosà, R., Versini, W., Cristofolini, A., Bregoli, M., Buckley, A., and Gould, E. 2007a. Early detection of TBEv spatial distribution and activity in the Province of Trento assessed using serological and remotely-sensed climatic data. *Geospatial Health* **1** (2): 169–176.

Rizzoli, A., Rosà, R., Rosso, F., Buckley, A., and Gould, E. 2007b. West Nile virus circulation detected in Northern Italy in sentinel chickens. *Vector Borne Zoonotic Dis* .

Rizzoli, A., Rosà, R., Mantelli, B., Pecchioli, E., Hauffe, H., Tagliapietra, V., Beninati, T., Neteler, M., and Genchi, C. 2004. [Ixodes ricinus, transmitted diseases and reservoirs] (in Italian). *Parassitologia* **46** (1-2): 119–122.

Robert Koch-Institut (RKI) 1998. Humane granulozytäre Ehrlichiose (HGE). *Epidemiologisches Bulletin* **42**: 295–297.

Rogers, D. J., Hay, S. I., and Packer, M. J. 1996. Predicting the distribution of tsetse flies in West Africa using temporal Fourier processed meteorological satellite data. *Annals of Tropical Medicine and Parasitology* **90** (3): 225–241.

Rogers, D. J. and Randolph, S. E. 2003. Studying the global distribution of infectious diseases using GIS and RS. *Nature Reviews Microbiology* **1** (3): 231–237.

Rogers, D. J., Randolph, S. E., Snow, R. W., and Hay, S. I. 2002. Satellite imagery in the study and forecast of malaria. *Nature* **415** (6872): 710–715.

Roiz, D., Rosà, R., Arnoldi, D., and Rizzoli, A. in press. Effect of temperature and rainfall on activity and dynamics of host-seeking Aedes albopictus females in Northern. *Vector Borne and Zoonotic Diseases* .

Rolland, C. 2003. Spatial and seasonal variations of air temperature lapse rates in alpine regions. *Journal of Climate* **16** (7): 1032–1046.

Roy, D. P., Borak, J. S., Devadiga, S., Wolfe, R. E., Zheng, M., and Descloitres, J. 2002. The MODIS Land product quality assessment approach. *Remote Sensing of Environment* **83** (1-2): 62–76.

Scharlemann, J. P., Benz, D., Hay, S. I., Purse, B. V., Tatem, A. J., Wint, G. R., and Rogers, D. J. 2008. Global data for ecology and epidemiology: A novel algorithm for temporal Fourier processing MODIS data. *PLoS ONE* **3** (1).

Scholte, E.-J. J., Dijkstra, E., Blok, H., De Vries, A., Takken, W., Hofhuis, A., Koopmans, M., De Boer, A., and Reusken, C. B. 2008. Accidental importation of the mosquito aedes albopictus into the netherlands: a survey of mosquito distribution and the presence of dengue virus. *Medical and veterinary entomology* **22** (4): 352–358.

Senior, K. 2008. Vector-borne diseases threaten Europe. *The Lancet Infectious Diseases* **8** (9): 531–532.

Sonenshine, D. E. 1993. *Biology of Ticks: Volume 2*. Oxford University Press, USA.

Intergovernmental Panel on Climate Change 2007. Summary for Policymakers. In *Climate Change 2007: The Physical Science Basis. Contribution of Working Group I to the Fourth Assessment Report of the Intergovernmental Panel on Climate Change* (eds. Solomon, S., Qin, D., Manning, M., Chen, Z., Marquis, M., Averyt, K. B., Tignor, M., and Miller, H. L.), pp. 1–18. Cambridge University Press.

Intergovernmental Panel on Climate Change 2008. *Climate Change 2007 - Impacts, Adaptation and Vulnerability: Working Group II contribution to the Fourth Assessment Report of the IPCC*. Cambridge University Press, 1st edition.

U.S. Geological Survey 2008. MODIS Reprojection Tool V4.0 software. URL `https://lpdaac.usgs.gov/lpdaac/tools/modis_reprojection_tool`.

Stahl, K., Moore, R., Floyer, J., Asplin, M., and Mckendry, I. 2006. Comparison of approaches for spatial interpolation of daily air temperature in a large region with complex topography and highly variable station density. *Agricultural and Forest Meteorology* **139** (3-4): 224–236.

Stanek, G. 2002. Tick-transmitted diseases in central Europe. *Wiener Klinische Wochenschrift* **114** (13-14): 471–472.

Stathopoulou, M., Cartalis, C., and Chrysoulakis, N. 2006. Using midday surface temperature to estimate cooling degree-days from noaa-avhrr thermal infrared data: An application for athens, greece. *Solar Energy* **80** (4): 414–422.

Steinacker, R., Ratheiser, M., Bica, B., Chimani, B., Dorninger, M., Gepp, W., Lotteraner, C., Schneider, S., and Tschannett, S. 2006. A mesoscale data analysis and downscaling method over complex terrain. *Monthly Weather Review* **134** (10): 2758–2771.

Straetemans, M. 2008. Vector-related risk mapping of the introduction and establishment of Aedes albopictus in Europe. *Euro surveillance: bulletin européen sur les maladies transmissibles = European communicable disease bulletin* **13** (7).

Strle, F. 2004. Human granulocytic ehrlichiosis in Europe. *International Journal of Medical Microbiology* **293**: 27–35.

Stuen, S. 2007. Anaplasma phagocytophilum - the most widespread tick-borne infection in animals in Europe. *Veterinary Research Communications* **31**: 79–84.

Sumilo, D., Asokliene, L., Bormane, A., Vasilenko, V., Golovljova, I., and Randolph, S. E. 2007. Climate change cannot explain the upsurge of tick-borne encephalitis in the Baltics. *PLoS ONE* **2**.

Suprit, K. and Shankar, D. 2008. Resolving orographic rainfall on the Indian west coast. *International Journal of Climatology* **28** (5): 643–657.

Süss, J. 2003. Epidemiology and ecology of TBE relevant to the production of effective vaccines. *Vaccine* **21**: S1/19–S1/35.

Tachiiri, K., Klinkenberg, B., Mak, S., and Kazmi, J. 2006. Predicting outbreaks: a spatial risk assessment of west nile virus in british columbia. *International Journal of Health Geographics* **5** (1): 21+.

Tatem, A. J., Goetz, S. J., and Hay, S. I. 2004. Terra and Aqua: new data for epidemiology and public health. *International Journal of Applied Earth Observation and Geoinformation* **6** (1): 33–46.

Tatem, A. J., Hay, S. I., and Rogers, D. J. 2006. Global traffic and disease vector dispersal. *Proceedings of the National Academy of Sciences of the United States of America* **103** (16): 6242–6247.

Teillet, P. M., Guindon, B., and Goodenough, D. G. 1982. On the slope-aspect correction of multispectral scanner data. *Canadian Journal of Remote Sensing* **8** (2): 84–106.

Thomson, M. C. and Connor, S. J. 2000. Environmental information systems for the control of arthropod vectors of disease. *Medical and Veterinary Entomology* **14** (3): 227–244.

Toma, L., Severini, F., Di Luca, M., Bella, A., and Romi, R. 2003. Seasonal patterns of oviposition and egg hatching rate of Aedes albopictus in Rome. *Journal of the American Mosquito Control Association* **19** (1): 19–22.

Tran, H., Uchihama, D., Ochi, S., and Yasuoka, Y. 2006. Assessment with satellite data of the urban heat island effects in asian mega cities. *International Journal of Applied Earth Observation and Geoinformation* **8** (1): 34–48.

Tsetsarkin, K. A., Vanlandingham, D. L., McGee, C. E., and Higgs, S. 2007. A single mutation in Chikungunya virus affects vector specificity and epidemic potential. *PLoS Pathogens* **3** (12).

Vancutsem, C., Ceccato, P., Dinku, T., and Connor, S. J. 2010. Evaluation of MODIS land surface temperature data to estimate air temperature in different ecosystems over Africa. *Remote Sensing of Environment* **114** (2): 449–465.

Vazeille, M., Jeannin, C., Martin, E., Schaffner, F., and Failloux, A. B. 2008. Chikungunya: a risk for Mediterranean countries? *Acta tropica* **105** (2): 200–202.

Veit, H. 2002. *Die Alpen – Geoökologie und Landschaftsentwicklung*. Ulmer, Stuttgart.

Vermote, E. F. and Vermeulen, A. 1999. Atmospheric correction algorithm: spectral reflectances (MOD09). Algorithm Technical Background Document (ATBD). URL `http://modis.gsfc.nasa.gov/data/atbd/atbd_mod08.pdf`.

Vinogradova, A. B. 2000. *Culex pipiens pipiens mosquitoes: Taxonomy, distribution, ecology, physiology, genetics, applied importance and control*. Pensoft Publishers.

Wahba, G. 1990. Spline models for observational data. In *SIAM*.

Walker, A. R., Alberdi, M. P., Urquhart, K. A., and Rose, H. 2001. Risk factors in habitats of the tick Ixodes ricinus influencing human exposure to Ehrlichia phagocytophila bacteria. *Medical and Veterinary Entomology* **15** (1): 40–49.

Wan, Z. 1999. MODIS Land-Surface Temperature. Algorithm theoretical basis document (LST ATBD): LST calculations. URL `http://modis.gsfc.nasa.gov/data/atbd/atbd_mod11.pdf`.

Wan, Z. 2003. MODIS Land-Surface Temperature products users' guide. URL `http://www.icess.ucsb.edu/modis/LstUsrGuide/usrguide.html`.

Wan, Z. 2008. New refinements and validation of the MODIS Land-Surface Temperature/Emissivity

products. *Remote Sensing of Environment* **112** (1): 59–74.

Wan, Z. and Dozier, J. 1996. A generalized split-window algorithm for retrieving land-surface temperature from space. *Geoscience and Remote Sensing, IEEE Transactions on* **34** (4): 892–905.

Wan, Z., Zhang, Y., Zhang, Q., and Li, Z. L. 2004. Quality assessment and validation of the MODIS global land surface temperature. *International Journal of Remote Sensing* pp. 261–274.

Wang, Q., Adiku, S., Tenhunen, J., and Granier, A. 2005. On the relationship of NDVI with leaf area index in a deciduous forest site. *Remote Sensing of Environment* **94** (2): 244–255.

Wood, B., Beck, L., Lobitz, B., and Bobo, M. 2000. Education, outreach and the future of remote sensing in human health. In *Remote sensing and geographical information systems in epidemiology* (eds. Hay, S., Randolph, S., and Rogers, D.), Advances in Parasitology Special Volume 47. Academic Press.

World Health Organization 2004. Using climate to predict disease outbreaks: A review.

World Health Organization 2008. Protecting health in Europe from climate change. Copenhagen, Denmark.

Xiao, X., Gilbert, M., Slingenbergh, J., Lei, F., and Boles, S. 2007. Remote sensing, ecological variables, and wild bird migration related to outbreaks of highly pathogenic H5N1 avian influenza. *Journal of Wildlife Diseases* **43** (3): S40–46.

Zeller, H. G. and Schuffenecker, I. 2004. West Nile Virus: An overview of its spread in Europe and the Mediterranean basin in contrast to its spread in the Americas. *European Journal of Clinical Microbiology & Infectious Diseases* **23** (3): 147–156.

A Appendix

A.1 Parallel processing for MODIS LST maps reconstruction on a cluster

FEM-CRI GIS and Remote Sensing unit cluster   The cluster of the FEM-CRI GIS and Remote Sensing unit[1] which was used to reconstruct the daily MODIS LST maps consists of 12 single-slot-blades with 2 processors each (4-core Xeon 2.5 GHz, 16 Gb/32 Gb RAM) and 2 double-slot-blades (4 x 4-core Opteron (2.2 GHz, 64 Gb RAM), all connected via 10 Gb ethernet, so in total 128 CPUs with 400 Gb RAM. The file server is a 4-core Xeon 2.66 GHz with 8 Gb RAM. The peak floating point performance of approximately 1.7 TeraFlops/s.

Blades:

- Dell PowerEdge M1000e Blade Enclosure
- 12 PE M600 Quad-Core Xeon E5420 2.5 GHz/2x6 MB 1333 FSB, RAM 16 GB 667 MHz FBD (8x2 GB dual rank DIMMs), 2 x 73 GB SAS (15,000 rpm) 2.5 in Hard Drive
- 2 PE M905 4x Quad Core Opteron 8354 (2.2 GHz, RAM 64 GB, 2 x 73 GB SAS (15,000 rpm) 2.5 in Hard Drive
- 2 PowerConnect M6220 switch 20 Port Redundant (FI)

File server:

- 1 PE2950 III Quad-Core Xeon E5430 2.66 GHz/2x6 MB 1333 FSB
- 1 MD3000 external SAS RAID array with 2 single-port controllers
- 14 * 750 GB

UPS:

- APC Smart-UPS RT (8000VA), Ethernet 10/100

Operating System:

- Scientific Linux 5.2: `http://www.scientificlinux.org`
- Blades: Scientific Linux 5.2 Live CD and DVD – Diskless Client: `http://www.livecd.ethz.ch/diskless.html`

---

[1]FEM-CRI GIS-RS platform cluster, `http://gis.fem-environment.eu/cluster/`

Job scheduler:

- Grid Engine (GE 6.1u5): `http://gridengine.sunsource.net` which allocates computational tasks among the available computing resources according to the requested resources.

The MODIS LST data were post-processed on this cluster with GRASS GIS 6.4 as outlined in this thesis.

The general procedure to use this or similar clusters from a user's point of view included:

Job definition

- estimation of calculation time, number of needed nodes, number of needed processors, amount of needed RAM for individual job; define these parameters in the job launch script;
- data storage in a centralized directory which is seen by all nodes (here: blades; via Network File System – NFS).

Job execution (launch of jobs)

- The user launches all jobs; they are submitted to the Grid Engine queue;
- the scheduler optimizes among all user the execution of the jobs according to available resources and requested resources;
- for the user this means that $0..n$ jobs (n is the maximal number of available nodes in the cluster) are executed in parallel.

For the MODIS LST reconstruction, all jobs were launched as serial jobs, i.e. each map was sent to a node. Due to this no special modification of the GRASS GIS was needed to process batch jobs in parallel since GRASS GIS is already a multi-user system.

Once a job is running, an email notification is sent to the user, the same again when a job is terminating (either finished or killed to to lack of resources).

Job planning   The challenging part for the user is to estimate the execution time since the scheduler kills jobs which exceed the requested time. The same applies to the request for number of nodes and CPUs per node as well as the amount of needed RAM. Usually tests are needed to minimise the request and to see the overall performance.

A.2   Air temperature data from meteo-stations versus reconstructed MODIS LST data

This section contains original data sets which are above shown as elaborated graphs. For explanations, see Section 5.2.2.

Name	Altitude	Tmin	Tmean	Tmax	LST	Tmin - LST	Tmean - LST	Tmax - LST
Arco	84.2				18.7			
Arsio	802.0	13.2	14.0	14.7	12.7	0.5	1.3	2.0
Avio	144.7	17.3	18.1	19.5	16.2	1.1	1.9	3.3
Borgo Valsugana	414.9	9.7	11.4	13.4	15.0	-5.3	-3.6	-1.6
Cavedine	561.2	13.5	14.5	16.5	15.3	-1.8	-0.8	1.2
Cunevo	558.8	14.3	17.4	18.3	13.0	1.3	4.4	5.3
Malga Flavona	2001.9				2.9			
Paneveggio	1537.5	7.0	7.8	8.0	7.7	-0.7	0.1	0.3
Passo Tonale	1876.3	4.2	4.9	5.7	9.3	-5.1	-4.4	-3.6
Rabbi	1399.9	7.7	9.4	9.5	8.2	-0.5	1.2	1.3
S. Michele a/A	207.1	16.7	17.5	18.3	16.3	0.4	1.2	2.0
S. Orsola	769.5	13.3	15.2	17.4	14.5	-1.2	0.7	2.9
Storo	385.4				14.7			
Terlago	424.9				14.9			
Trento Sud	187.0	15.2	16.6	18.1	16.0	-0.8	0.6	2.1
Average						*-1.1*	*0.2*	*1.4*
StdDev						*2.23*	*2.46*	*2.40*

Table A.1: **Comparison of air temperature data (2m) with MODIS LST data from reconstructed LST map: autumn, 10:30 overpass, actual map gradient used**
Comparison of air temperature data (2m) with MODIS LST data from reconstructed LST map (10% void in the filtered map; actual map gradient used) in the position of the stations (date: 1 Nov 2001, air temperatures from 10:00-11:00 local solar time; MODIS LST 10:30). R^2=0.78 for Tmin/LST linear regression. See also LST maps in Figure 5.1 and Figure 5.10.

Name	Altitude	Tmin	Tmean	Tmax	LST	Tmin - LST	Tmean - LST	Tmax - LST
Arco	84.2	10.5	11.2	11.9	10.7	-0.2	0.5	1.2
Arsio	802.0	14.6	15.4	16.3	11.4	3.2	4.0	4.9
Avio	144.7	11.4	12.0	12.6	11.7	-0.3	0.3	0.9
Borgo Valsugana	414.9	16.7	17.5	18.4	12.2	4.5	5.3	6.2
Cavedine	561.2	15.0	15.5	16.3	9.6	5.4	5.9	6.7
Cunevo	558.8	17.1	17.3	17.7	12.7	4.4	4.6	5.0
Malga Flavona	2001.9	3.6	4.4	5.5	-2.6	6.2	7.0	8.1
Paneveggio	1537.5	4.6	5.5	6.7	2.7	1.9	2.8	4.0
Passo Tonale	1876.3	5.6	6.0	6.5	0.8	4.8	5.2	5.7
Rabbi	1399.9	8.8	9.5	9.9	7.2	1.6	2.3	2.7
S. Michele a/A	207.1	17.9	18.1	18.4	11.6	6.3	6.5	6.8
S. Orsola	769.5	15.8	16.3	16.6	11.2	4.6	5.1	5.4
Storo	385.4	14.7	15.5	16.3	11.3	3.4	4.2	5.0
Terlago	424.9	16.2	16.7	16.9	12.7	3.5	4.0	4.2
Trento Sud	187.0	17.0	18.3	19.0	12.3	4.7	6.0	6.7
Average						*3.6*	*4.2*	*4.9*
StdDev						*2.06*	*2.02*	*2.06*

Table A.2: **Comparison of air temperature data (2m) with MODIS LST data from reconstructed LST map: winter, 13:30 overpass, actual map gradient used**
Comparison of air temperature data (2m) with MODIS LST data from reconstructed LST map (38% void in the filtered map; actual map gradient used) in the position of the stations (date: 12 Jan 2007, air temperatures from 13:00-14:00 local solar time; MODIS LST 13:30). R^2=0.83 for Tmin/LST linear regression. See also LST maps in Figure 5.2 and Figure 5.10.

Name	Altitude	Tmin	Tmean	Tmax	LST	Tmin - LST	Tmean - LST	Tmax - LST
Arco	84.2	6.7	6.8	6.8	2.9	3.8	3.9	3.9
Arsio	802.0	2.2	2.5	2.6	-2.0	4.2	4.5	4.6
Avio	144.7	6.1	6.2	6.3	2.4	3.7	3.8	3.9
Borgo Valsugana	414.9	3.0	3.2	3.4	0.5	2.5	2.7	2.9
Cavedine	561.2	3.3	3.4	3.6	-0.3	3.6	3.7	3.9
Cunevo	558.8	3.8	4.0	4.2	-0.2	4.0	4.2	4.4
Malga Flavona	2001.9				-12.3			
Paneveggio	1537.5	-4.3	-3.0	-2.3	-7.3	3.0	4.3	5.0
Passo Tonale	1876.3				-10.4			
Rabbi	1399.9	-2.4	-2.2	-2.0	-6.4	4.0	4.2	4.4
S. Michele a/A	207.1	5.6	5.8	6.2	2.0	3.6	3.8	4.2
S. Orsola	769.5	1.8	2.1	2.4	-1.8	3.6	3.9	4.2
Storo	385.4	3.4	3.6	3.8	0.7	2.7	2.9	3.1
Terlago	424.9	4.2	4.5	4.6	0.5	3.7	4.0	4.1
Trento Sud	187.0	5.9	6.2	6.4	2.1	3.8	4.1	4.3
Average						*3.6*	*3.9*	*4.1*
StdDev						*0.51*	*0.51*	*0.56*

Table A.3: **Comparison of air temperature data (2m) with MODIS LST data from reconstructed LST map: spring, 01:30 overpass, actual map gradient used**
Comparison of air temperature data (2m) with MODIS LST data from reconstructed LST map (74% void in the filtered map; actual map gradient used) in the position of the stations (date: 11 Apr 2003, air temperatures from 01:00-02:00 local solar time; MODIS LST 01:30). R^2=0.98 for Tmin/LST linear regression. See also LST maps in Figure 5.3 and Figure 5.11.

Name	Altitude	Tmin	Tmean	Tmax	LST	Tmin - LST	Tmean - LST	Tmax - LST
Arco	84.2	15.8	16.4	20.0	12.2	3.6	4.2	7.8
Arsio	802.0	7.8	8.5	9.1	5.4	2.4	3.1	3.7
Avio	144.7	15.6	16.1	16.8	11.1	4.5	5.0	5.7
Borgo Valsugana	414.9	9.1	10.5	12.8	7.5	1.6	3.0	5.3
Cavedine	561.2	9.2	9.9	10.6	9.2	0.0	0.7	1.4
Cunevo	558.8	9.9	10.6	11.2	6.9	3.0	3.7	4.3
Malga Flavona	2001.9	-1.5	-1.1	-0.8	-4.0	2.5	2.9	3.2
Paneveggio	1537.5	-0.5	0.7	1.5	0.8	-1.3	-0.1	0.7
Passo Tonale	1876.3	1.9	2.3	2.8	-1.8	3.7	4.1	4.6
Rabbi	1399.9	4.5	5.7	6.4	1.3	3.2	4.4	5.1
S. Michele a/A	207.1	13.9	14.6	15.6	9.6	4.3	5.0	6.0
S. Orsola	769.5	9.5	10.3	10.8	6.4	3.1	3.9	4.4
Storo	385.4	10.9	11.4	12.2	8.9	2.0	2.5	3.3
Terlago	424.9	10.6	11.2	11.7	8.6	2.0	2.6	3.1
Trento Sud	187.0	14.3	14.5	14.6	10.1	4.2	4.4	4.5
Average						*2.6*	*3.3*	*4.2*
StdDev						*1.60*	*1.46*	*1.78*

Table A.4: **Comparison of air temperature data (2m) with MODIS LST data from reconstructed LST map: spring, 22:30 overpass, actual map gradient used**
Comparison of air temperature data (2m) with MODIS LST data from reconstructed LST map (25% void in the filtered map; actual map gradient used) in the position of the stations (date: 25 Apr 2008, air temperatures from 22:00-23:00 local solar time; MODIS LST 22:30). R^2=0.92 for Tmin/LST linear regression. See also LST maps in Figure 5.4 and Figure 5.11.

Name	Altitude	Tmin	Tmean	Tmax	LST	Tmin - LST	Tmean - LST	Tmax - LST
Arco	84.2	20.9	21.3	21.6	28.1	-7.2	-6.8	-6.5
Arsio	802.0	17.9	18.5	22.8	24.2	-6.3	-5.7	-1.4
Avio	144.7	19.8	20.1	20.7	27.7	-7.9	-7.6	-7.0
Borgo Valsugana	414.9	20.4	21.0	21.4	26.3	-5.9	-5.3	-4.9
Cavedine	561.2	18.9	19.3	19.7	25.5	-6.6	-6.2	-5.8
Cunevo	558.8	18.9	19.2	19.7	25.5	-6.6	-6.3	-5.8
Malga Flavona	2001.9	11.1	11.5	11.7	17.7	-6.6	-6.2	-6.0
Paneveggio	1537.5	13.5	14.2	15.1	20.2	-6.7	-6.0	-5.1
Passo Tonale	1876.3	9.5	9.7	10.0	18.4	-8.9	-8.7	-8.4
Rabbi	1399.9	12.5	12.9	13.5	21.0	-8.5	-8.1	-7.5
S. Michele a/A	207.1	20.2	20.9	23.7	27.4	-7.2	-6.5	-3.7
S. Orsola	769.5	16.9	17.5	17.8	24.4	-7.5	-6.9	-6.6
Storo	385.4	18.6	19.0	19.3	26.4	-7.8	-7.4	-7.1
Terlago	424.9	19.1	19.5	19.9	26.2	-7.1	-6.7	-6.3
Trento Sud	187.0	19.8	20.6	21.1	27.5	-7.7	-6.9	-6.4
Average						*-7.2*	*-6.8*	*-5.9*
StdDev						*0.83*	*0.90*	*1.68*

Table A.5: **Comparison of air temperature data (2m) with MODIS LST data from reconstructed LST map: summer, 10:30 overpass, 16-day period map gradient used**
Comparison of air temperature data (2m) with MODIS LST data from reconstructed LST map (96% void in the filtered map; 16-day period map gradient of 10:30 overpass phase used) in the position of the stations (date: 24 Jul 2003, air temperatures from 10:00-11:00 local solar time; MODIS LST 10:30). The LST map is generated from the 16-day period mean gradient model since no sufficient number of valid pixels was available. Therefore Tmin and LST are highly correlated (R^2=0.95 for Tmin/LST linear regression). See also LST maps in Figure 5.5 and Figure 5.12.

Name	Altitude	Tmin	Tmean	Tmax	LST	Tmin - LST	Tmean - LST	Tmax - LST
Arco	84.2	8.1	8.9	10.0	7.9	0.2	1.0	2.1
Arsio	802.0	7.0	7.8	8.2	3.8	3.2	4.0	4.4
Avio	144.7	7.7	8.2	8.6	6.6	1.1	1.6	2.0
Borgo Valsugana	414.9	5.7	6.0	6.5	5.2	0.5	0.8	1.3
Cavedine	561.2	5.2	6.0	6.3	6.3	-1.1	-0.3	0.0
Cunevo	558.8	4.3	4.9	5.8	4.6	-0.3	0.3	1.2
Malga Flavona	2001.9	-0.6	-0.4	-0.2	-1.7	1.1	1.3	1.5
Paneveggio	1537.5	-0.7	0.1	1.0	1.0	-1.7	-0.9	0.0
Passo Tonale	1876.3	-0.7	0.2	0.6	-1.0	0.3	1.2	1.6
Rabbi	1399.9	3.0	3.4	3.9	1.4	1.6	2.0	2.5
S. Michele a/A	207.1	4.5	5.5	6.6	5.6	-1.1	-0.1	1.0
S. Orsola	769.5	4.9	5.3	5.8	4.2	0.7	1.1	1.6
Storo	385.4	4.3	4.9	6.5	4.9	-0.6	0.0	1.6
Terlago	424.9	2.1	2.5	2.8	4.8	-2.7	-2.3	-2.0
Trento Sud	187.0	5.3	5.8	6.3	5.8	-0.5	0.0	0.5
Average						*0.0*	*0.6*	*1.3*
StdDev						*1.46*	*1.44*	*1.41*

Table A.6: **Comparison of air temperature data (2m) with MODIS LST data from reconstructed LST map: autumn, 01:30 overpass, actual map gradient used**
Comparison of air temperature data (2m) with MODIS LST data from reconstructed LST map (27% void in the filtered map; actual map gradient used) in the position of the stations (date: 18 Oct 2006, air temperatures from 01:00-02:00 local solar time; MODIS LST 01:30). R^2=0.76 for Tmin/LST linear regression. See also LST maps in Figure 5.6 and Figure 5.12.